Romanian Journal of Earth Sciences, vol. 89, issues 1-2, p. 35-250

FLUIDS IN THE EARTH CRUST AND UPPER MANTLE: AN ATLAS OF THE FLUID AND MELT INCLUSIONS FROM ROMANIA

Ioan Pintea

Geological Institute of Romania, Cluj - Napoca branch, ipinteaflincs@yahoo.com

Key words: fluid and melt inclusions, Carpathians, Romania

Abstract. The geological history of the Romanian territory spanned ca. 2.0 Ga from the Proterozoic to the present time (Balintoni 2000). There are plenty of geological events where one or more fluid/melt phases were involved during their formation time. Metamorphic, magmatic and sedimentary rocks were generated during Wilson cycles characterized by various fluid mixtures trapped as carbonic, aqueous and melts inclusions in petrogenetic and hydrothermal or evaporate ore minerals. A complex fluid assemblage can also be encountered in the upper mantle peridotite nodules and in the high to low grade metamorphic rocks in all crystalline chains of the Carpathians. In this work the fluid and melt inclusions trapped in mineral formed during various geological processes and ages from Carpathian area from author's collection are presented, based mainly upon petrography and microthermometry.

1. Introduction

The main goal of this paper is to present in an atlas form the principal fluid and melt inclusions types and assemblages from mineral growth in various geological conditions and time period from Romania, based upon the personal author's collection. Magmatic-hydrothermal and sedimentary deposits are well represented by many fluid and melt inclusions types, related to the most important ore deposit from the Eastern Carpathians, Metaliferi Mountains, North Apuseni Mountains and South Carpathians in the Banat region. Igneous and hydrothermal processes are related to the Alpine subduction zones and to the magmatism of late Cretaceous and Neogene age, to which the most productive events of the studied areas are associated (Borcoş et al., 1998).

Hydrous silicate melt and aqueous-carbonic fluids evolved in shallow subvolcanic or plutonic rocks generating huge geochemical anomalies as associated ore deposits, including porphyry copper, skarn and epithermal ore deposits and occurrences, many of them being of economic interest from immemorial times (Borcoş and Udubaşa, 2012). Complex silicate melt inclusions were described inside the shallow magmatic – hydrothermal systems from Moldova-Nouă, Oraviţa, Birtin and Vlădeasa granite – pegmatite complex (Pintea, 1991b; Pintea 2012 and

unpublished data). Complex fluid phase immiscibility between hydrous salt melt–silicate and Fe-S-O phases was documented in the Miocene porphyry copper system from Metaliferi Mountains and Ţibles massif in the subvolvanic zone of the Eastern Carpathians (Pintea, 1993c; 1995b; 1996b; 2014a). Silicate glass and multiphase aqueous inclusions were described in the bipyramidal quartz phenocrysts from Roşia Montană, "Laleaua Albă" and Dăneşti-Piatra Roşie dacite or plagioclase from the Bătarci hyalodacitic rocks from Oaş Mountains. Glass "foam-like" silicate melt inclusions were described in the Dej tuff formation (Pintea, 2013).

Epithermal fluids were studied mostly in the gangue minerals (quartz, calcite, anhydrite, gypsum, barite etc) but also in ore minerals such as enargite and wolframite (Bailly, com pers) and sphalerite (Pintea, 1995a). Greisens-like fluids were evolved during the Variscan emplacement of the Highiş massif and they are characterized by a saline rich liquid phase trapped as primary, pseudosecondary and secondary fluid in quartz from veins and druses (Pintea, 2002 unpublished). Generally, the metamorphic fluids trapped in the quartzite fissures systems from the Carpathian crystalline chain, including amphibolite facies rocks, contain also saline rich fluids and CO_2-H_2O± CH_4 ±N_2 fluid assemblages. (Pintea, 1987, unpublished data). Complex fluid inclusion assemblages were described in quartz from the REE-Mo mineralization at Jolotca ore deposit, belonging to Ditrău alkaline massif metallogenetic prospect (Pintea, 1991b; Pintea and Diamond, 1994).

Evaporite minerals from various sedimentary environments, including the recent and ongoing process such as saline crust generation around saline lakes and above salt mining prospects, contain mostly monophase liquid inclusions (Pintea, 2008b). The diagenetic processes up to anchizone facies shown complex fluid and solid fluid inclusion assemblages trapped mostly in salt diapire bodies in Transylvania basin and outer Carpathians. Carbonic fluids (CO_2, CH_4) were found in halite from Badenian salt deposits, while liquid hydrocarbons and methane was found in the "Maramureş diamond" quartz crystals in fissures within the upper Cretaceous carbonaceous flysch from north Romania (Pintea, 1995a).

The methods used by the author during about 25 years of work on fluid and melt inclusions in Romania started with microscopic petrography and continued by low and high temperature microthermometry (Pintea, 1995a; 1998, unpublished), crush-leach techniques coupled with selective ion devices and AAS, CG-MS (Cuna et al., 2001) for gas extraction, SEM-EDS, PIXE, Raman microspectroscopy (Pintea, 1996b) and chlorine isotope measurement (Pintea et al., 1999b). Significant benefits were gained by working, visiting and collaborating with various European laboratory from Lvov, Zurich, Amsterdam, Nancy, Utrecht and Univ. "Babes-Bolyai" - Physics department; INCTDIM and "Raluca Ripan" Chemical and Physical Institutes in Cluj - Napoca. SEM-EDAX analyses were carried out using the facilities of the Geological Institute of Romania and METAV in Bucharest. Based upon these data, it is concluded that there is still much work to be done to characterize the diversity of Fluid and Melt Inclusions assemblages trapped in minerals within the geological history of the Romania's environment.

2. General principles and techniques of the fluid and melt inclusion study.

"*From simple optical techniques to the use of particle accelerators, no stone has been left unturned in the search for analytical perfection"* stated T.J. Shepherd and A.H. Rankin (1998) to argue the exceptional evolution of fluid and melt inclusion research in the last few decades. This started from the 1970s, when the first Chaixmeca microthermometric stage (Poty et al., 1976) became commercially available, followed by USGS (Were et al., 1979), Linkam (Shepherd, 1981; Esposito et al., 2012), Leitz 1350 (e.g. Tissot and Rodriguez, 1999; Amorim et al., 2012) and the Vernadsky stage (Zappuny et al., 1989). Nowadays, these were completed by HDAC (hydrothermal diamond anvil cell - Basset et al., 1993; Schmidt et al., 1998) or internally heated

pressure vessel for "in situ" observations at high T and P conditions (Gondé et al., 2011). Fluid and melt inclusion petrography and microthermometry are *fundamental* and precede any further investigation or sophisticated analytical technique (Weisbrod, 1979; 1984).

2.1. Fluid and melt inclusion petrography. The general philosophy of the fluid and melt inclusion study is based on the natural entrapment of representative samples from the melt and/or fluid, from which their mineral hosts crystallized or precipitated. After being trapped, it is assumed that they recorded the initial PVTX – time as the unique snapshot of the entrapment conditions. Relative to the entrapment time, there are *primary inclusions*, formed during crystal growth and arranged following internal growing zones or random isolated distribution. The *pseudosecondary inclusions,* trapped during the rehealing of internal microfractures, formed during crystal growth, while the *secondary inclusions,* which decorated the microfissure planes, formed after the crystal growth had ceased. Based upon the nature and number of phases present at room temperature conditions, the fluid and melt inclusion are monophase (liquid, gas or glass), biphasic (liquid + gas, glass+ vapour), triphasic (liquid + gas + solid; glass + vapour + solid) and multiphase. The first step in this study starts with the optical microscopy, when fluid and melt inclusions are identified, described and classified, according to the "golden rules" stated by Roedder (1984) as follows (Bodnar, 2003a):

1. The inclusions trapped a single, homogeneous phase;

2. The inclusions represent an isochoric (constant volume) system;

3. after trapping, nothing has been added to, or removed from, the inclusions.

Commonly, there is little chance for a fluid or melt inclusion to *follow strictly* these petrographic rules because of many perturbations, which can occur after their sealing. During petrogenesis, several post entrapment processes must be recognized and, amongst them, decrepitation, necking-down and stretching are the most common (Roedder, 1984). Heterogeneous trapping (two or more phases trapped simultaneously in the same cavity) and post-entrapment re-equilibration processes are also recognised frequently (Sterner et al., 1995; Audétat and Gunther, 1999; Bodnar, 2003b; Steele-McInnis et al., 2011). In the last few years a plenty of papers deal with the *in* or *out* movement of several chemical compounds from the fluid inclusions, such as H_2O, H_2, Cu, Na (Hall and Sterner, 1993; Li et al., 2009). The most important achievement of the petrographic method is the introduction of the concept of fluid and melt inclusion assemblages (**FIAs** - Goldstein and Reynolds, 1994; **MIAs** - Bodnar and Student, 2006) which delineate a homogeneous group of fluid/melt inclusions having almost the same PVTX-t characteristics related to a specific internal feature of the host microtexture such as growth zone or microfissure planes (e.g. Chi et al., 2003). Microtexture internal feature are analysed by the OM/CL and/or SEM/CL techniques which help to elucidate significant relationships between fluid/melt inclusions and their occurrence and distribution in their hosts (e.g., van den Kerkhof and Hein, 2001), although simply optical microscopy is still useful for studying the growing characteristics of these minerals (Pintea, 2010). Size, shape and distribution of fluid inclusions are analysed with various techniques including the spindle stage (Anderson and Bodnar, 1993; Bakker and Diamond , 2006) or 3D imaging by x-ray-fluorescence - micro- tomography (Ménez et al., 2001) and multimodal nonlinear microscopy using coherent anti-Stokes - Raman – scattering (CARS- Burrus et al., 2012). Fluid phase evolution in various fluid system is performed by synthetic fluid/melt

inclusion techniques, for determination of phase equilibria properties, fluid - rock interaction or the physical and chemical data of model fluid systems (e.g. Bodnar and Sterner,1987; Bodnar,1989; Simon et al., 2007).

2.2. Analytical techniques. In fluid and melt inclusion analysis two groups of method are generally used function of complexity of the chemical content and trapping conditions. These are destructive and non-destructive methods which using single or bulk chemical analyses, respectively. Theoretically, the analysis of any given inclusion should be complete (Roedder, 1990): The major solvent H_2O and/or CO_2, the major solute ions Na, K, Ca, Mg, Cl, SO_4 and HCO_3, the minor solute ions Al, Fe, B, Ba, Br, Mn, NH_4, P, F, and Si, metals with high atomic mass such as Au, Ag, U, also pH and Eh, other species of elements with variable valences Fe, Mn, S (SO_4^{2-}), H_2S, HS^-, and C (CO_2, CH_4, CO, C_xH_y, H_2CO_3, HCO_3^-), the organic compound when present (acetate, oxalate, amino acids, etc), others gaseous species (H_2, He, N_2, O_2, Ar), the isotopic ratio of the major elements (H, C, N, O, S and also Sr, Ar, He). It must remind that these components participate in variable mixtures from an inclusion to another function of their origin, but the quantity of material available for chemical analysis is about 10^{-9} to 10^{-13}g in each of them (Shepherd and Rankin, 1998). Therefore, it is not an easy operation to do this in normal chemistry or physical laboratory facilities. For this reason, the majority of preparation techniques and even analytical methodologies were adapted for such low available sample-quantity for analysis.

2.2.1. Non-destructive analyses. The most important analytical tool in this group is represented by microthermometry from the lowest temperature i.e. – 190°C to + 700°C for fluid inclusions and up to 1500°C for silicate melt inclusions in several commercially microthermometric stages mentioned above. These elaborated techniques allow us to determine the main PTX data of the fluid/melt phases included. They are completed by micro-spectroscopic methods such as micro-Raman (e.g. Dubessy et al., 1989; Frezzotti et al., 2012), FTIR and UV fluorescence, PIXE (proton induced X-ray emission), PIGE (proton induced gamma ray emission) or more sophisticated synchrotron X-ray fluorescence microanalysis (SXFMA). These methods are capable of analysing the elemental and molecular species, polyatomic gaseous species and polynuclear ones, in solution for single unopened inclusion (Roedder, 1990; Shepherd and Rankin, 1998). Other methods of this category are: Transmission electron microscopy (TEM) used for nanoscale structures and fluid inclusion shape, Confocal Laser Scanning Microscopy and Atomic- Force Microscopy (AFM) which are used for 3D images of fluid inclusion cavities and bubbles (Chi, et al., 2003; Bodnar, 2003a). Estimation of the viscosity and water content of silicate melt using homogenization measurements were delineated by Thomas (1994) in silicate melt inclusions from granites and rhyolites. PVTX evolution of crystalline melt inclusions during heating and cooling were determined by Student and Bodnar (1996), using available phase equilibrium data for the hydrous haplogranite system (albite-ortoclaze-quartz-water).

2.2.2. Destructive methods. They were the first techniques used in fluid inclusion study (e.g. Roedder et al., 1963; Petrichenko, 1973) and consist of extract the fluid inclusion content, opening the microcavities during mechanical crushing, or decrepitation by heating in vacuum or even opened in atmospheric conditions in the case of evaporites (halite). There are techniques suitable only for volatile analyses, such as GC (gas-chromatography)-MS (mass spectrometry), Gas Chromatography (GC) or simply gas (G)

- mass (M) - spectrometry (S) especially for high hydrocarbons. Modern "crush-leach" analyses based upon the protocols designed by Roedder et al., (1963), Weisbrod and Poty (1975), Botrell et al., (1988); Banks and Yardley (1992), Halbauer (1997) are used for solute ion analysis in conjunction with atomic absorption spectrometry (AAS), Ion Chromatography (IC), ICP-OES, ICP-MS, selective ionic electrodes (SIE) and capillary electrophoresis (CE). By these combined methodologies, a wide variety of chemical compounds can be analysed, including Na, K, Li, Rb, Ca, Mg, Fe, Mn, Zn, Cu, Pb, (Al), Ba, Sr, Cl, Br, F, B and SO_4^{2-}, and also REE (Shepherd and Rankin, 1998). All the techniques mentioned above are bulk analyses, thus they involve the opening of several hundreds or thousands of inclusions mixed together in the leachate solutions and the results characterizes several generation of fluid inclusions related to different processes. This approximation was avoided by the new generation of high- technology methods based upon laser technique which are able to analyse the content of one single inclusions and the advantage is now described in many papers (e.g. Heinrich et al., 2003; Mason et al., 2008; Pettke et al., 2012). There are three method based on laser ablation technique (Shepherd and Rankin, 1998): laser-ablation-inductively-coupled plasma mass spectrometry (LA-ICP-MS), laser ablation coupled plasma atomic emission spectroscopy (LA-ICP-AES), and laser ablation emission spectroscopy (LA-AES). This are in situ sampling analysis of major, trace and isotopic analyses by opening the cavity with a pulsed laser beam (Heinrich et al., 2003). The methods involving the single fluid or melt inclusions analysis are now calibrated (e.g. Pettke, 2008; Jackson, 2008; Pettke et al., 2012) and used routinely in many fluid inclusion laboratories worldwide. SEM/EDS techniques involving mechanical opening, coating and analysed in high vacuum chambers are used to identify daughter solid mineral in transparent and opaque minerals, as well (Hallbauer, 1983; Nedelcu et al., 2003), the composition of the evaporate mound released by thermic decrepitation (Kontak, 2004) and the crio - technique used mainly for the evaporate minerals (halite) which work in two variants; Crio-SEM/EDS (Ayora and Fontarnau, 1990) and ESEM/EDS (Timofeeff et al., 2000). Electron probe microanalyzer (EPMA) is used routinely to analyse the chemical composition of silicate melt inclusions after these were re-homogenized in the microthermometric stage, in muffle furnace or high pressure vessels. These results are used in petrochemistry and petrologic investigations in all petrogenetic minerals from ultramafites to felsic rocks (e.g. Clocchiatti, 1975; Sobolev, 1996; Danyushevsky et al., 2002; Thomas, 2003; Blundy et al., 2006; Naumov et al., 2013 among others). Quantitative microanalysis of entire silicate and sulphide melt inclusion by excimer Laser-ablation inductively-coupled-plasma-mass spectrometry (LA-ICP-MS) has been applied by Halter et al., 2004 in a suite volcanic rocks and subvolcanic Farallon Negro Volcanic Complex from Argentina. The authors used silicate melt from pyroxene, amphibole, plagioclase and quartz together with sulphide melt trapped in amphibole to evaluate the accuracy of this technique. The quantification of the inclusion composition is performed by using an internal standard which corrects for the crystallization of the host mineral onto the inclusion wall upon cooling and consequently it is not necessary to pre-homogenize the melt inclusions content before analyses (Halter et al., 2005). Secondary ion mass spectrometry (SIMS) is frequently used for isotopic and halogen content of silicate melt inclusions (e.g. Hauri et al., 2002, Thomas, 2003). Petrography and microthermometry of silicate melt inclusions from eruptive, subvolcanic and plutonic rocks were treated on many published articles

and book chapters as following: Sorby, 1858; Clochiatti, 1975, Takenouchi and Imai, 1975; Roedder, 1979; Li, 1994; Lowenstern,1995; Frezzotti, 2001 Bodnar and Student 2006, and related endogene process such as fluid-melt or melt-melt immiscibility (Roedder, 1992; Frezzotti, 1992; Naumov et al., 1996; Davidson, 2004; Heinrich, 2007; Webster and Mandeville, 2007; Kamenetsky, 2006; Kamenetsky and Kamenetsky, 2010; and many others)

3. Data interpretation and applications.

After a complete chemical analysis, the data are interpreted based upon the evolutionary topology of the model - systems for which a large range of experimental data are known, i.e. H_2O, CO_2, (Dubessy, 1994; Diamond, 2003ab); H_2O-NaCl (Bodnar et al., 1985; Bodnar and Vityk, 1994; Bodnar, 2003c; Driesner and Heinrich, 2007); H_2O-CO_2 (e.g. Sterner and Bodnar, 1991; Diamond, 1994); H_2O-CO_2-NaCl (Schmidt and Bodnar, 2000); H_2O-NaCl-KCl (Chou, 1987; Sterner et al.,1988); CO_2-CH_4-N_2 (Van den Kerkhof, 1988). The chemical composition of the silicate melt inclusions are projected in the common petrologic diagrams and also using fluid-melt equilibria in specific diagrams of the vapour saturated silicate melt-CO_2-H_2O or vapour saturated silicate melt-NaCl-KCl-H_2O systems (Student and Bodnar, 1996; Steele - MacInnis et al., 2011). Oil-bearing fluid inclusions in carbonate cement, "Marmarosh diamond" quartz crystals as single inclusions were analysed by microthermometry (e.g. Godstein and Reynolds, 1994; Pintea, 1995; Jones and Macleod, 2000) to determine the minimum trapping temperature and the gas composition derived by confocal microscopy and P-V-T- simulation. Thermal decrepitations, GC-MS, µFT-IR, µRaman spectroscopy were used with microthermometry to calibrate high precision curves from synthetic hydrocarbon inclusions in halogenide and sulphate crystals at low temperatures (Pironon, 1990). Fluid phase evolution at elevated P-T conditions in the water - oil mixtures were used to study the interaction of natural petroleum and hydrothermal fluids in the range of 180 – 500°C and 1-150MPa (e.g. Balitsky et al., 2009). A combination between time-of - flight-mass spectrometry - SIMS and GC-MS analyses were applied on single oil-bearing fluid inclusions from fluorite veins (Siljeström, 2011).

Nowadays, Fluid and Melt inclusions are not simple geothermometers or geobarometers anymore but they became (mainly because of their abundance in the majority of terrestrial and extraterrestrial minerals crystallized from melt and precipitated from solution and also because of the tremendous technical analytical advance *from* (of) the last decades), the most valuable source of information about the initial geochemical media of the rocks and mineral formation. In fact, they are part of the rocks and minerals and must be studied together with their hosts in any magmatic, metamorphic and sedimentary environment. From the beginning (e.g. Sorby, 1858, Zirkel, 1893; Vogelsang, 1869; Deicha, 1955; Bakker, 1999; Zhili et al., 2008) following the evolution in the last 150 years (Touret, 1984), their practical applications could be summarized, for the purpose of the atlas topic, *based upon the main authors and milestone works*, as follows: **magmatic petrology** (i.e. Roedder, 1979; Roedder, 1992; Frezzotti, 1992, 2001; Touret and Frezzotti, 1993; Yang and Bodnar, 1994; Student and Bodnar, 1996; Sobolev, 1996; Naumov et al., 1996, 2013; Larocque et al., 2000; Kamenetsky et al., 2002; Danyushevsky et al., 2002; Thomas, 2003; Bodnar, Student,

2006; Kamenetsky, 2006; Mason et al., 2008; Hansteen and Klügel, 2008; Kamenetsky and Kamenetsky, 2010; Steele-Maccinnis et al., 2011); **volcanism (**e.g. Clocchiatti, 1975, Takenouchi and Imai, 1975; Lowenstern, 1995; 2003; Webster and Mandenville, 2007; Anderson, 1991; Pintea, 2013; Blundy et al., 2006); **porphyry-copper types and pegmatites** (e.g. Roedder, 1971; Nash, 1976; Bodnar, 1995; Thomas et al., 2000; Campos et al., 2002; Student and Bodnar, 2004; Williams-Jones and Heinrich, 2005; Heinrich et al., 2005; Heinrich, 2005, 2006, 2007; Halter et al., 2005; Bodnar, 2010; Audetat and Simon, 2012; Pintea, 2014a); **hydrothermal ore deposits** (e.g. Bodnar et al., 1985a; Roedder and Bodnar, 1997; Bailly et al., 1998; Brown, 1998; Wilkinson, 2001; Kesler, 2005; Heinrich, 2005; Kouzmanov et al., 2010; Kouzmanov and Pokrovski, 2012; Bodnar et al., 2014); **fluid and multiphase solid inclusions in metamorphic rocks** (e.g. Touret, 1977, 2001; Frezzotti and Ferrando, 2007; Cesare et al., 2009; Van den Kerkhof et al., 2014); **sedimentary and oil-bearing fluids** (e.g. Petrichenko, 1973; Roedder, 1984a; Shepherd et al., 1985; Robert and Spencer, 1995; Lowenstein et al., 1998; Pironon, 1990; Jones and Macleod, 2000; Dubessy, 2004; Balitsky et al., 2009; Kovalevich, Vovnyuk, 2010); **upper mantle and subduction zone fluids** (e.g. Roedder, 1965; Pintea and Mârza, 1989; Varela, 1997; Chalot-Prat and Arnold, 1999; Scambeluri and Philippot, 2001; Harlov, 2014); **fluids in planetary systems** (Bodnar, 2005; Madden, 2005); **fluid and melt inclusions books, short courses, computer programs and workshop proceedings** (e.g. Pomârleanu, 1971, 1975, 2007; Pomârleanu and Neagu, 2003; Ermakov and Dolgov, 1979; Hollister and Crawford, 1981; Roedder, 1972; 1984; Shepherd et al., 1985; De Vivo and Frezzotti, 1994; Bakker, 1999; Samson et al., 2003; Bakker, 2003; Bakker and Brown, 2003; Webster, 2006; Driesner and Heinrich, 2007; Van den Kerkhof and Sosa, 2012; Bodnar et al., 2013; Yardley and Bodnar, 2014; Hurai et al., 2015).

Important web links: The "world of fluid inclusions" at www.geology.wisc.edu; Bodnar's Fluid's Research Lab Web Site-; Ron Bakker's Home Page - University of Leoben; Linkam Scientific Web; Site IMA Home Page and link to Working Group on Inclusions in Minerals; Geo-Petro-ETH Zurich- http://www.geopetro.ethz.ch; Fluid Inclusion Technologies, Inc-http://fittulsa.com; http://rruff.geo.arizona.edu.

Acknowledgements. The published work on "*Decrepitometry and their application to ore mineral prospection*" by V. Pomârleanu (1975) was my first encounter with the "*Fluid and melt inclusions*" geological research field, and I am indebted to V. Pomârleanu, L. Ghergari, A. Moţiu. I. Imreh and I. Mârza for their encouragements on the Fluid Inclusion Research. I express my gratitude to G. Udubaşa and E. Constantinescu, who supported me to study consistently and accurate fluid and melt inclusions in a wide variety of fluid and melt inclusions in minerals, formed in various conditions during the geologically history of the Romania's territory. I am also grateful to I. Seghedi, S. Boştinescu, V. Ghiurcă, I. Mârza, M. Borcoş, L. Nedelcu, M. Tatu, G. Săbău, T. Berza and L. Robu for their courtesy of handing me samples of their own. I am indebted to S. Cuna, C. Cuna and N. Palibroda from the "Institute of Isotopic and Molecular Technology" (INCDTIM) of Cluj Napoca which allowed me to use their analytical facilities and experience in gas analyses from minerals. I thank V. Cosma, G. Morar and E. Hopârtean from "Raluca Ripan" Institute of Chemistry in Cluj-Napoca for their help on the chemical characterisation of fluid inclusions by "crush-leach" technique.

Figures

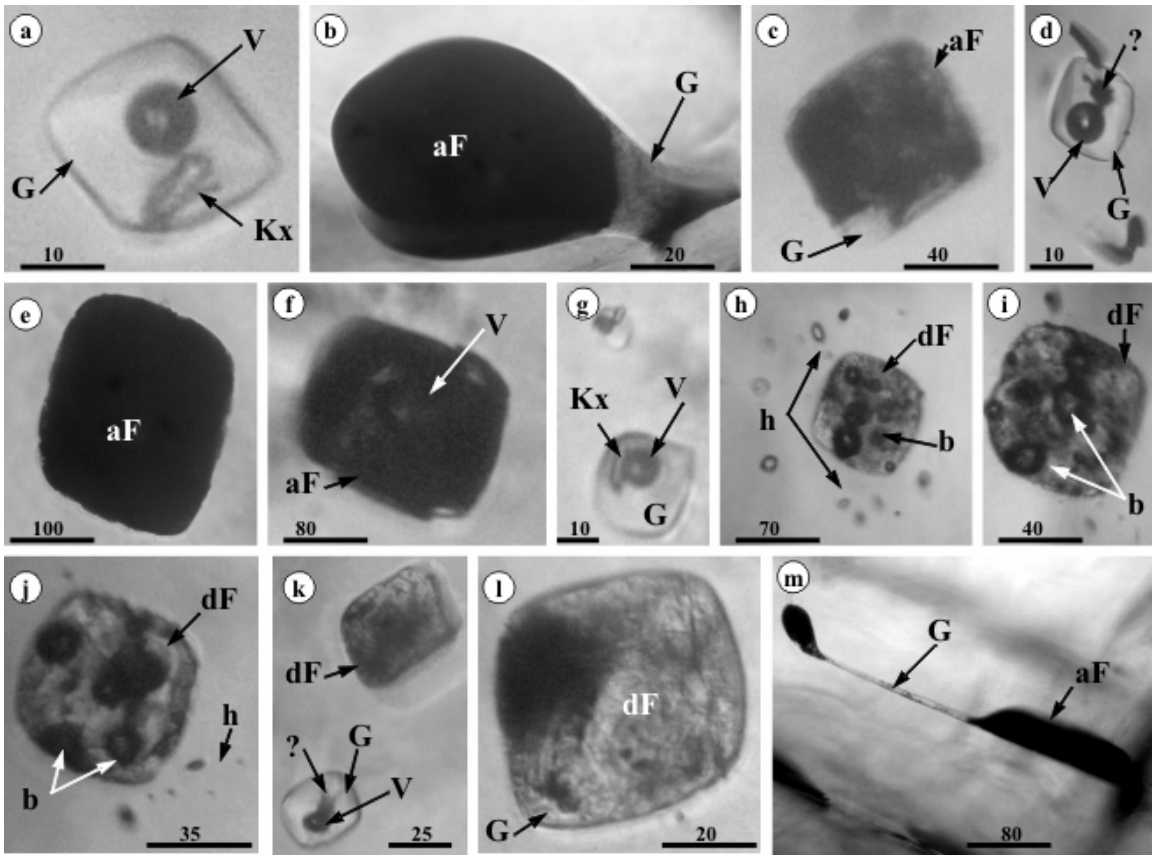

Fig. 1. Silicate melt inclusions types in bipyramidal quartz phenocrysts extracted from the bentonites from Valea Chioarului (Maramureş County). **a, d, g, k**, - three-phase inclusions with glass (G) + vapor (V) + solids (Kx- transparent quartz or feldspar microcrystal, ?-unidentified); **b**- altered "foam-like" hourglass inclusion (aF), G-glass; **c, e, f, m** - altered glass "foam - like" inclusions; **h, i, j, k, l**- decrepitated "foam-like" glass inclusions (dF). Total homogenization temperature recorded in six silicate glass inclusions ranged between 845°-1045°C, and the solid microcrystals melted between 550°-990°C (Pintea, unpubl. data). Scale bar in µm.

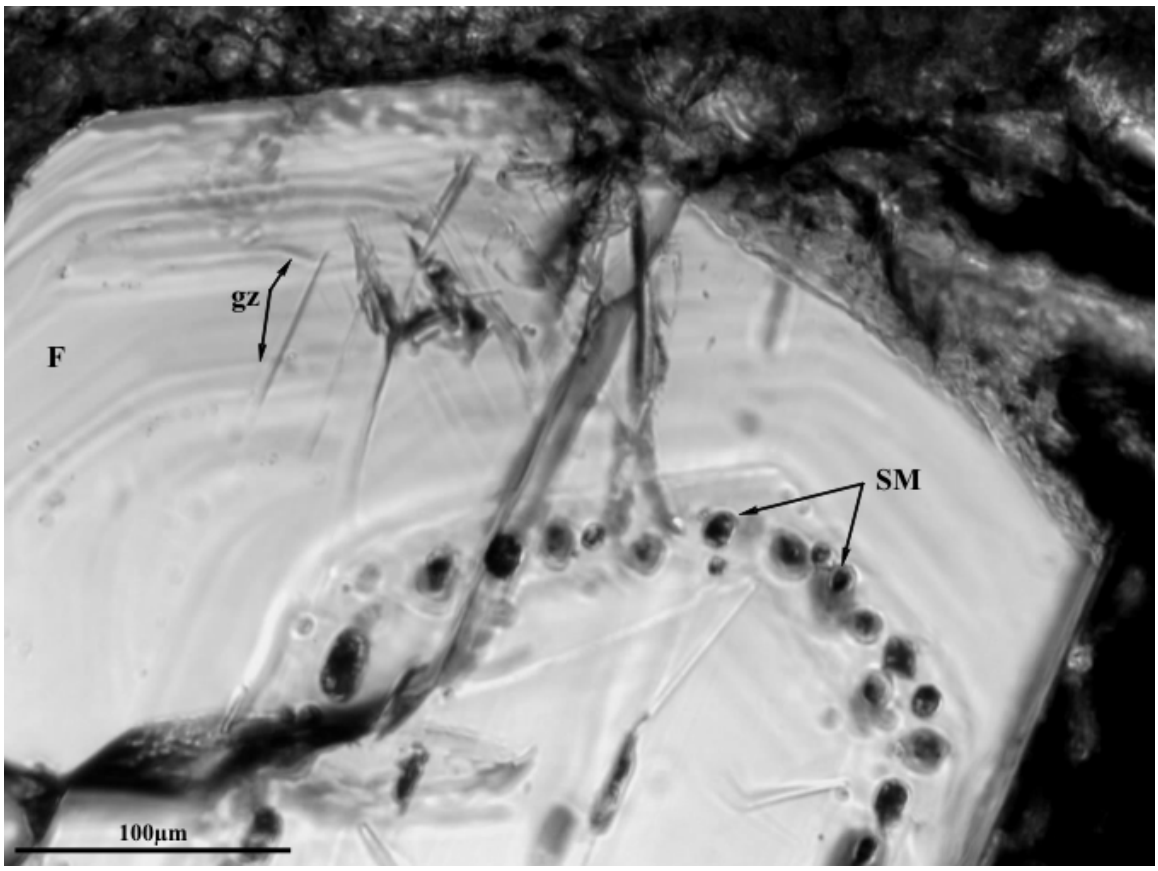

Fig. 2. Overgrowth zonation in plagioclase from Bătarci hyalodacite (e.g. Jude, 1977) decorated with silicate melt inclusions, F-feldspar, gz- oscillatory growth zones, SM- silicate melt inclusions (Bătarci Valley, Oaş Mountains).

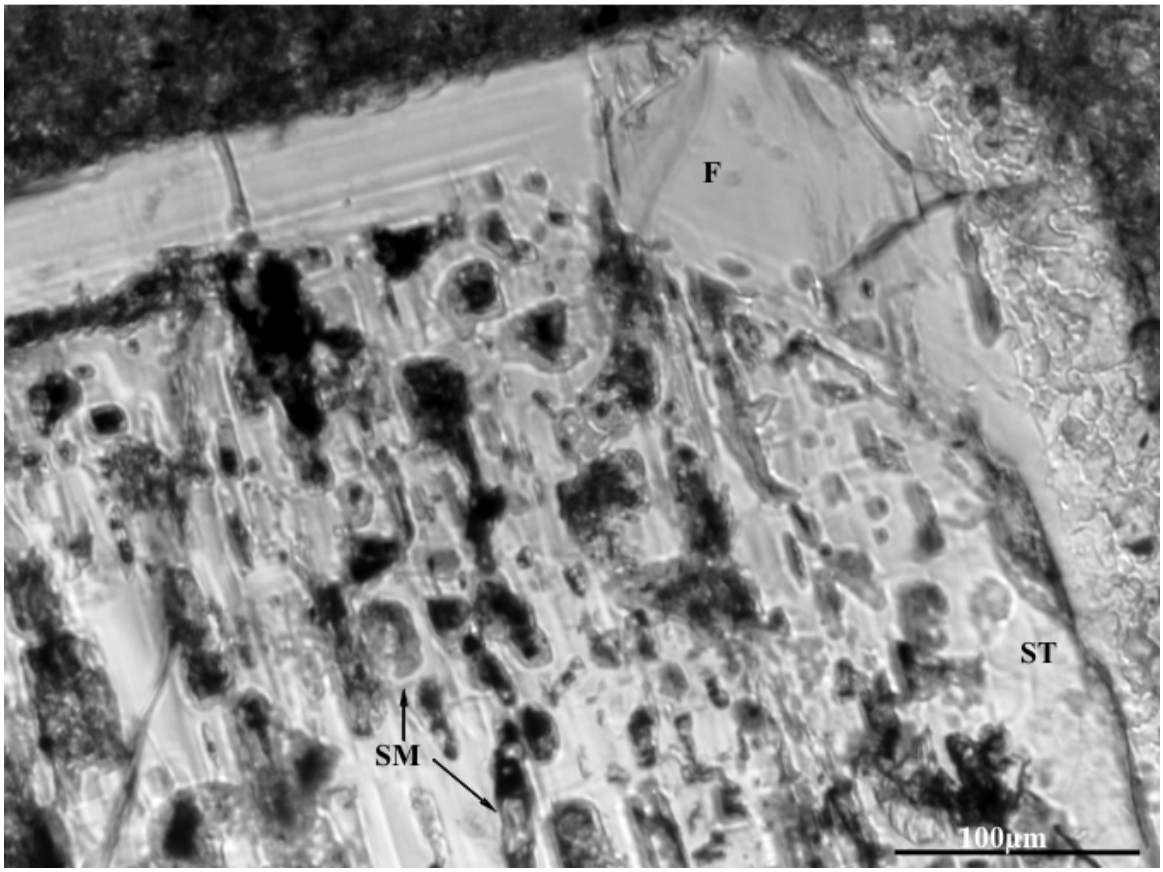

Fig. 3. Internal sieve microtexture (ST) containing multiple silicate melt inclusions (SM) formed in a dissolved feldspar microcrystal during a subsequent magmatic melt influx, overgrowth with new feldspar (F) zone equilibrated with the Bătarci hyalodacite groundmass(Bătarci Valley, Oaş Mountains). Crystal host interference imaging, electron microprobe analysis, petrography and microthermometry of the silicate melt inclusions are the favorites in study of sieve-texture significance in magmatic-volcanic processes (e.g. Stewart and Pearce, 2004; Pintea et al., 2003; Blundy et al., 2006).

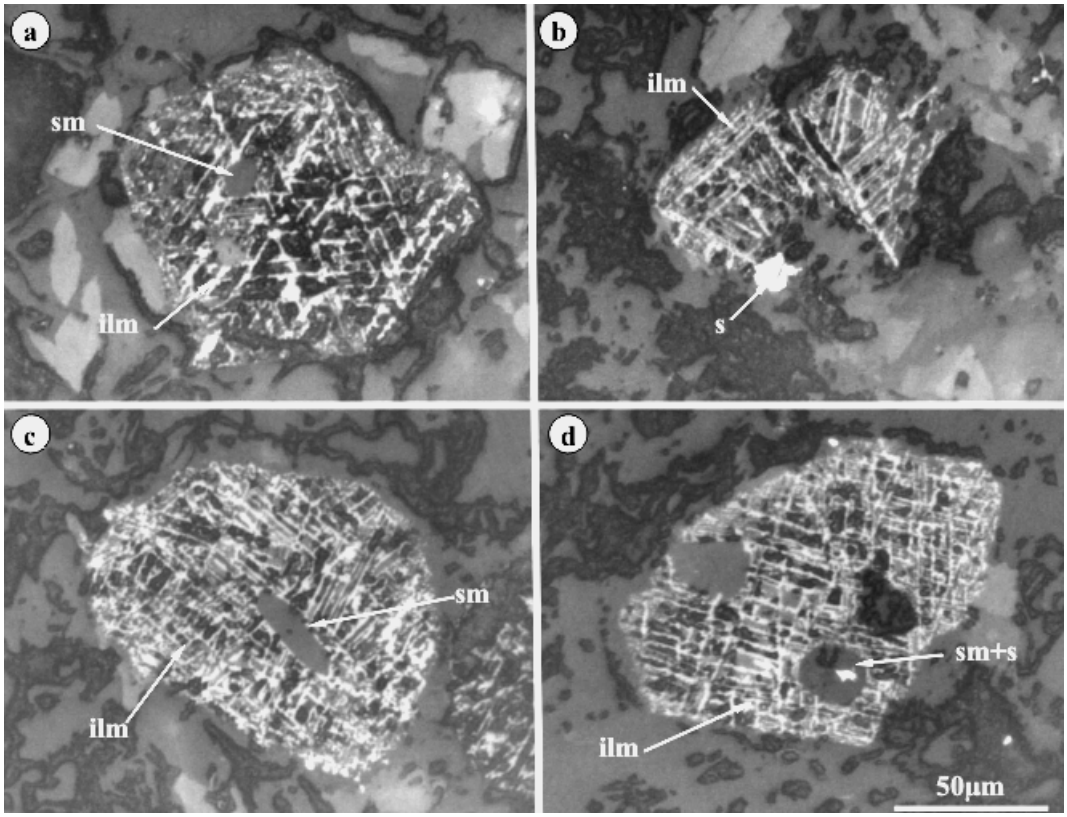

Fig. 4. Trellis type ilmenite lamellae exsolution microtexture features in the Bătarci hyalodacite containing silicate melt inclusions. ilm-ilmenite, sm- silicate melt, s- sulfide. (Bătarci Valley, Oaş Mountains) (e.g. sphenitization described by Udubaşa, 1984).

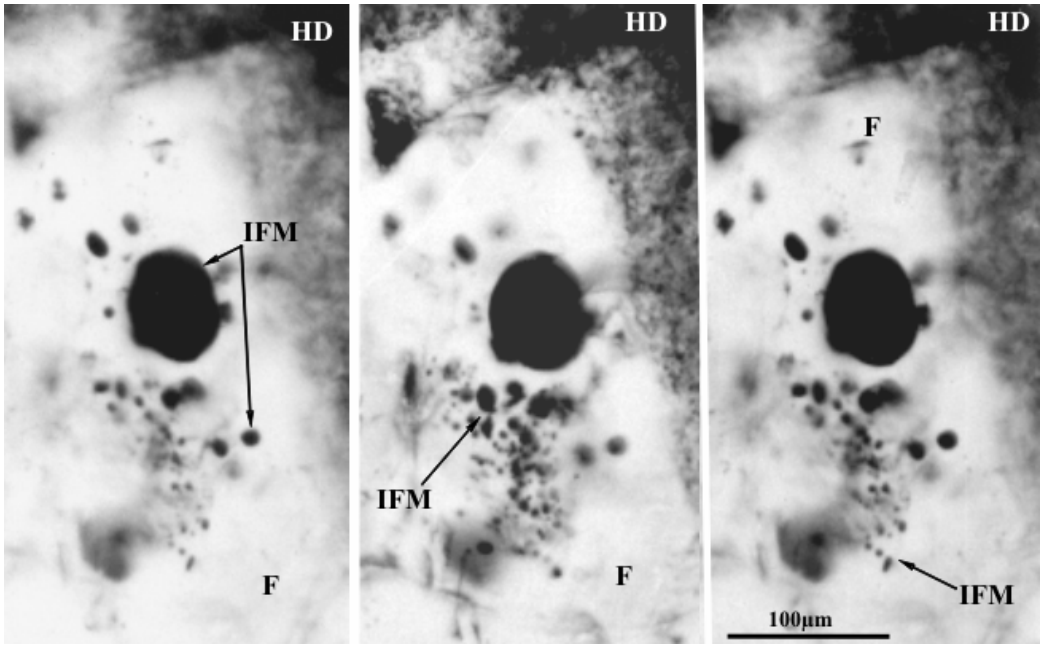

Fig. 5. Immiscible Fe-S-O melt assemblage trapped in plagioclase phenocrysts from Batarci hyalodacite. IFM- immiscible opaque globules, F- plagioclase, HD- hyalodacite (Larocque et al., 2000; Pintea, 2002).

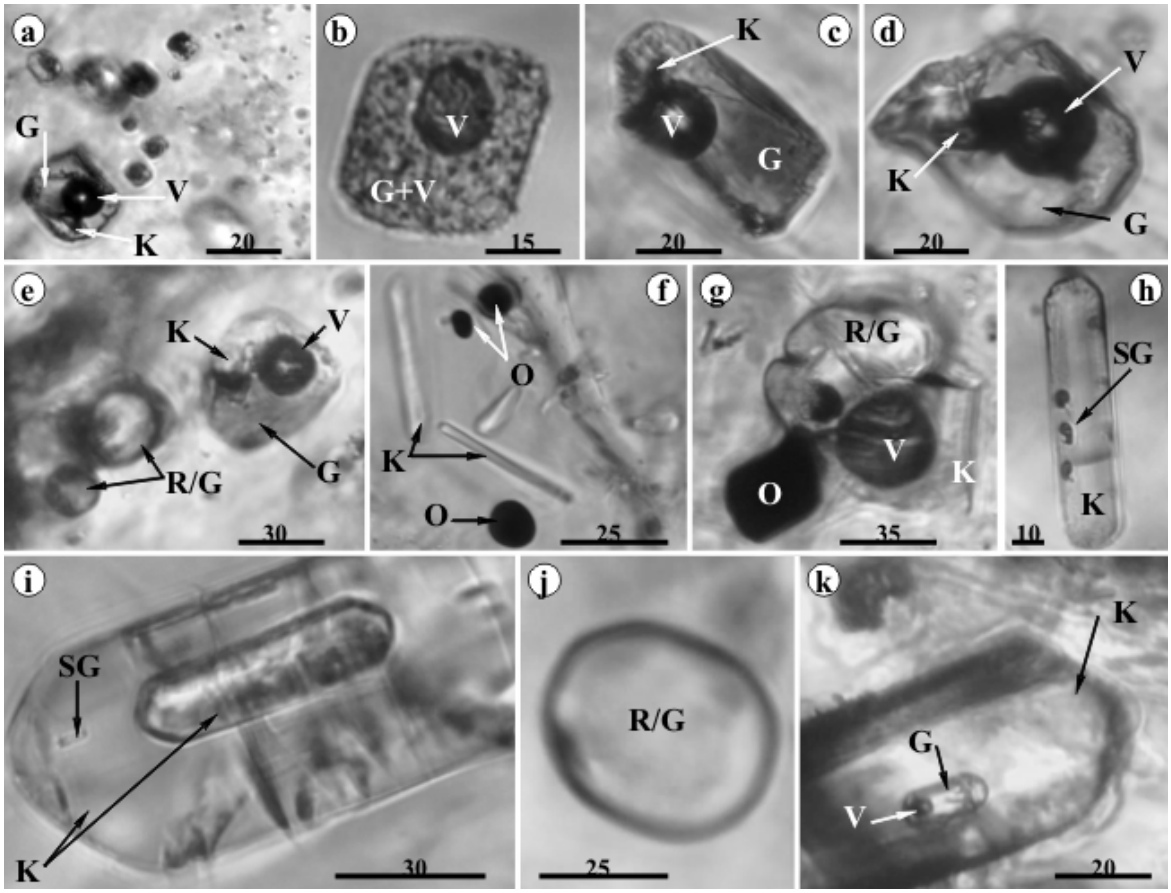

Fig. 6. Silicate melt and solid microinclusions in the Batarci hyalodacite. **a**, **c**, **d**, **e**, **g** - silicate melt inclusions; **b**- silicate glass inclusion; **e**, **h**, **i**, **j**, **k**- solid microinclusion, probably several generation of restitic apatite microcrystal sometimes with early silicate melt inclusion pictured in **k**; K- apatite, zircon or plagioclase solid microcrystal (undefined), R- restitic microcrystal or simply glass inclusions (**e**, **g**, **j**); O- opaque (Fe-S-O immiscible melt); G-glass, V-vapor, SG- silicate glass inclusion. (Bătarci Valley, Oaş Mountains). Scale bar in µm.

Fig. 7. Fluid and melt inclusions in quartz xenoliths, phenocrysts and fragments from Săpânţa caldera (Pintea, 2014b). **a**, **b**, **c**, **d**, **e**, **f**, **g**, **n**, **t**- silicate melt inclusions; **d**, **g**, **h, i, j**, **k**, **m**, **o**, **p**, **q**, **r**, **s**, **u**, **v**, **w** – vapor rich inclusions, **l**- quenched from 1000°C in the high temperature microthermometric stage, three grain sublimated from the vapor-rich phase; G-glass, Gm- mafic silicate glass, Ks- silicate solid phase, Kx- salt mineral phase (halite, and others), V-vapor, H-halite, O-opaque, f- fissure, Kxy-undetermined, Q- presumably β-quartz. Scale bar in µm.

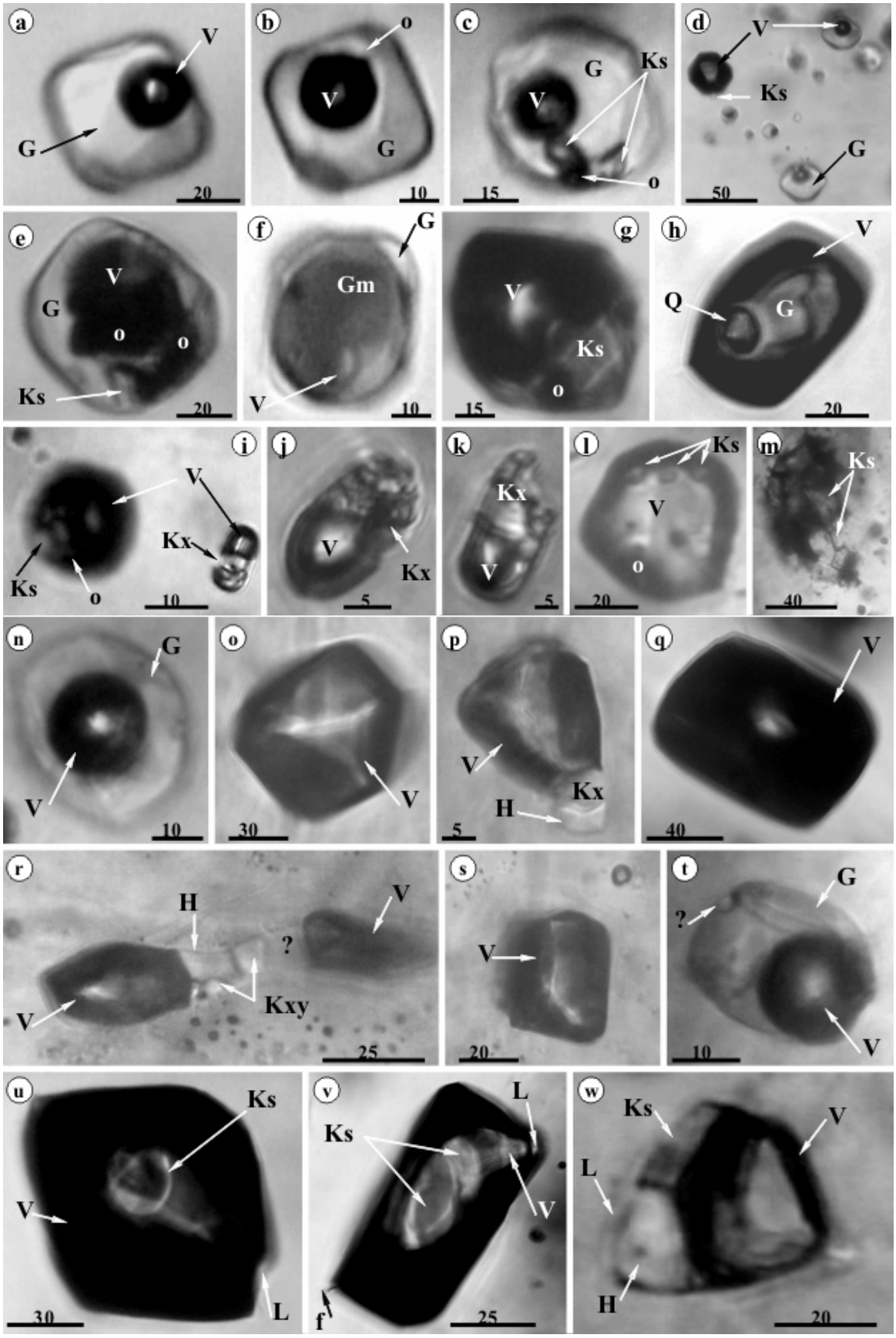
a
V
G
20
b
o
V
G
10
c
G
Ks
V
o
15
d
V
Ks
G
50
e
V
G
o
o
Ks
20
f
G
Gm
V
10
g
V
Ks
o
15
h
V
Q
G
20
i
V
Kx
Ks
o
10
j
V
Kx
5
k
Kx
V
5
l
Ks
V
o
20
m
Ks
40
n
G
V
10
o
V
30
p
V
Kx
H
5
q
V
40
r
H
V
?
Kxy
V
25
s
V
20
t
G
?
V
10
u
Ks
V
L
30
v
L
Ks
V
f
25
w
Ks
V
L
H
20

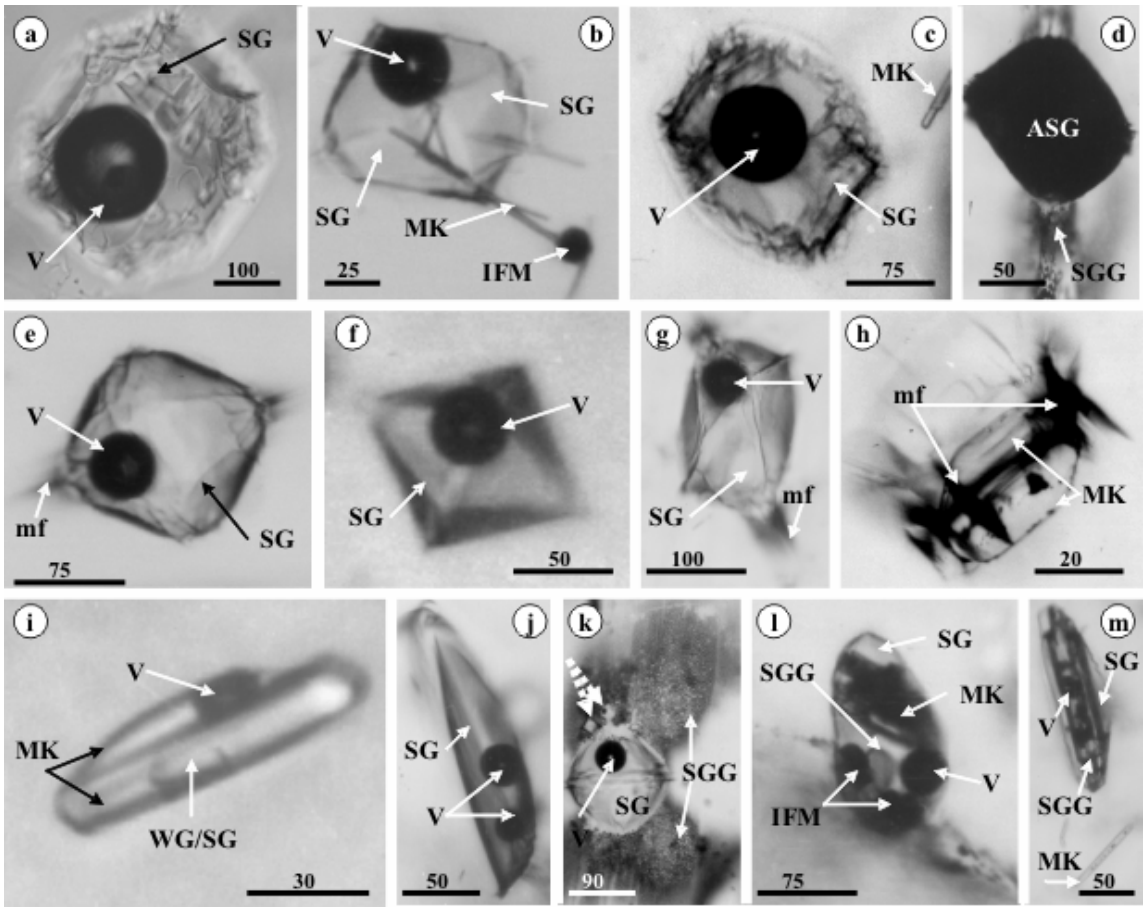

Fig. 8. Silicate melts inclusions in quartz and feldspar phenoclasts from "Laleaua Alba" dacite quarry from Baia Mare region. Macroporphyric dacite nucleus with quartz, biotite, amphiboles and pyroxene surrounded by quartz andesite with pyroxene, amphibole and biotite; gabbros xenoliths are quite frequent too (Kovacs, 2002). The majority of primary melt inclusion were thermally decrepitated and late-hydrothermally altered by the volatile rich phases associated with the mafic magma pulse and magma mixing processes. Decrepitated and remelting features show characteristic halos around primary melt inclusions and melted and deformed edges in a plastic state during the reheating processes (Pintea, 1986). Generally, they cannot be homogenized in the heating stage at 1 bar pressure only up to 950°C - 1100°C (e.g. 986°C, n = 3; biphasic silicate melt inclusions in zircon embedded in plagioclase homogenized at 923°C - Pintea, 2006. The primary silicate melt changed the initial vapor/melt ratio and so the homogenization values are characteristic for the re-equilibration conditions. SG- silicate glass, MK-microcrystal, V-vapor, SGG- secondary silicate glass globule, mf- microfissures; ASG- altered glass inclusion, IFM- (Fe-S-O) melt, k – the dashed arrow indicates the separation of new silicate glass inclusions from the principal inclusions during the natural reheating process; Comprehensive geochemistry and geothermometry of the silicate melt inclusions from the Laleaua Alba dacite was recently published by Naumov et al., 2014. Scale bar in µm.

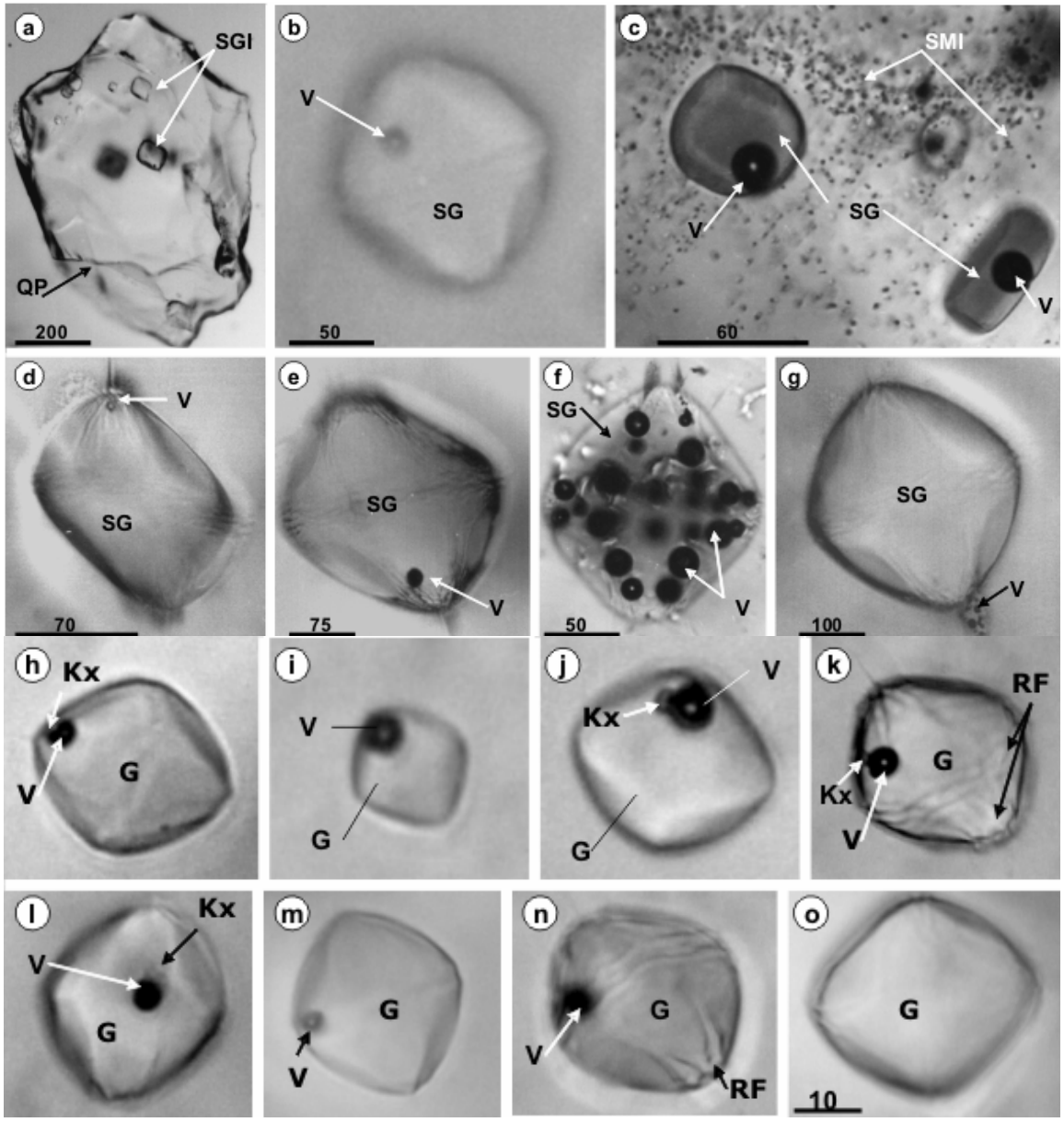

Fig. 9. Silicate glass inclusions in quartz and feldspar phenoclasts from Dăneşti-Piatra Roşie dacite. Dacite lava dome produced by mingling/mixing between mafic /ultramafic melt and rhyolitic magma matrix located near Baia Sprie and Cavnic areas (Kovacs, 2002). They also contain ultrabasic xenoliths with Mg-hastingsite amphibole, probably the primary metallic source of the epithermal ore deposit in the region as globular sulfide/oxide as immiscible melt of (Fe-S-O) type. **a** - Quartz phenoclast(QP) containing silicate glass inclusions (SGI), c- silicate melt inclusions (SMI) in plagioclase, SG- silicate glass; **b**, **d**, **e**, **f**, **g**, **h**, **i**, **j**, **k**, **l**, **m**, **n**, **o**- silicate glass inclusions (SG) containing glass (G), vapor (V), Kx- undetermined solid phase, RF- natural remelting feature; Silicate melt inclusions(G +V ± solid) homogenized between 700-1000°C (n= 172) in quartz (e.g. one reliability test for one inclusion ranged between 730-780°C, n= 15) and from 800-1060°C (n= 22), in plagioclase; n - number of measurements (Pintea, 2006). Geochemistry and petrologic significances of the silicate melt inclusions from Dăneşti dacite were published by Grancea et al., 2003. Scale bar in µm

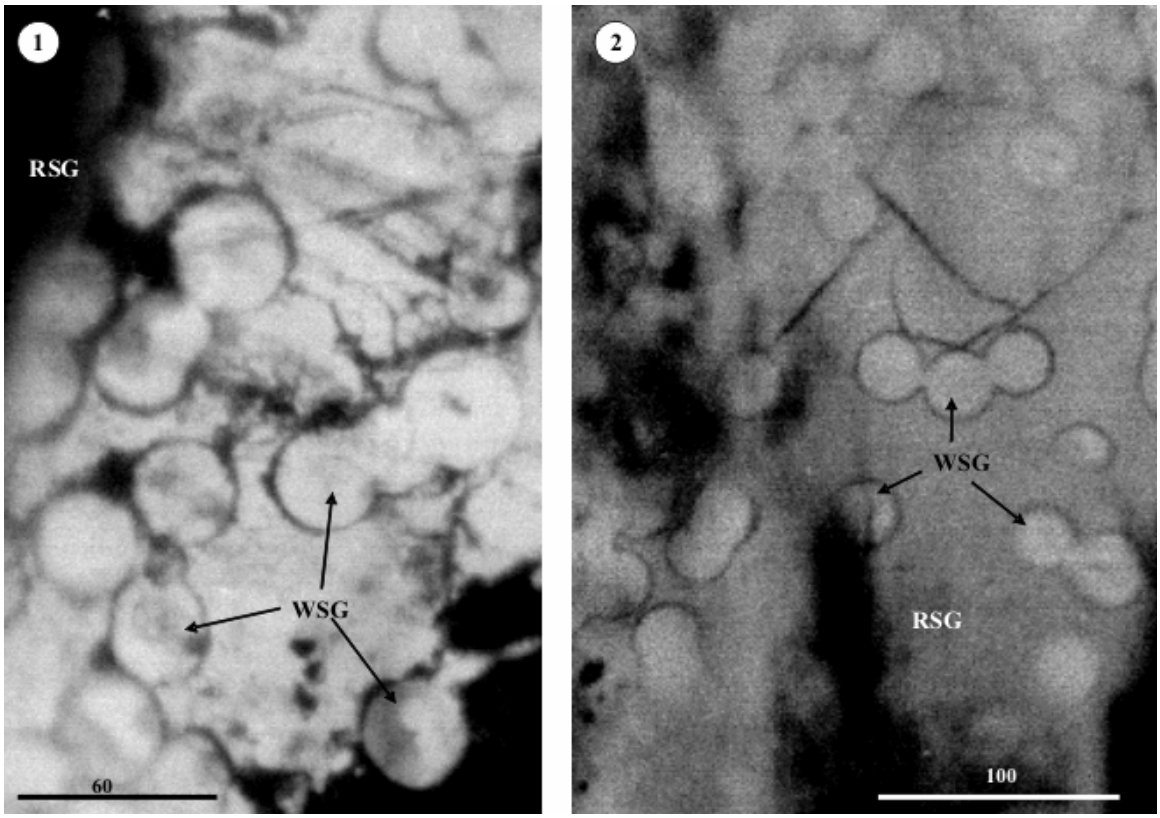

Fig. 10. Thinly white silicate glass globules (WSG) in reddish colored silicate glass matrix (RSG) in the dacite groundmass from Piatra Roşie-Dăneşti dacitic extrusive rocks. (Pintea, 2010). Scale bar in µm.

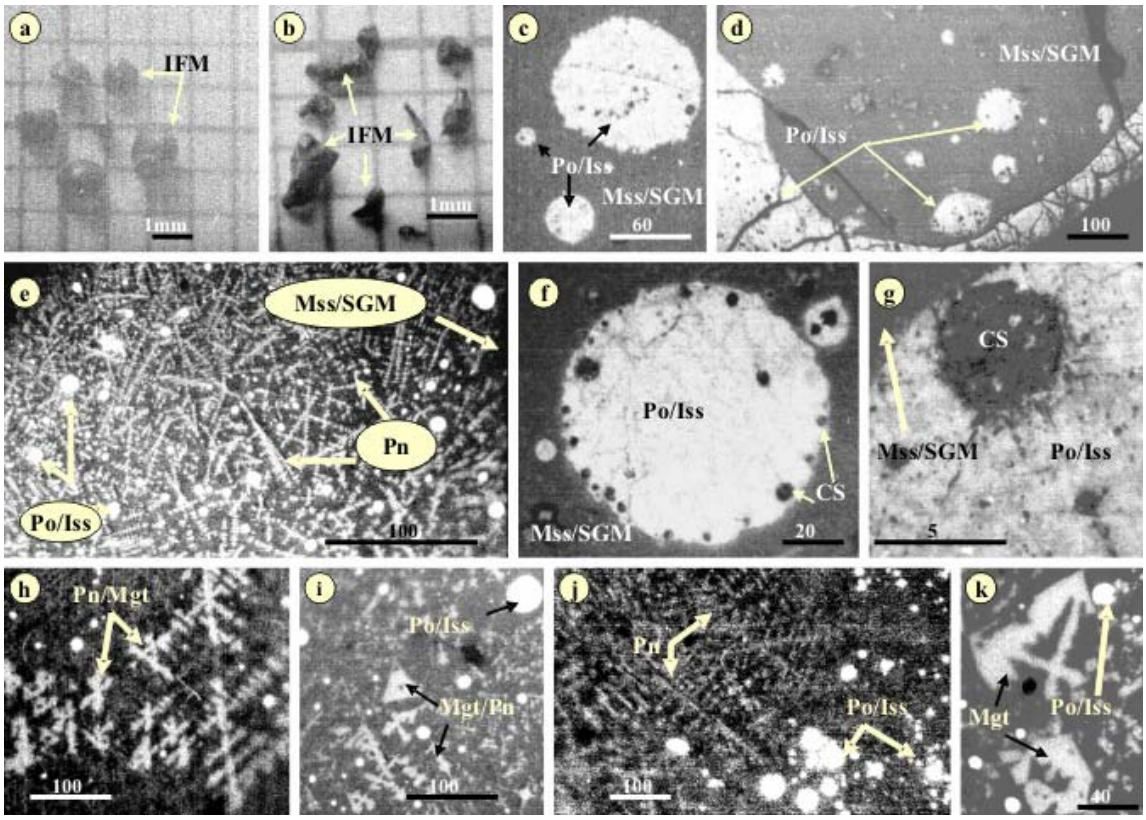

Fig. 11. Globular sulfide melt from Dăneşti - Piatra Roşie dacite (Maramureş county).**a**-perfect spherical globules collected from a dry outcrop of the dacitic lava dome near Dăneşti village; **b**- elongate shaped (Pelees's tears-like); **e**, **h**, **i**, **j**, **k**- microphotographs in reflected light suggesting the presence of monosulfide solid solution (Mss) an/or intermediate solid solution (Iss), pyrrhotite (po) magnetite (mgt) and pentlandite-like dendrites (pn), and another immiscible compound as black globules (CS) inside the Mss or Iss, all embedded probably in mafic glass matrix (SGM); their identification is based upon textural features in reflected light microscopy and comparative literature data (e.g. Desborough et al., 1968; Kelly and Vaugham, 1983; Stone and Fleet, 1991; Guo et al., 1999; Craig, 2001; Török et al., 2003; Etschmann et al., 2004); **c**, **d**, **f**, **g**- under high magnification in reflected light the globular phases embedded in presumable pyrrotite, Mss or Iss, a second immiscible Cu-Fe sulfide phase formed mainly at the border of the host globules, based upon optical reflectivity and comparative references data (e.g. Ranjamani and Naldrett, 1978; Ballhaus et al., 2001, Baker et al., 2001). This interpretation is only qualitative there are no analytical data yet, but the trace distribution of Sc, Ni, Co (which presumably are relate the immiscible silicate melt) was used to separate the subvolcanic bodies in the region, as suggested many years ago by Rădulescu and Dimitrescu(1982). Scale bar in µm.

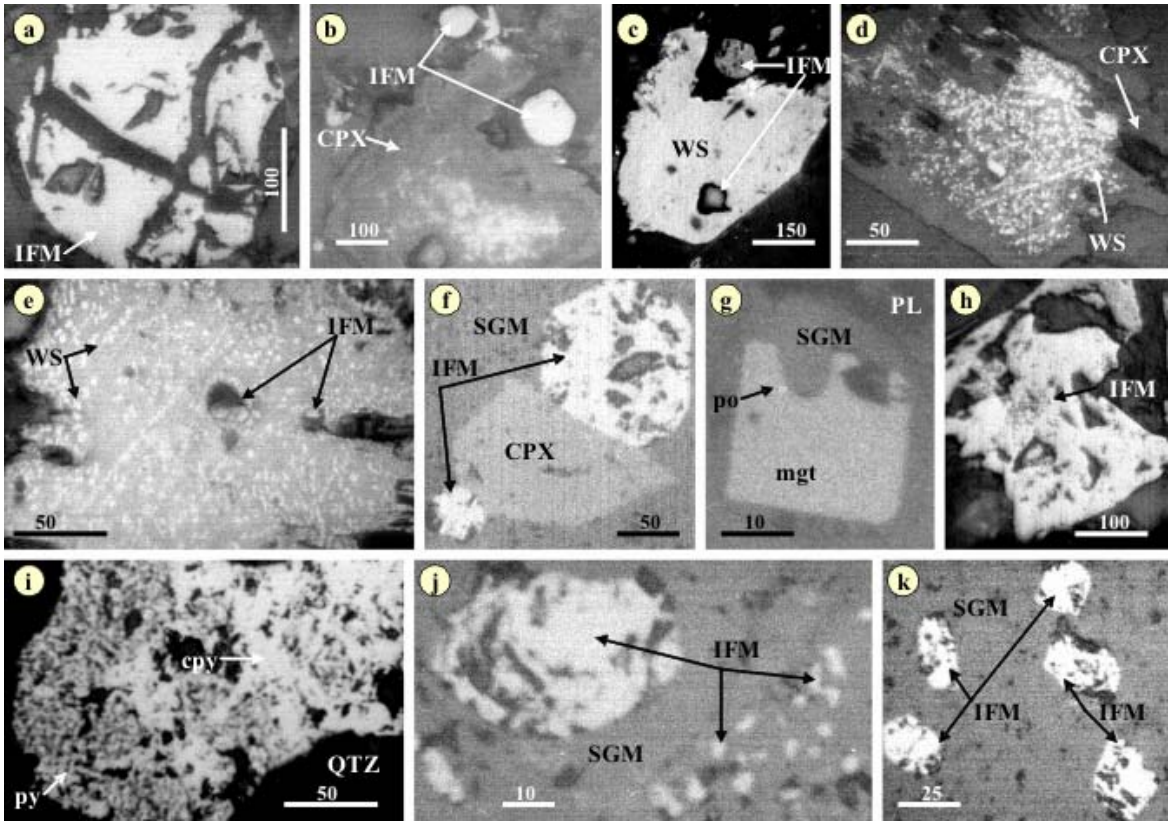

Fig. 12. Globular sulfide (IFM) from Dăneşti - Piatra Roşie dacite trapped in pyroxene (CPX) and glass matrix pictured in **a**, **b**, **f**, **g**, **h**, **j**, **k**; **c**, **d**, **e** - microphotographs showing a sulfide film (decrepitated mound-WS) wetting the host mineral surface after experimentally heating around 1000°C; **i**- chalcopyrite (cpy) exsolution from pyrite (py) during the autometasomatism in quartz grain from Valea Morii porphyry copper deposit (Apuseni Mountain, Romania). Scale bar in µm.

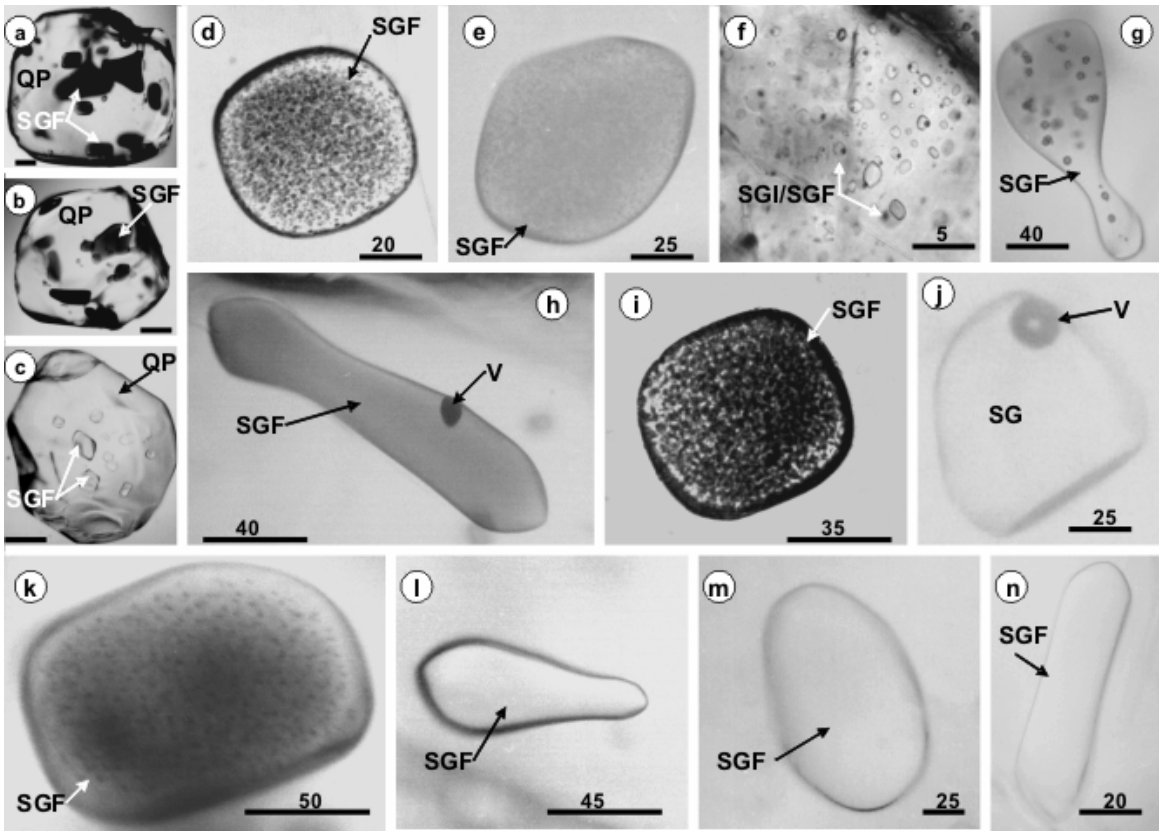

Fig. 13. "Foam-like" glass inclusions types in quartz phenocrysts from "Dej Tuff" formation, Transylvania basin, Romania. Quartz phenoclasts (QP) containing glass foam inclusions (SGF) partially decrepitated in **a.** and **b.**, **c.** - clear "bubble-free" glass inclusions; **d., e., i., k**.- natural reheated glass foam inclusions revealing silicate foam microtexture; **g.**- biphasic glass inclusions (SGI) with glass+ contraction bubble; **f.** cluster of primary glass foam inclusions in sanidine, some of them contain contraction bubble ; **l., m., n.,**- silicate glass inclusions bubble-free which shown obviously homogeneous foam microtexture above 500°C, and they homogenized on further heating in the stage (minimum trapping temperature). It should be noticed that during repeated microthermometric cycles some of them lost all bubbles and become "real" "bubble-free" silicate glass inclusions. (Pintea 2005a; 2006; Pintea, 2013); Scale bar: a, b, c- 250 µm; d, e, f, g, h, i, j, k, l, m, n – in µm.

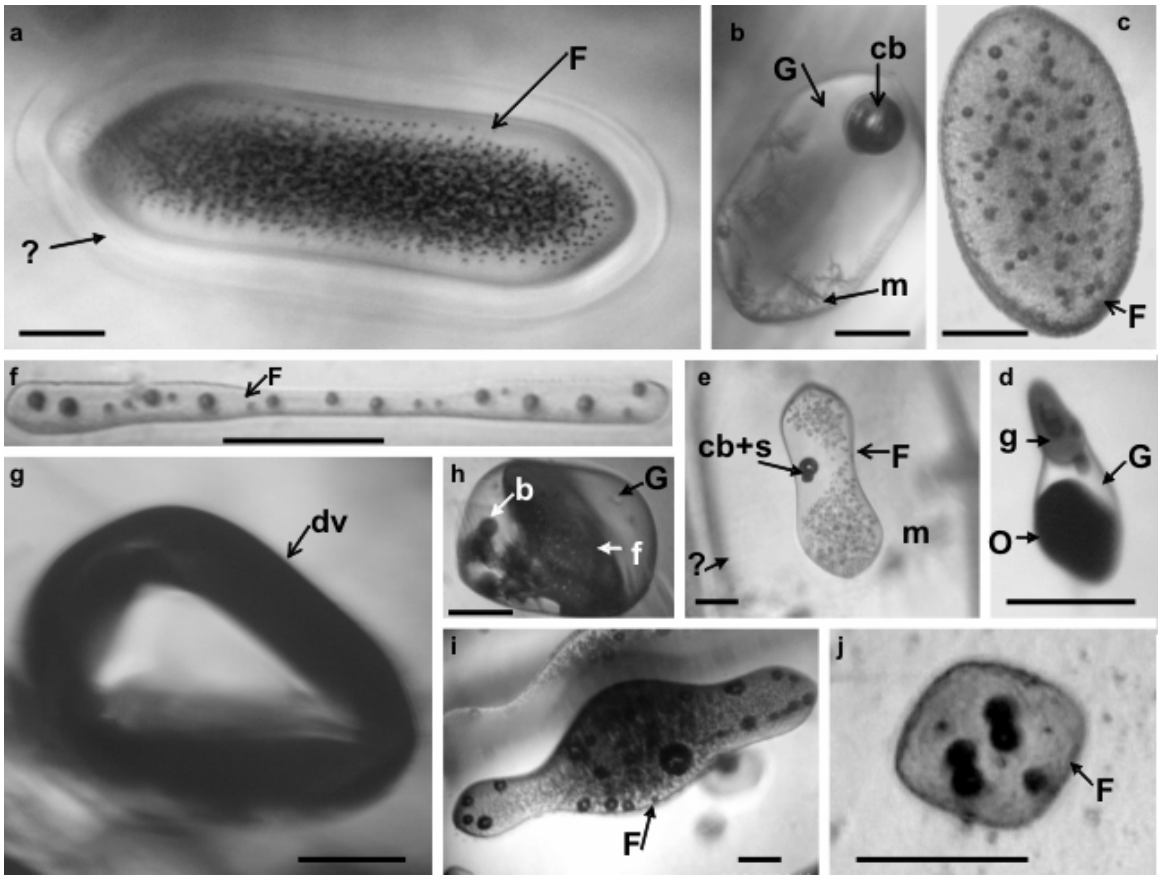

Fig. 14. More microtexture features of the glass foam inclusions from Dej tuff trapped in quartz phenoclasts. **a.** Foam glass inclusion(F) surrounded by decrepitation halo(?), developed in the stage during heating, cannot be homogenized; **b.** Glass + contraction bubble (+ CO_2-?) and microlites (m); **c.** Partly devitrified foam glass inclusion (F); **d.** Multiphase glass inclusion containing glass (G), opaque globule (O) and probably another droplet of immiscible silicate melt (mafic-g); **e.** Foam glass inclusion with one contraction bubble and an attached solid phase (cb+s) surrounded by an unknown ellipsoidal halo (reequilibration- ?); **f.** Elongated secondary glass foam inclusion (F), partially decrepitated showing several ripened-? bubbles(b); **g.** Empty void(dv) left behind after complete decrepitation of a glass foam inclusion; **h.** Glass foam inclusion partially decrepitated containing glass(G), fissure (f) and bubbles (b); **i., j.** Typical partially decrepitated glass foam inclusion which never homogenized during the heating procedure in the stage. (Pintea, 2013). Scale bar in µm.

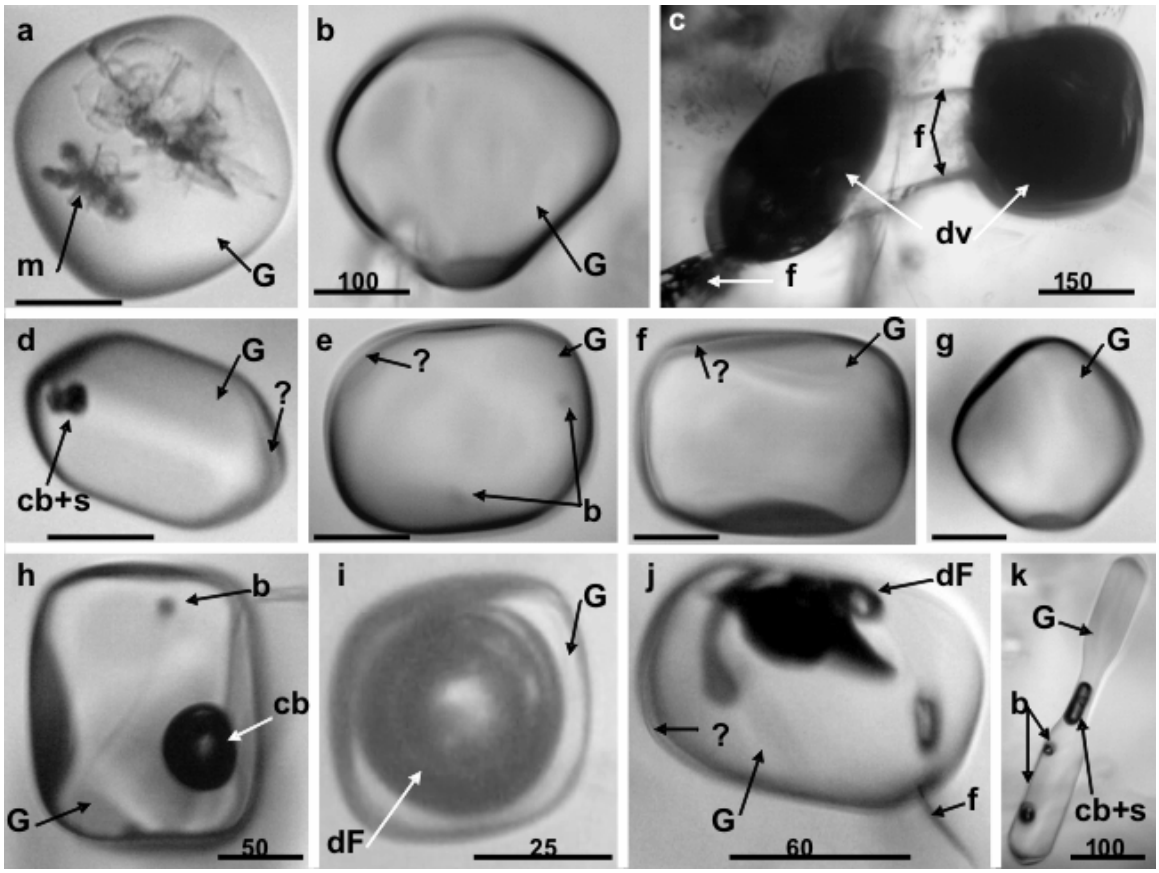

Fig. 15. Glass foam inclusions in quartz from ignimbrites (Măgura Ciceului) with various natural reheated microtextures. **a.** Silicate glass (G) and microlites (m); **b**, **c**, **f**, **g**- contracted (? - menisci) clear silicate glass bubble-free at room temperature (the same type as in Fig 4); **c**- Voids (dv) formed after decrepitation of two glass foam inclusions, f- microcracks; d. Silicate glass with contraction rim (?) contain contraction bubble(cb) and a solid grain (s); **h**.- Slightly decrepitated glass foam inclusions with contraction bubble(cb) and another small bubble(b); **i.** Decrepitated glass foam inclusion with a silicate glass (G) surrounding concentrically bubbles (b); **j.** Partially decrepitated glass foam inclusion contain contracted (?) silicate glass, disrupted foam (dF), f- microfissure; **k.** Elongated glass foam inclusions with contracted bubble containing a solid grain(s) in contracted silicate glass (G), b- bubbles. (Pintea, 2013). Scale bar: µm (a, d, e, f, g = 40 µm).

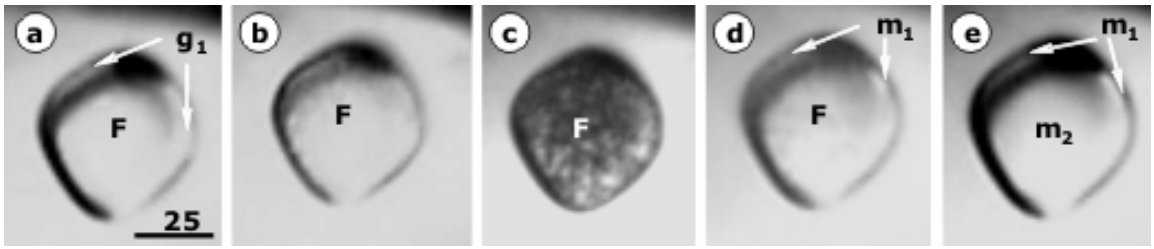

Fig. 16. Microthermometric cycle in silicate foam-like inclusions from quartz phenoclast from the Dej tuff collected at Măgura Ciceului ignimbrite outcrop. During heating it seems that two silicate phases were separated formed by a rim of silicate melt (m_1) around the silicate foam (F).**a.** 25°C, **b**.332°C, **c**.616°C, **d**.814°C, **Th=831°C**, **e**.834°C. The first observable change in silicate glass inclusion was mentioned around 300°C by Clocchiatti, 1975, when ephemeral cracks were formed or the glass seem to be separated from the cavity wall in the still solid state. Our observation suggests that the separation menisci are still there around the homogenization temperature (see Fig. 17). Scale bar in µm.

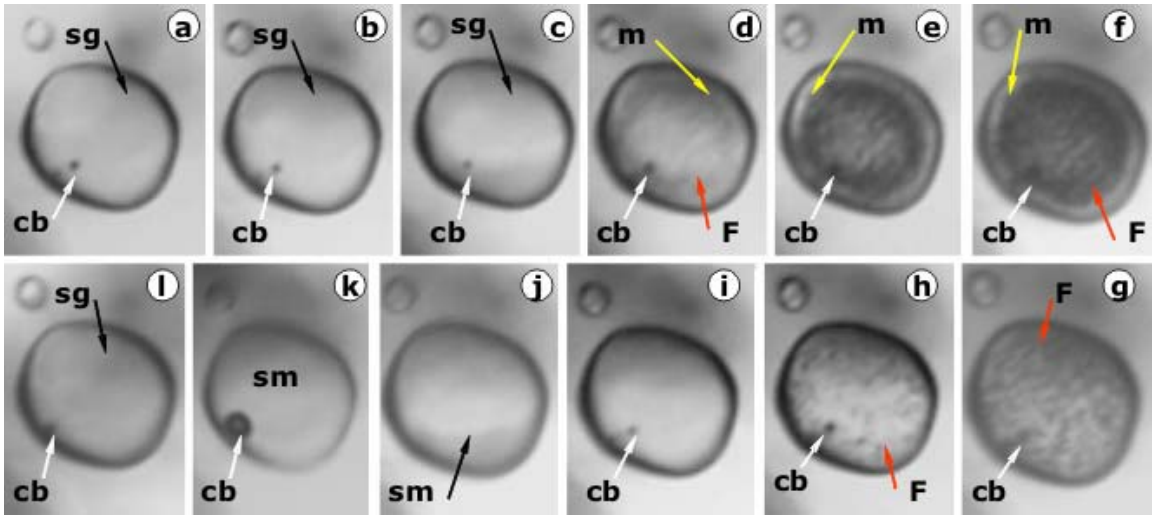

Fig. 17. Complete microthermometric cycle of silicate foam-like inclusion in quartz phenoclasts from Jichisul de Sus. A second silicate phase was developed during heating as an immiscible rim around the silicate foam (**d**, **e**, **f**) which disappeared on further heating before final bubble homogenization (j). Such kind of immiscibility between two silicate melt phases was envisaged by Rădulescu (1979) as a possible process for ignimbrite genesis **a.** 25°C, **b**.390°C, **c**.477°C, **d**.550°C, **e**.570°C, **f**.578°C, **g.** 580°C, **h**.710°C, **i**.721°C, **Th=818°C**, **j**.823°C, **k**.581°C, **e**.25°C. Scale bar in µm.

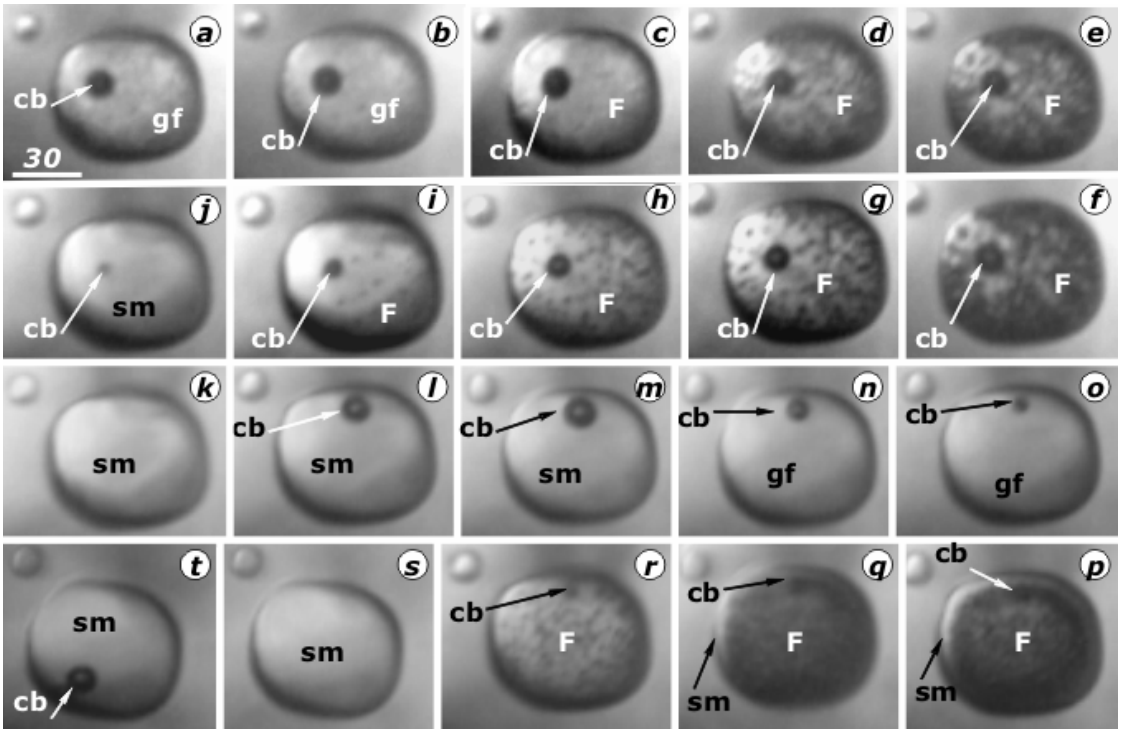

Fig. 18. Replicated microthermometric cycle in the silicate foam-like inclusion (homogeneous foam) from Jichisul-de Sus in quartz phenoclasts showing a large contraction bubble at starting temperature in **a**. and homogenized first at **Th= 882°C**. In the second cycle this homogenized at **Th=848°C**. This seem to be a common feature of the silicate foam-like inclusion, as it was documented by Pintea (2013) in a lot of microthermometric cycles from inclusions trapped in phenoclasts from the Dej tuff. **a**.25°C, **b**.219°C, **c**.396°C, **d**.546°C, **e**.569°C, **f**.601°C, **g**.744°C, **h**.784°C, **i.**859°C, **j**.879°C, **k**.881°C, **l**.639°C, **m**.585°C, **n**.517°C, **o.**471°C, **p**.662°C, **g**.720°C, **r**.761°C, **s.**853°C, **t**.713°C. Scale bar in µm.

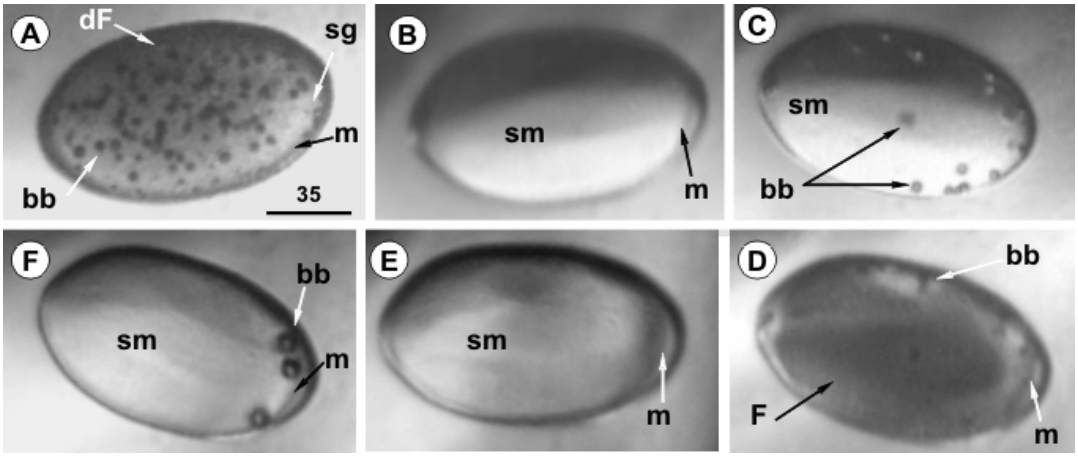

Fig. 19. Microthermometric cycle in a partial decrepitated silicate foam-like inclusion (heterogeneous foam) in quartz phenoclast from Jichişul de Sus. **A**. Starting at 25°C with a silicate glass (sg) + bubbles (bb) mixture it homogenized completely at 913.5°C, but still showing meniscus (m) suggesting silicate melt immiscibility. In the replicated cycle the final homogenization increased at 919.5°C because of the initial decrepitated state. **A**.25°C, **B**.914°C, **Th=913.5°C**, **C**.582°C, **D**.619°C, **E**.928°C, **Th=919.5°C**, **F**.547°C. Scale bar in µm

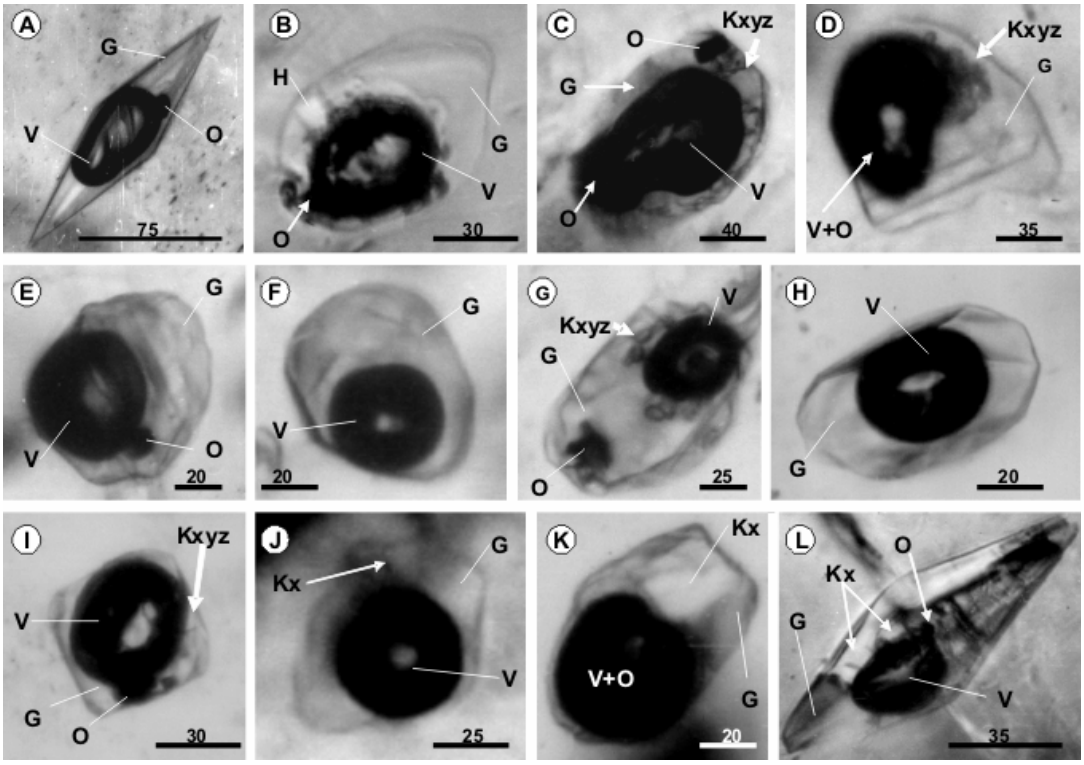

Fig. 20. Silicate melts inclusions in fluorapatite from Tibles massif. Fluorapatite euhedral phenocrysts are associated with phlogopite, rutile, quartz and metallic minerals (Kovacs et al., 1982), formed by reaction between the monzogranodiorite host magma and embedded Paleogene sedimentary material (Edelstein et al., 1981- Geological Map of the Ţibles Mountains- unpubl. report). The silicate melt inclusions contain several solid transparent phases (Kxyz-undetermined), probably silicate, carbonates and chlorides etc, in a glassy matrix (G). Opaque O, are also present. Homogenization tentative failed around 850°C, because thermic decrepitation (Pintea, 1998, unpubl.). Calculated formulae based upon chemical composition of Tibles fluorapatite is $Ca_5\ (PO_4)_3[F_{0.73}\ Cl_{0.25}\ (OH)_{0.02}]$ (Kovacs et al., 1995). The sample described occurred in the N-E part of Ţibles Massif on the Izvorul Mesteacănului Valley. Scale bar in µm.

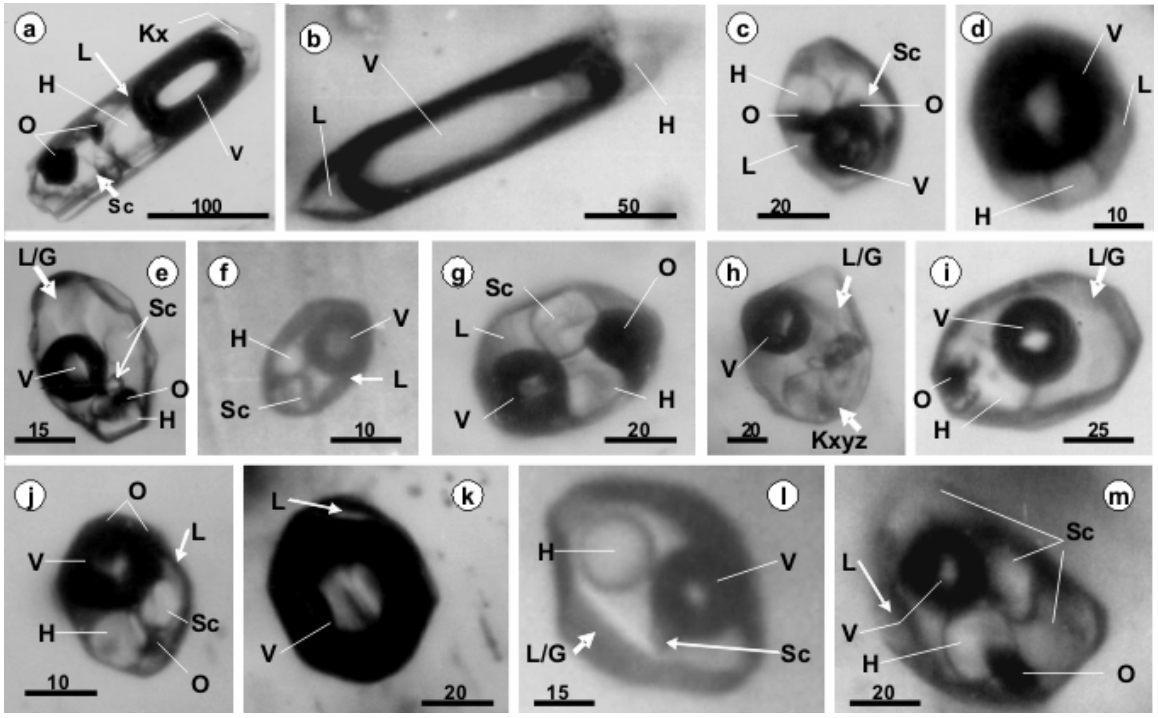

Fig. 21. Brine and vapor rich inclusions in fluorapatite phenocrysts from Tibles massif. Primary isolated or random distributed and pseudosecondary and secondary fluid inclusions parallel to the cleavage planes and microfissures are representative for high salinity high temperature saline fluids. They are fluid separated during magma crystallization and fluid-rock high-Mg metasomatic processes. L-liquid, V-vapor, H-halite, Sc- carbonate, O- opaque, kx- transparent solid phase. Halite melting temperature shown 30- 40 wt% NaCl eq and Th > 400-600°C, indicating fluid phase immiscibility at high temperatures (Pintea, 1998; Kovacs et al., 1995). Scale bar in µm.

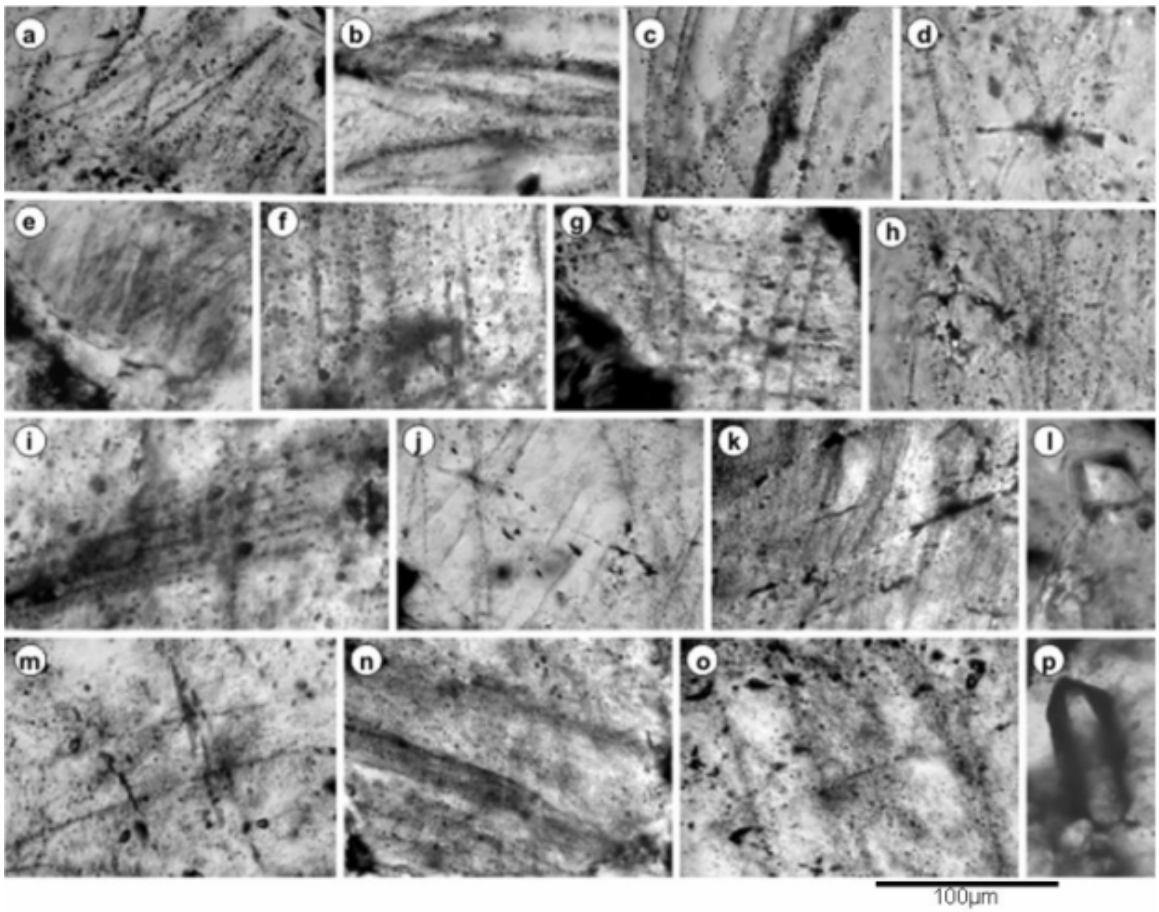

Fig. 22. Plan deformation features in quartz from Măgura-Neagră - Suplai porphyry - type ore deposit suggesting post "shock" events related to variable UHPT conditions supported probably during exhumation processes (argued by thermochronology, fission track" and (U-Th)/(He). Similar features are characteristic also in the Miocene porphyry copper deposits from Apuseni Mountains (e.g. Deva, Valea Morii, Talagiu etc) and were also described by CL at Butte porphyry system (Rusk et al., 2005, their Fig.2G). e.g. others similar features between Ţibles porphyry copper system with Butte were mentioned by Udubaşa et al., 1984. **a, b, c, d, e, f, g, h, i, j, k, m, n, o** – planar elements (cracks) probably structural controlled in quartz similar to the shocked quartz frequently described in the high pressure environment (e.g. Langenhorst, 2002; Trepmann and Spray, 2006). Solid microinclusions in quartz, probably titanite in **l** and zircon in **p**.

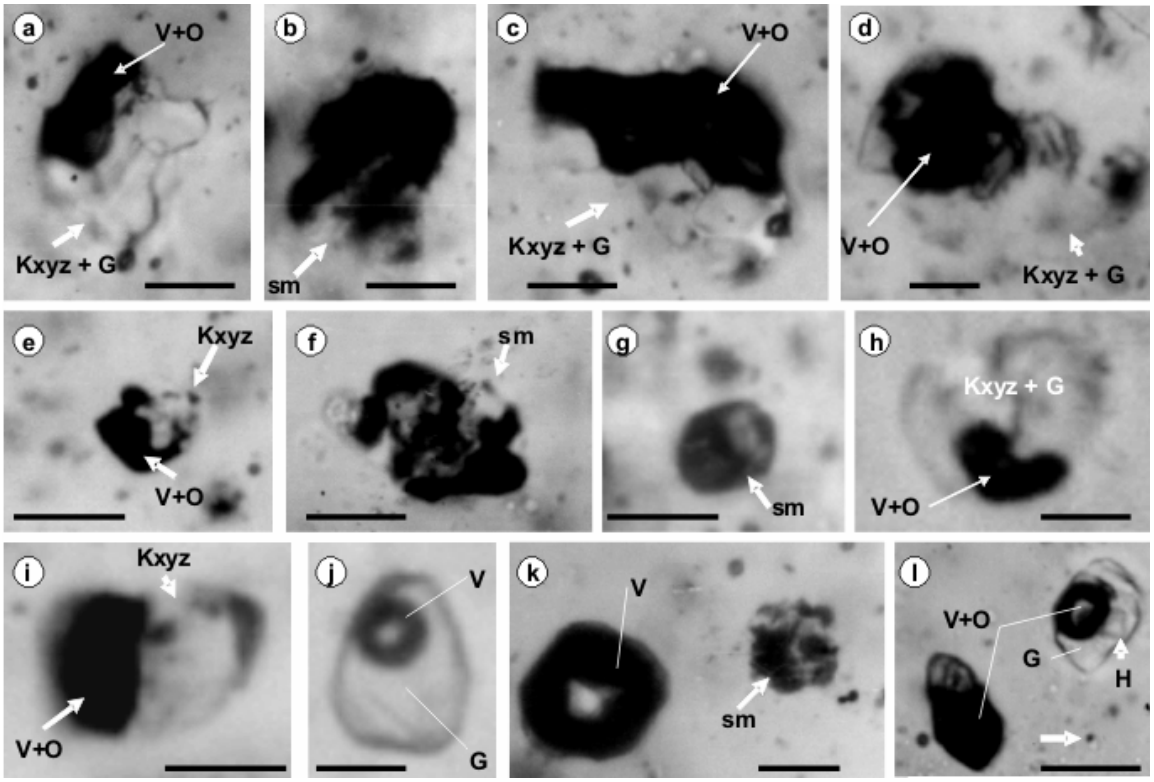

Fig. 23. Silicate – brine assemblages in the Măgura-Neagră–Suplai mining district (Ţibles massif). Kxyz-undetermined solid transparent microminerals, undifferentiated vapor and opaque solid phases, together trapped in sm-silicate melt (now glass-G). Associate aqueous fluid inclusions, vapor rich (k) and/or brine (l) seem to be contemporaneous at high temperatures. Homogenization temperature exceeded frequently 1000°C, the silicate melted around 600-900°C, and salt mineral melted around 500°C (Pintea, 1998; Pintea et al., 1999).

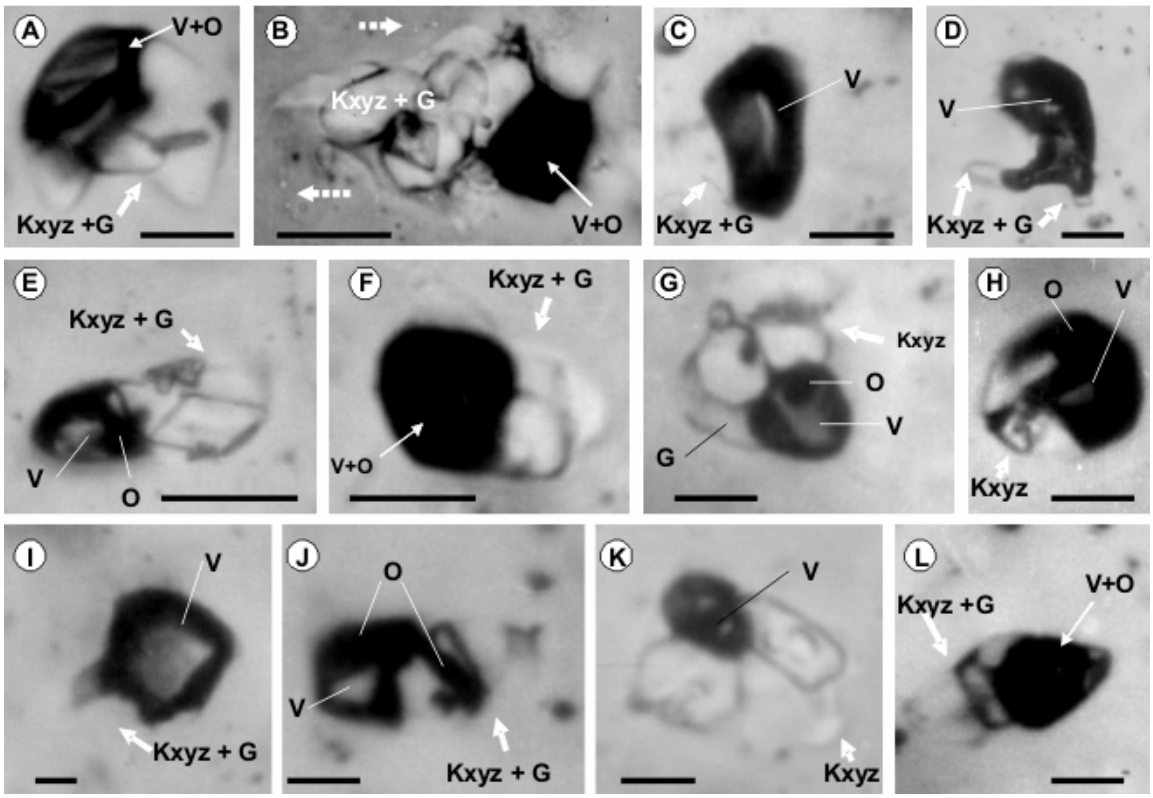

Fig. 24. Silicate-brine inclusion assemblages in quartz from Măgura-Neagră-Suplai mining district (Ţibles massif). Frequently the brine inclusions are liquid-free at room temperature suggesting the existence of salt melt at trapping conditions. Kxyz- salty and silicate daughter minerals undifferentiated, but obviously halite is the dominant transparent solid. Vapor (V) and opaque (O) were separated after trapping inside the microcavities. G-glass. Variable homogenization temperature between 1000-550°C, salinity between 60 - 80 wt % NaCl eq. suggesting single fluid phase separation by decompression in a magmatic - to - hydrothermal transition (Pintea, 1998; Pintea et al., 1999a); Scale bar 10 µm.

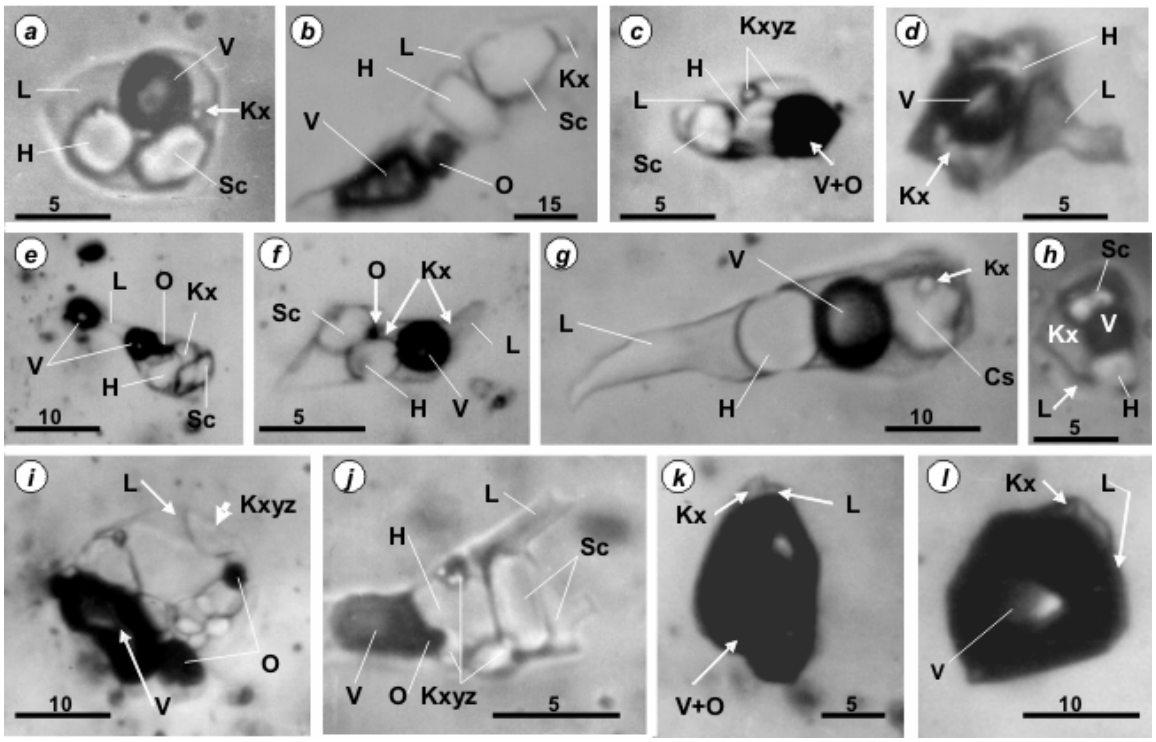

Fig. 25. Brine and vapor-rich inclusions in quartz from Măgura-Neagră-Suplai mining district from Ţibles massif. Complex salt daughter minerals including halite (H), sylvite sometimes anhydrite (Cs) are noted as Kx, Kxyz ; Sc- presumably carbonate rich salt; O- opaque, L-liquid, vapor (V), O- opaque frequently undifferentiated at room temperature (V+O). Intermediate to low temperature homogenization by vapor bubble disappearance between 400 – 600°C, or by halite homogenization at low than 450°C showing variable salinity between 30 and 70 wt% NaCl eq. More data in tables 1 an 2 (Pintea et al., 1999a). Scale bar in µm.

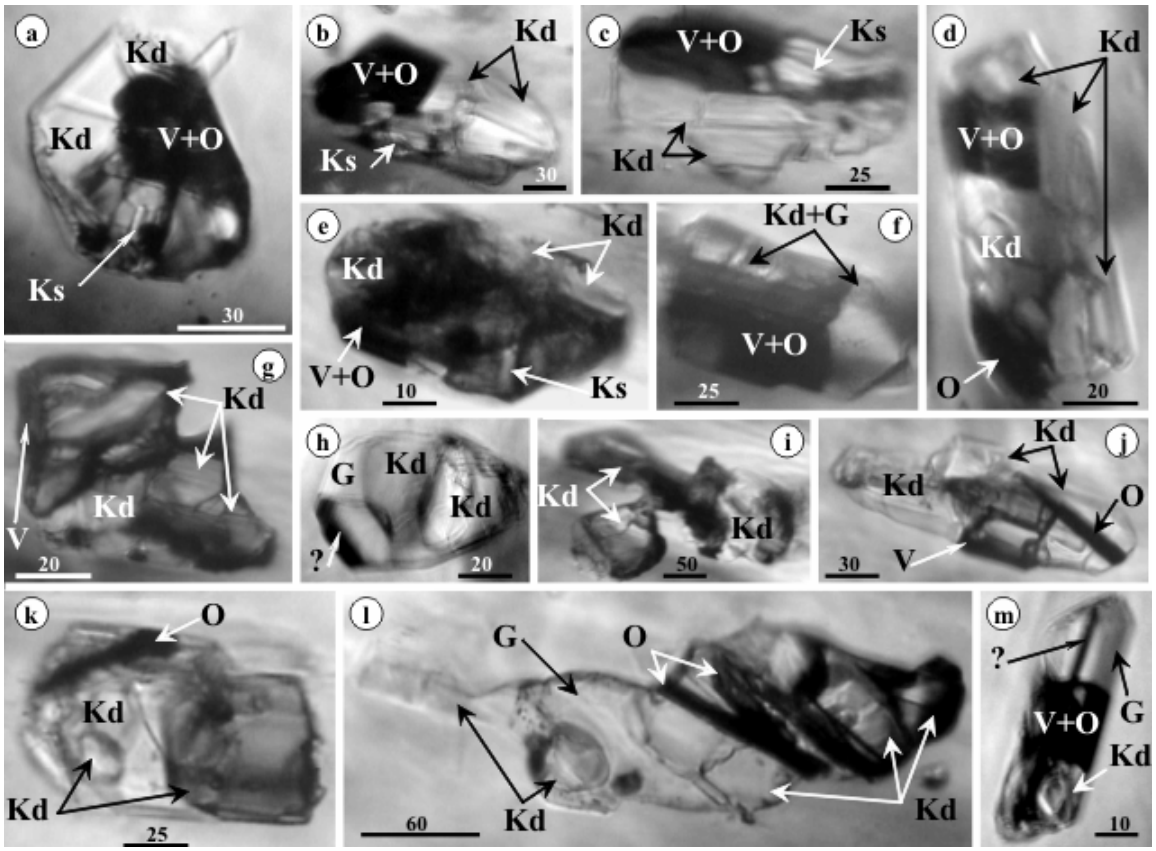

Fig. 26. Complex silicate melts plus brine inclusions in pargasite from the high temperature magnezian skarn from Ţibles massif. More than 40 minerals were described for the first time in relation with the wide temperature processes from the contact between quartz monzodiorite and Oligocene sedimentary rocks mainly described in the Saci transversal (Udubaşa et al., 1981).V-vapor, Kd- silicate mineral, Ks- saline daughter phase, G-glass, ?-unknown, O-opaque. Microthermometric experiments (Pintea, 1998 and unpubl.) indicated very high final homogenization temperatures (≥ 960°C) in good accord with experimental published data for pargasite formation in the presence of diobside, forsterite, spinel, nepheline, anorthite and silicate melt between 995-1103°C and 1.2-8 kbars (e.g. Holloway, 1973).Scale bar in µm.

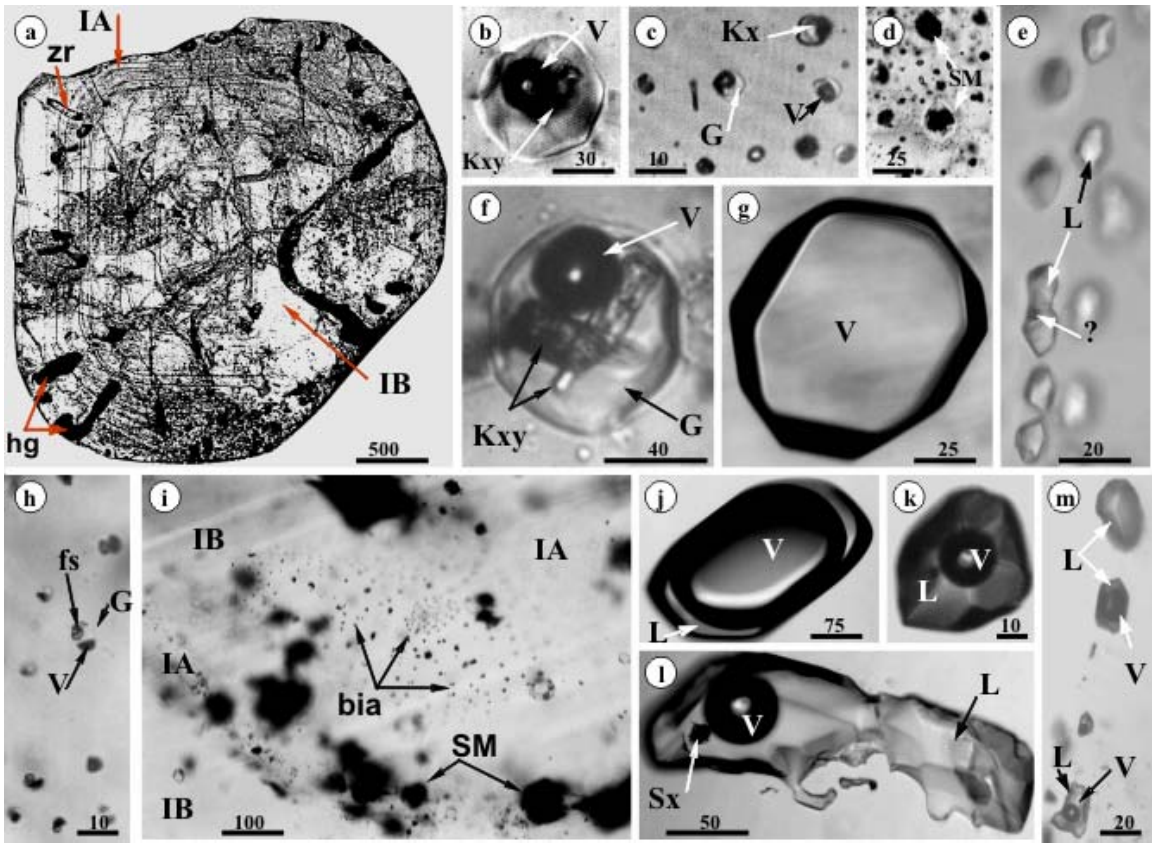

Fig. 27. Silicate melt and fluid inclusions in quartz phenocrysts from Roşia Montană. **a**.-Transversal double polished thin section on typical β-quartz crystal from Roşia Montană dacite showing oscillatory zoned feature of a thin resorption layer- IA and a wide growing zone- IB. Specifically they contain various silicate melt-, fluid inclusions and sometimes embedded solid inclusions as zircon-zr, and hourglass inclusions - hg; **b.** and **f.-** Silicate melt inclusions containing glass (G), vapor (V) and daughter solid phases (Kxy); **d.-** Completely altered silicate melt inclusions with characteristic decrepitation halos formed by secondary fluid inclusions; **e.-** Monophase liquid (L) rich inclusion +/- vapor (V) in epithermal quartz; G. Vapor (V) rich inclusion looking empty at room temperature conditions, but during microthermometry a special kind of phase transition were recorded (see Fig. 116). **h.** - Brine (fs) trapped in silicate glass inclusions (G-glass, V-vapor); **i. -** Brine inclusions assemblage (bia) formed "in situ" in a large zone (IB) of β-quartz from decrepitated silicate melt inclusions (SM) in a subsequent decompression stage; **j. k.-** Biphasic vapor – rich and liquid – rich inclusions in epithermal quartz phenocrysts (L-liquid, V-vapor);**l-** Three phase fluid inclusion in epithermal quartz trapped frequently a liquid (L), vapor (V) and accidentally a solid grain phase of carbonate, silicate or sulfate, but never a real daughter saline (halite) mineral; **m**.- Biphasic fluid inclusions with variable phase ratios between vapor (V) and liquid (phase) in a secondary trail in magmatic quartz formed "in situ" around decrepitated silicate melt inclusions (Pintea, 1999; Pintea, Iatan, 2013). Scale bar in µm.

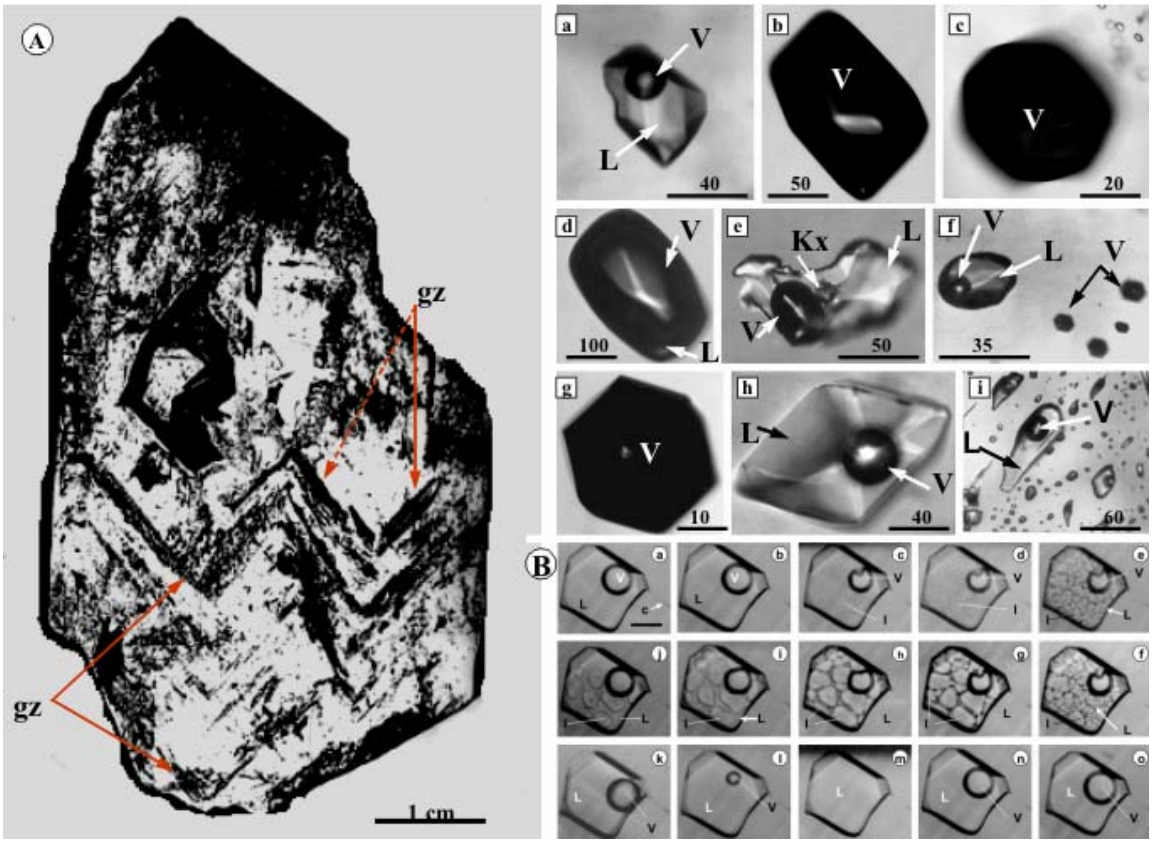

Fig. 28. Typical aqueous fluids trapped in epithermal quartz from Roşia Montană. **A.** Double terminated prismatic quartz crystal with parallel double zonation (gz). **a, h**.- Primary biphasic fluid inclusion with vapor (V) and liquid (L); **b, c, d, g**- Isolated vapor-rich inclusions containing a vapor phase (V) and a film of liquid (L); Presumably boiling event recorded by pairs of aqueous- rich (L+V) and vapor- rich (V), trapped in a restricted zone; **j.-** Pseudosecondary biphasic (L+V) assemblage in epithermal quartz. **B**. Sequences shown the complete microthermometric cycle, typical for aqueous-rich inclusions in the epithermal quartz from Roşia Montană, first recorded with an original microthermometric stage, working between -196 to +750°C (Pintea et al., 1992). **a.** and **o.** +25°C, **d.** - 40°C (Tf), **e**. -20.8°C (Te), **k.** -0.2°C (Tmi), **m.**+221.5°C (Th), salinity = 0.35 wt% NaCl eq. **b. c. f. g. h. i. j. l. n.** intermediate temperatures; the fine capillary (*c* in **a.**) had no visible influence on microthermometry; Notations: L- liquid, I-ice, V- vapor; Scale bar = 20µm.

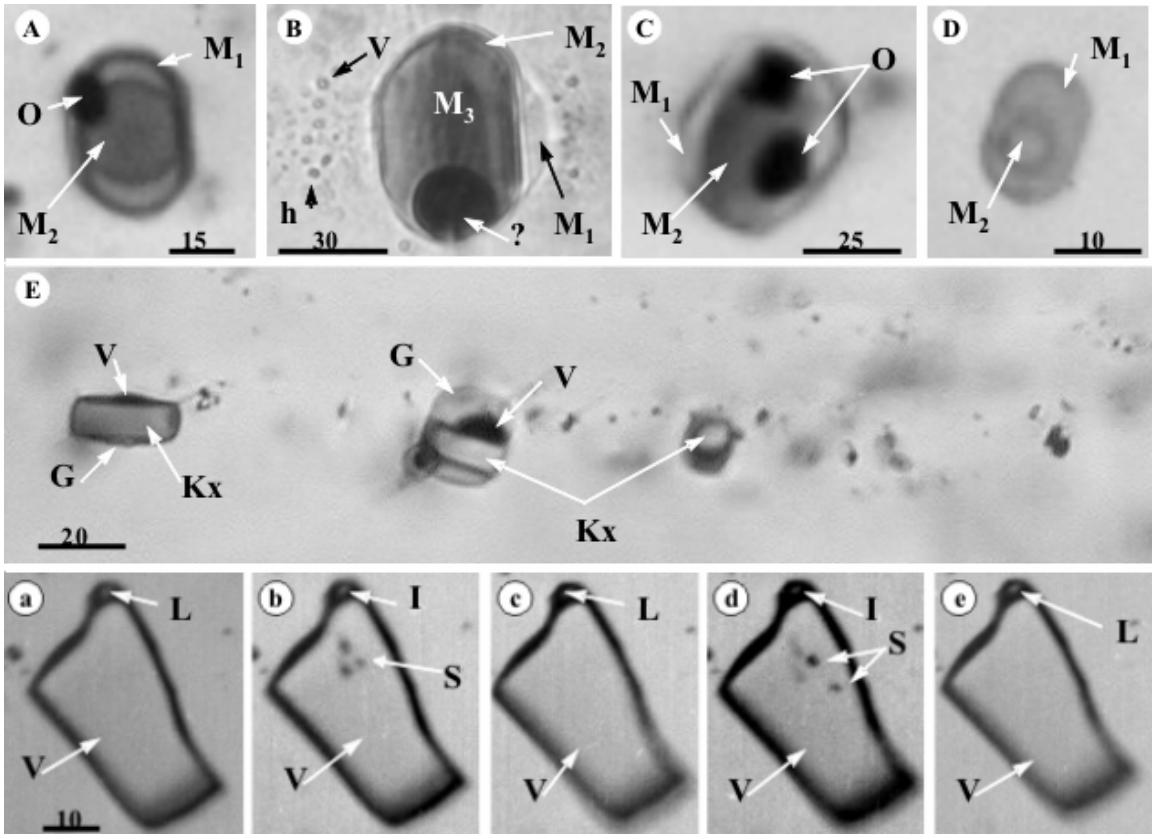

Fig. 29. Roşia Montană melts and fluid inclusion feature in ß- quartz phenocrysts. **A**, **B**, **C**, **D**- multiphase glass inclusion formed by heterogeneous trapping or in situ fractionation after thermic decrepitation (e.g. **B** from Pintea and Iatan, 2013); M_1+M_2 reproducible homogenization temperature around 1050°C was determined by microthermometry (Pintea, 2003). **E**.- Recrystallized melt inclusions along a resorption layer. **a**, **b**, **c**, **d**, **e** - Duplicated low-T microthermometry in low density vapor- rich inclusion trapped in hydrothermal quartz from Roşia Montană. **a.** +25°C (L-liquid rim, V- vapor phase), **b.** to –196°C (S-sublimated gas phase, I-ice), **c.** +25°C (Liquid + Vapor), **d**. –196.7^{o}C (ice + sublimated grains), **e.** + 25°C. In this fluid inclusion, and similar ones the liquid phase have a salinity of 0.71 wt % NaCl eq, and homogenized between 362 -373.8^{o}C for n= 10 determinations. (Pintea, 1999). Review on melt inclusion study from Roşia Montană magmatic quartz phenocrysts were published by Naumov et al., 2013. Scale bar in µm.

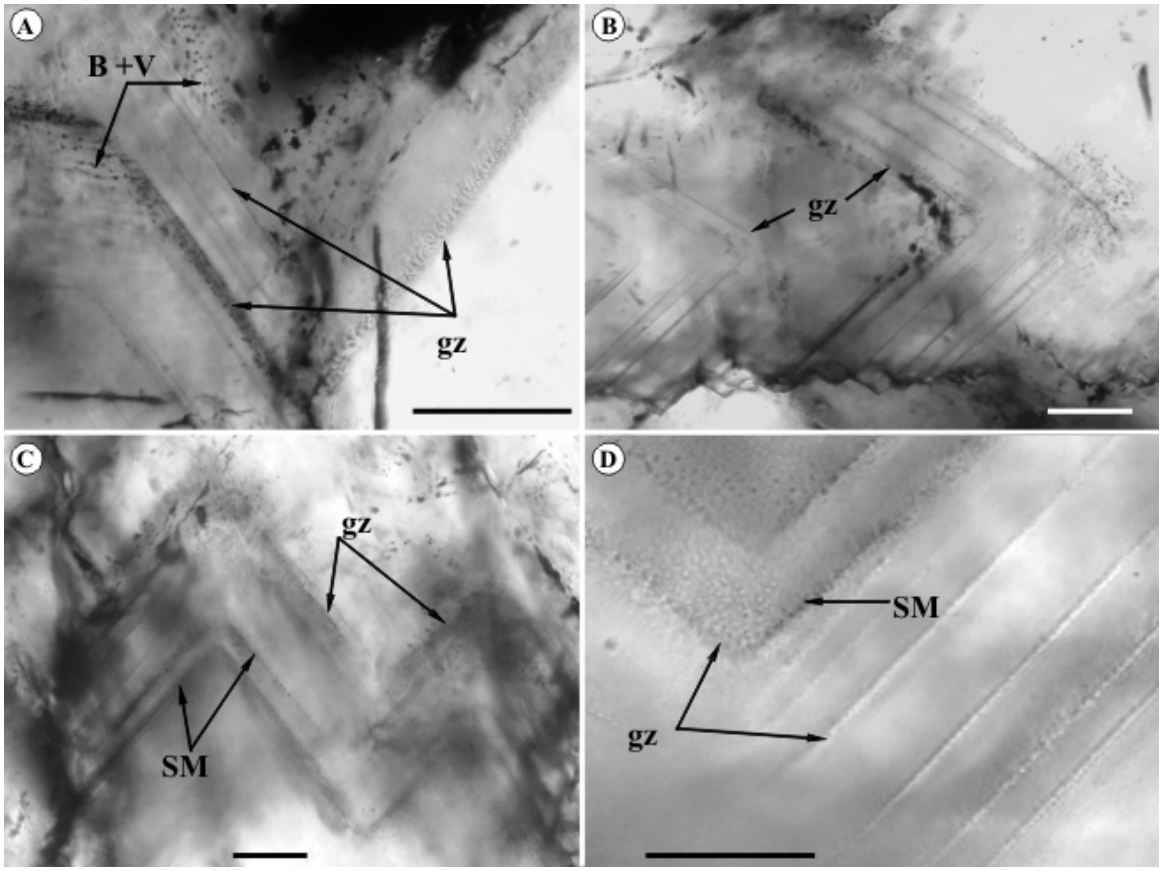

Fig. 30. Multiple growth zones (gz) in quartz coarse grain in veinlets from Deva porphyry copper deposit (**A**, **B**, **C**, **D**- level -450, Pintea 1996, 2014a) Generally, they are decorated by silicate (SM), hydrous saline melt inclusions (B) and vapor rich inclusions (V). More than 20 growth zones could be counted for small quartz veinlets of max 10 mm wide and zonation could be the result of the retreating downward crystallization, mafic influx, autometamorphism, dissolution or diffusion. Complex imaging methodology by using SEM-CL technique was applied to decipher episodes in porphyry copper genesis based upon zonation and trace element distribution (e.g. Penniston-Dorland, 2001; Landtwing et al., 2005; Rusk et al., 2004). Microtextural feature on quartz zonation from Deva porphyry copper also in Ivăşcanu et al., 2003. Scale bar: 100µm.

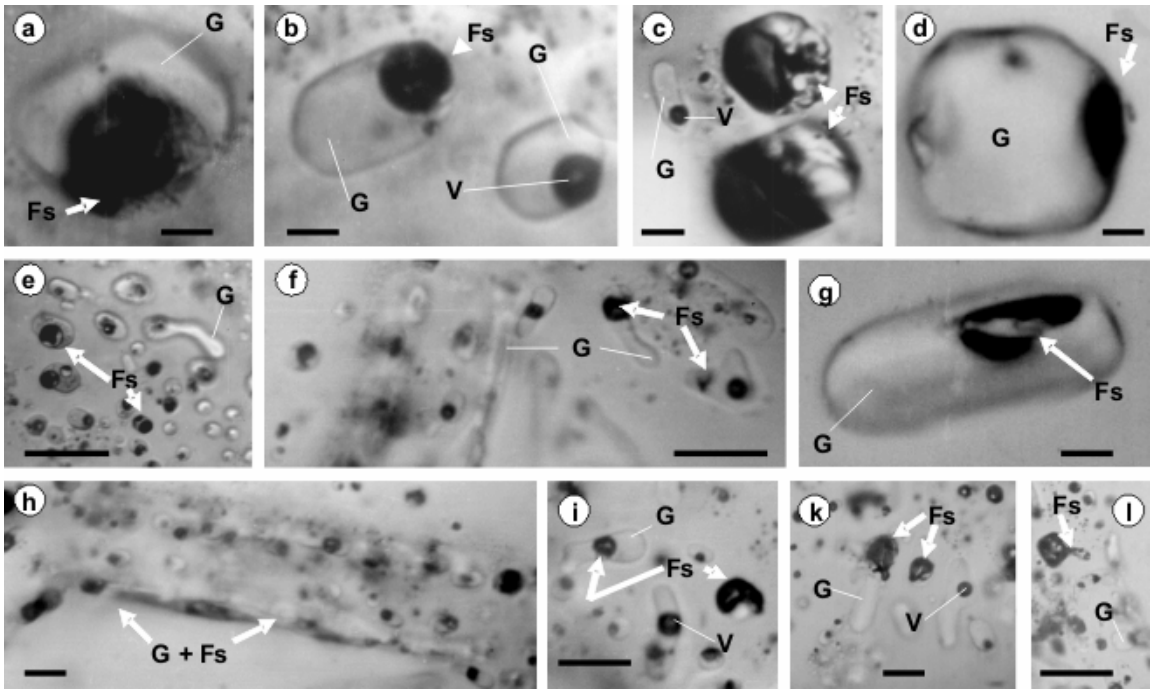

Fig. 31. Immiscible silicate melt (G) and hydrous salt melt (Fs) trapped together (**a**, **b**, **d**, **e**, **f**, **g**, **h**) and/or coeval inclusions (**c**, **i, k**, **l**) decorating quartz growth zones in quartz from Deva porphyry copper deposit. These are common feature of immiscibility when two fluid/melt phases were trapped in various proportion in the host mineral (Roedder, 1992), documented also by large P-T range, e.g. $\geq 900^{o}$-1100°C and 0.3 to 12.8 kbars (Pintea, 1996b; 2014a). Scale bar: 10µm.

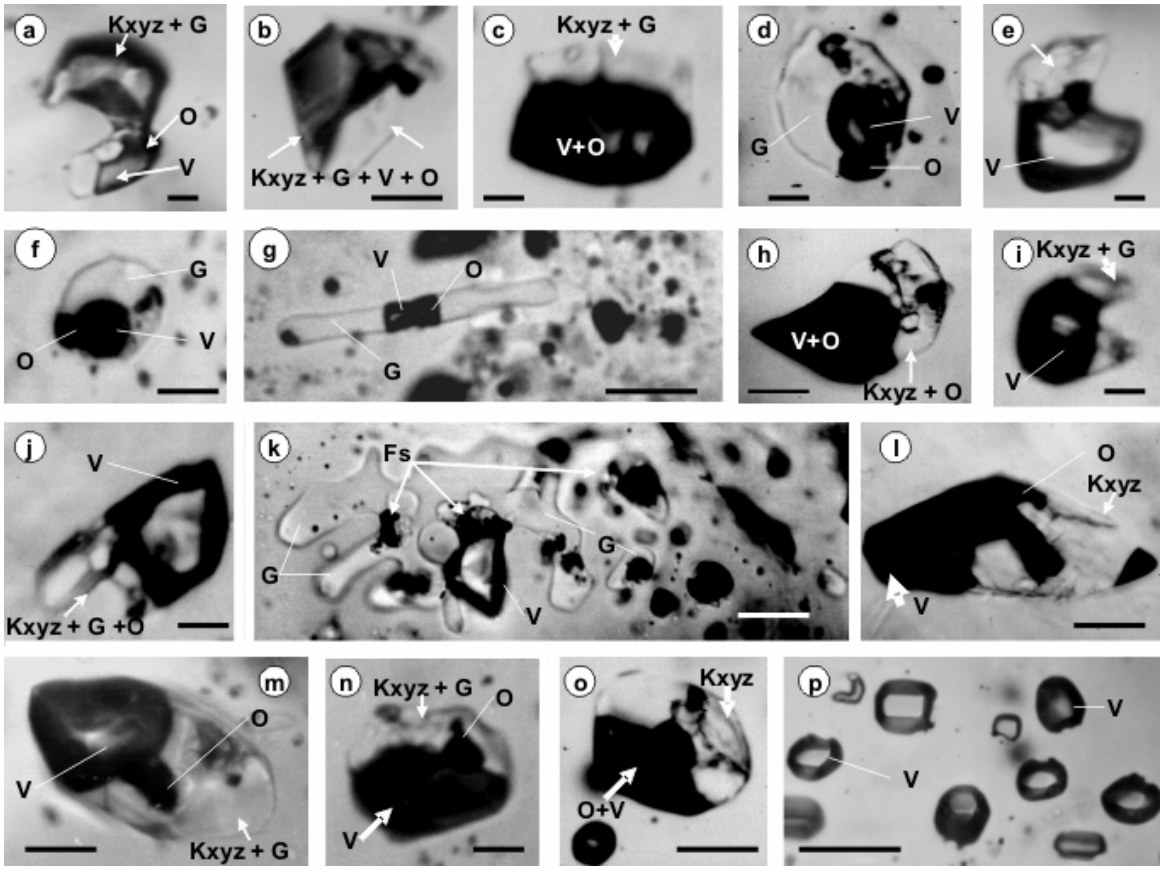

Fig. 32. Compositional variation at room temperature between silicate melt (now glass) and the hydrous saline melt in individual complex inclusions trapped in quartz from Deva porphyry copper deposit. **a**, **b**, **c**, **e**, **h**, **i**, **j**, **l**, **m**, **n**, **o**- hydrous salt melt; **d**, **f**, **k**, - complex silicate melt (now glass) inclusions and hydrous salt melt. G-glass, V-vapor, O-opaque, Kxyz- solid phase association, Fs-hydrous salt melt. Scale bar: 10μm.

Fig. 33. Individual hydrous salt melt inclusions without liquid phase at room temperature condition formed in quartz as primary, pseudosecondary or secondary inclusions in quartz grain from veinlets from Deva porphyry Cu-Mo (Au) ore deposit. **a**, **b**, **c**, **d**, **e**, **f**, **g**, **h**, **i**, **k**, **l**, **m**, **o**, **q**, **r**, **t**, **w**, **x**, **y**,- hydrous saline melt inclusions; **n**, **p**, **s**, **u**, **v**- vapor rich inclusions; kxyz- multiple solid daughter mineral association. Amongst them halite, anhydrite, sylvite, complex K, Fe, Mg, Ca – chlorides and K-feldspar were positively identified by microthermometry and SEM/EDS (Pintea, 1996b; 2014a). Complete microthermometry was firstly documented up to 1500°C (Pintea, 1993ac, 1996ab, 1997, 1998-unpubl., 2001ab, 2014a), showing multiple immiscibility between silicate-sulfide-salt-sulfate liquid phases and vapor. Scale bar: 10μm (n to y).

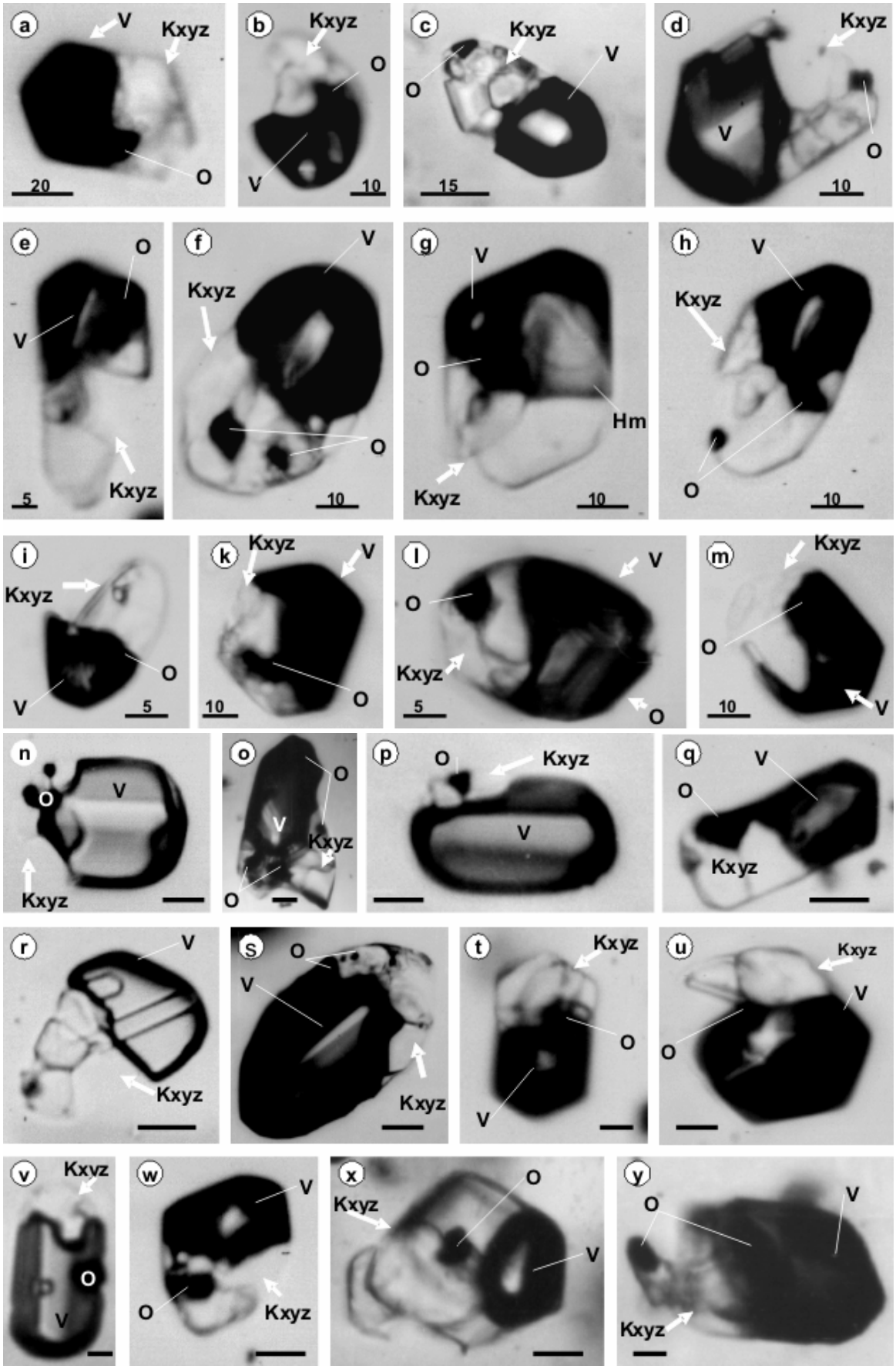
a
V
Kxyz
O
20
b
Kxyz
O
V
10
c
Kxyz
V
O
15
d
Kxyz
V
O
10
e
O
V
Kxyz
5
f
V
Kxyz
O
10
g
V
O
Hm
Kxyz
10
h
V
Kxyz
O
10
i
Kxyz
O
V
5
k
Kxyz
V
O
10
l
V
O
Kxyz
O
5
m
Kxyz
O
V
10
n
O
V
Kxyz
o
O
V
Kxyz
O
p
O
Kxyz
V
q
V
O
Kxyz
r
V
Kxyz
s
O
V
Kxyz
t
Kxyz
O
V
u
Kxyz
V
O
v
Kxyz
O
V
w
V
O
Kxyz
x
O
Kxyz
V
y
O
V
Kxyz

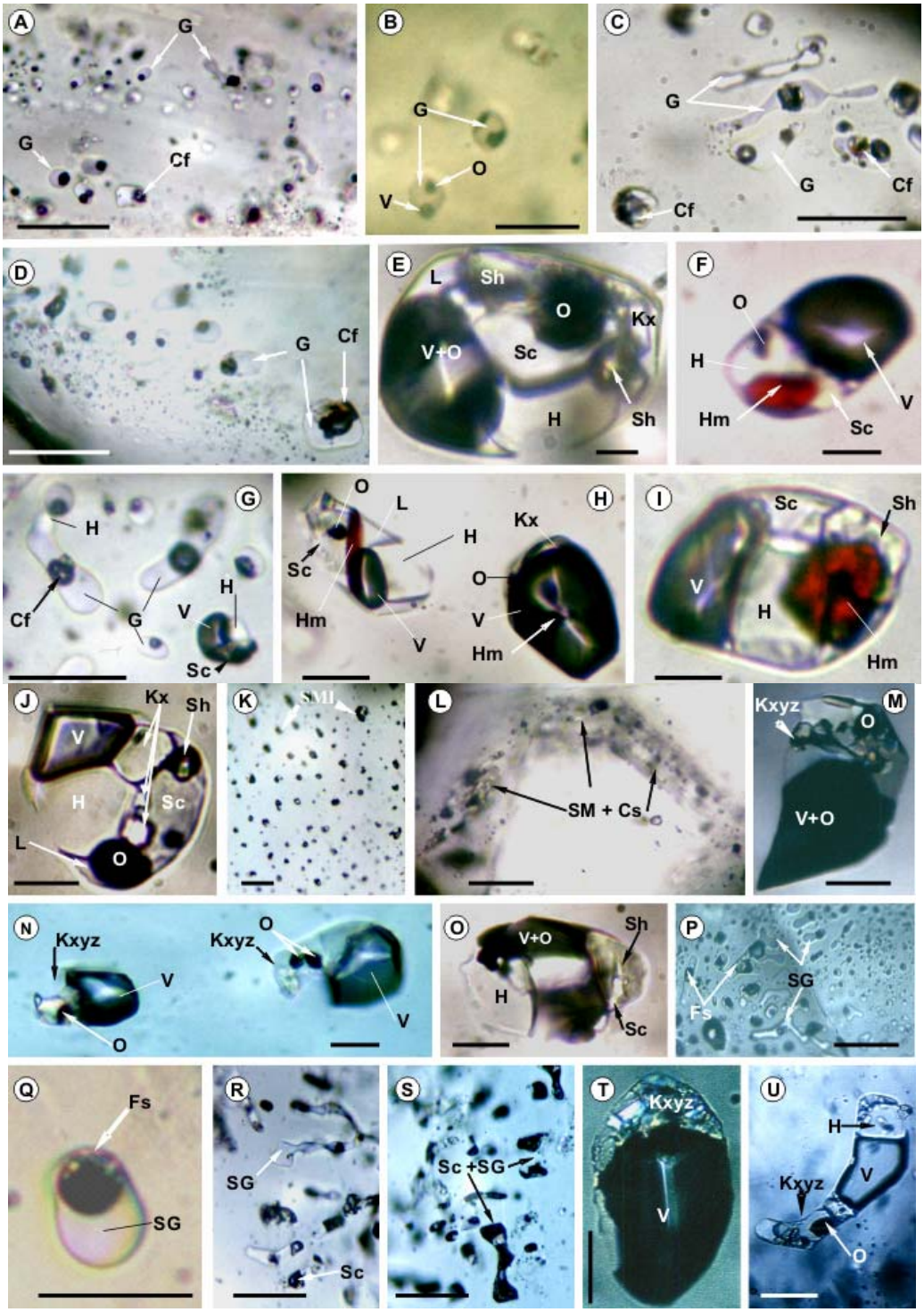

Fig. 34. Coloured microphotographs showing several kind of silicate glass inclusions, vapor-rich and hydrosaline melt inclusions in quartz from Deva (**A, C, D, E, F,G, I**) and Rosia Poieni (**B**, **H**) porphyry copper systems. G-glass, Cf- saline fluid, H-halite, V-vapor, Sc- another salt daughter phase, Hm- hematite, Kxyz- unidentified solid phases, Sh- unknown, O-opaque solid phases (pyrite, magnetite, bornite etc (Pintea, 2014a); Scale bar: 20 µm.

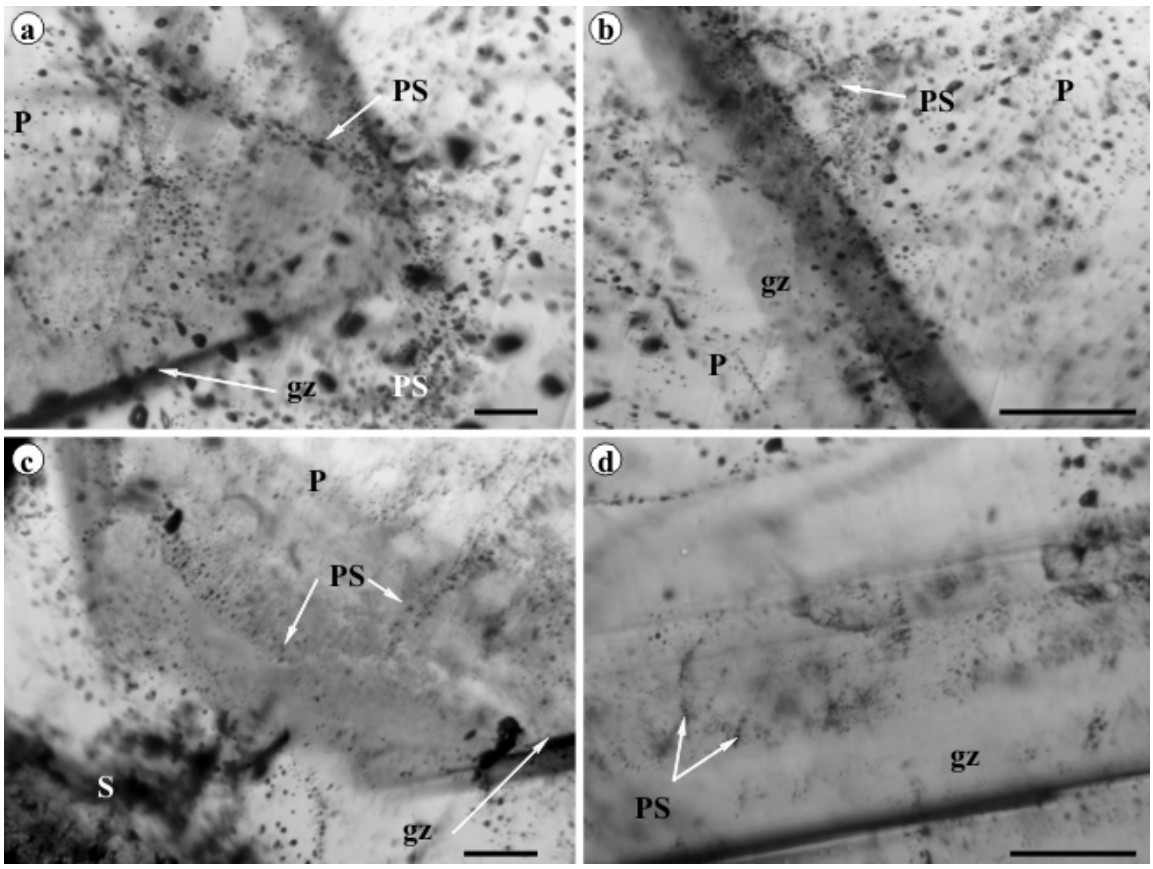

Fig. 35. Longitudinal sections through the prismatic quartz crystals from potassic zone - brecciate veinlets during overprinting by high-sulfidation stages from Roşia Poieni porphyry copper deposit **(a**, **b**, **c**, **d**). Early potassic quartz veins were fragmented and (re) cemented by high sulfidation mineralization described as pebble dike by Kouzmanov et al., 2010. Quartz is multiple zoned (gz) and decorated with primary fluid inclusions (vapor - rich and brine) and intersected by pseudosecondary (PS) and secondary (S) trails. Microthermometry and LA-ICP-MS analyses were published by Damman et al., 1996, Pintea, 1996; Pettke et al., 2001; Ivăşcanu et al., 2001; Heinrich et al., 2005, Kouzmanov et al., 2010. Scale bar in µm.

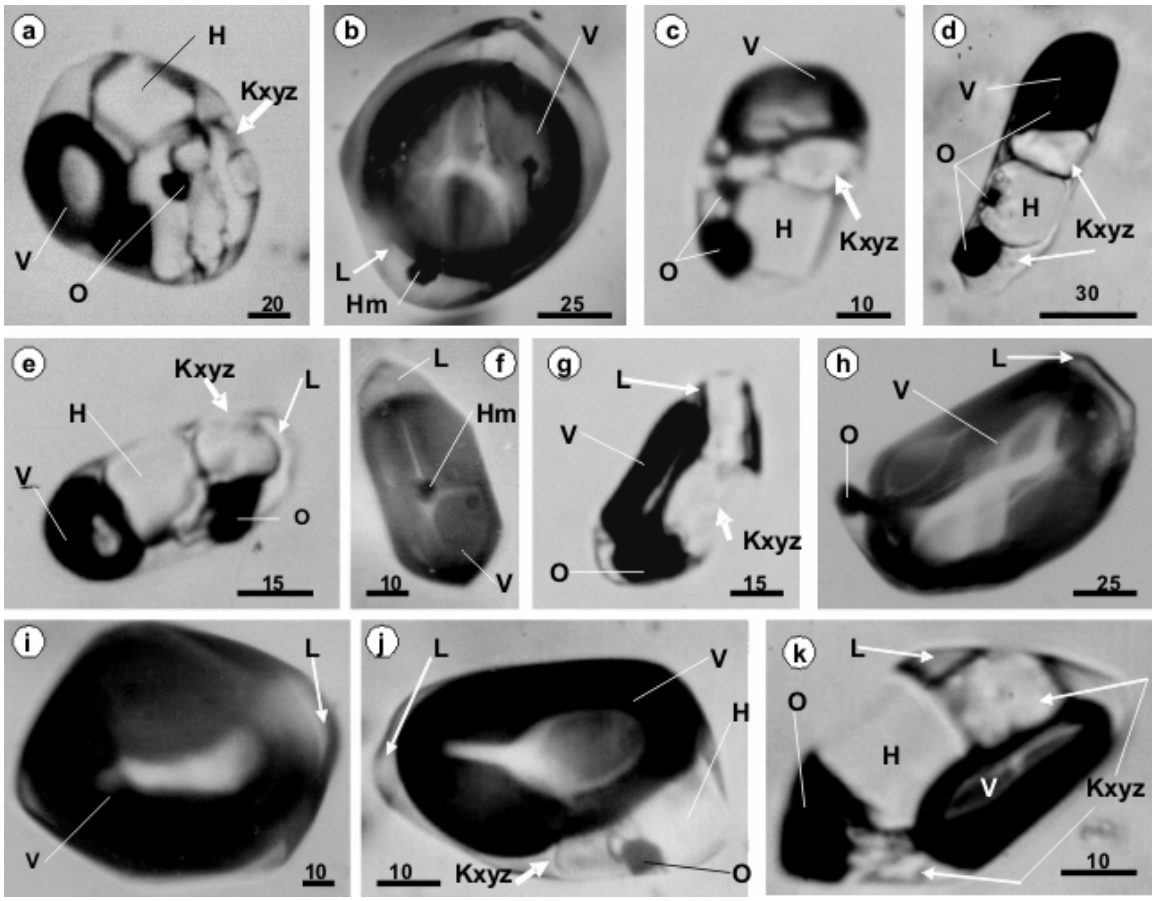

Fig. 36. Fluid and brine inclusions trapped in quartz from Roşia Poieni porphyry Cu-Au (Mo) deposit. **a**, **c**, **d**, **e**, **g**, **k**- brine inclusions containing halite (H), Kxyz- transparent salt and silicate solid daughter phases, O-opaque, V-vapor, L-liquid; **b**, **f**, **h**, **i**, **j-** vapor-rich inclusions with vapor-V, Hm-hematite, O-opaque (py, cpy), L- liquid, Kxyz- salt and/or silicate solid daughter phases. Scale bar in µm.

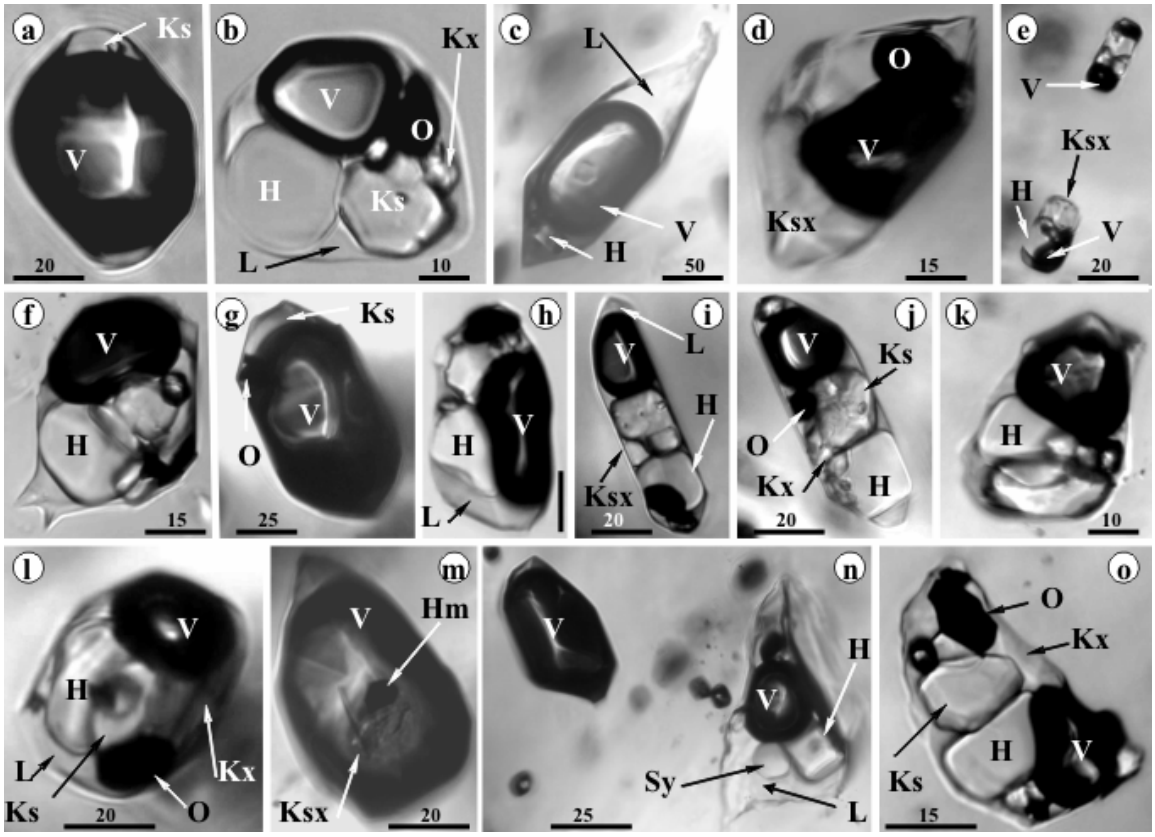

Fig. 37. Vapor-rich and multiphase (brine) inclusions in prismatic quartz crystals from Roşia Poieni porphyry Cu-Au (Mo) deposit; **a**, **c**, **g**, **m**- vapor rich inclusions with vapor-V, Ks- chloride daughter phase, O-opaque, Hm-hematite, Ksx- others salt/silicate phases. **b**, **d**, **e**, **f**, **h**, **i**, **j**, **k**, **l**, **o**- brine inclusion containing H-halite, Ks- complex (K, Fe, Mg ,Ca – chloride), O-opaque, Ksx- other solid transparent daughter phases (chloride or silicate), **n**- coeval vapor-rich and brine inclusion trapped from a boiling episode (Damman et al., 1996; Pintea 1996b; Pintea, 2000; 2001ab; Heinrich, 2007). Scale bar in µm.

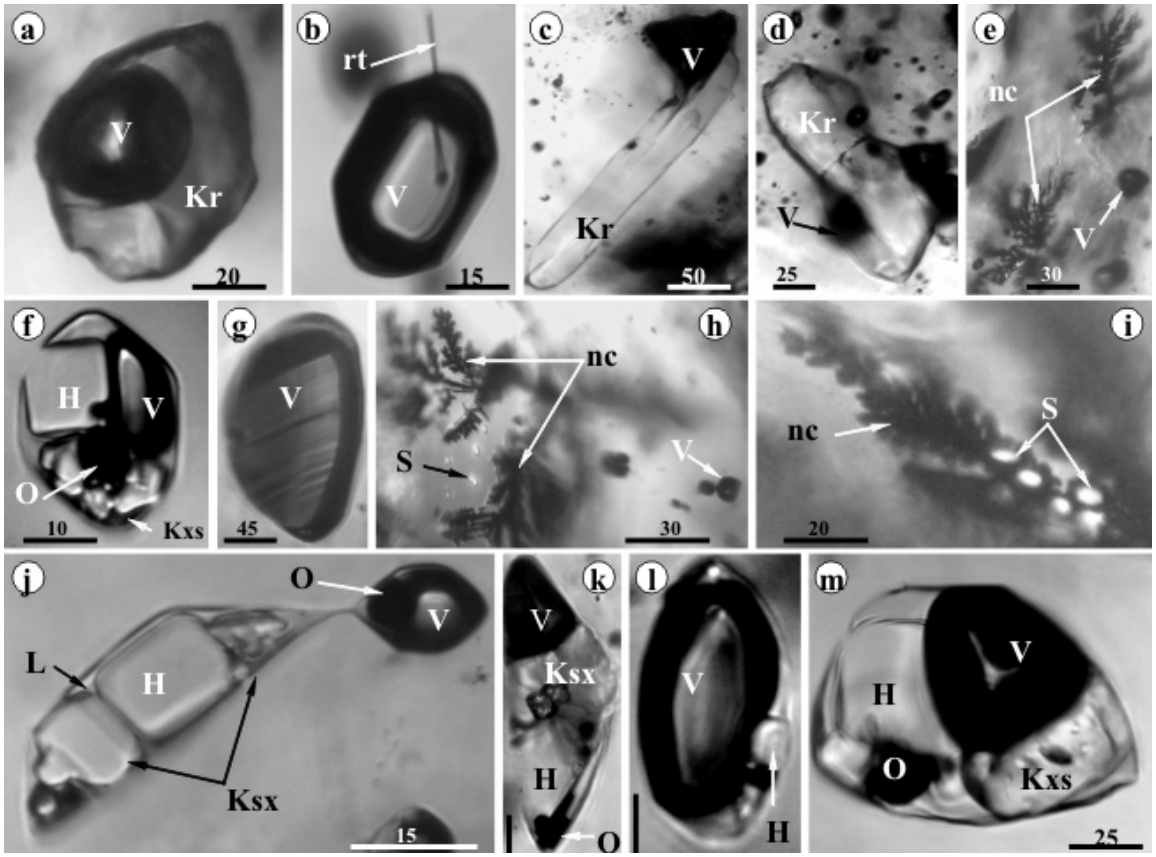

Fig. 38. Various fluid and solid inclusion types in quartz from Roşia Poieni porphyry Cu-Au (Mo) deposit; **a**, **c**, **d**- biphasic with solid remnants (Kr) and vapor (V); **b**, **g**, **l**- vapor rich, V-vapor, rt- rutile, H-halite; **f**, **j**, **k**, **m**- brine, H-halite, O-opaque, Ksy, Kxs- daughter solid phases association (chloride, sulphate, silicate; **e**, **h**, **i-** unknown globular (S) and dendrites (arborescent- nc) feature in microfissures (possible liquid/solid hydrocarbons or sulfide or native Cu). "Crush-leach" solution analyzed by Mass Spectrometry at department of geochemistry of Utrecht University (VG SIRS 24 EM mass spectrometer), showed chlorine isotopes ranges between -0.6 and -0.3‰ relative to the SMOC (Pintea et al., 1999b; Pintea, 2014a). Scale bar in μm.

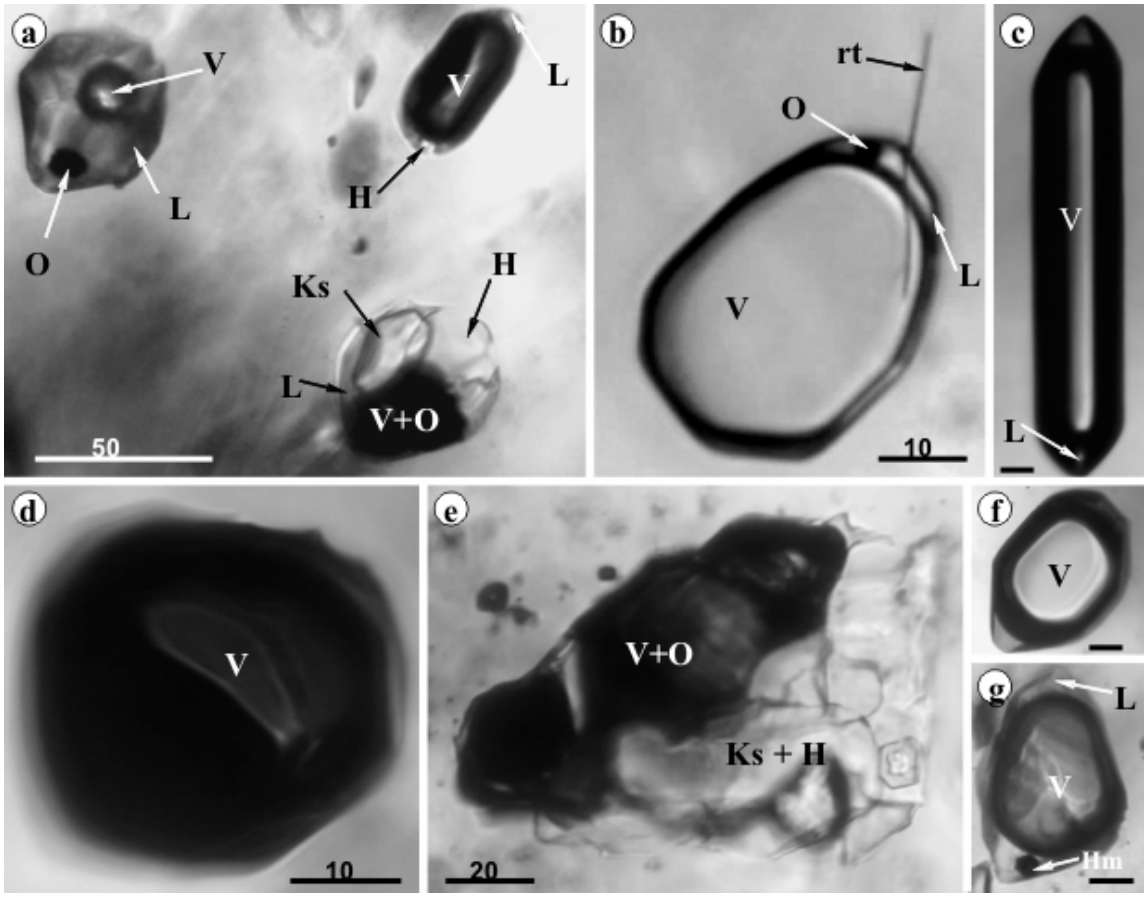

Fig. 39 Coeval association (**a**) of the liquid-rich (L), vapor (V) and brine inclusion containing variable content of liquid (L), vapor (V), halite (H), other chloride (Ks), V-vapor and opaque-O; **b**, **c**, **d**, **f**, **g** – vapor rich inclusions with V-vapor, L-liquid, O-opaque, rt- rutile, Hm-hematite; **e**- decrepitated and recrystallized brine inclusion showing multiple daughter phases association including halite (H), V-vapor, and opaque-O. All inclusions were hosted by quartz crystals from Roşia Poieni porphyry Cu-Au (Mo) deposit. Scale bar in µm; **c**, **f**, **g**-10µm.

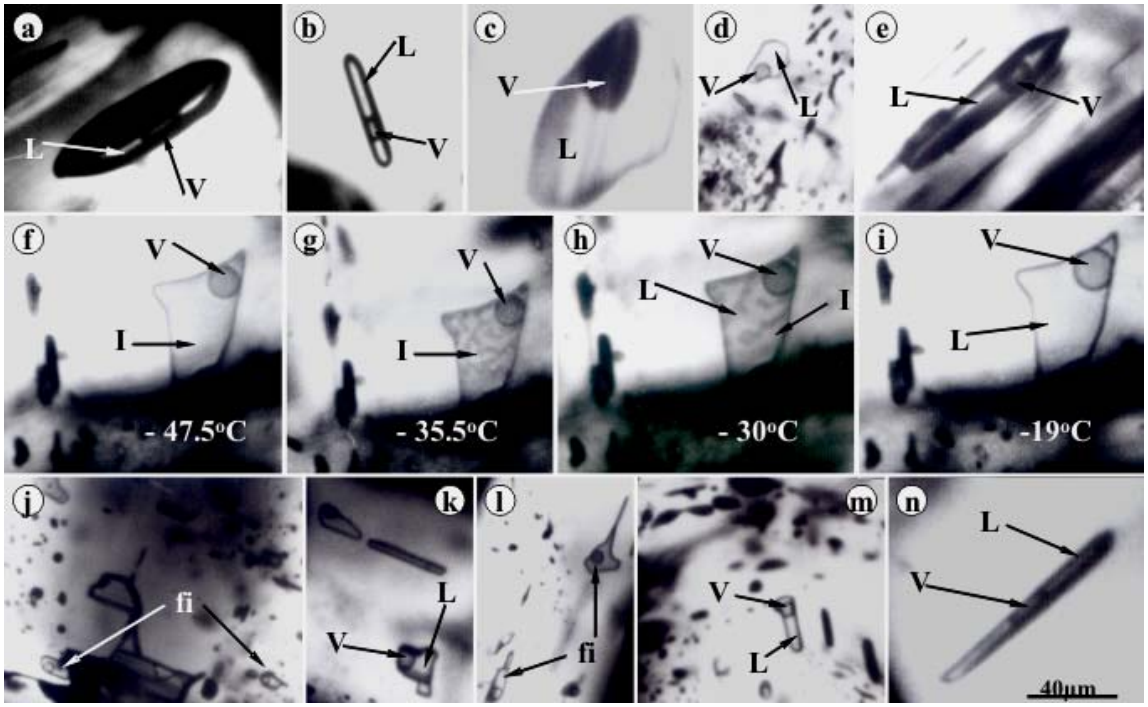

Fig. 40. Fluid inclusions trapped in enargite-luzonite from high-sulfidation epithermal overprinting from the Roşia-Poieni porphyry Cu-Au(Mo) deposit (L. Bailly, com. pers., 2002); **a**, **b**, **c**, **e**, **n**- primary liquid-rich inclusions, L-liquid, V-vapor; d, j, l, m-pseudosecondary fluid inclusions (fi) with liquid (L) and vapor (V) phases; f, g, h, i-microthermometric sequences at indicated temperatures, I-ice, V-vapor, L-liquid. From 29 determinations Th (homogenization temperatures) = 243-284°C and salinity = 4.03-14.15 wt% NaCl eq. (Pintea, 2008a; 2012). Scale bar from n in all microphotographs.

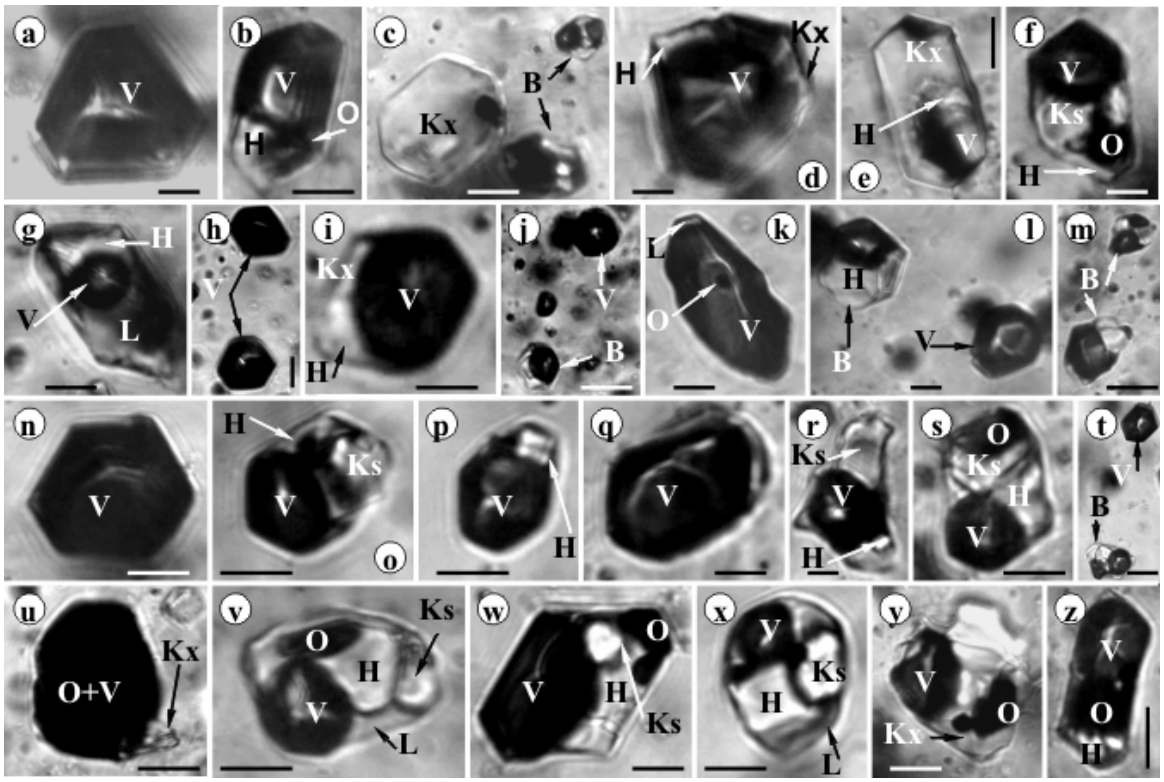

Fig. 41. Fluid-, brine-, vapor-rich and solid microcrystals from Tarniţa porphyry copper deposit (belonging to the Roşia Montană-Roşia Poieni-Bucium-Tarniţa caldera zone from Metaliferi Mountains, (e.g. Popescu and Neacşu, 2012); **a**, **b**, **d**, **h**, **i**, **k**, **n**, **p**, **q**, **u**, **w**- vapor rich inclusions; **c**, **g**, **f**, **m**, **o**, **r**, **s, v**, **x**, **y**, **z –** brine inclusions**; c, e -** microcrystals sometimes with attached brine; **j**, **l**, **m**, **t**- coeval brine(B) and vapor-rich inclusions. V-vapor, H- halite, O-opaque, Ks, Kx- anhydrite, silicate or other solids, L-liquid. Microthermometry: brine inclusions frequently floating in silicate melt at Th=885°-969°C, salinity=68 wt%NaCl eq., P=1.1-1.5kbars (Pintea, unpubl.); Scale bar 10µm.

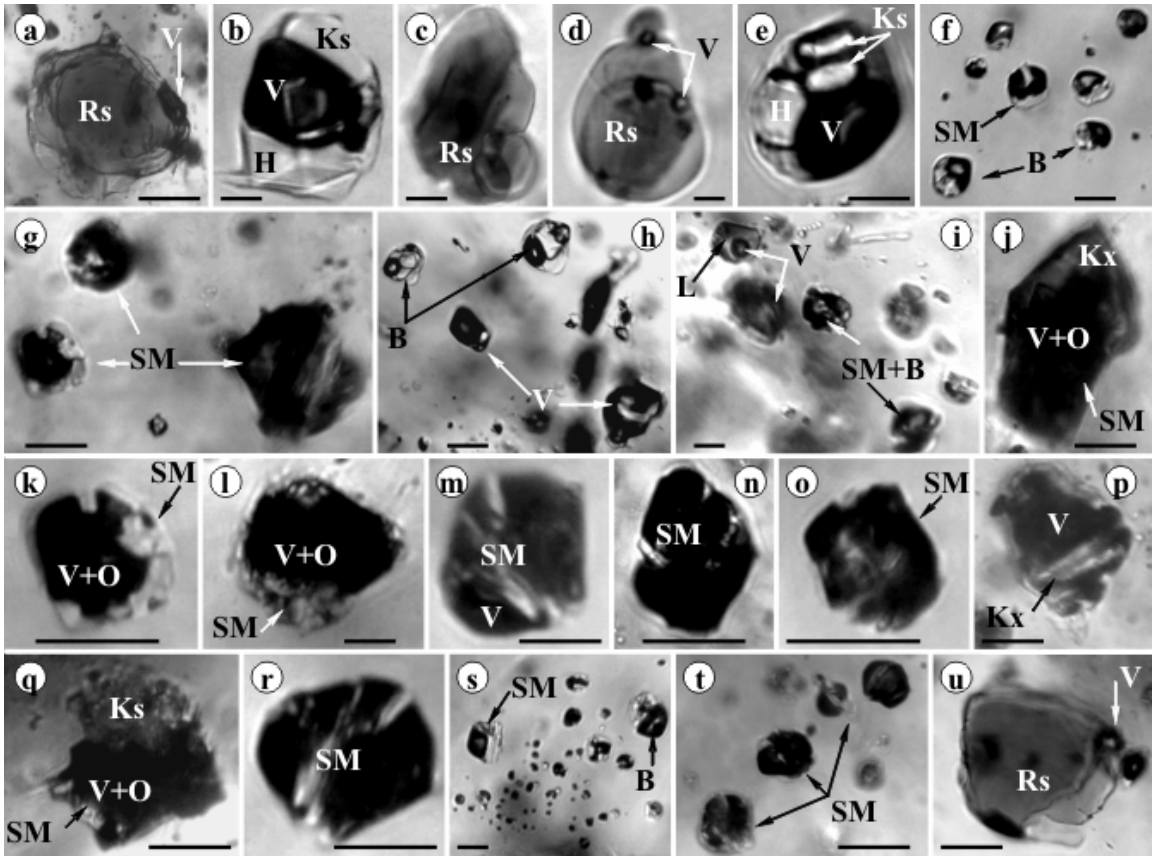

Fig. 42. Magmatic hydrous silicate-, and hydrous saline melt inclusions from quartz grains in veinlets from the Bolcana porphyry Au-Cu (Mo) –Metaliferi Mountains; **a**, **c**, **d**, **u**- restitic solid microcrystals or glass inclusions; **b**, **e**, **h**- brine inclusions; **f**, **g**, **i**, **j**, **k**, **l**, **m**, **n**, **o**, **p**, **q**, **r**, **s**, **t**- silicate melt inclusions (SM) often coeval with vapor-rich (V) and/or brine (B) inclusions. Generally, silicate melt inclusions are completely recrystallized after trapping and their petrography and microthermometry encountered by many difficulties (Student and Bodnar, 2004). V-vapor, H-halite, Ks, Kx-solid salt or silicate daughter phases. Scale bar: 10μm.

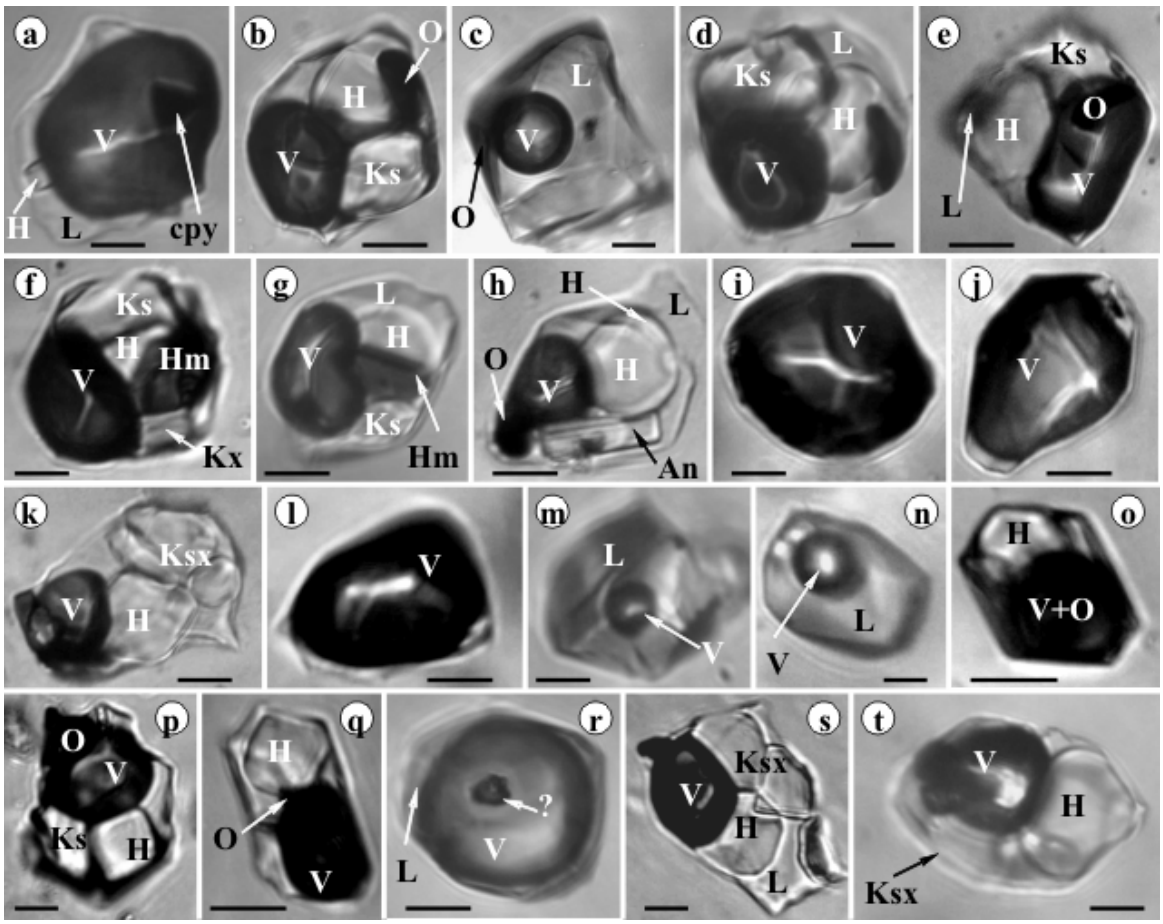

Fig. 43. Fluid inclusion types trapped in the quartz veinlets from the potassic zone of the Bolcana porphyry Au-Cu (Mo) deposit (Metaliferi Mountains); **a**, **i**, **j**, **l**, **r**- vapor-rich inclusions; **b**, **d**, **e**, **f**, **g**, **h**, **k**, **o**, **p**, **q**, **s**, **t**- brine inclusions; **c**, **m**, **n**- aqueous liquid-rich inclusions. H-halite, cpy- chalcopyrite, O-opaque, L-liquid, V-vapor, Ks, Kx, Ksx- solid salt and/or silicate daughter phases, An- anhydrite, ?-unknown. Scale bar: 10µm. Petrography and microthermometry were published (e.g. Pintea, 1996a, Milu and Pintea, 2001; Cioaca, 2011; Dénes et al., 2014). Scale bar: 10µm.

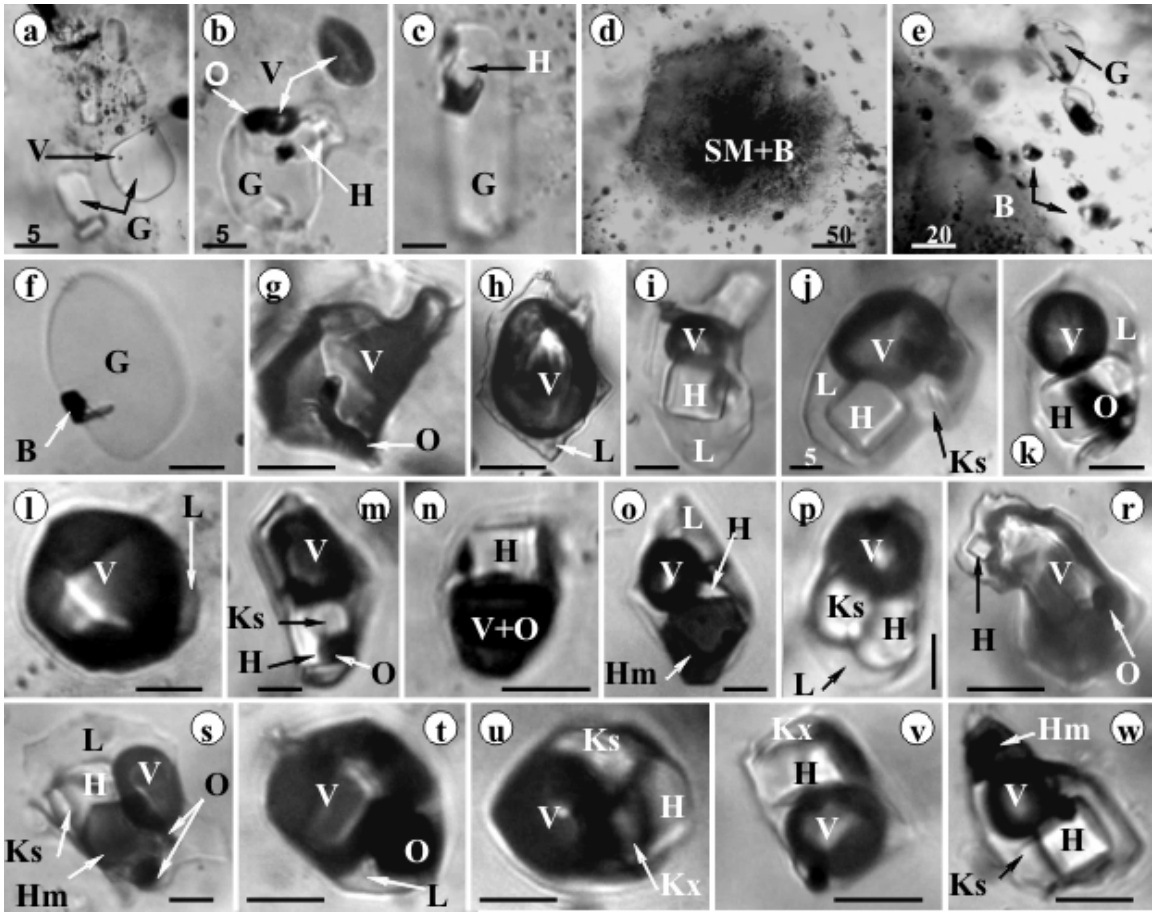

Fig. 44. Fluid and melt inclusions types from the deep potassic zone of the Bolcana porphyry Cu-Au (Mo) deposit. Alteration and mineralization associations described from the column of F4 drill-hole (Milu et al., 2003). **a**, **b**, **c**, **d**, **e**, **f**- silicate melt inclusions (SM); **g**, **h**, **l**, **n**, **r**, **t**- vapor rich inclusions; **i**, **j**, **k**, **m**, **o**, **p**, **s**, **u**, **v**, **w**- brine inclusions (B); V-vapor, G-glass, H-halite, O-opaque, L-liquid, Hm-hematite, Ks, Kx - other solid daughter phases (complex chloride, anhydrite, silicate). Scale bar: 10µm.

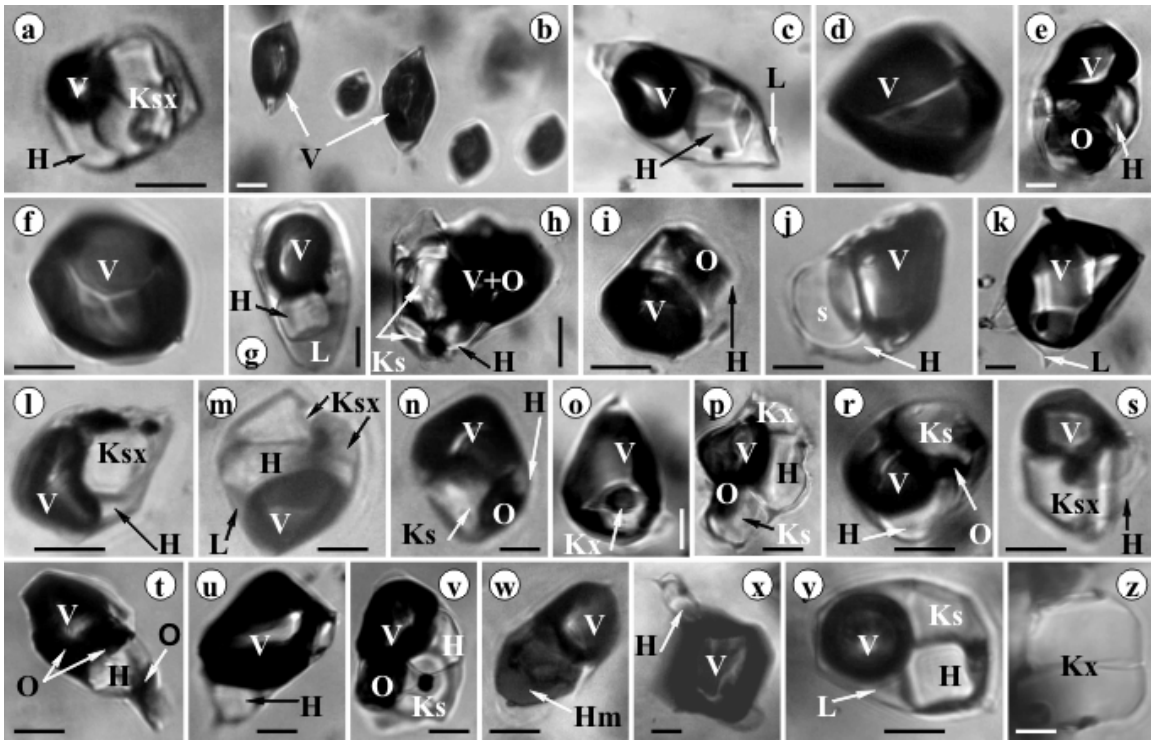

Fig. 45. Fluid and solid inclusions types from Bucuresci-Rovina porphyry copper deposit (from Metaliferi Mountains - Boştinescu, 1984); **a**, **c**, **e**, **g**, **h**, **i**, **j**, **l**, **m**, **n**, **p**, **r**, **s**, **t**, **v**, **w**, **y-** brine inclusions; **b**, **d**, **f, k**, **o**, **u**, **x-** vapor-rich inclusions; z- solid microcrystal, sometimes with attached brine. Informative microthermometry (Pintea, 1996b and unpubl. data): Th= 598-1017°C, 0.6-1.6 kbars, 56-70 wt% NaCl equiv. Scale bar:10µm.

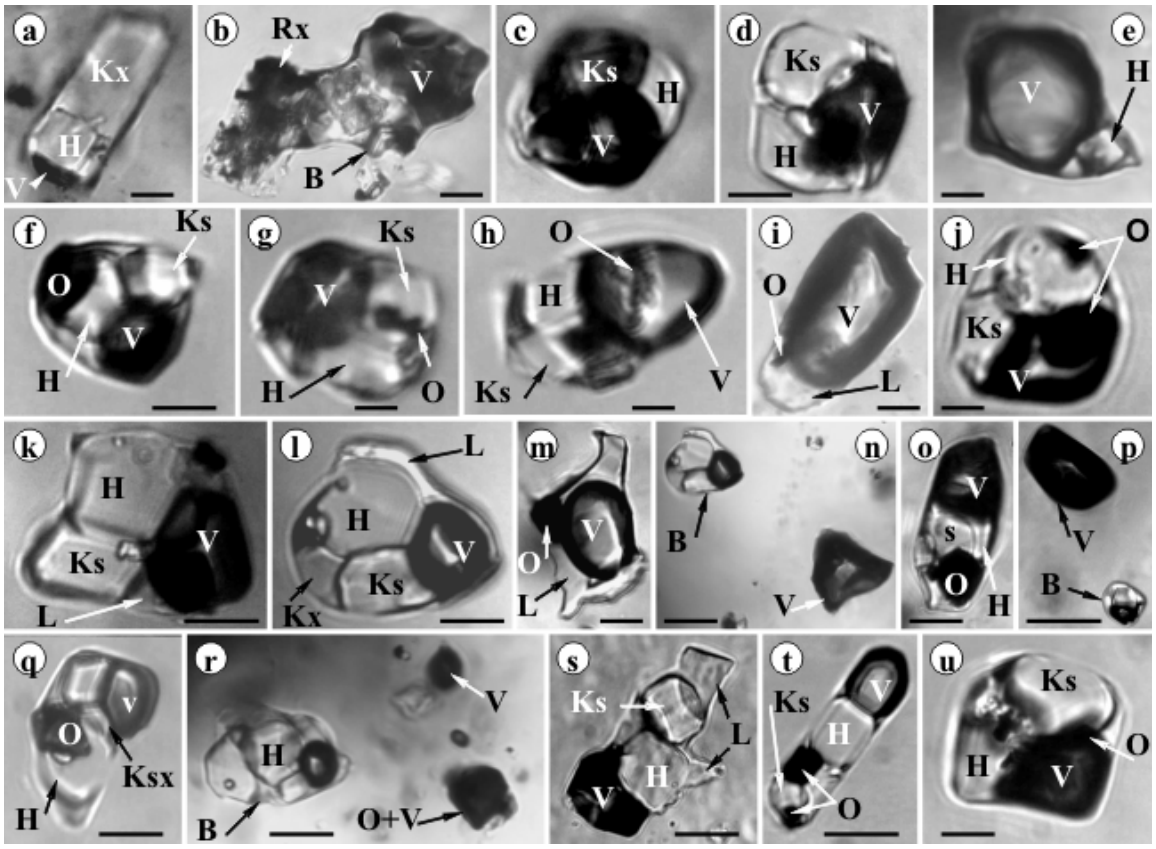

Fig. 46. Fluid inclusions types from Valea Morii porphyry Cu-Au (Mo) deposit (Metaliferi Mountains); **a**, **b**- solid microcrystals with brine; **c**, **d**, **f**, **g**, **h**, **j**, **k**, **l**, **o**, **p**, **s**, **t**, **u**- brine inclusions; **e**, **i**, **m**- vapor rich inclusions; **n**. **p**, **r**- coeval brine(B) and vapor rich (V) inclusions; V-vapor, H-halite, Rx- solid remnants, Ks, Kx, Ksx- other solid daughter phases, O-opaque. Petrography and microthermometry were documented by Pintea, 1996b; André-Mayer et al., 2001; Nedelcu et al., 2001; Kouzmanov et al., 2003). Silicate melt inclusions in plagioclase were studied by Grancea et al., 2001. Scale bar: 10µm.

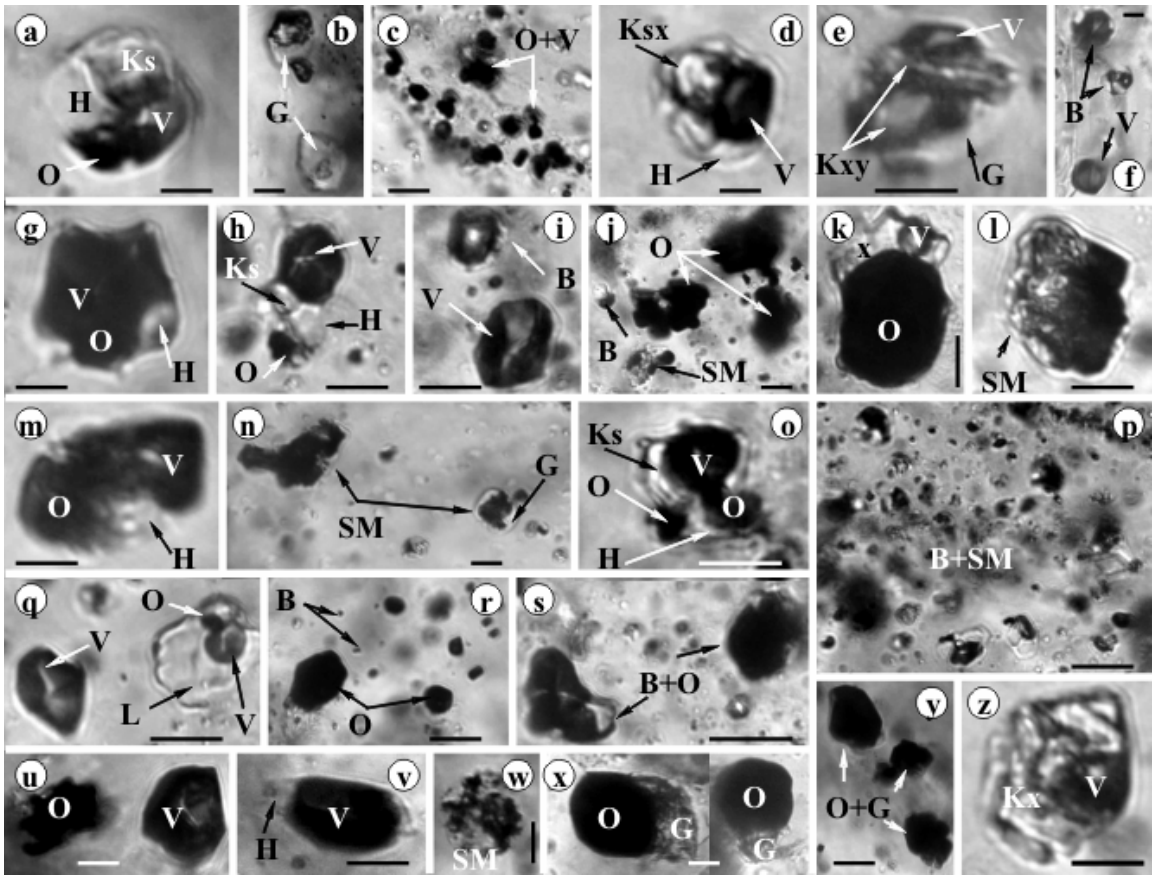

Fig. 47. Fluid and melt inclusions types from the endogenous (autometasomatism- Roşu et al., 2001, Pintea, 2010) zone from the Valea-Morii – Barza underground (Spiros adit; Nedelcu sample courtesy); **a**, **d**, **h**, **m**, **o** – brine inclusions; **b**, **d**, **h**, **m**, **o**- silicate melt inclusions, **v**- vapor – rich inclusions; **c**, **f**, i, **j**, **p**, **q**, **r**, **s**, **u**,- coeval inclusions of different phases as opaque-vapor, brine (B)- silicate melt (SM), vapor-liquid, sulfide – vapor; V-vapor, L- liquid, H-halite, O-opaque, x-unknown, Ks, Kx- solid daughter phases, G-glass. Microthermometry (Pintea, 2014, unpubl.): 420-1060°C, 0.2-1.5 kbars, 44-73 wt% NaCl eq. Scale bar: 10 µm.

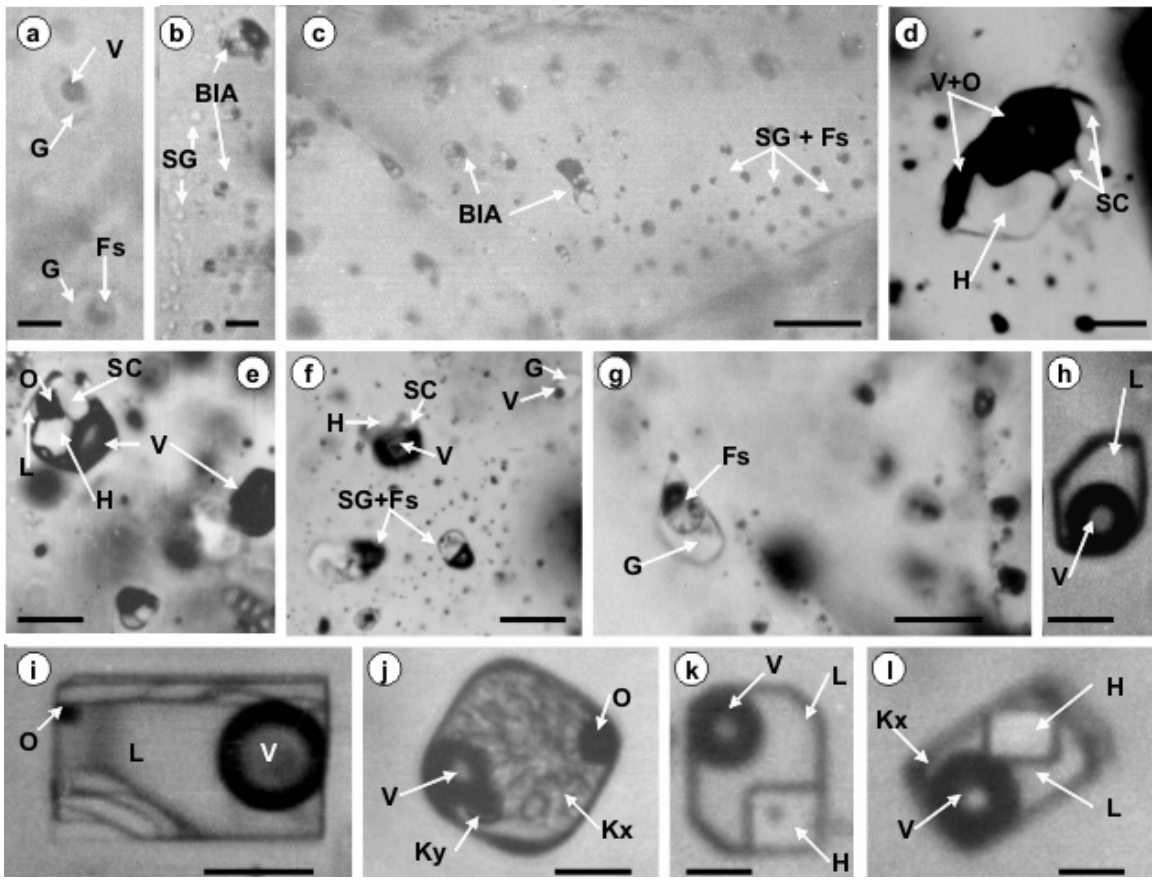

Fig. 48. Fluid and melt inclusions from Bolcana, Valea Morii and Tălagiu trapped in quartz and anhydrite; **a**, **b**, **c** - coeval silicate melt and brine assemblages (BIA) as heterogeneous mixtures, rejuvenated after microthermometry up to 1000°C (Bolcana-Pintea, unpubl.); **f**, **g**- heterogeneous inclusions containing silicate glass and brine from quartz at Valea Morii porphyry Cu-Au(Mo) deposit (microthermometry: Th=665°C, Salinity = 63 wt% NaCl eq., P = 0.7 kbars- Pintea, 2008a); **d**, **e** - brine inclusions from quartz and **h**, **i**, **j**, **k**, **l** fluid inclusions types in anhydrite from Talagiu porphyry Cu-Au(Mo) deposit; V-vapor, G-glass, Fs-brine, SC- another salt or silicate solid daughter phases, L-liquid, Kx, Ky-unknown, H-halite, O-opaque. Scale bar: 10μm.

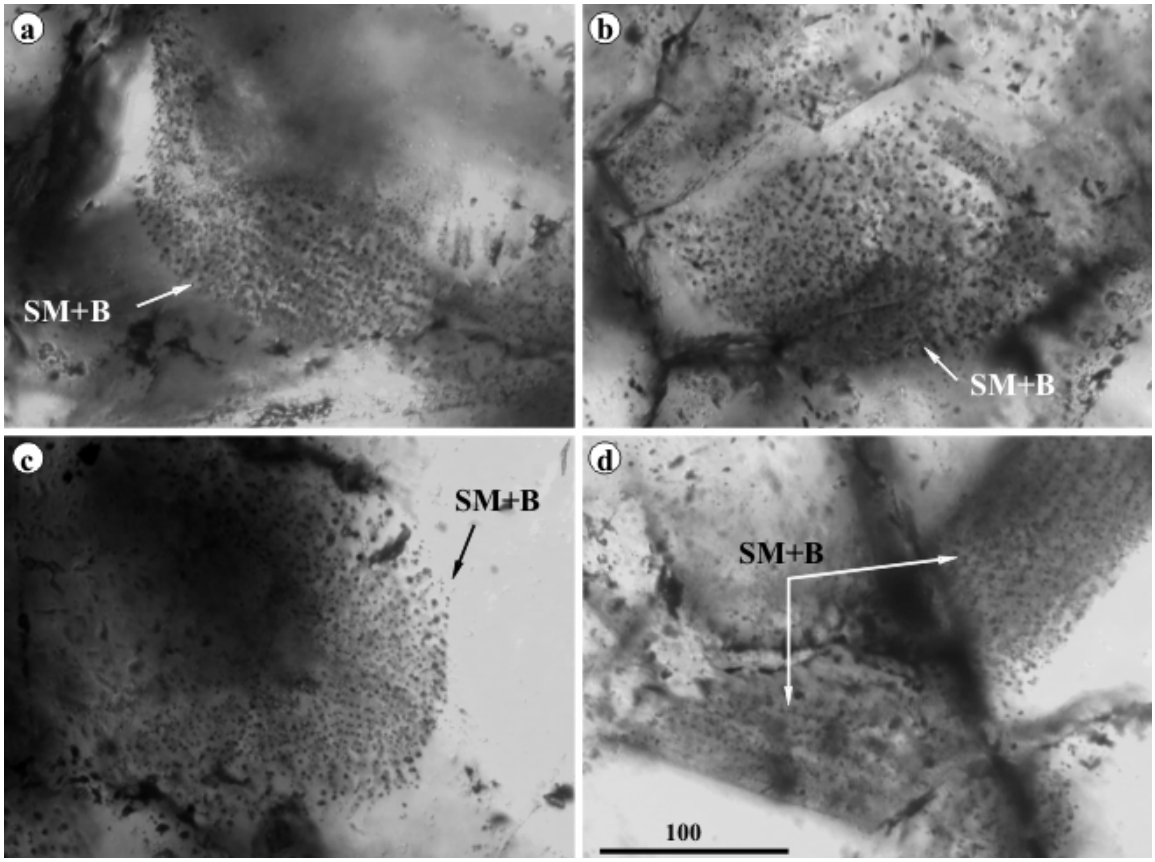

Fig. 49. Internal (re)crystallized microtexture features in the quartz grains from veinlets in the potassic zone of the Tălagiu porphyry Cu-Au (Mo) deposit. Tiny silicate melts (SM) and brine (B) inclusions are the main components decorating the growth zones. Because their small size are very difficult to be study by petrography and microthermometry (e.g. Student and Bodnar, 2004); Scale bar in µm.

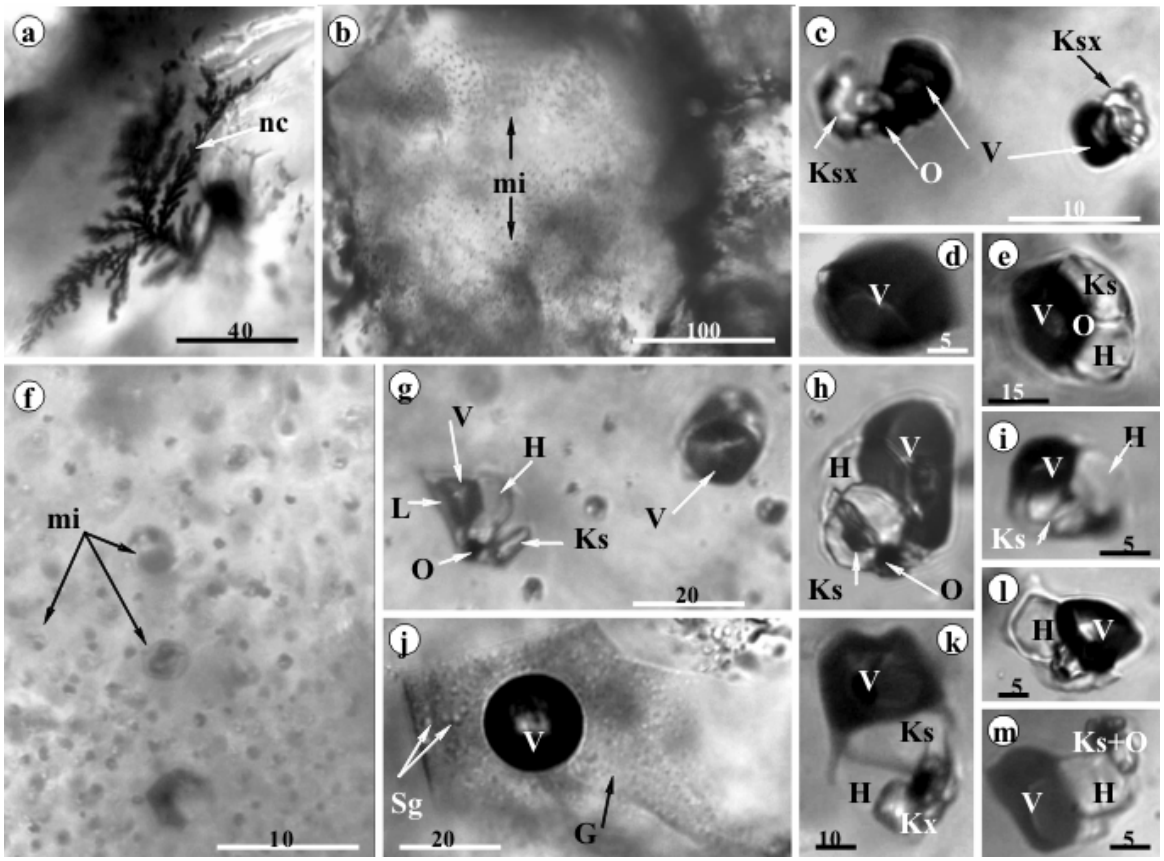

Fig. 50. Fluid and melt (solid) inclusions from Tălagiu porphyry Cu-Au(Mo) deposit; **a**- unknown dendrites feature (nc) formed by (sulphides, native copper, possible solid hydrocarbons or phosphate phases -?; **b**, **f**, **j**- complex melt inclusions (mi) including brine, silicate glass (g), silicate globules (Sg) and vapor (V); **c**, **e**, **h**, **i**, **k**, **l**, **m**- brine inclusions without liquid phase at Troom conditions; **d**- vapor-rich inclusion; **g**- coeval (boiling) brine and vapor-rich inclusions; V-vapor, H-halite, L-liquid, Ks, Kx- other solid daughter phases (complex chloride, sulphate, silicate), O- opaque. Scale bar in µm. Petrography and microthermometry were documented by Pintea, et al., 1992; Pintea, 1996 – unpubl.; Stovold, 2009 – unpubl. (web item 21035474). Traces of CO_2, CH_4, and H_2S were detected by CG/MS in quartz and anhydrite (Cuna et al., 2001); Scale bar in µm.

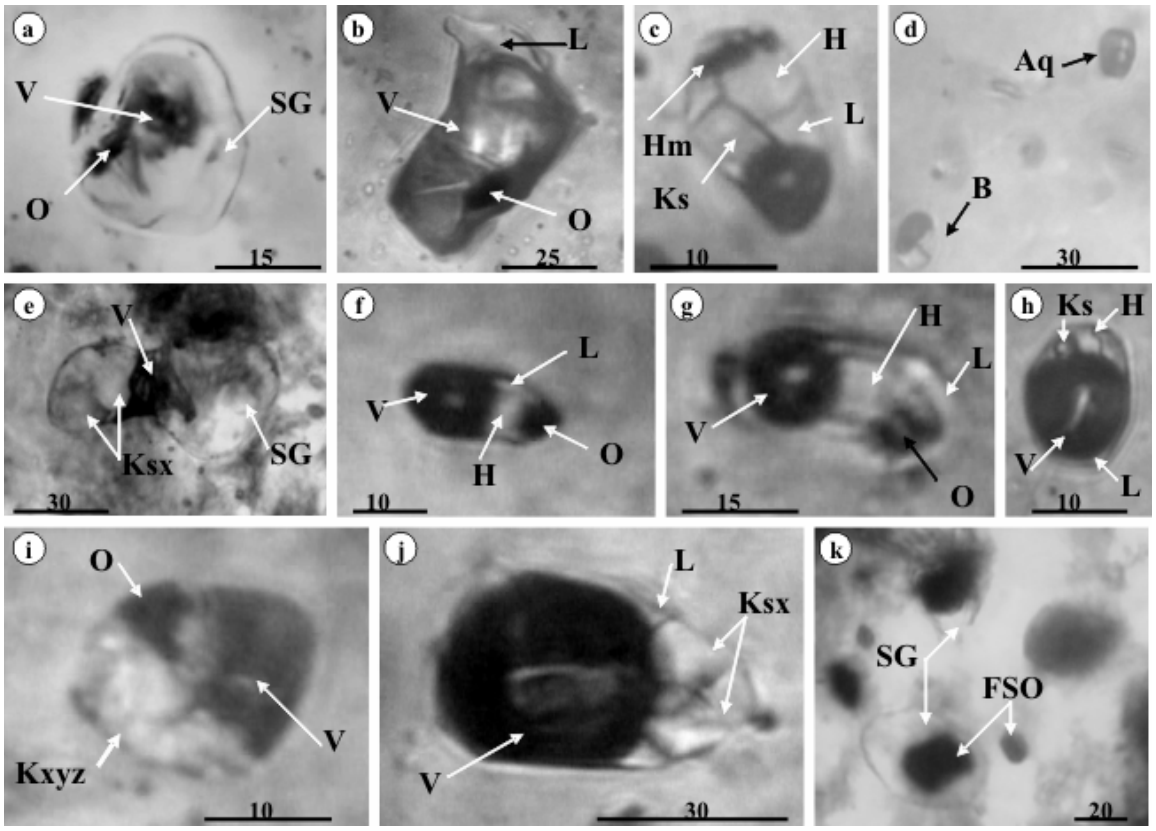

Fig. 51. Melt and fluid inclusions types inherited in a rounded quartz-veinlet fragment (xenoliths) from propylitic andesite suggesting the collapse of the volcanic edifice after Tălagiu porphyry copper system genesis, overprinted by high–sulphidation mineralization (Pintea, 2012- unpubl.); **a**, **e**, **k**- complex silicate melt (SG) and fluid (FSO); **b**, **h**, **j**- vapor rich inclusions; **c**, **f**, **g**, **i**- brine inclusions, **d**- coeval (boiling) brine (B) and biphasic aqueous (Aq) inclusions; V-vapor, L-liquid, O-opaque, Ksx, Ks, Kxyz- other solid daughter phases (complex chloride, sulphate, silicate). Microthermometry (Pintea, 2012-unpubl.): Th = 618-1037°C, P= 0.5-2.2 kbars, salinity = 52-81 wt % NaCl eq. Scale bar in µm.

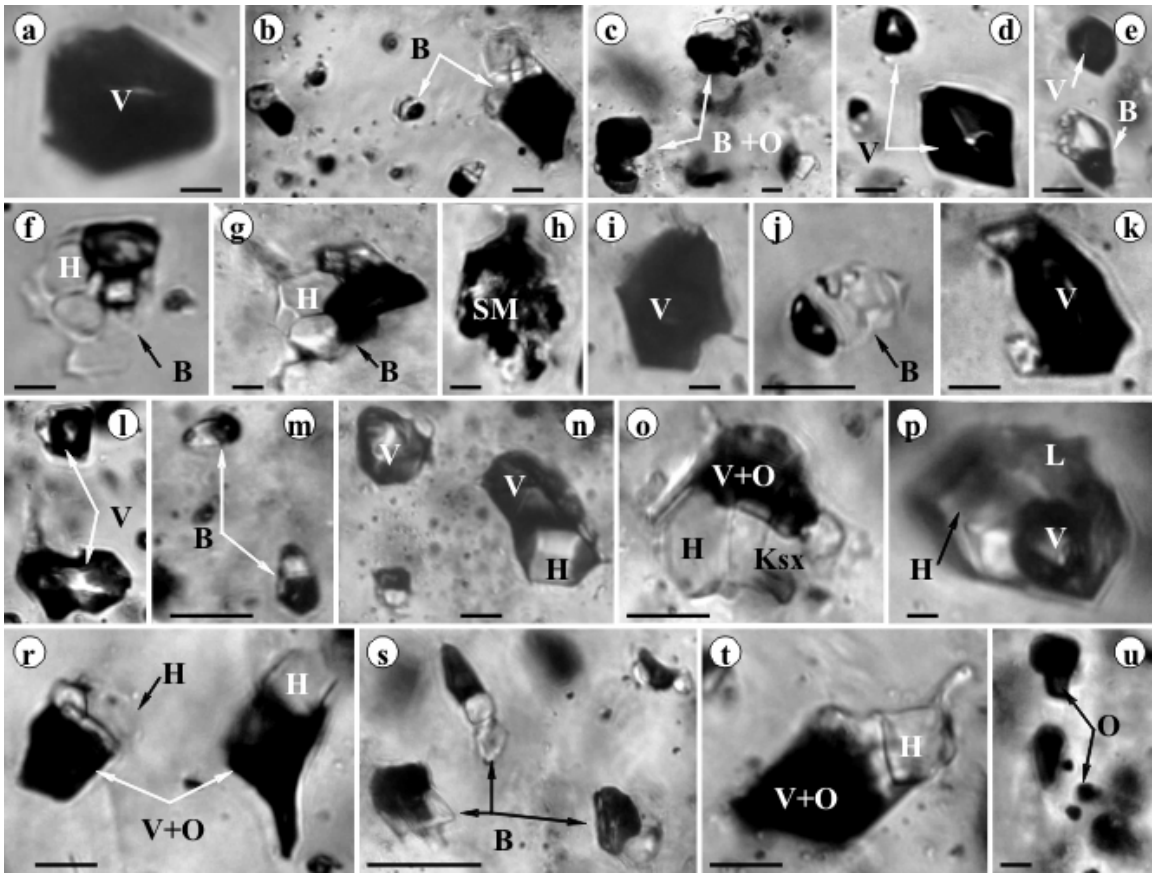

Fig. 52. Fluid and melt inclusion types from quartz sampled from drill-holes S1 (Dl Roatei – Larga , M. Borcoş- sample courtesy), L1, L2 (Larga –Trâmpoiele; L. Nedelcu –sample courtesy) from Larga-Trâmpoiele porphyry Cu-Au(Mo) deposit in the Zlatna zone (Pintea, 1998- unpubl.); **a**, **d**, **i**, **k**, **l**- vapor – rich inclusions; **b**, **c**, **f**, **g**, **j**, **m**, **o**, **p**, **r**, **s**, **t**- brine (B) inclusions; **h**- silicate melt inclusion (SM); **e**, **n**- coeval brine (B) and vapor rich (V) inclusions; **u**- globular opaque (sulphide); V-vapor, O-opaque, H-halite. Scale bar: 10μm.

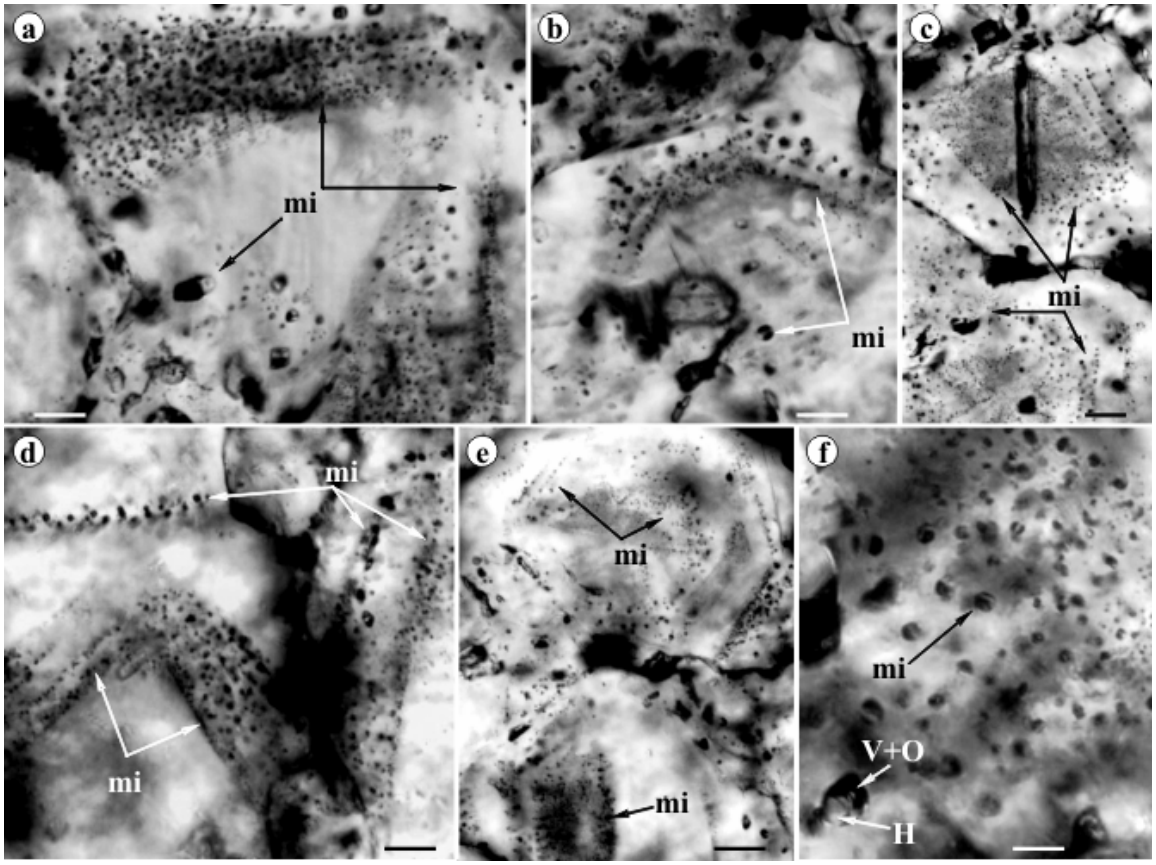

Fig. 53. Primary melt inclusion assemblages (mi) decorating growth zones in quartz grains in veinlets from Moldova Nouă Upper Cretaceous porphyry Cu-Mo (Au) deposit (**a**, **b**, **c**, **d**, **e)**. Some of these features could be generated by grain boundary dynamic recrystallization (in a similar way as in experimental run product of several analogues, (i.e. Schmatz and Urai, 2008). It is suggested that immiscible fluid globules were dispersed in a hydrosilicate matrix formed by metasomatic reactions between supercritical fluids and crystallizing country rocks during stock formation. Their generation is possibly related to the hydrosilicate recrystallization processes (e.g. Vasyukova, 2011) showing internal euhedral zonation (phantom) and isolated or trail of inclusions in the former grain boundaries; **f-** the petrography and microthermometry is difficult to be done especially because their small size (obviously less than 10μ) and are completely recrystallized (e.g. Student and Bodnar, 2004). Scale bar: 50 μm.

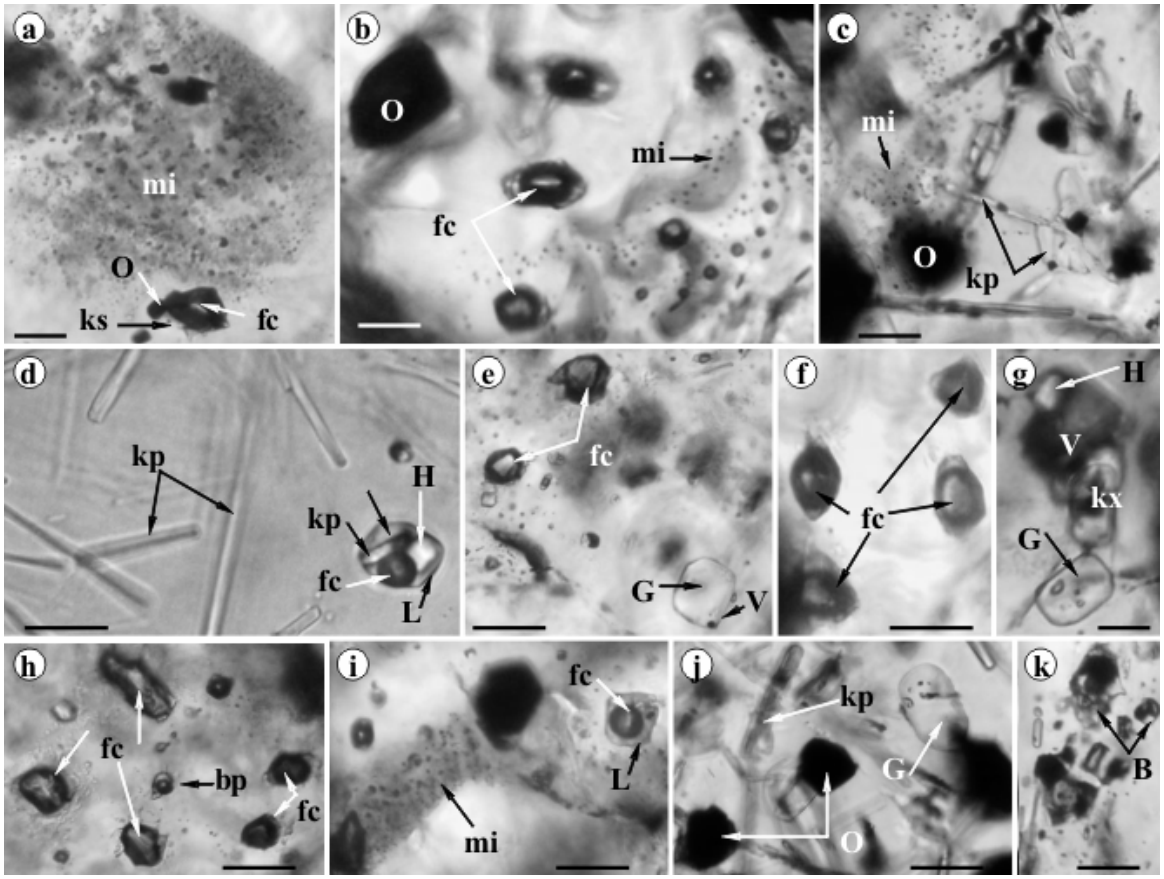

Fig. 54. Fluid and melt inclusions types from the Moldova Nouă (Suvorov) porphyry Cu-Mo (Au) deposit; **a**, **i**- Recrystallized quartz grain microtexture decorated by silicate melt inclusion assemblages (mi); **b**, **e**, **f**, **h**- vapor rich inclusion containing complex fluid mixture (fc) of (H_2O + CO_2), suggested by the presence of a second bubble or solid hydrate at low temperature; **c**, **d**, **e**, **g**, **j**, **k**- solid microcrystals (kp) and silicate glass inclusions (G); **b**, **j**, **k**-opaque globular sulphides (O); V-vapor, H-halite. Scale bar: 50 µm.

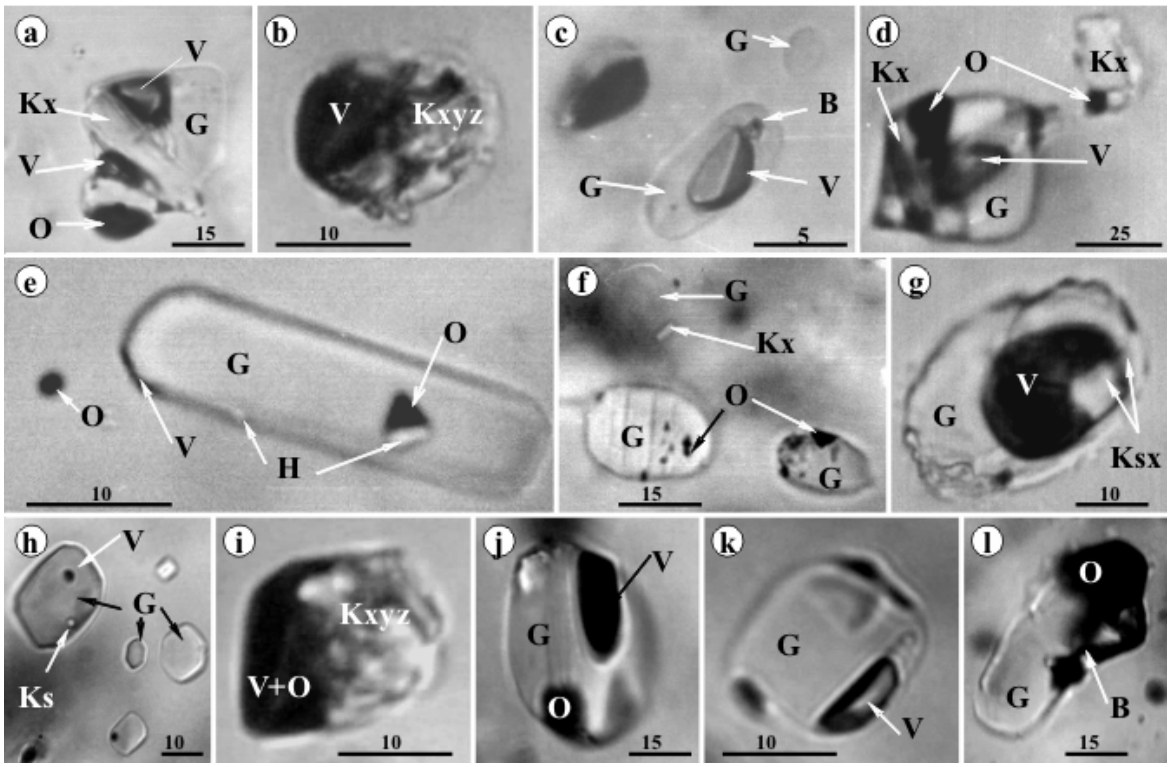

Fig. 55. Silicate melts inclusion types from Upper Cretaceous porphyry Cu-Mo (Au) deposits. **a**, **c**, **d**, **e**, **f**, **g**- Oraviţa (Nicolae adit); **b**, **h**, **i, j**, **k**, **l**- Moldova Noua; V-vapor, H-halite, Kx, Ksx, Kxyz, Ks-other solid daughter phases (i.e. chloride, silicate, sulfate), G-glass, O-opaque, L-liquid, B-brine (L+V+H+O); Microthermometry of the complex inclusion from **e** indicated Th=925°C, salinity=52 wt% NaCl eq, P=1.8 kbars and the opaque phases melted completely at Tm= 909°C, becoming an immiscible opaque phase stable up to 1037°C where the experiment was stopped (Pintea in Roşu et al., 2002-unpubl.). Scale bar 10 μm.

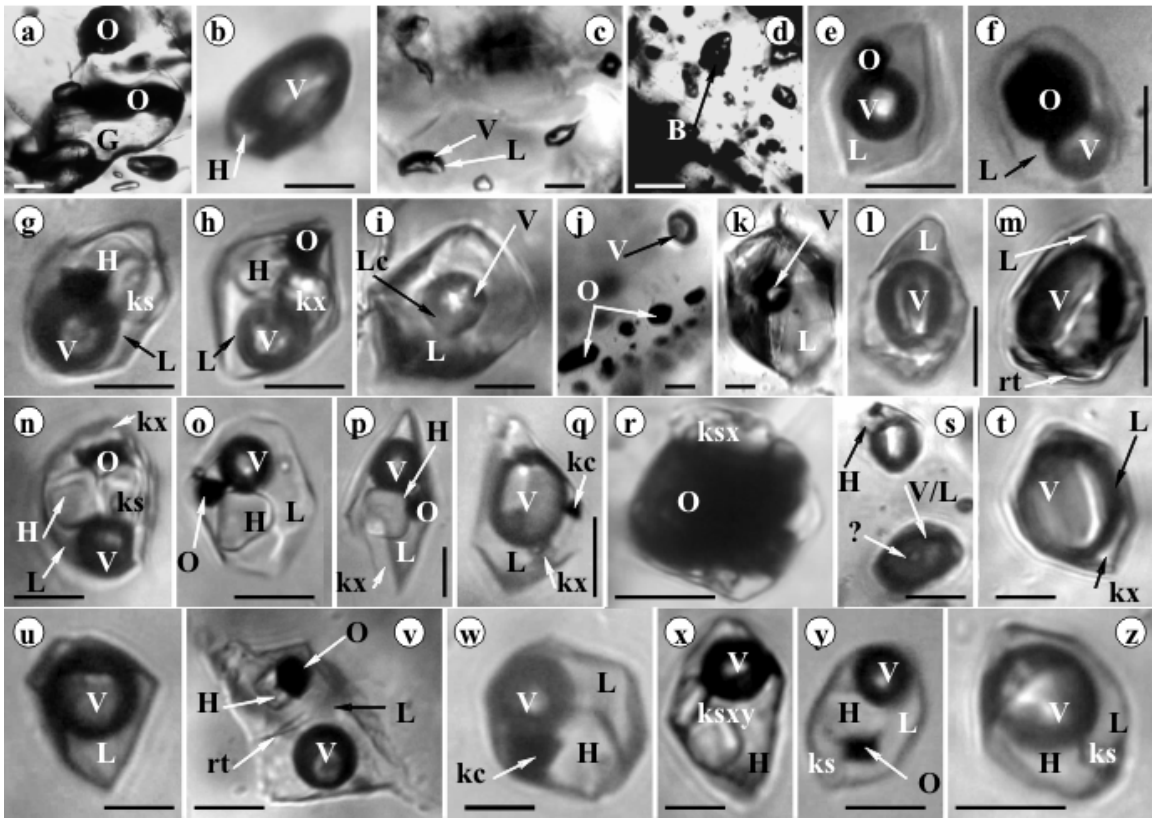

Fig. 56. Silicate melt and fluid inclusion types from garnet and quartz from the potassic zone or the Moldova Noua porphyry Cu-Mo (Au) deposit; **a**, **b**, **c**, **d**- glassy, vapor-rich and brine inclusions from garnet; **e**, **i**, **k**, **l**, **m**, **q**, **t**, **u**, **z**- aqueous rich + vapor inclusions; **g**, **h**, **n**, **o**, **p**, **v**, **w**, **x**, **y**- brine inclusions; **f**, **j**, **r**- opaque dominated inclusions; O-opaque, B-brine, G-glass, H-halite, V-vapor, L-liquid, ks, kx, ksx, ksxy- other daughter solid phases, kc-chalcopyrite or nantokite(?), rt- rutile, ?- vapor bubble or solid at Troom; V/L- carbonic vapor rich or liquid carbonic phase at Troom (?), (e.g. Rusk et al., 2008). Scale bar in µm. Microthermometry of brine inclusions from Moldova Nouă and other porphyry Cu-Mo (Au) deposits (Pomârleanu and Întorsureanu, 1986; Pintea, 2002; Pintea in Roşu et al., 2002- unpubl.), evidentiated Th between 350° and up to 1050°C, salinity = 32 - 76 wt% NaCl eq., P= 0.1-1.9 kbars, suggesting boiling episodes and sulfide/oxide-silicate-chloride magmatic immiscibility. Endogenous metasomatism is also emphasized (Pintea, 2010).Scale bar: 10µm.

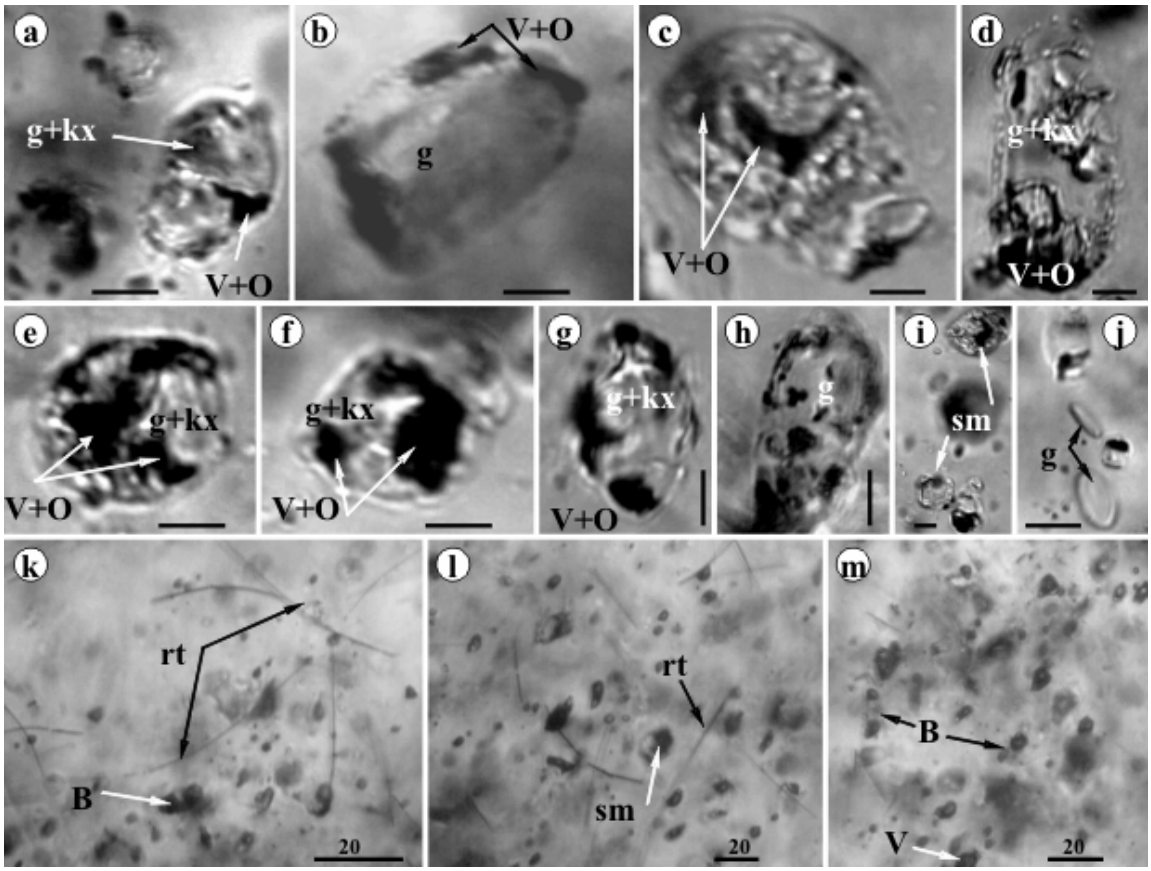

Fig. 57. Fluid and melt inclusions types in quartz grains from Sasca-Montana porphyry Mo-Cu deposit (Upper Cretaceous); **a**, **b**, **c**, **d**, **e**, **f**, **g**, **h**, **i**, **j**- silicate melt inclusions; g-silicate glass, kx-solid daughter phases (silicate, possible chloride, anhydrite etc); **k**, **l**, **m**- fluid and melt inclusions; B- brine and aqueous biphasic inclusions, rt- rutile needles, V-vapor. Scale bar: 10µm.

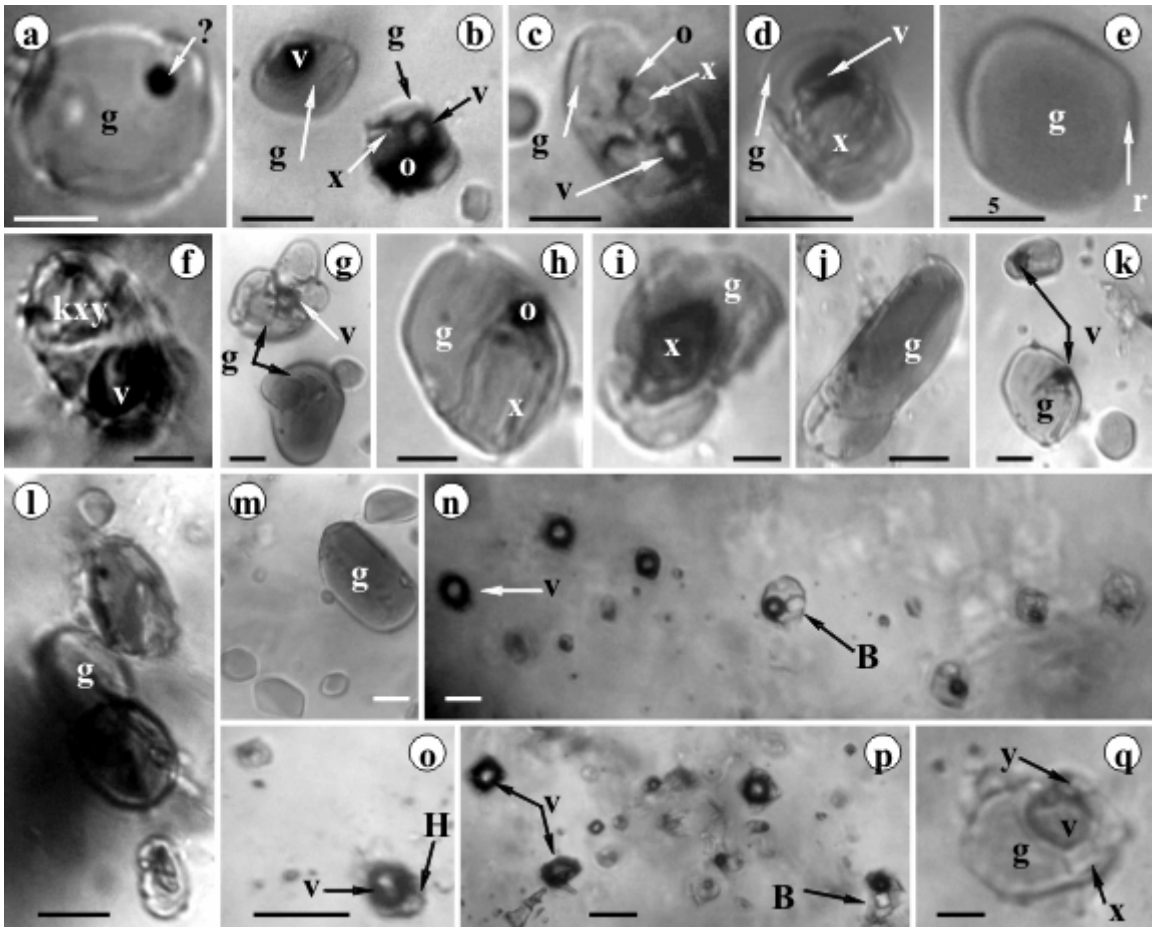

Fig. 58. Fluid and melt inclusions types in quartz veinlets from the Bocşa granititic massif ("Cracul cu Aur" creek); **a**, **b**, **c**, **d**, **e**, **f**, **g**, **h**, **i**, **j**, **k**, **l**, **m**, **q**- silicate melt inclusions; g-glass, x- crystallized daughter phases, o-opaque, V-vapor,?-unknown; **n**, **o**, **p**-vapor-, liquid-rich and brine (B) inclusions, H-halite., r-silicate rim. Scale bar: 10μm.

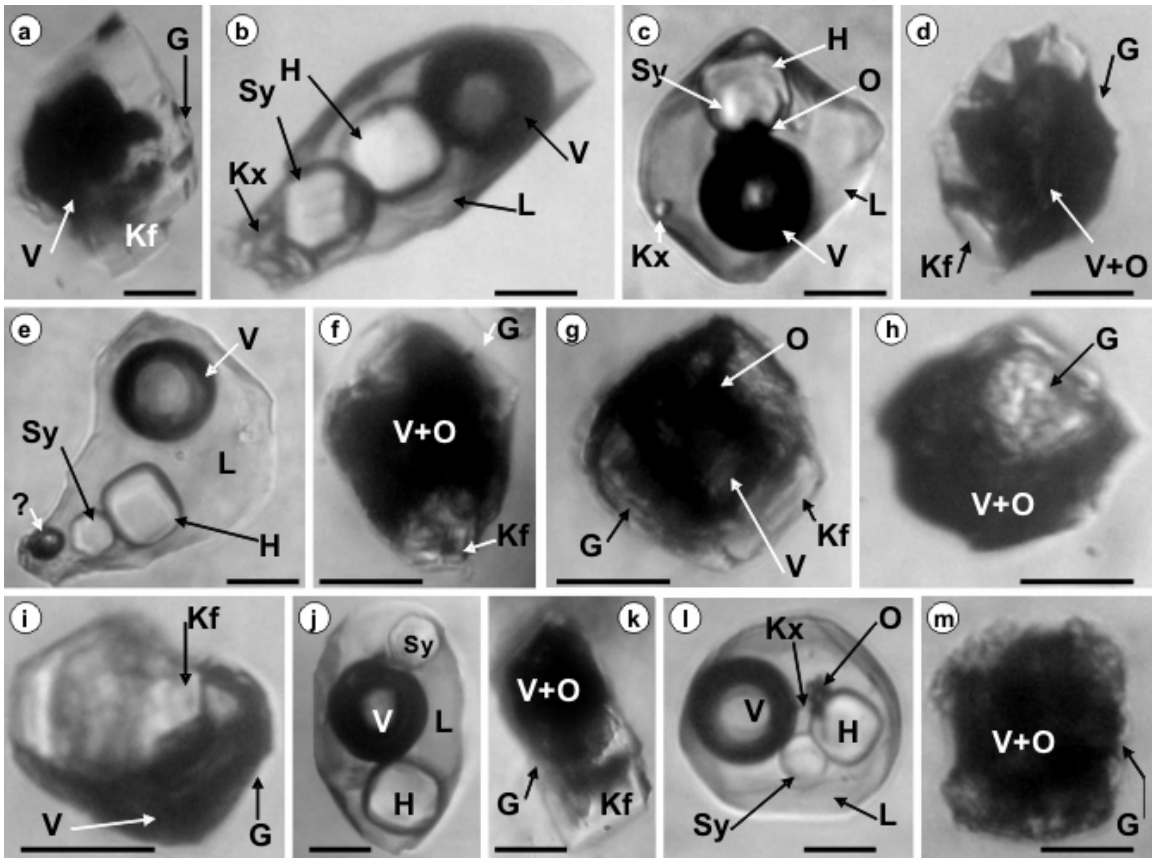

Fig. 59. Hydrous silicate melt and brine inclusions trapped in miarolitic smoky quartz from Vlădeasa granite (North Apuseni Mountains, upper Cretaceous); **a**, **d**, **f**, **g**, **h**, **i**, **k**, **m**- completely crystallized silicate melt; **b**, **c**, **j**, **l** - brine inclusions; V-vapor, G-glass, Kf- orthoclase, H-halite, Sy-sylvite, Kx- other solid daughter phase (chloride, silicate, sulfate), O- opaque, L-liquid; Microthermometry under microscope at 1 bar, indicated Th= 979-1083°C (n=10; Pintea, 2012); Scale bar 10µm.

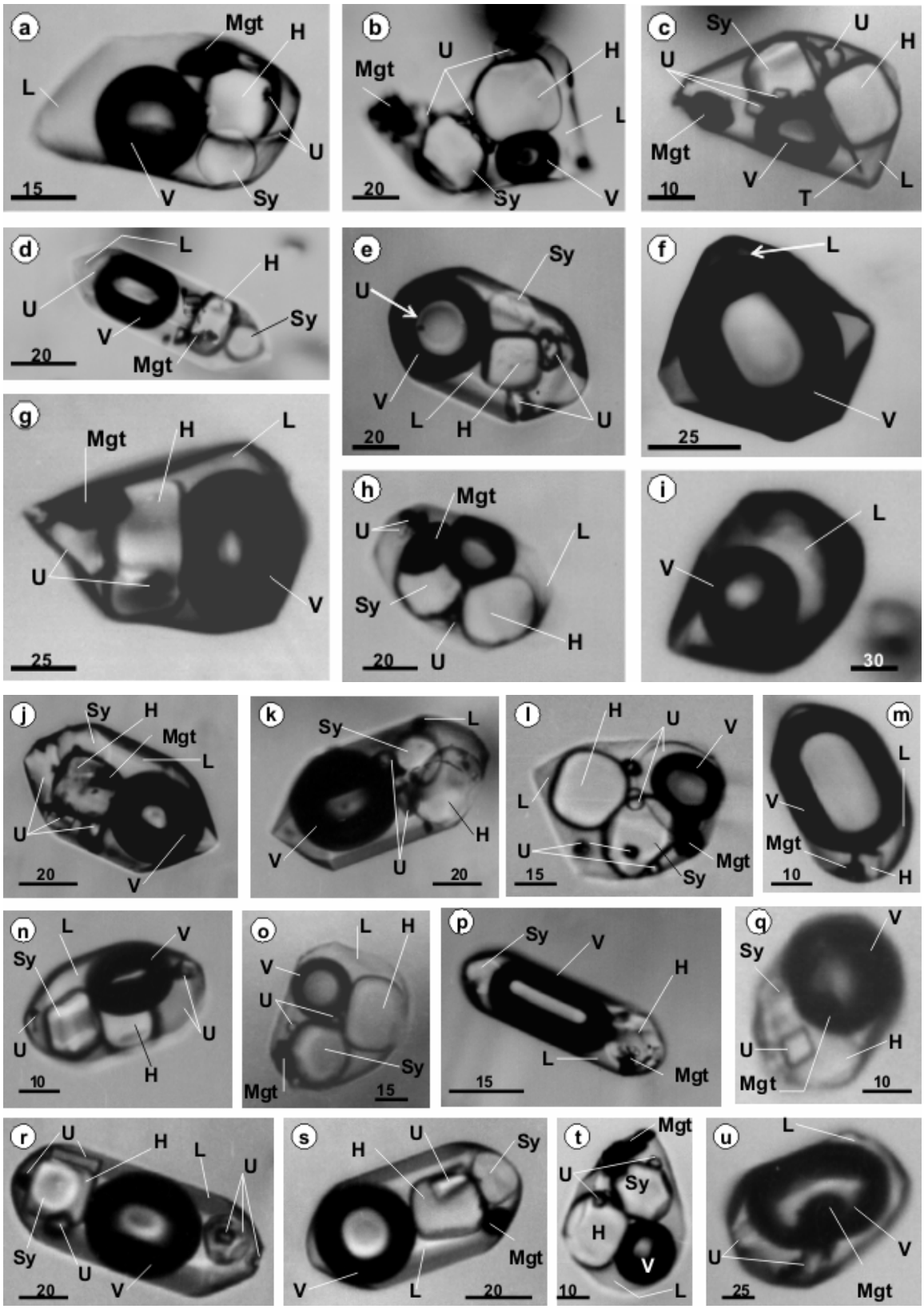
a
Mgt
H
L
U
V
Sy
15
b
U
Mgt
H
L
Sy
V
20
c
Sy
U
H
U
Mgt
V
T
L
10
d
L
H
U
Sy
V
Mgt
20
e
Sy
U
V
L
H
U
20
f
L
V
25
g
Mgt
H
L
U
V
25
h
Mgt
U
L
Sy
H
U
20
i
L
V
30
j
Sy
H
Mgt
L
U
V
20
k
Sy
L
H
V
U
20
l
H
U
V
L
U
Mgt
Sy
15
m
L
V
Mgt
H
10
n
L
V
Sy
U
U
H
10
o
L
H
V
U
Sy
Mgt
15
p
Sy
V
H
L
Mgt
15
q
V
Sy
U
H
Mgt
10
r
U
H
L
U
Sy
U
V
20
s
U
Sy
H
Mgt
V
L
20
t
Mgt
U
Sy
H
V
L
10
u
L
U
V
Mgt
25

Fig. 60. Fluid inclusions types from zoned miarolitic quartz crystals from Vlădeasa granite; **a**, **d**, **e**, **g**, **j**, **k**, **n**, **q**, **r**, **s**- S_1-type brine inclusions (Pintea, 1991b; 1993b); **b**, **c**, **h**, **l**, **o**, **t**- S_2 type brine inclusion (Pintea, 1993); **f**, **m**, **p**, **u**- vapor rich inclusions; **i**- liquid rich inclusion; L-liquid, V-vapor, Mgt-magnetite, u-unknown, H-halite, Sy-sylvite, T-tourmaline (rutile-?). Microthermometry (Pintea, 1993a, 1995a, 2012) aqueous rich inclusions : Th (L) = 295-372°C, salinity = 1-6 wt % NaCl eq.; vapor - rich inclusions: Th (V) = 363-414°C, salinity= 2wt% NaCl eq.; S_1-brine: Th (L) = 570-1070°C, salinity = 41-74 wt% NaCl eq., P = 0.6-2.3 kbars; S_2 brine: ThV=179-405°C, TmH = 420°C, salinity = 46 wt % NaCl eq., P= 7.9kbars. Scale bar in µm.

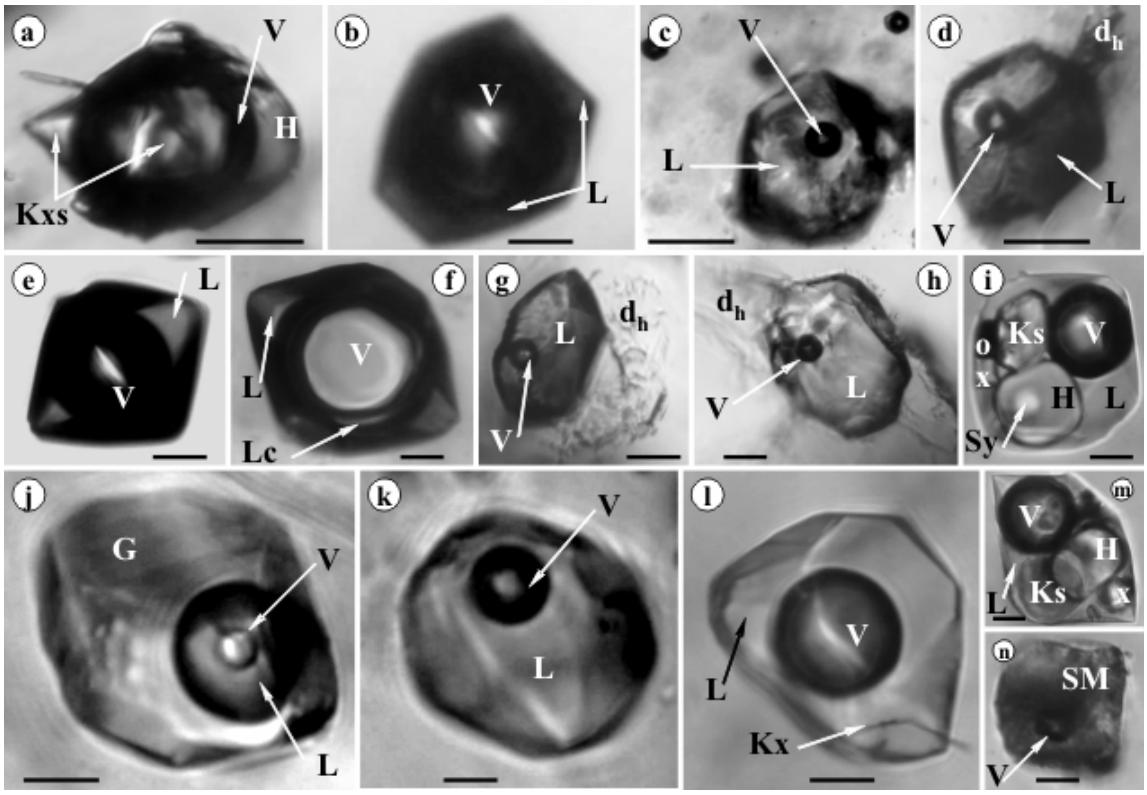

Fig. 61. Vapor-, high density(?) aqueous liquid and brine inclusions in recrystallized pegmatitic quartz from Vlădeasa granite; **a**, **b**, **e**, **f**- vapor rich fluid inclusions; **c**, **d**, **g**, **h**- decrepitated high density (?) aqueous- liquid inclusions; j- silicate glass (G) with aqueous or carbonic fluid (L+V); **k**, **l**- biphasic liquid – rich, **i**, **n**- brine inclusions, **n**- (re) crystallized silicate melt inclusion (SM). Scale bar: 10µm.

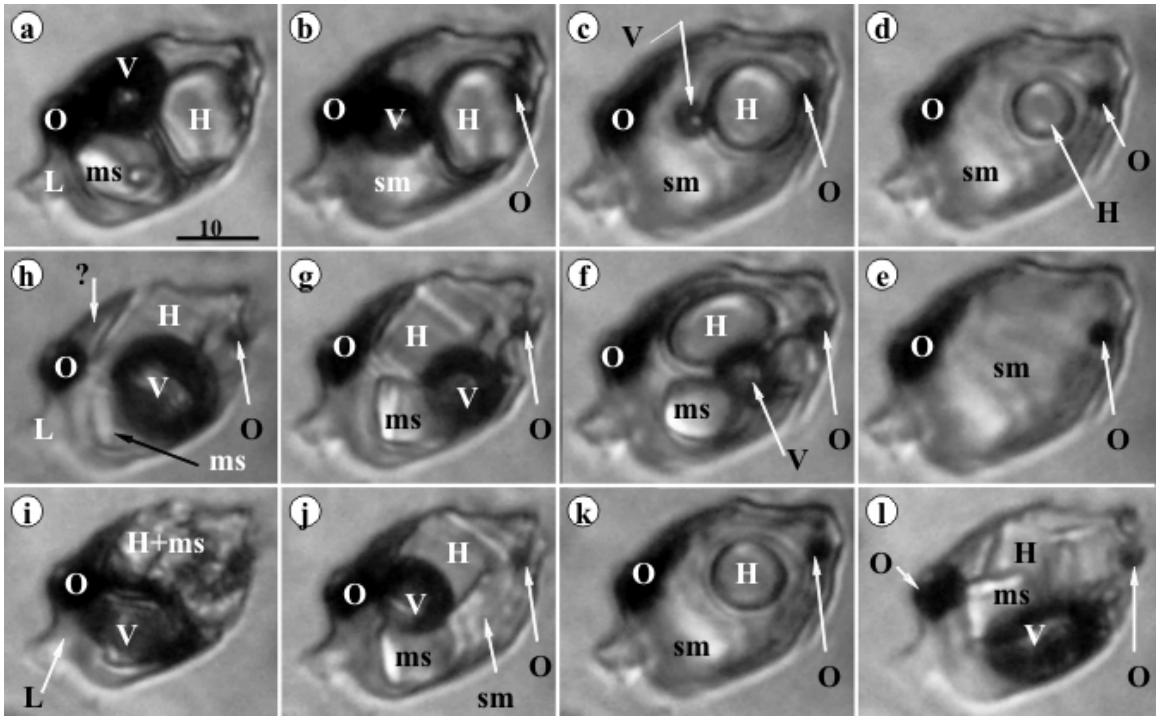

Fig. 62. Microthermometric replicated cycles of brine inclusion microthermometry in quartz from miarolitic quartz from Vlădeasa granite; I cycle: **a**. 25°C, **b**. 267°C, **c**. 496°C, Thv=513°C, **d**. 533°C, TmH= 553°C (salinity = 67 wt% NaCl eq.), **e**. 556°C, **f**. 344°C, **g**.196°C, **h**. 25°C; IIcycle: **i**. 25°C, **j**. 261°C, Thv= 511°C, **k**. 515°C, TmH=553°C (salinity= 67 wt% NaCl eq.), **l**. 25°C; Calculated trapping P= 0.7kbar; L-liquid, O-opaque, H-halite, ms- solid salt mixture, sm-salt melt, V-vapor; Thv- vapor bubble disappearance temperature, TmH- halite melting temperature. There are three homogenization mode of the brine or hydrous salt melt inclusions:**1**. by vapor bubble homogenization after halite melting temperature; **2**. by halite final homogenization after bubble disappearance temperature and **3**. simultaneous homogenization temperature of vapor bubble and halite phases (details in Bodnar et al., 1985; Pintea, 1993a; Becker, 2008; Becker et al., 2008; Lecumberri-Sanchez et al., 2012). Scale bar in µm.

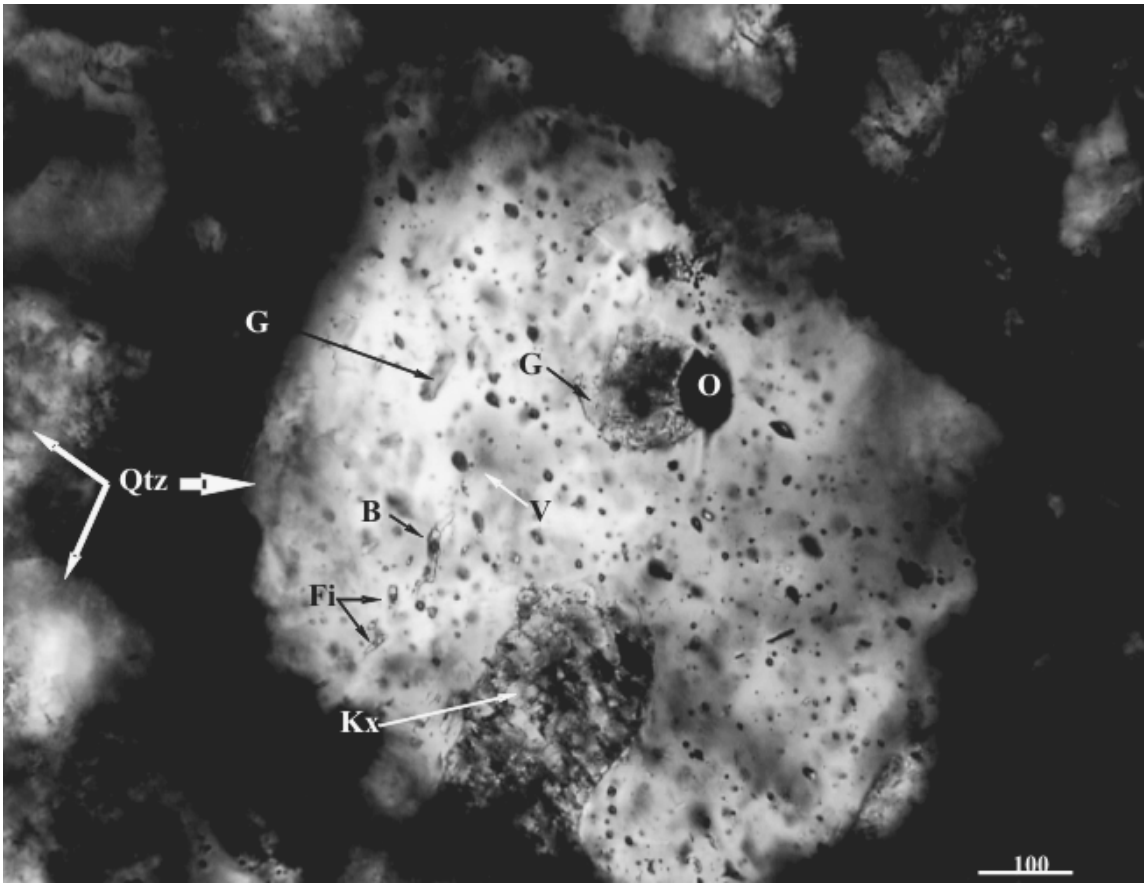

Fig. 63. Quartz eyes (Qtz) from endogenous metasomatized quartz-monzonite from Birtin-dyke (Upper Cretaceous- Ştefan et al., 1982); B- brine, Fi- biphasic aqueous inclusions, G-glass, V- vapor-rich inclusions, O-opaque. Microthermometry: Th= 339-1004°C, salinity= 39-74 wt% NaCl eq., P=0.1-1.3 kbars (Pintea, 2012 unpubl.). Scale bar in μm.

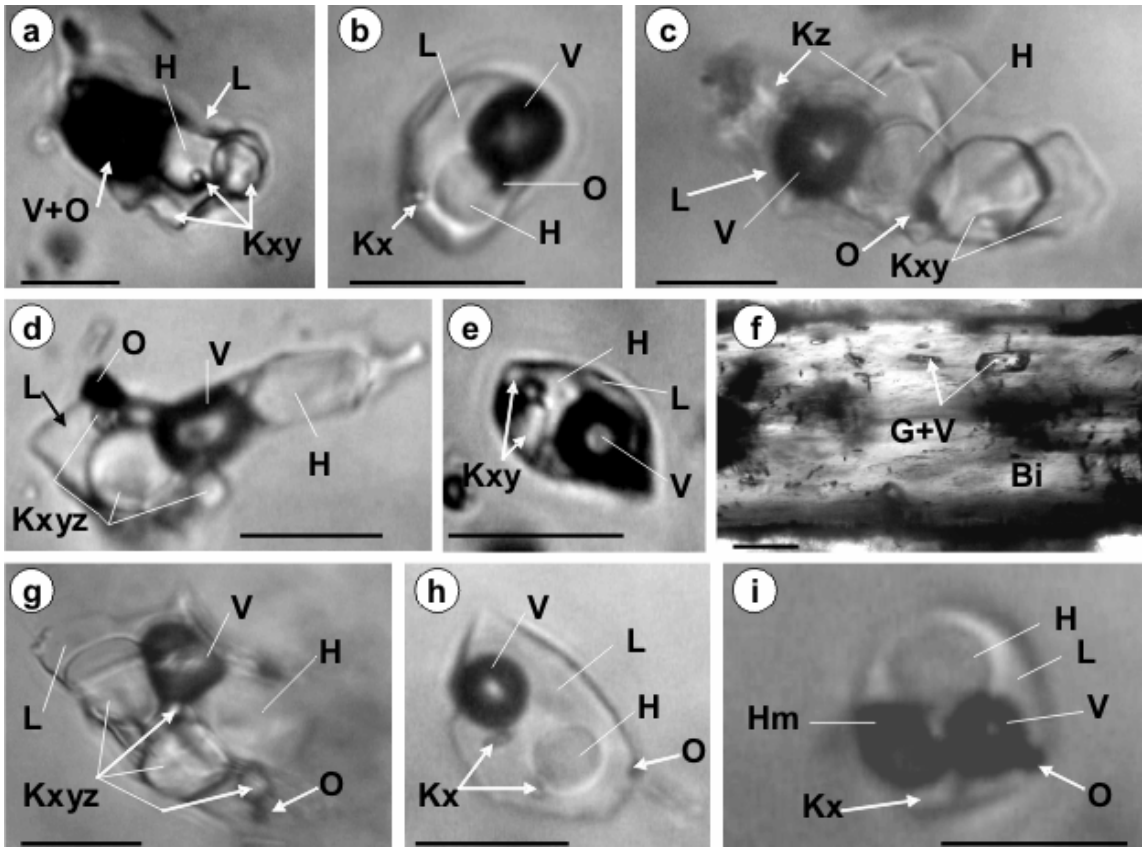

Fig. 64. Silicate melts and brine inclusions types from quartz veinlets and biotite from the Birtin-dyke (Upper Cretaceous). **a**, **b**, **c**, **d**, **e**, **g**, **h**, **i**- brine inclusions in quartz; **f**- silicate glass (G) + vapor inclusions in biotite (Bi); V-vapor, O-opaque, H-halite, L- liquid, Kx, Kxy, Kxyz-other solid mineral daughter phases (chloride, sulfate, silicate), O-opaque, Hm-hematite. Scale bar: 10µm.

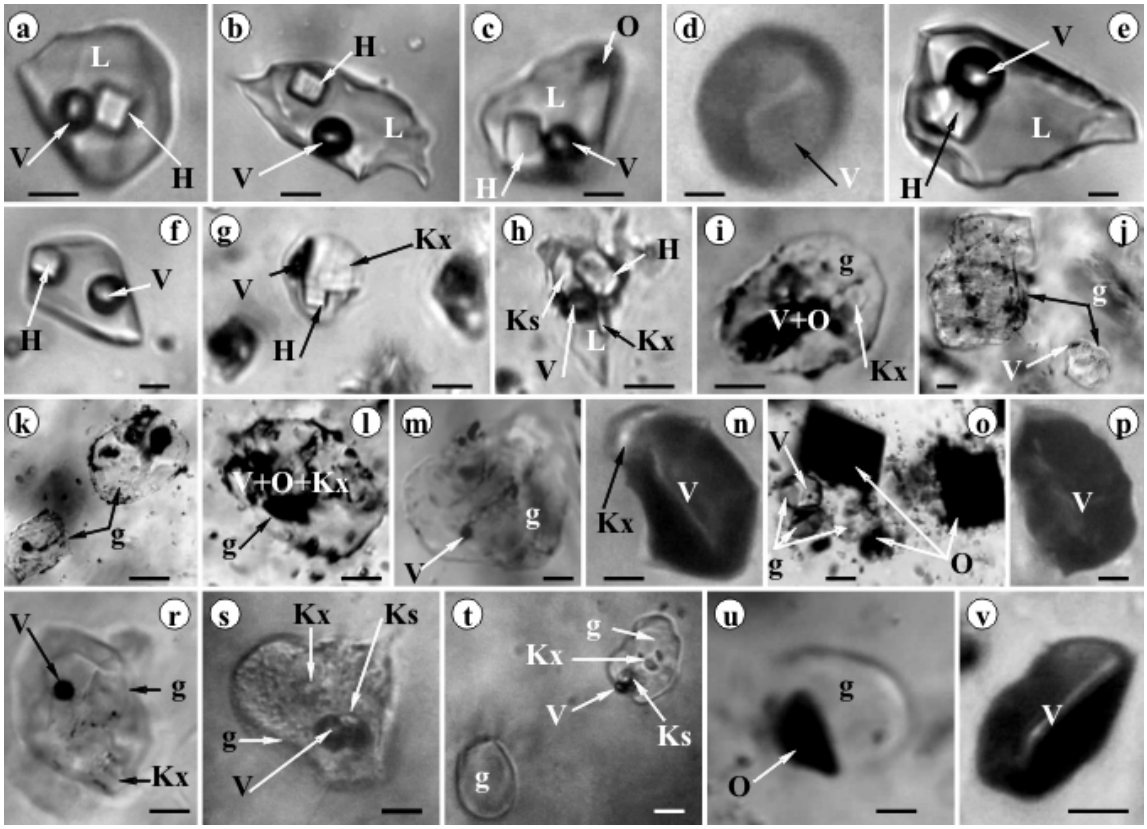

Fig. 65. Fluid and melt inclusions types from quartz related to the Highis granite massif (Hercynian) from Apuseni Mountains; **a**, **b**, **c**, **e**, **f**, **g**, **h**- brine inclusions; **d**, **n**, **p**, **v**- vapor rich inclusions, **i**, **j**, **k**, **l**, **m**, **o**, **r**, **s**, **t**, **u**- silicate melt inclusions; V-vapor, L-liquid, H-halite, O-opaque, kx, ks- other solid daughter phases (chloride, silicate), g-glass, Brine inclusions microthermometry: Th =193-298°C, salinity= 31-38wt% NaCl eq; Bulk crush leach analyses: NaCl= 25.20-46.90 wt%; KCl= 11.18-27.00 wt%, $CaCl_2$= 13.36-42.33, $MgCl_2$=0.07-2.96, $FeCl_2$=2.80-23.07 wt% (Pintea, 2003-unpubl.); Scale bar:5µm.

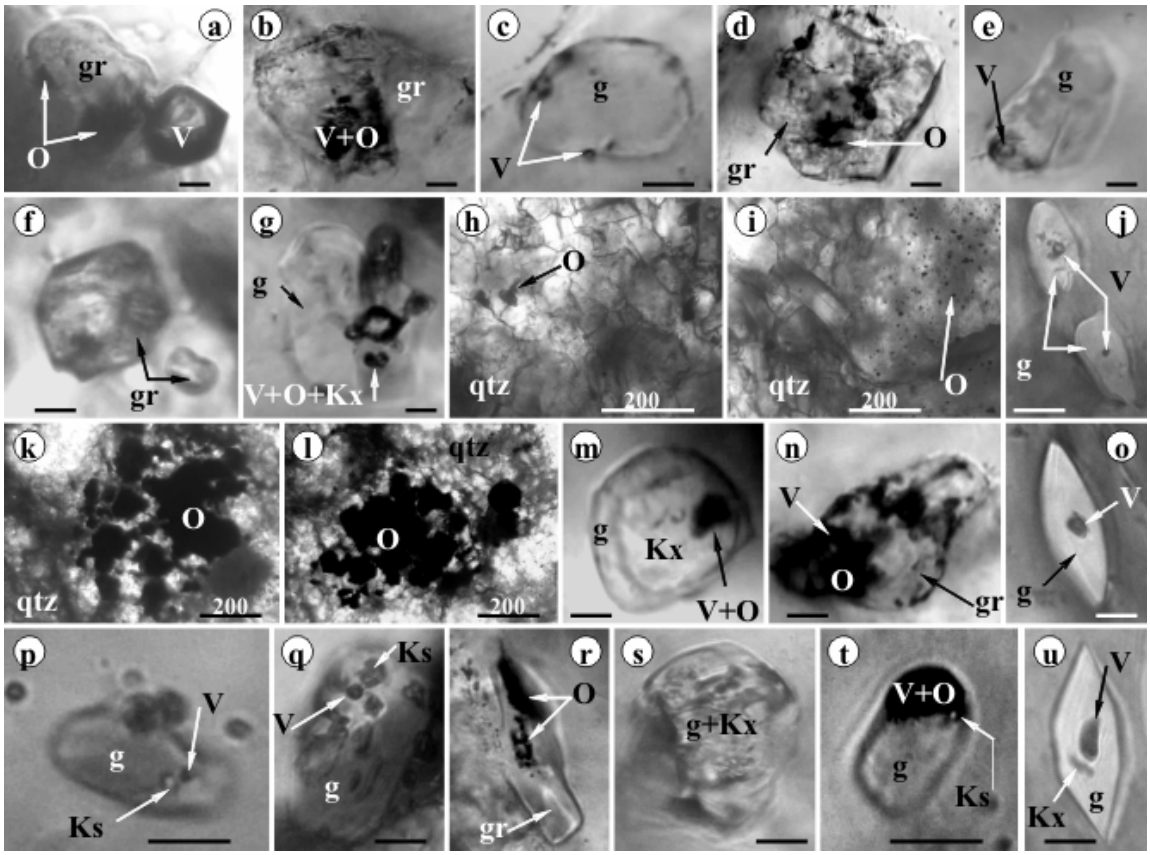

Fig. 66. Silicate melt inclusion types from quartz phenocrysts in rhyolitic- dyke sample G5 (M. Tatu-sample courtesy) from the Highiş massif; **a**, **b**, **c**, **d**, **e**, **f**, **g**, **m**, **n**- silicate remnants; **j**, **o**, **q**, **r**, **s**, **t**, **u**-microthermometric experiments showing the exsolution of multiple fluid bubbles during heating up to 1100°C at 1 bar pressure condition under the microscope (Pintea, in Rosu et al., 2002-unpubl.); frequently the unheated silicate melt inclusion shown similar features with the experiments, suggesting natural reheating (endogenous remelting); gr- glass remnants (glass + microcrystal), O-opaque, V-vapor, g-silicate glass, Ks, Kx- daughter phases (chloride, silicate, opaque); Scale bar: 10µm; h, i, k, l- 200µm.

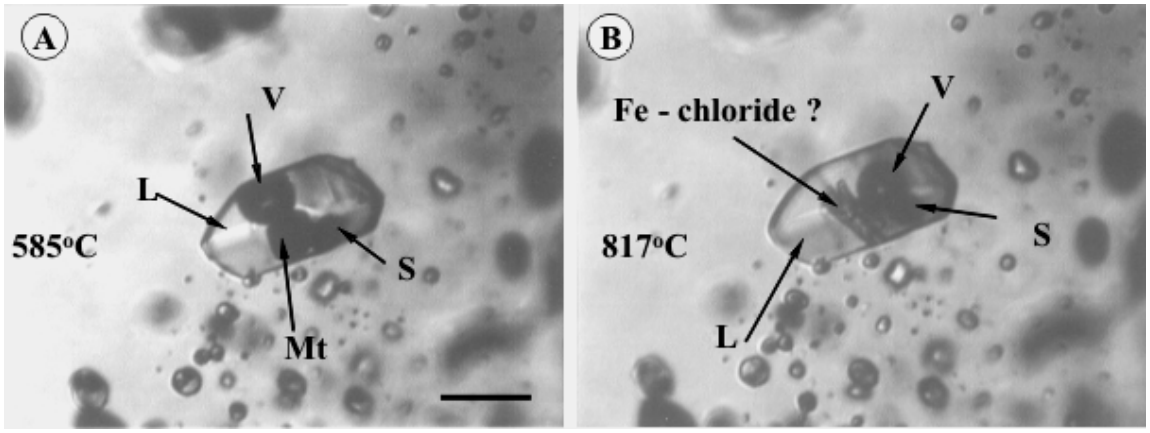

Fig. 67. Brine inclusion microthermometry in quartz from Bolcana porphyry Cu-Au (Mo) deposit showing the sudden formation of $FeCl_2$ (?) phase from magnetite around 816°C. Pictures **A**, **B** take at indicated temperatures; L-liquid, V-vapor, Mt-magnetite, S-opaque. Microthermometry (Pintea, 2009): Th (L) =901°C, P= 1.1 kb, salinity=72 wt% NaCl eq. Scale bar 10µm.

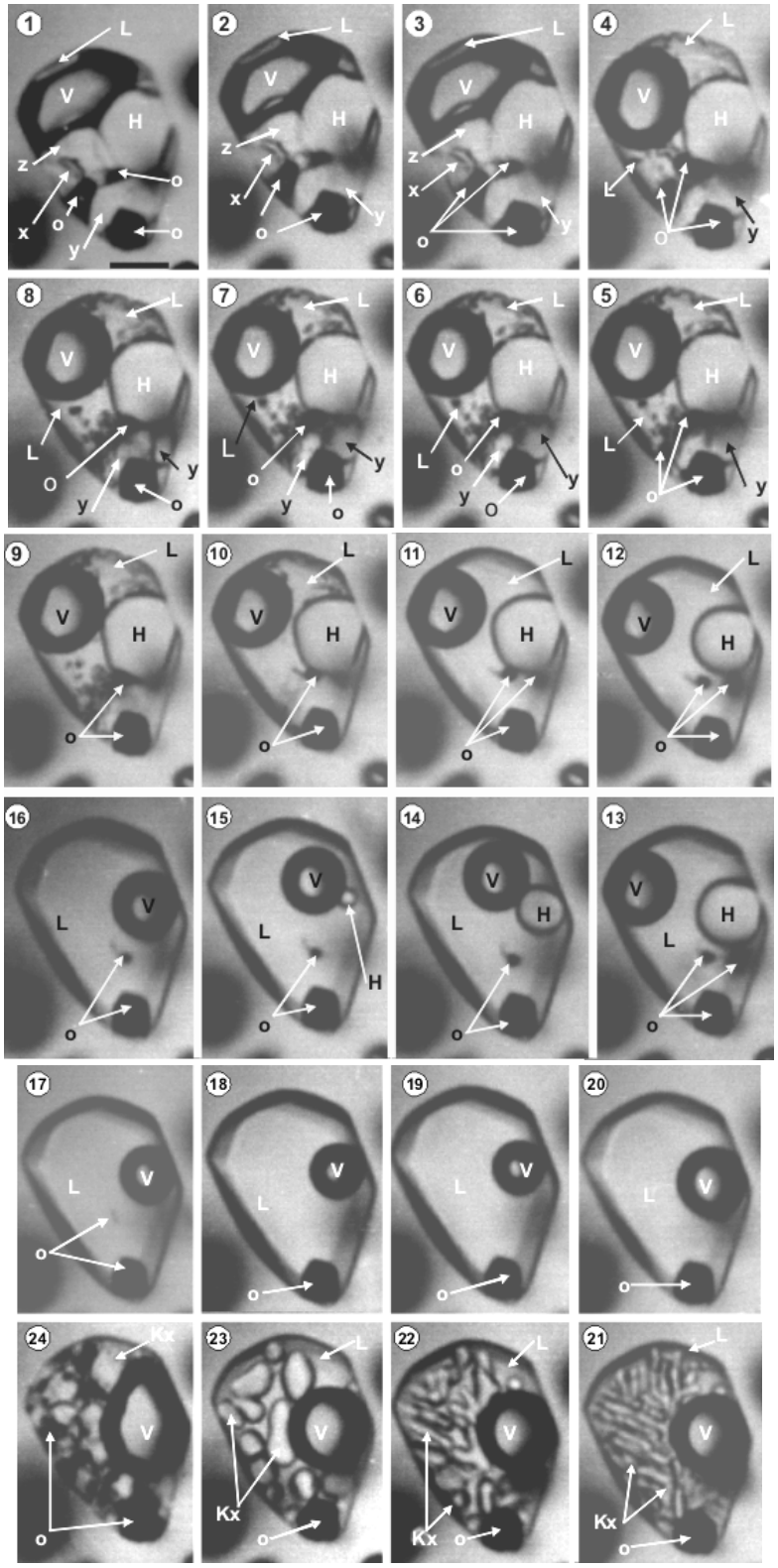

Fig. 68. Sequential microphotographs in brine inclusions from Roşia Poieni porphyry Cu-Au (Mo) deposit. Selected values: **1.** 25°C, **4.**133°C, **11.**302°C, **15.** 530°C, **19.**712°C, **21.** 363°C, **24.** 25°C. Th (L) = 712°C (corrected by Sowat), P = 0.8kb, salinity = 64 wt% NaCl eq. Tmhalite = 532°C. Pintea, 1998, unpubl.). Scale bar 20µm.

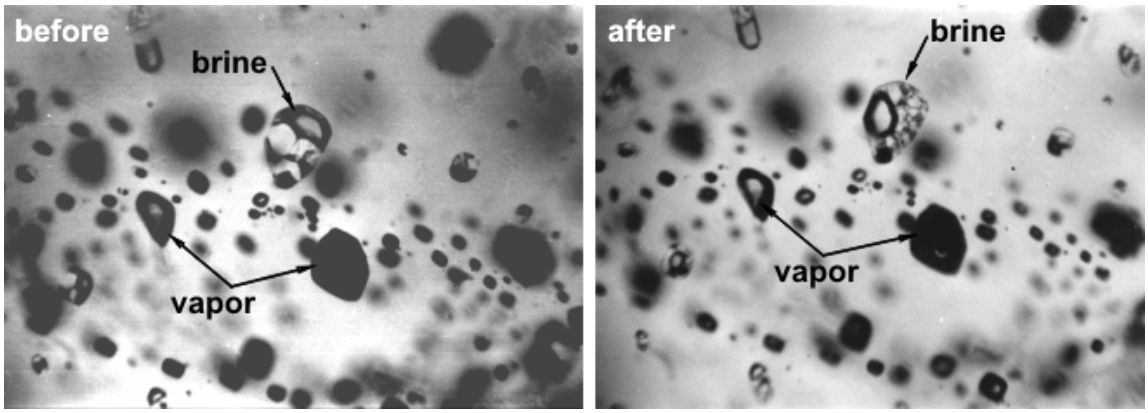

Fig. 69. Microphotographs showing features of the brine inclusion cycled in Fig. 68 before and after the microthermometric experiment, at 25°C. This is a typical microcrack in quartz from Roşia Poieni porphyry Cu-Au (Mo) deposit with coeval brine and vapor-rich inclusions defining so called "boiling assemblage" (see also Heinrich et al., 2005).

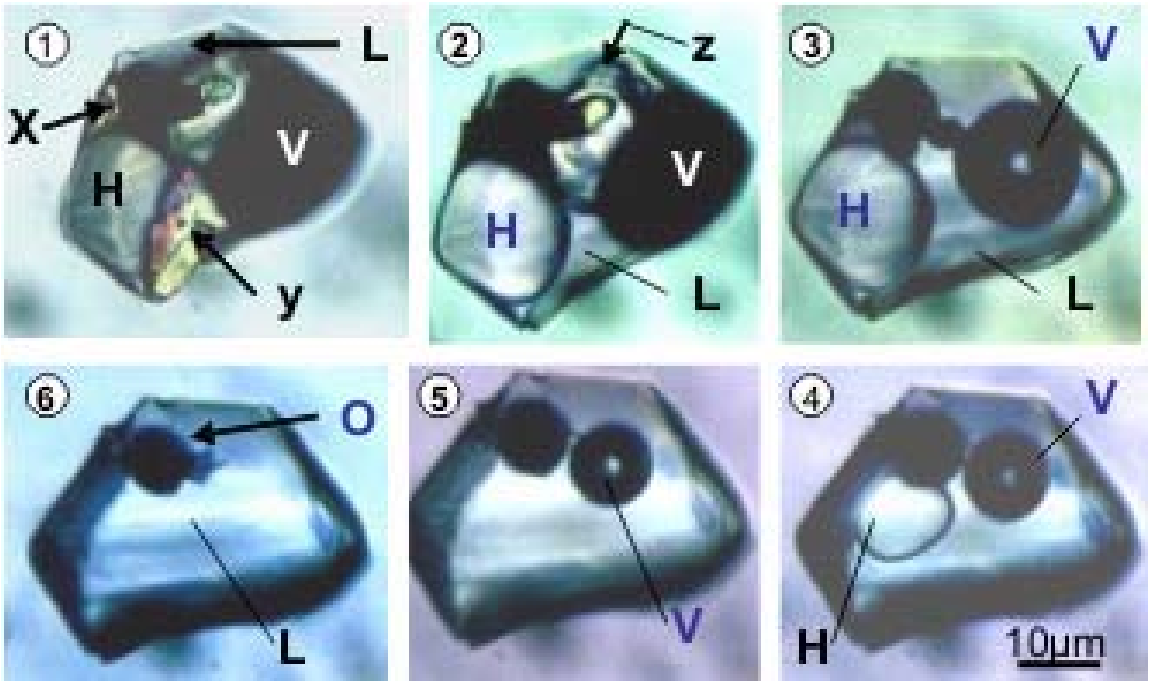

Fig. 70. Hydrous salt melt inclusion with liquid phase at room temperature from Roşia-Poieni porphyry Cu-Au (Mo) deposit, homogenized in "single phase state" in a completed microthermometric run. **1**. 25°C), **2**. 126°C, **3**. 309°C, **4**. 575°C, **5**. 601°C, **6**.750°C, Tm NaCl=585°C, Th (liquid + solid (s) = 749°C; x,y-unknown solid phases, probably salt hydrates and/or complex salts, H- halite, V- vapor, O-opaque (Fe-S-O), L- liquid (Pintea, 2014a).

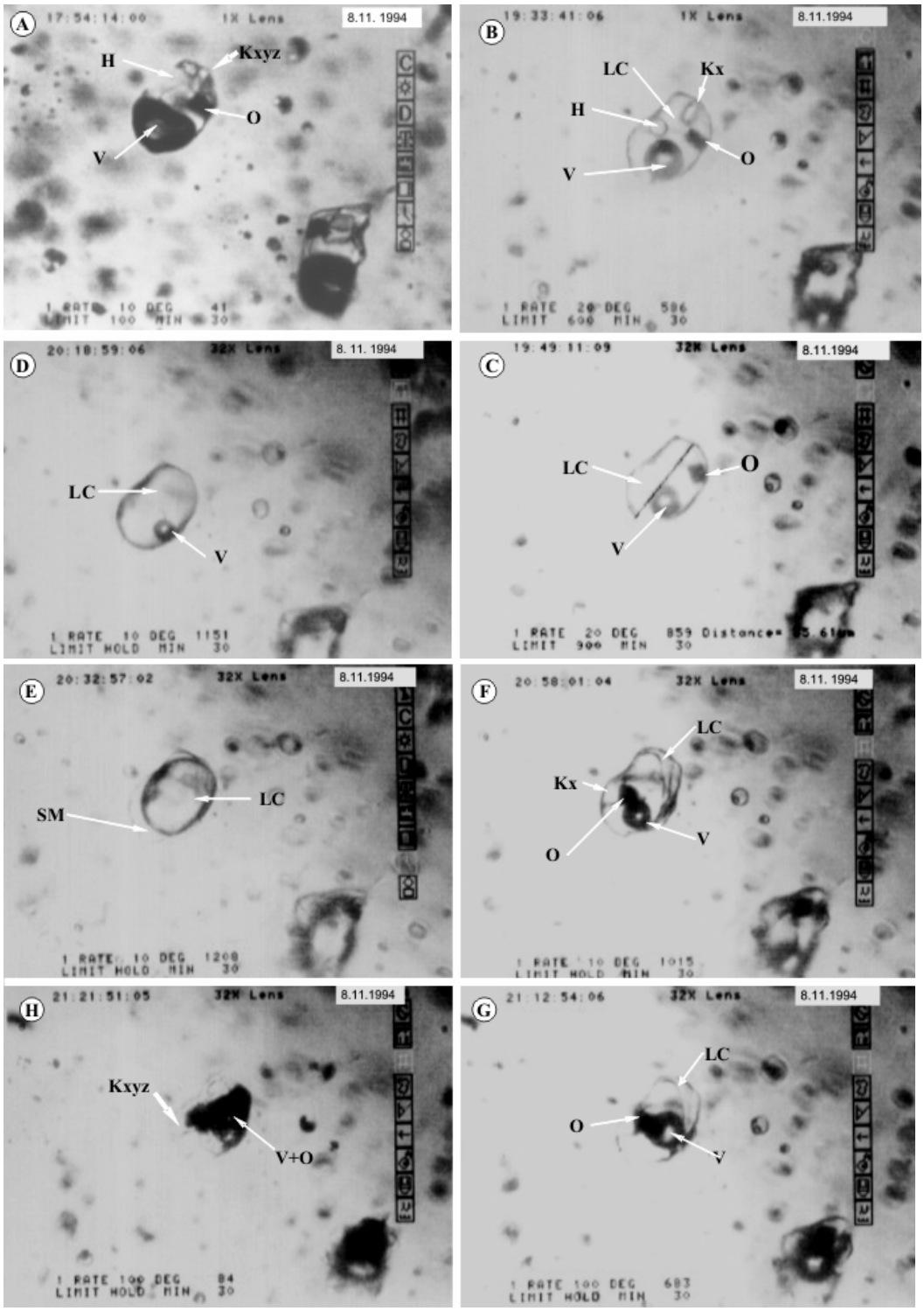

Fig. 71. Sequential Linkam-overlaid microphotographs showing a complete microthermometric cycle of the typical hydrous salt melt inclusion (without liquid phase at room temperature) in quartz from Deva porphyry Cu-Au(Mo) deposit; H-halite, Kx,y,z- other solid daughter phases, O-opaque, V-vapor, LC- salt melt, SM-silicate melt, Scale bar around 35µ.

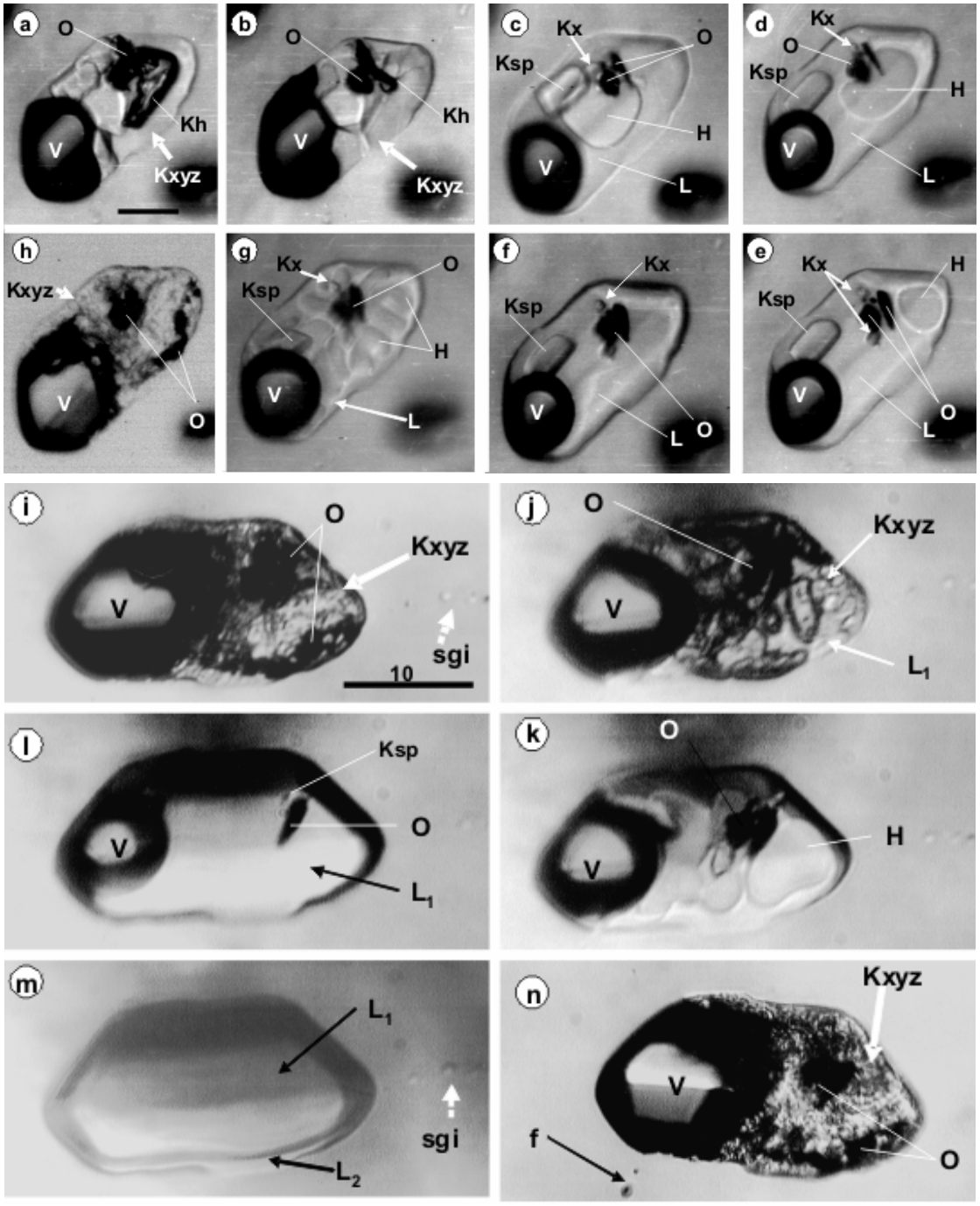

Fig. 72. Sequences of the first (**a** to **h**) and the second (**i** to **n**) microthermometric run, repeated after 2 years in a liquid-free hydrous salt melt inclusion trapped in quartz crystal from Deva porphyry Cu-Au(Mo) deposit; **a**. 25°C, **b**.187°C, **c**. 349°C, **d**. 597°C, **e**.589°C, **f**. 561°C, **h**. 450°C, **i**. 25°C, **j**. 220°C, **k**. 345°C, l. 678°C, **m**. 1305°C, **n**. 25°C, Tmh= 555°C,Th(L)=1262°C. Notations: Kxyz- mixture of salt microcrystals with halite (H) dominant solid daughter phase, O- opaque, Ksp- feldspar, L_1- salt melt released by melting of the salt mixture, L_2- a tiny film of silicate melt released by melting the silicate phases, SMI-silicate glass inclusions formed in fissure probably during the first microthermometric cycle (indicated by dashed arrow in a) suggesting a slight leaking process (re-equilibration) but the salt melt volume remains almost the same because this recrystallized and filled up the microcavity as in the starting moment (vol in a = vol in f) even if another small fissure (c) is formed in the second cycle (f).(Pintea, 1993ac; 2014a). Scale bar in µm.

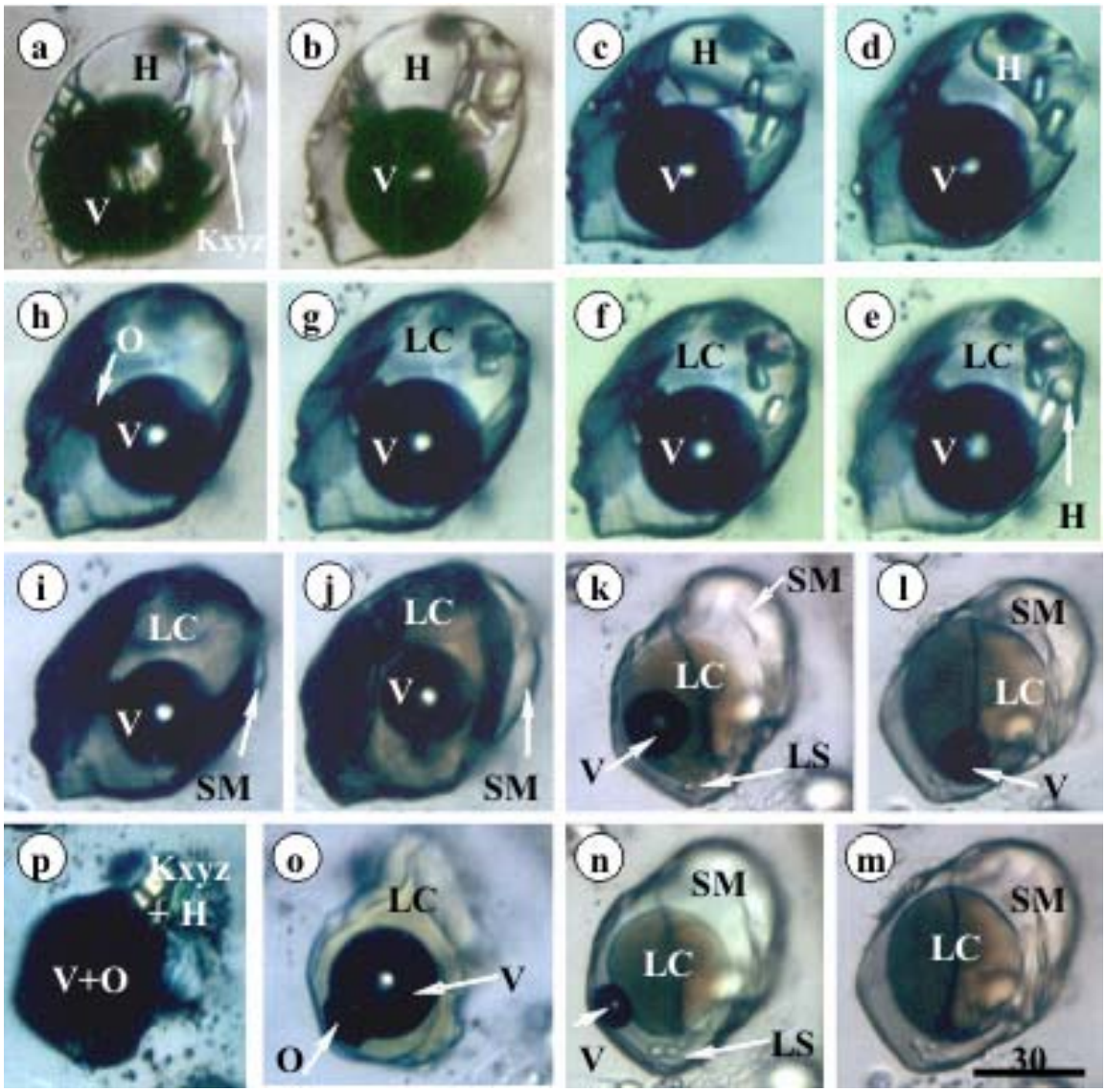

Fig. 73. Sequence of microphotographs showing the complete microthermometric cycle in a hydrous salt melt inclusion trapped in a primary quartz growth zone from Deva porphyry Cu-Au(Mo) deposit (Pintea, 1995b, 2014a modified) **a**. 25°C, **b**. 243°C, **c**. 450°C, **d**. 504°C, **e**. 594°C, **f**. 599°C, **g**. 648°C, **h**. 840°C, **i**. 1086°C, **j**. 1219°C, **k**. 1284°C, **l**. 1317°C, **m**. 1394°C, **n**. 1284°C, **o**. 1062°C, **p**. 25°C. TmNaCl=598°C, Th (melt- V (melt) =1347°C. Other melting temperature recorded for x (Tm_1=113°C), y (Tm_2=122°C, 288°C-sylvite), z (Tm_4= 602°-840°C), Tmo= 1170°C and renucleated at 1130°C. x, y- chloride hydrates-sylvite solid phase, z- silicate phase(s), and anhydrite-?, O- Fe,Cu sulphide-?, V-Vapor, L_1- chloride liquid, L_2-silicate liquid, g- sulphate globules-?, K- mixture of salt microcrystals renucleated at room temperature.. Experiment duration = 5h. Note: Above ca. 1100°C the microcavity have been seriously damaged and their volume increased probably because the chloride liquid phase have dissolved quartz from the walls, and silicate melt liquid increased also in volume, but chloride part seem to be unchanged during the overheating steps. In this case it was estimated that immiscibility occurred at 1086°C, which could be considered as the real "heterogeneous" trapping temperature of the (L+V) chloride mixture and the silicate melt counterpart (see also Steele-MacInnis and Bodnar, 2013). Scale bar µm.

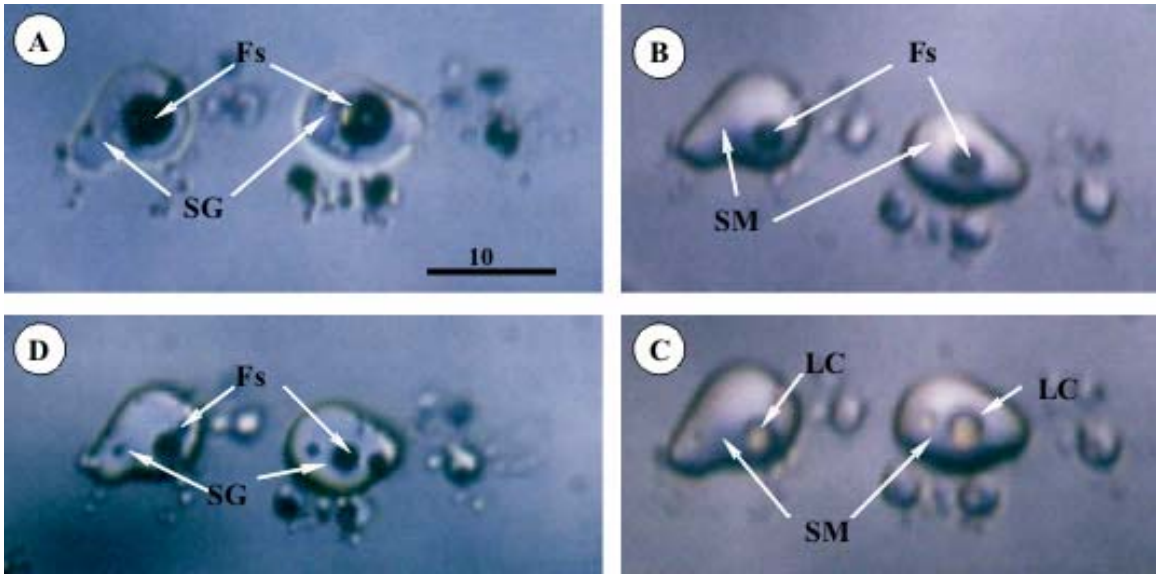

Fig. 74. Sequence of microphotographs showing HT-microthermometry in complex silicate-hydrous salt melts inclusions in quartz from Deva porphyry Cu-Au (Mo) deposit. At room temperature conditions (**A**) the microcavities contains a rich silicate glass and a fluid formed by vapor- rich phase, a halite cube and some opaque. On heating the halite melted around 550°C and at 1085°C (**B**) the fluid bubble is more reduced in volume and contain silicate melt and a dark vapor bubble from which was released around 1267°C a yellow chloride melt (LC) surrounded by a vapor film (dark meniscus), (**C**). Back again to the room temperature (**D**) the fluid is redistributed in several small dark bubbles and the microcavities have changed their shape. The final homogenization temperature is impossible to be determined accurately because of the permanent immiscibility between the two trapped phases, the silicate melt and the hydrosilicate melt, +/- vapor rich. Scale bar in microns (modified from Pintea, 2014a). It should be emphasized that the silicate melt rim appearance in hydrous salt melt inclusions depicted in **Fig 73i**, and the first appearance o the salt melt rim in silicate melt inclusions from this sequence in **B** could be the maximum "normal" trapping temperature of hydrous salt melt inclusions in the porphyry copper systems as already was proved experimentally by Burnham (1979) and reloaded by Becker, 2008 ; Bodnar, 2010. More recently, magmatic control on porphyry copper genesis was published by Audetat and Simon, 2012. Scale bar in µm.

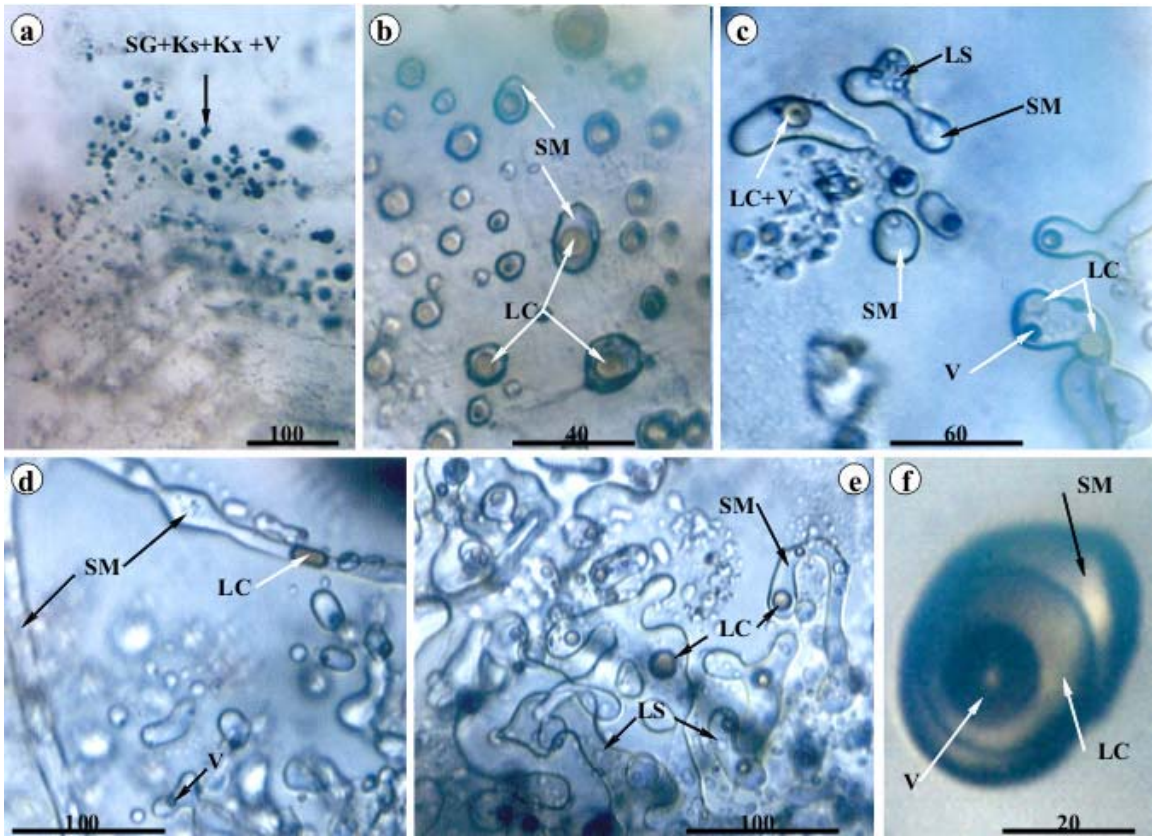

Fig. 75. Coeval silicate melt and hydrous salt melt inclusions in zoned quartz from veinlet of the Deva porphyry Cu-Au(Mo) deposit; **a**. complex silicate melt- salt melt inclusions formed by silicate glass (SG), salt crystal (Ks), silicate (sulfate) daughter phase (Ks) and vapor; **b**, **c**, **d**, **e**, **f**- silicate - salt melt immiscibility depicted around 1300°C; SM-silicate melt, LC-salt melt, LS-sulfate melt (?), V-vapor. Scale bar in µm.

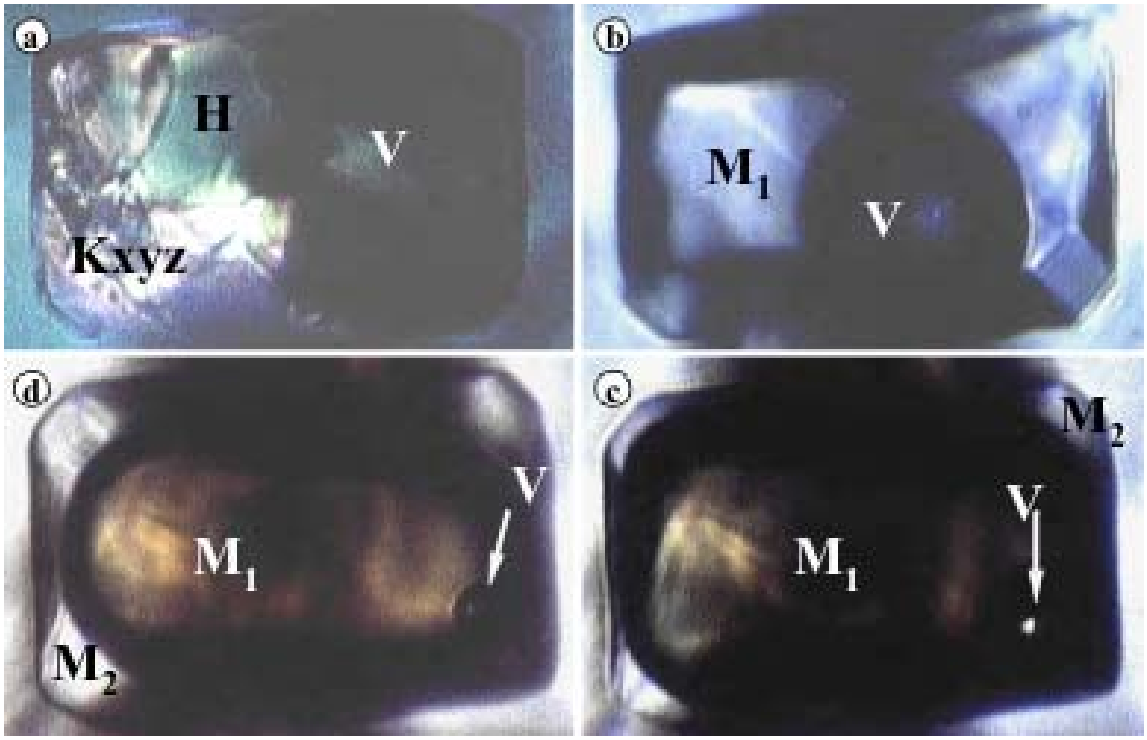

Fig. 76. Rectangle shaped (high pressure form-?) hydrous salt melt inclusion without liquid phase at Troom showing HT immiscibility in quartz from Deva porphyry Cu-Au(Mo) deposit; V-vapor, H-halite, Kxyz-other solid daughter phase including complex chloride, silicate, sulfate), M_1- salt melt, M_2-silicate melt; **a**. 25°C, **b**. 641°C, **c**.1170°C, **d**.1226°C. Microthermometry: Th (L) = 1234°C, P=8kb, salinity=72 wt% NaCl eq. (Pintea, 1994a, unpubl.). Inclusion size=70µm.

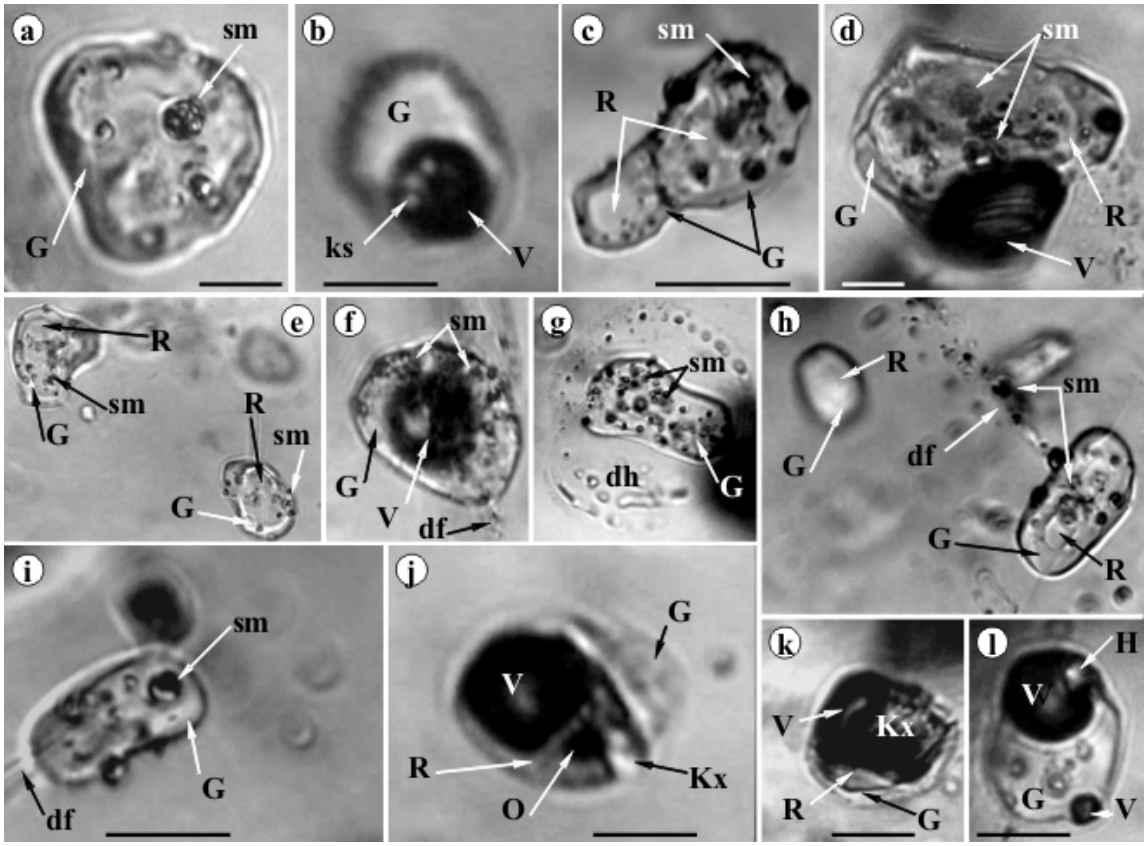

Fig. 77. Experimentally re-melted features in silicate melt inclusions from Upper Cretaceous porphyry Mo-Cu (Au) occurrence from Oraviţa (Nicolae adit); **a**, **c**, **e**, **g**, **h**, **i**- immiscible saline droplets exsolved from silicate melt depicted around 1000°C; **b**, **d**, **f**, **j**, **k**, **l**- two phase silicate melt inclusion (glass + vapor) and separate immiscible globules exolved around 1000°C; G-glass, sm-silicate melt, R-restitic glass (unmelted), dh/df-decrepitation halo/fissure, O-opaque, Kx- other daughter solid phase (silicate, chloride). Scale bar 10µm.

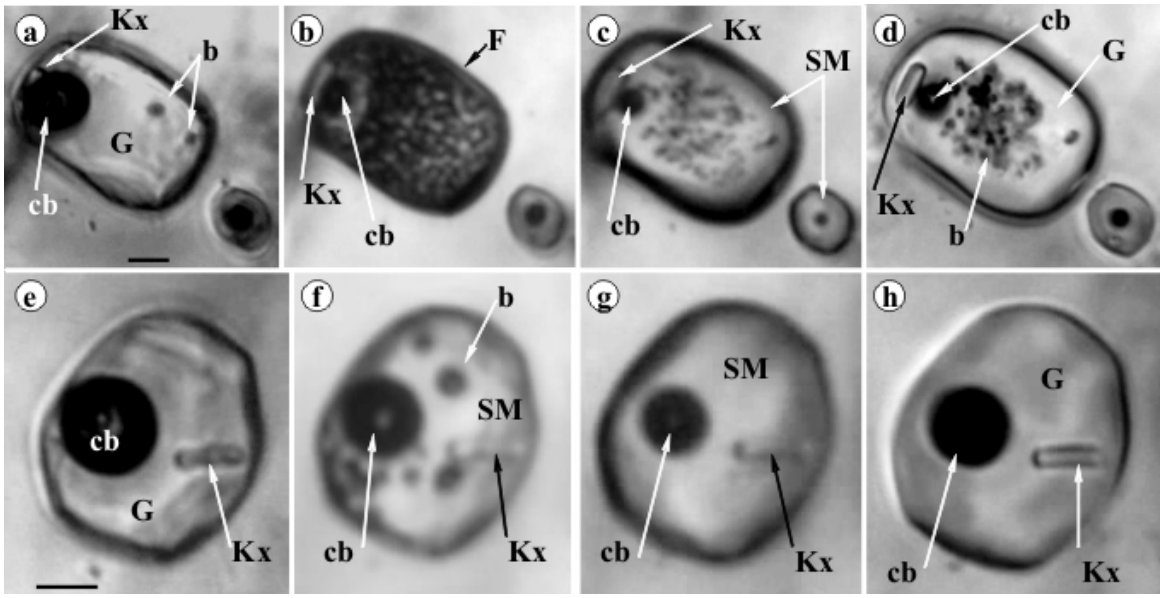

Fig. 78. Microthermometric sequences in two contemporaneous silicate melt inclusions (assemblage) in plagioclase from Danesti-Piatra Rosie dacite showing different internal features during heating up around 1100°C; a, b, c, d- homogeneous silicate foam-like inclusion; e, f, g, h- silicate melt inclusion; cb= contraction bubble, G-glass, b- erratic bubbles, Kx- daughter silicate , SM- silicate melt. **a**. 25°C, **b**.1048°C, **c**.1080°C, **d.** 25°C, **e.** 25°C, **f**. 1047°C, **g.** 1094°C, **h**. 25°C. Scale bar: 10µm

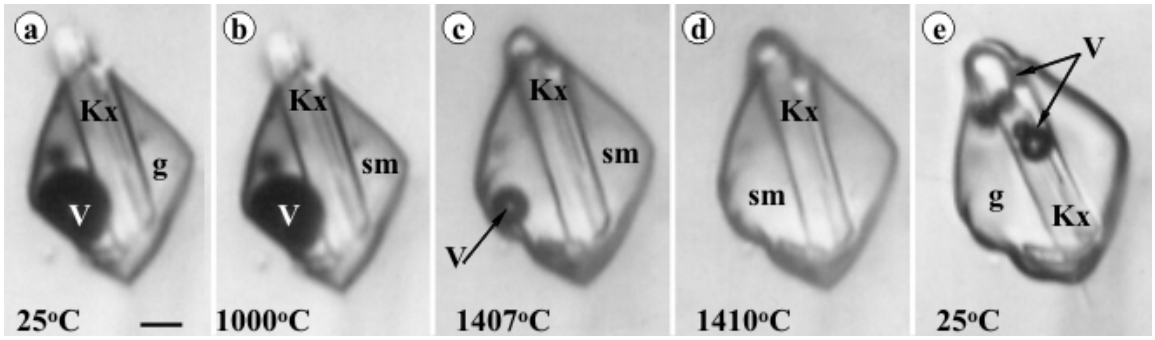

Fig. 79. Three phase silicate melt inclusion (glass + crystal + vapor) showing uncommon high temperature disappearance of the vapor bubble, suggesting heterogeneous trapping. Nevertheless the recent published data on contemporaneous silicate melt inclusions in quartz from Laleaua Alba dacite (Naumov et al., 2014) suggested very deep trapping conditions (about 30 km ≈ 8kb). Moreover xenocrystic pyroxene geothermometry from acidic rocks indicate high temperature values up to 1416°C, suggesting magma mixing by hot mafic magma influx (Kovacs, 2002; Pintea 2007; 2008a). Scale bar cca 20 µm.

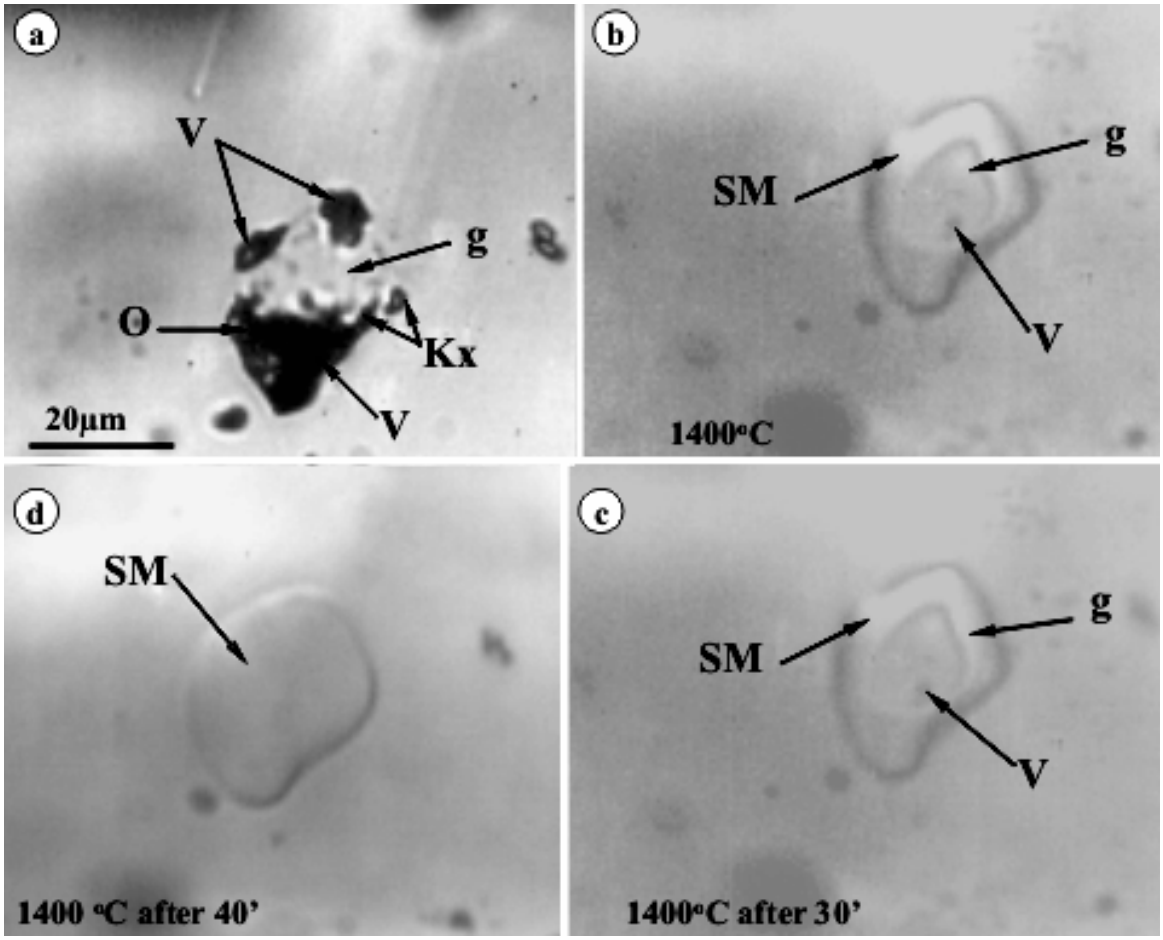

Fig. 80. Microthermometry of an silicate melt remnant in ß-quartz crystal from Roşia Montană dacite dome (Metaliferi Mountains).The inclusion contain at room temperature in **a**. silicate glass (G), a vapor phase as multiple bubbles (V) and solid silicate phases (kx) and opaque (O). During heating procedure in the stage around 1400°C, the phase disappeared one by one and now contains only silicate melt (SM), a vapor bubble (V) and remaining glass in **b**. and **c**. which melted completely at 1370°C showed in **d** (uncorrected temperature, see Pintea and Iatan, 2017). This behavior is uncommon and trapping temperature cannot be estimated, but this seems to be the initial temperature of a new melt influx. The new overheating magma influx induced overgrowth of the β-quartz phenocrysts, after homogenization of the mafic and felsic melt during decompression (Pintea and Iatan, 2013). Such high temperature fluid and/or melt phases seem to be extracted from the astenospheric mantle wedge in postcollisional environment followed by an extensional regime as was emphasized in the Miocene volcanism from Metaliferi Mountains (Harris et al., 2013). Scale bar in µm.

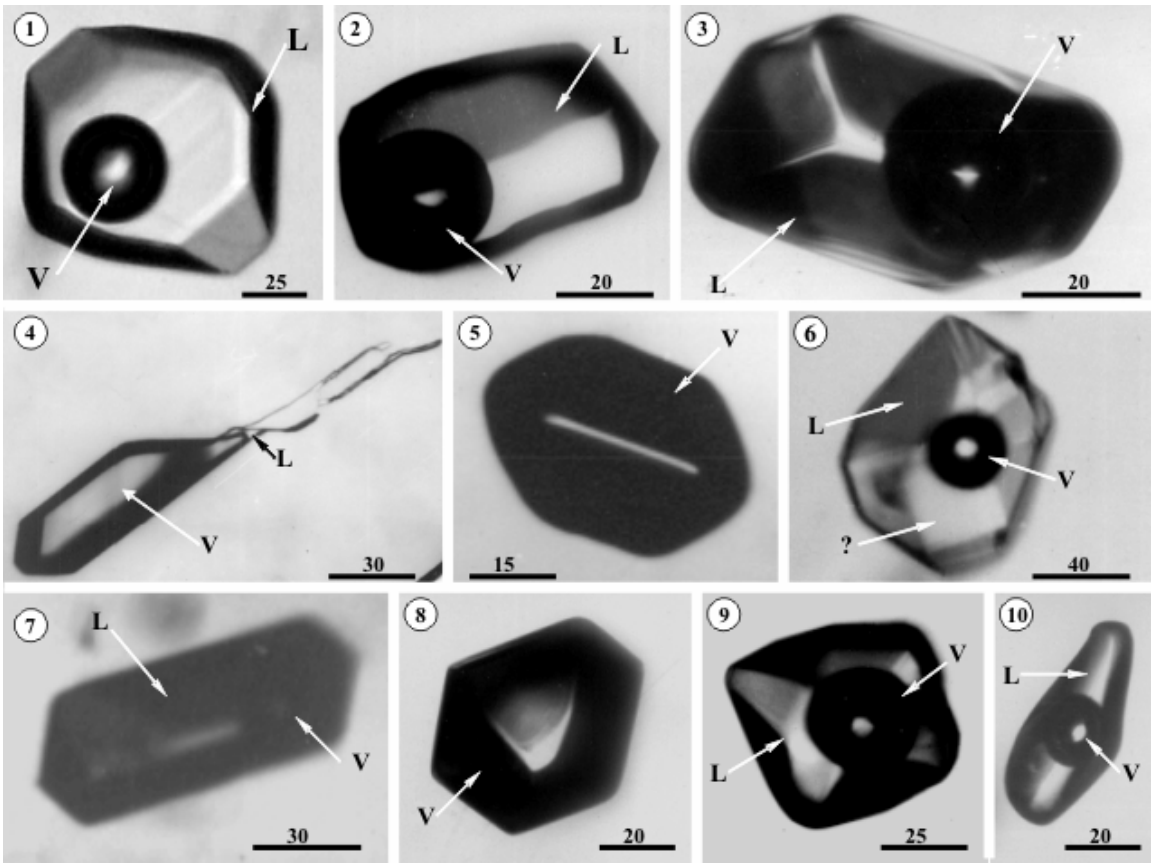

Fig. 81. Aqueous fluid inclusions (monophase and biphase) in various Neogene epithermal deposits from Carpathians (Romania).**1**. Herja (low sulfidation); **2**, **4**. "Cucu" crater in Harghita Mountains, **3**. Baia Sprie (low sulfidation), **5**, **9**.Tălagiu (possible high sulfidation fluids overprinting the porphyry copper system); **6**, **7**, **8**, **9**, **10**. Roşia Montană Au-Ag epithermal deposit (Gold Quadrilateral- Metaliferi Mountains). V-vapor, L-liquid, ?- unknown solid daughter phase. Scale bar in µm.

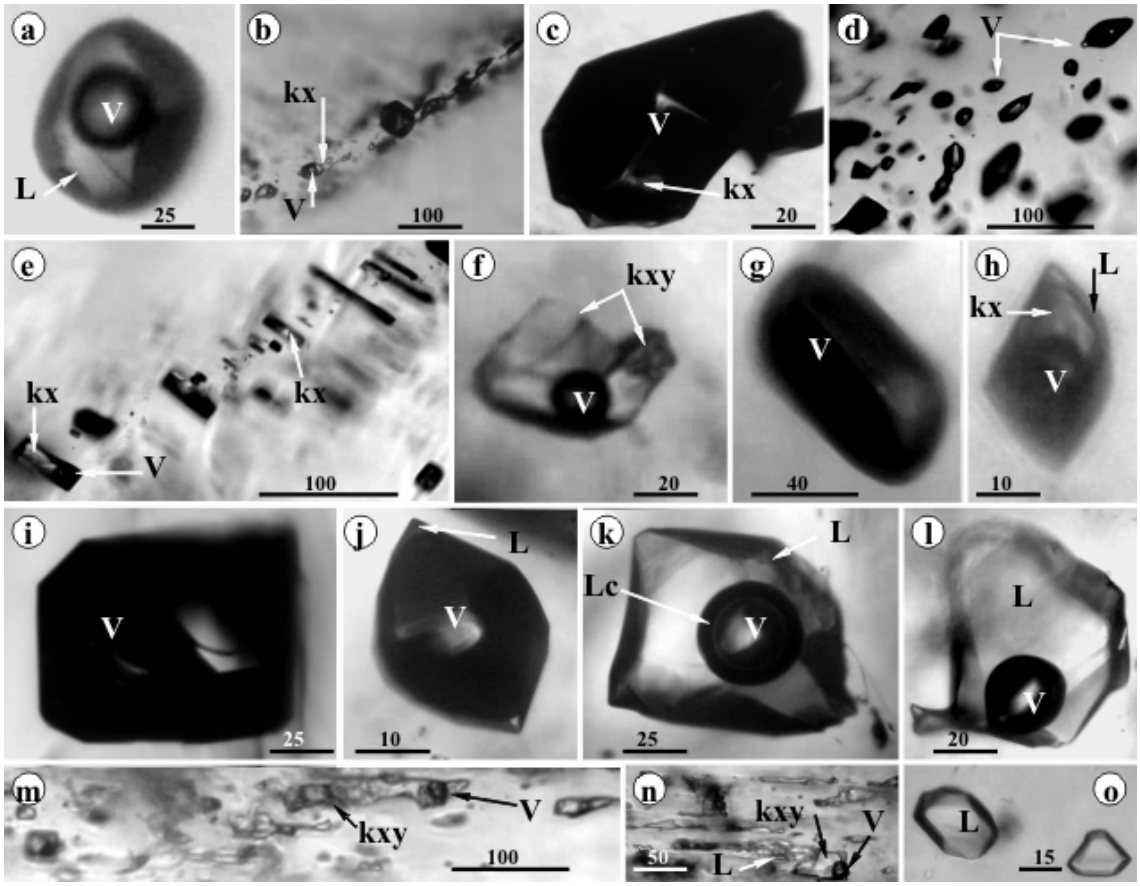

Fig. 82. Fluid inclusions types in quartz from Herja epithermal ore deposit (Baia Mare mining district); **a**, **k**, **l**- biphasic fluid inclusions; **b**, **e**, **f**, **h**, **m**, **n**- multiphase fluid inclusions; **c**, **d**, **g**, **i**, **j**- vapor-rich inclusions; **o**- monophasic liquid inclusions; As it was pointed out by Damian (2003) that the Herja low sulfidation ore deposit could be related at depth with a subvolcanic body activated as a porphyry copper - like system, suggesting that the early fluid were high- salinity ones, as now proved by the presence of solid phases precipitated (?) in the fluid inclusions in quartz (this Figure). The salinity estimated by Pintea (1995a; 1996b) ranged between 4.9 to 19.5 wt % NaCl eq at temperatures between 175°C and 370°C. Moreover it is suggested that the early mineralization stage was characterized by high temperature values as indicated by the S-isotope compositions of coexisting pyrite-galena pairs between 417±75°C and 320±70°C. The famous stibnite and sulphosalt parageneses including "plumosite" probably crystallized below 220°C (Pomârleanu 1971; Cook and Damian, 1997); L-liquid, Lc-CO_2 liquid, kx, kxy- solid phases (silicate, carbonate, sulfate), V-vapor. Scale bar in µm.

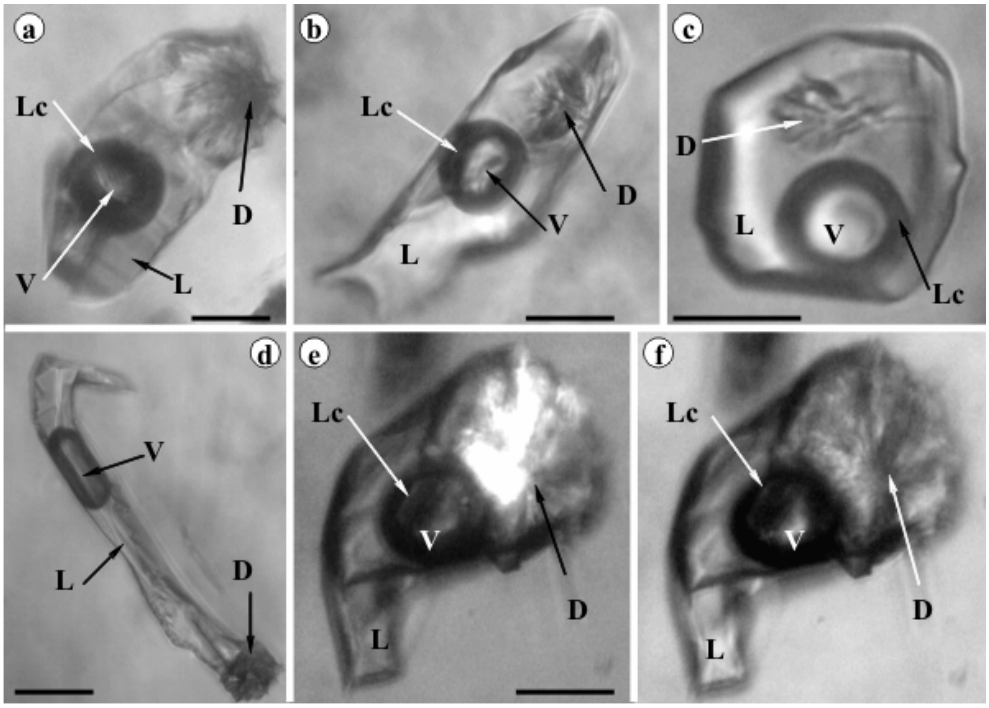

Fig. 83. Typical aqueous biphase (± carbonic fluid) fluid inclusions from Baia Sprie epithermal ore deposit containing dawsonite as solid daughter (?) phase.; L-liquid, Lc- liquid carbonic rim, V-vapor, D-Dawsonite – $NaAl(CO_3)(OH)_2$. Despite metastability during heating in the stage under the microscope, it is considered a real daughter phase formed in inclusions after trapping of Al- rich carbonaceous alkaline solution in low T-P epithermal environments (e.g. Coveney and Kelly, 1971) or in granitic-pegmatites formations by Sîrbescu and Nabelek (2003) at relatively high T (~ 340°C) and P(2.7 kbars). Generally a CO_2 - rich phase is necessary present as a thin rim of liquid CO_2 around the vapor bubble at Troom conditions (Nedelcu and Pintea, 1993; Pintea, 1995a; 1996b). Scale bar 40µm.

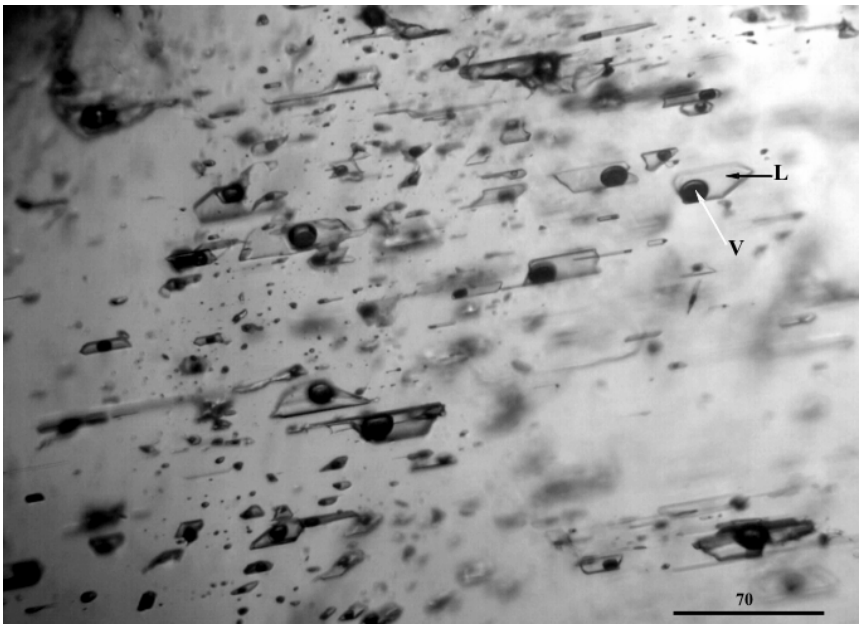

Fig. 84. Pseudosecondary parallel alignements (overgrowths) decorated with aqueous-rich biphasic fluid inclusions in epithermal quartz from Baia Sprie ore deposit. V-vapor, L-liquid. Scale bar in µm.

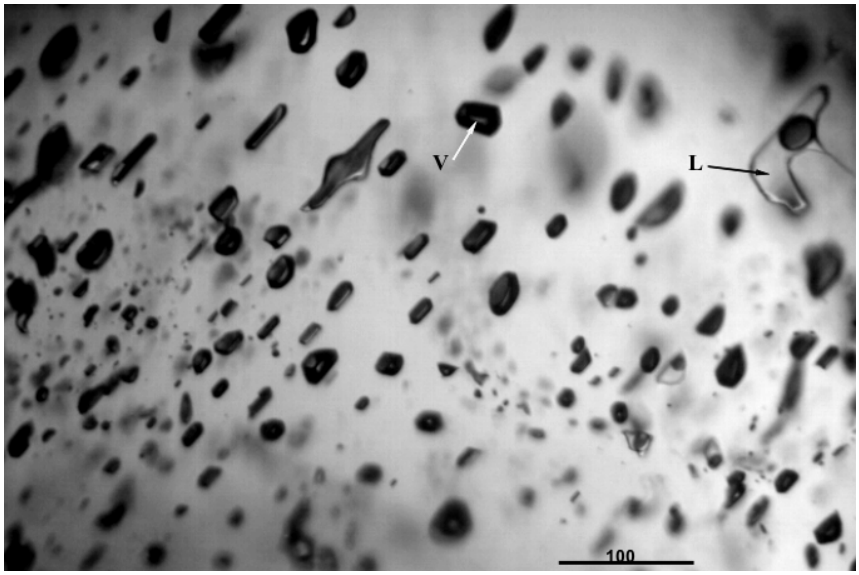

Fig. 85. Pseudosecondary trail containing coeval vapor-rich (V) and liquid-rich (L) fluid inclusions representing a presumptive boiling episode during quartz crystallization in the main vein from Baia - Sprie ore deposit (level X). There are many episodic boiling and effervescence or evaporation stages in the "Main Vein" from Baia Sprie (e.g. Manilici et al., 1965, Pomârleanu et al., 1985; Nedelcu and Pintea, 1993) precipitating successive mineral parageneses all together suggesting the characteristic ore elements distribution with precipitation height column (cca 800m): (Au-Ag) on the top, (Pb-Zn) and (Pb-Zn-Cu) ± Bi ±W intermediate depth to the bottom, deposited between 150-360°C, rarely more, and 0 to 21.0 wt % NaCl eq. (Manilici et al., 1965; Pintea, 1995a; Grancea et al., 2002). Mixed fluids (magmatic and meteoric) with low salinity (4.6-6.4 wt% NaCl eq) and intermediate Th between 154° and 240°C was estimated in wolframite for primary biphase fluid inclusions (Bailly comm. pers, 2001; Bailly et al., 2002). Scale bar in µm.

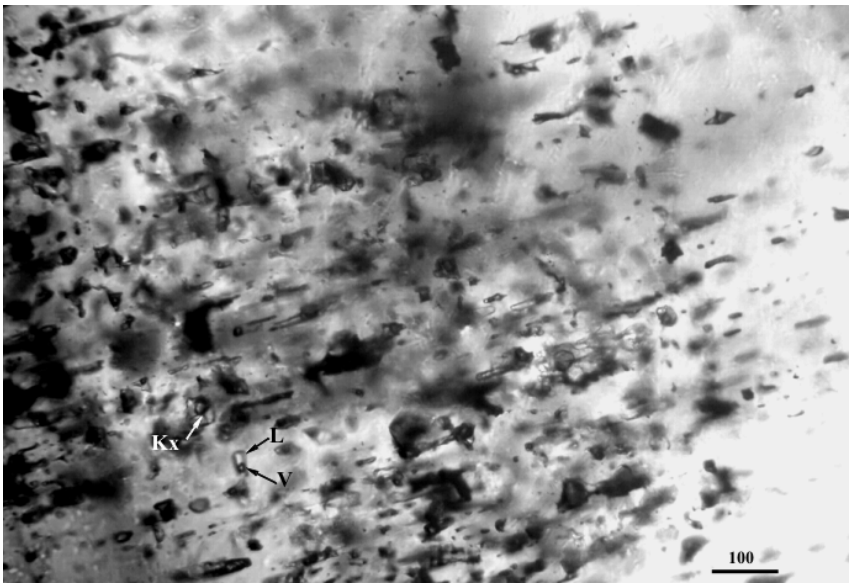

Fig. 86. Overgrowths zones in quartz decorated with multiphase (L+V+solids) fluid inclusions in the second crystallization stage from the "Main Vein" of the Baia Sprie epithermal system (Nedelcu and Pintea, 1993; Pintea, 1995a; 1996b). L-liquid, V-vapor, Kx- crystal (silicate, carbonate, sulfate or silicate glass-?). Scale bar in µm.

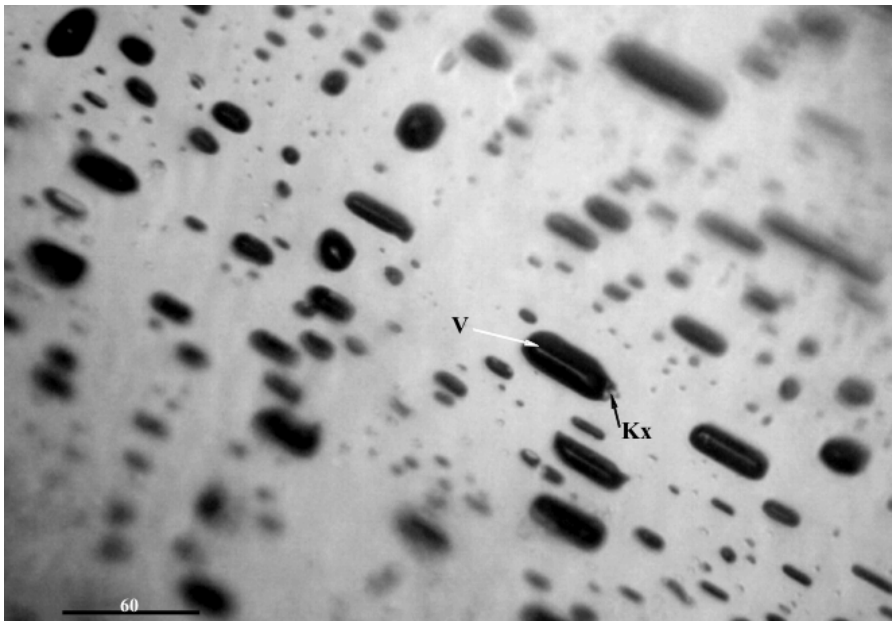

Fig. 87. Presumptive magmatic vapor-rich fluid inclusions as pseudosecondary parallel alignment in a microfissure plane in quartz from Baia Sprie – "Main Vein". V- vapor, Kx- sublimated solid phase (silicate or carbonate). Scale bar in µm.

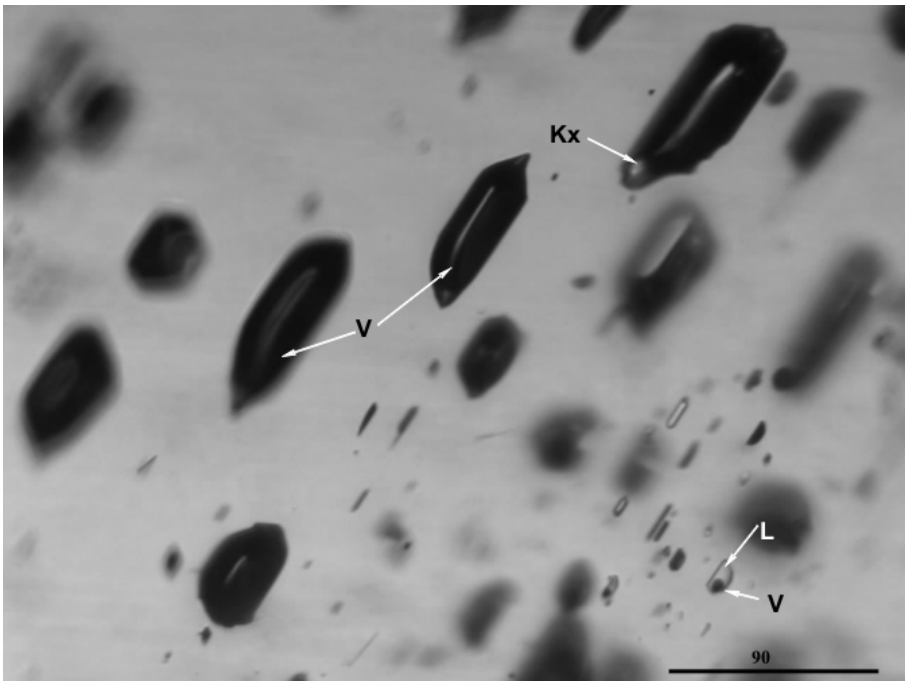

Fig. 88. Coeval presumptive magmatic vapor- rich inclusions trails with aqueous biphasic fluid inclusions in the same microfissure plane in epithermal quartz from Baia Sprie ore deposit. V-vapor, Kx- solid condensate (silicate or carbonate), L-liquid. Scale bar in µm.

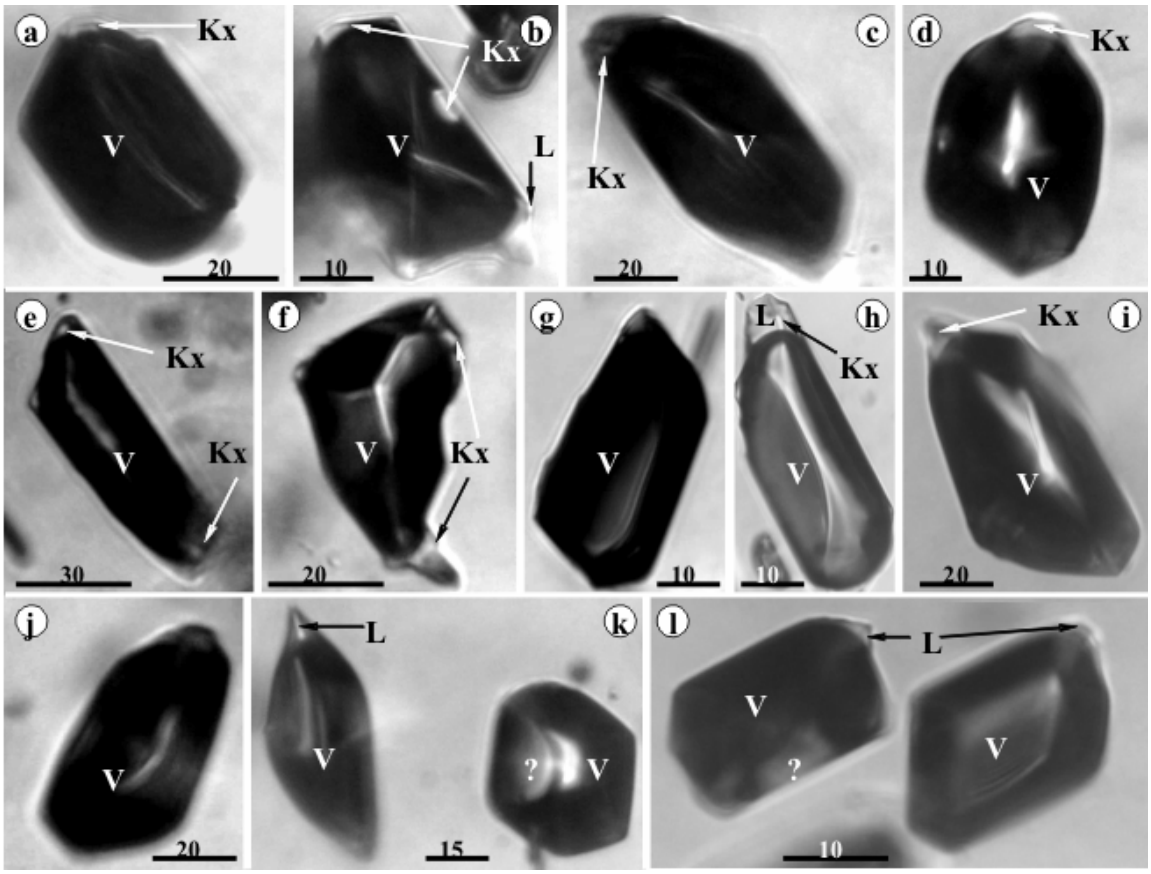

Fig. 89. Individual presumptive magmatic vapor-rich inclusions types (**a, b, c, d, e, f, g, h, i, j, k, l**) trapped in epithermal quartz in the "Main Vein" from Baia Sprie ore deposit. Recent (Pintea, 2014b) petrographic and microthermometric evidences suggested a deep source of silicate- rich vapor phase as it was envisaged by Wyllie and Ryabchikov, (2000) in the join $NaAlSi_2O_6$-$KAlSi_3O_8$-H_2O at 2GPa and 700^oC, where the silicate content in the vapor increase from ~30 wt% in the $NaAlSi_2O_6$-H_2O boundary system to ~60 wt% for vapor coexisting with both jadeite and muscovite; Chalot-Prat F., Arnold M.(1999) documented immiscibility between carbonate and silicate melts at mantle depth in the Persani Mountains quaternary alkaline magmatism. V-vapor, Kx-solid (silicate, carbonate, sulfate), L-liquid, ?- unknown. Scale bar in µm.

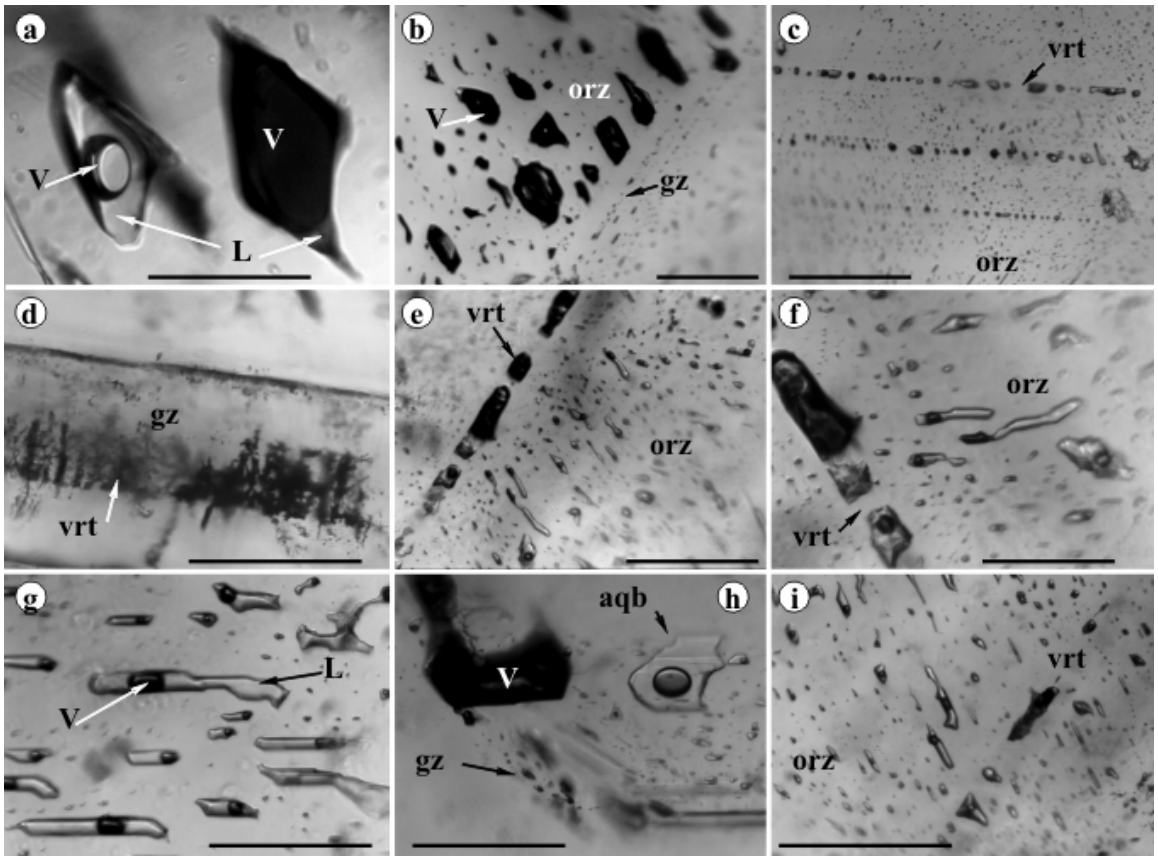

Fig. 90. Primary and pseudosecondary microtexture features in zoned epithermal quartz from "Main Vein" of Baia Sprie ore deposit; **a**, **b**, **h**- coeval liquid -, and vapor-rich inclusions; **c**, **d**, **e**, **f**, **g**, **i**- growth zones decorated by biphasic aqueous inclusions with variable orientation in the same horizontal plan section; gz- growth zone, orz- horizontal perpendicular growth zone, vrt- vertical parallel growth zones in horizontal plane-view, aqb- aqueous fluid inclusion, V- vapor, L-liquid.. (similar feature mentioned also in Heinrich, 2007, fig 1c). Scale bar in µm

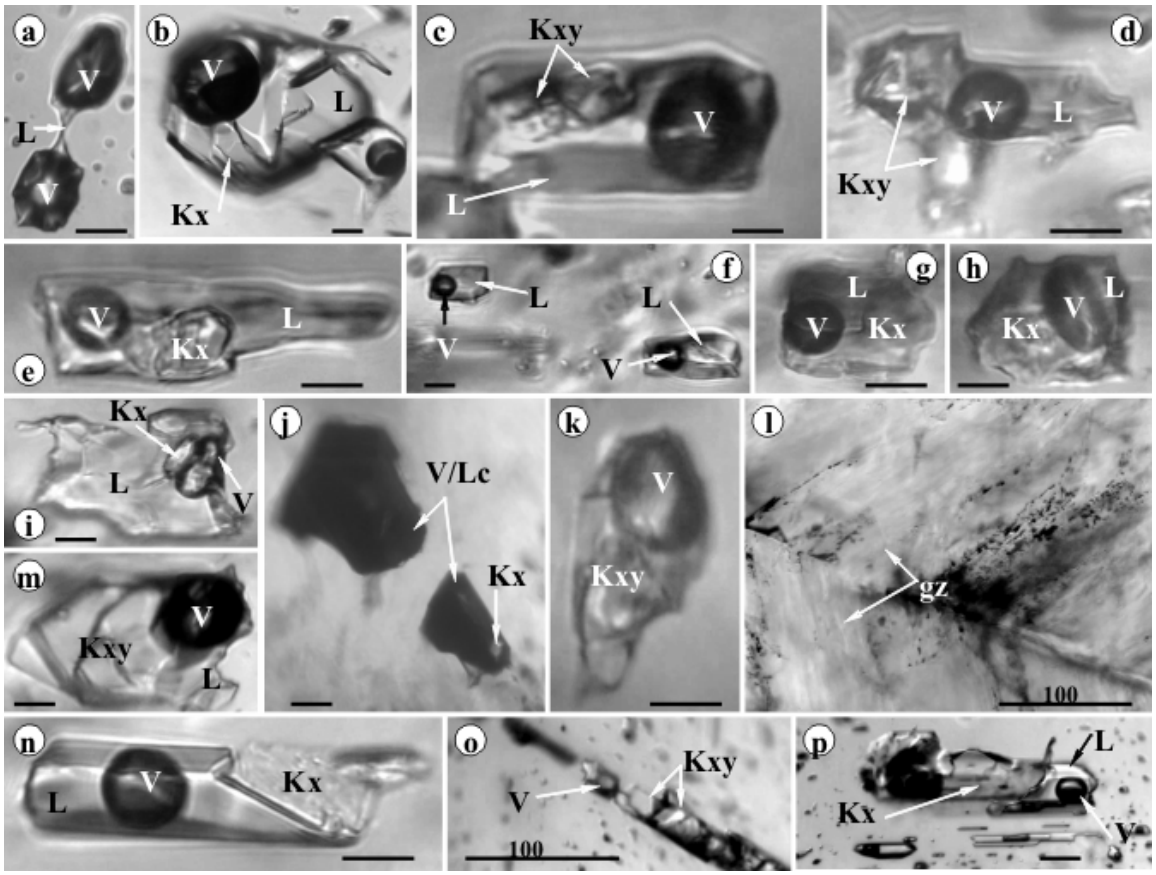

Fig. 91. Vapor - rich inclusion (**a**, **j**), biphasic (**f**) and multiphase (**b**, **c**, **d**, **e**, **g**, **h**, **i**, **k**, **m**, **n**, **o**, **p**) fluid inclusions (in quartz growth zone of the second mineralization stage (Nedelcu and Pintea, 1993; Pintea, 1995a;1996b) of the "Main Vein" from the Baia Sprie epithermal ore deposit; **l**. dihedral growth zones; V-vapor, L-liquid, Lc- CO_2-liquid rim, Kx, Kxy – solid phases (silicate, carbonate, sulfate); These solid phases are characteristic trapped phases in fluid inclusions from all epithermal ore deposit from Baia Mare mining district suggesting complex fluid phase composition (primary and secondary silica and carbonate) probably responsible for intensive adularization and silicification processes (Giuşcă, 1960, Manilici et al., 1965; Stanciu, 1984). Scale bar in µm.

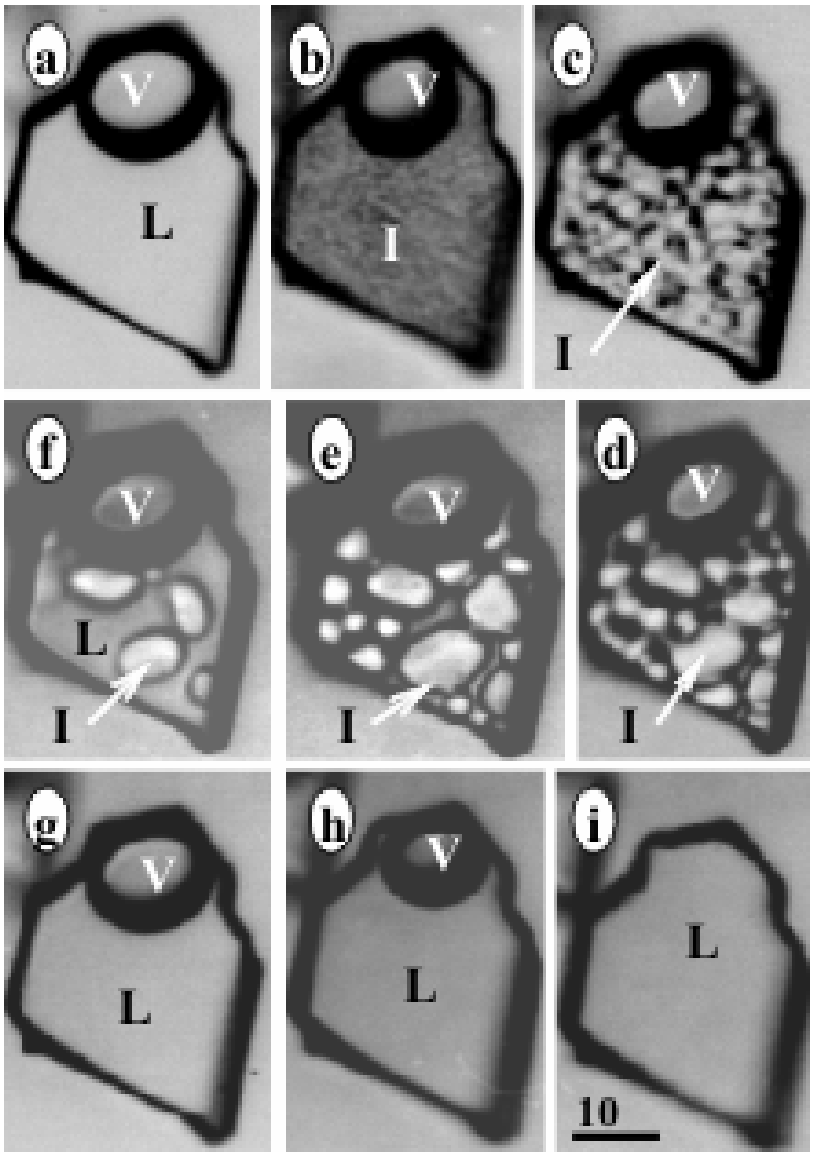

Fig. 92. Aqueous fluid inclusion microthermometry from Baia Sprie hydrothermal quartz. **a**.+25°C, **b**.-79°C, **c**.-28°C (Te), **d**.intermediate, **e**. -11.4°C (Tmi), f.-7°C, **g**. +25°C, **h.** to **i**. Th= +250°C (first fluid inclusion criometry in Romania – I. Pintea in Nedelcu et al., 1987, unpubl. report IGG; Pintea, 1995a, 1996b); L-liquid, V-vapor, I-ice, Scale bar in µm.

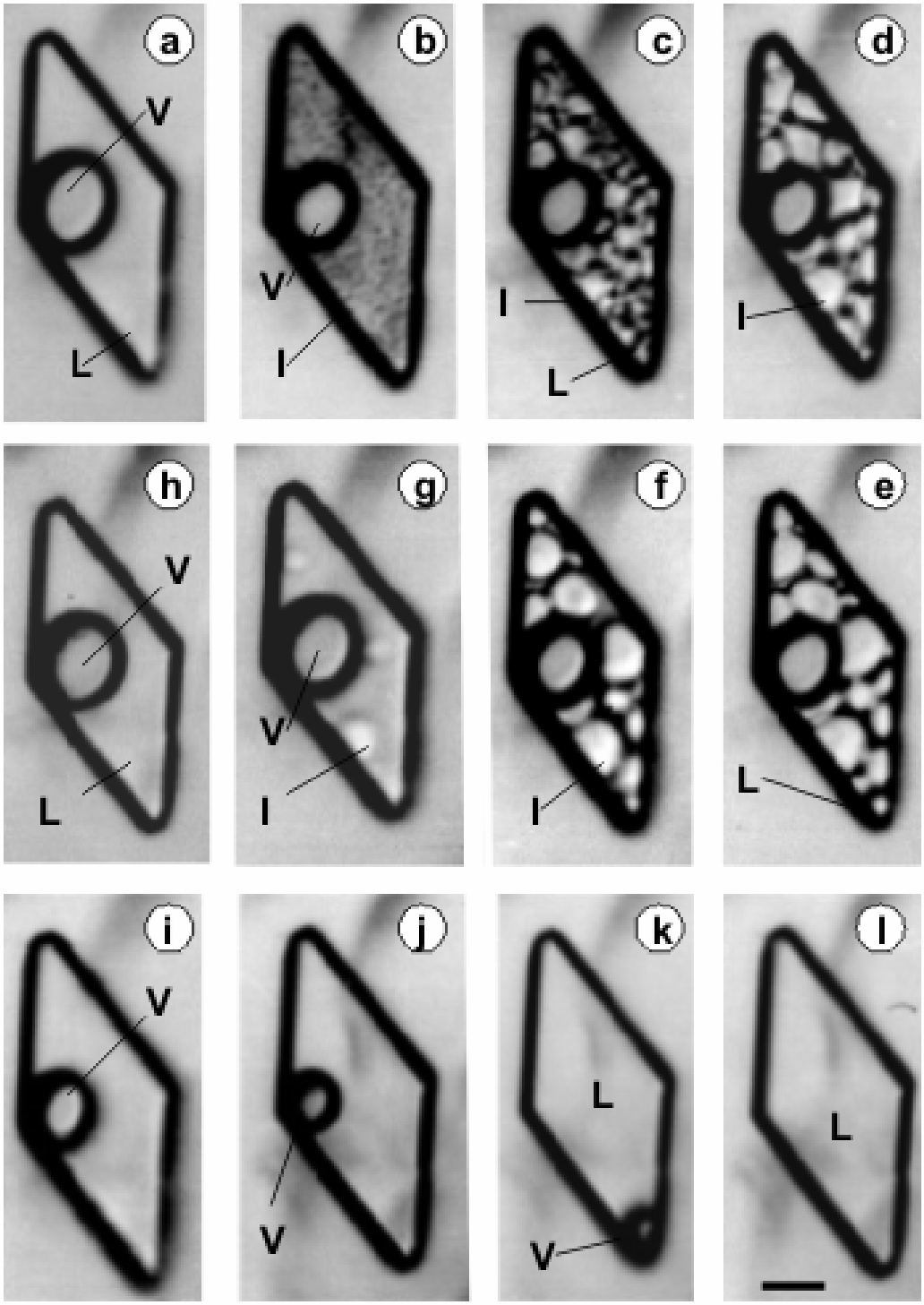

Fig. 93. Aqueous fluid inclusion microthermometry from Baia Sprie hydrothermal quartz. **a**.+25°C, **b**.-63°C, **c**.-28°C, **d**.-25°C, **e**.-23.8°C, **f**. -19.8°C, **g**. to **h**. Tmi =-4.6°C, **i**.+130°C, **j**.+167°C, **k**. to **l**. Th= +250°C, salinity =7.31wt % NaCl eq (Bodnar ,1993) (modified from Pintea, 1995a).Scale bar 15µm.

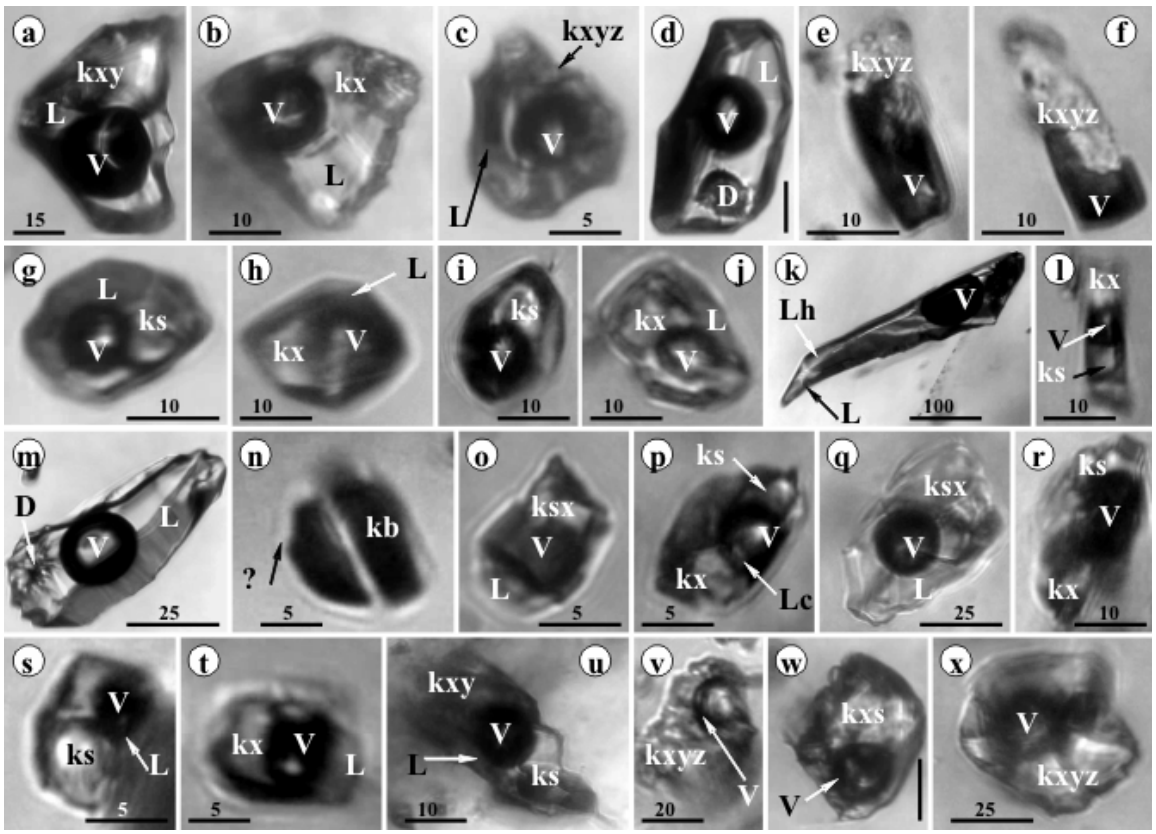

Fig. 94. Solid-bearing liquid-rich inclusions in epithermal quartz from Cavnic Pb-Zn-Cu deposit (Baia Mare mining district); **a**, **b**, **c**, **h**, **j**, **r**, **t**, **u**- liquid rich with insoluble solid phases (silicate, carbonate); **g**, **i**, **l**, **o**, **p**, **r**, **s**, **u**, **w**- liquid-rich with possible soluble solid phases (rounded unknown salt-? etc); **d**, **m**- liquid – rich with dawsonite; **e**, **f**, **n**, **x**- multiple solid and vapor (no liquid at room temperature); kx, kxy, kxyz- insoluble solid phases; ks-ksx- possible soluble solid phases; kb- biotite-like flakes embedded in another solid phase (glass-?); L-liquid, V-vapor, Lh-liquid hydrocarbon (?), D- dawsonite. The nature and origin of the solid phases are unkown yet but some of them could be precipitate from the silicate rich magmatic vapor phases (Pintea, 2014b), others were formed before trapping during fluid-rock interaction processes as alteration products. There is not mention yet about the halite daughter phase in these fluid inclusions (Pintea, 2012). Scale bar in µm; **d**- 20µm, **w**-10µm.

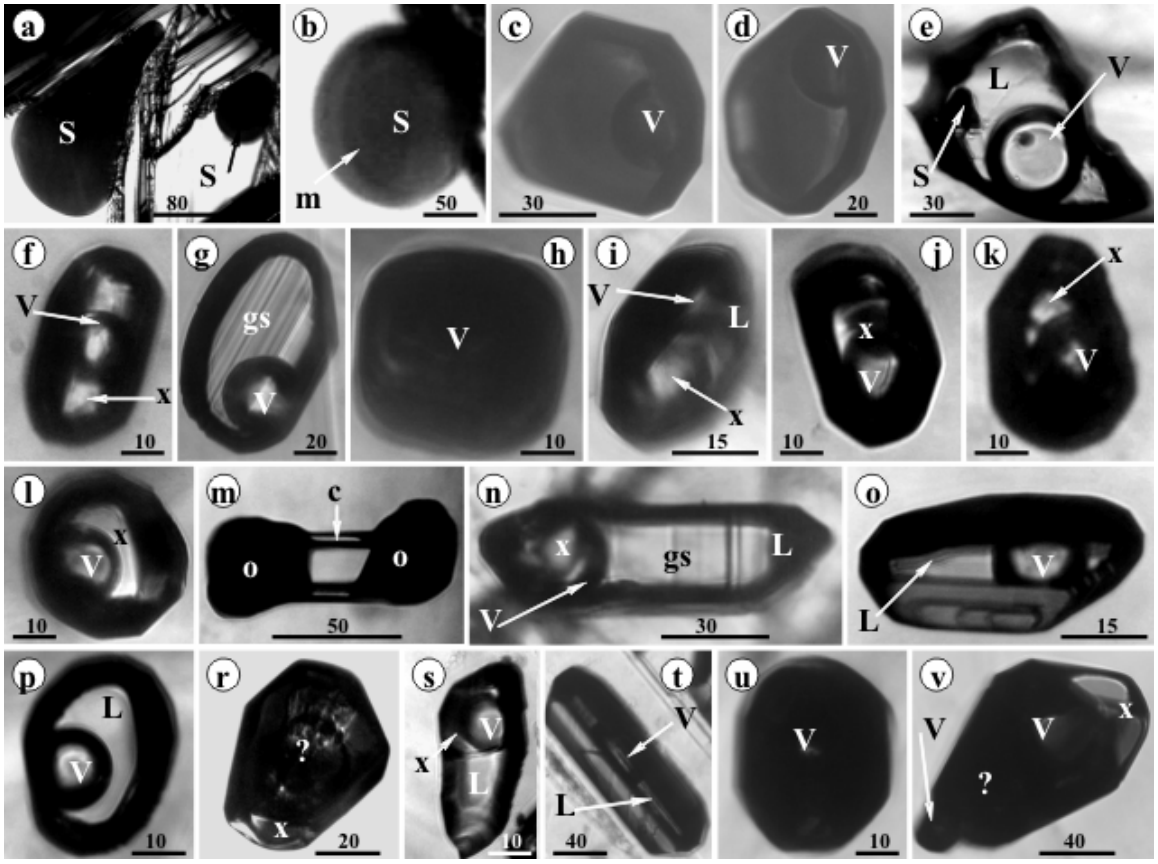

Fig. 95. Solid and fluid inclusions in Cavnic-Bolduţ sphalerite; **a**, **b**- globular sulphides (immiscibility-?); **c**, **d**, **o**, **p**, **t**- biphasic fluid inclusions; **g**, **n**- biphasic fluid inclusions showing oscillatory stria (varves-?) on the cavity walls (see Roedder, 1972); **e**, **f**, **i**, **j**, **k**, **l**, **s**- liquid rich inclusions with unknown solid phases;h,u,v- vapor (?) rich like fluid inclusions; **m**, **o**, **r**- multiple solid microinclusions; S- sulfide, x- unknown solid phase, o-opaque, c- capillary with liquid (?), L-liquid, V- vapor, ?- unknown. Scale bar in µm.

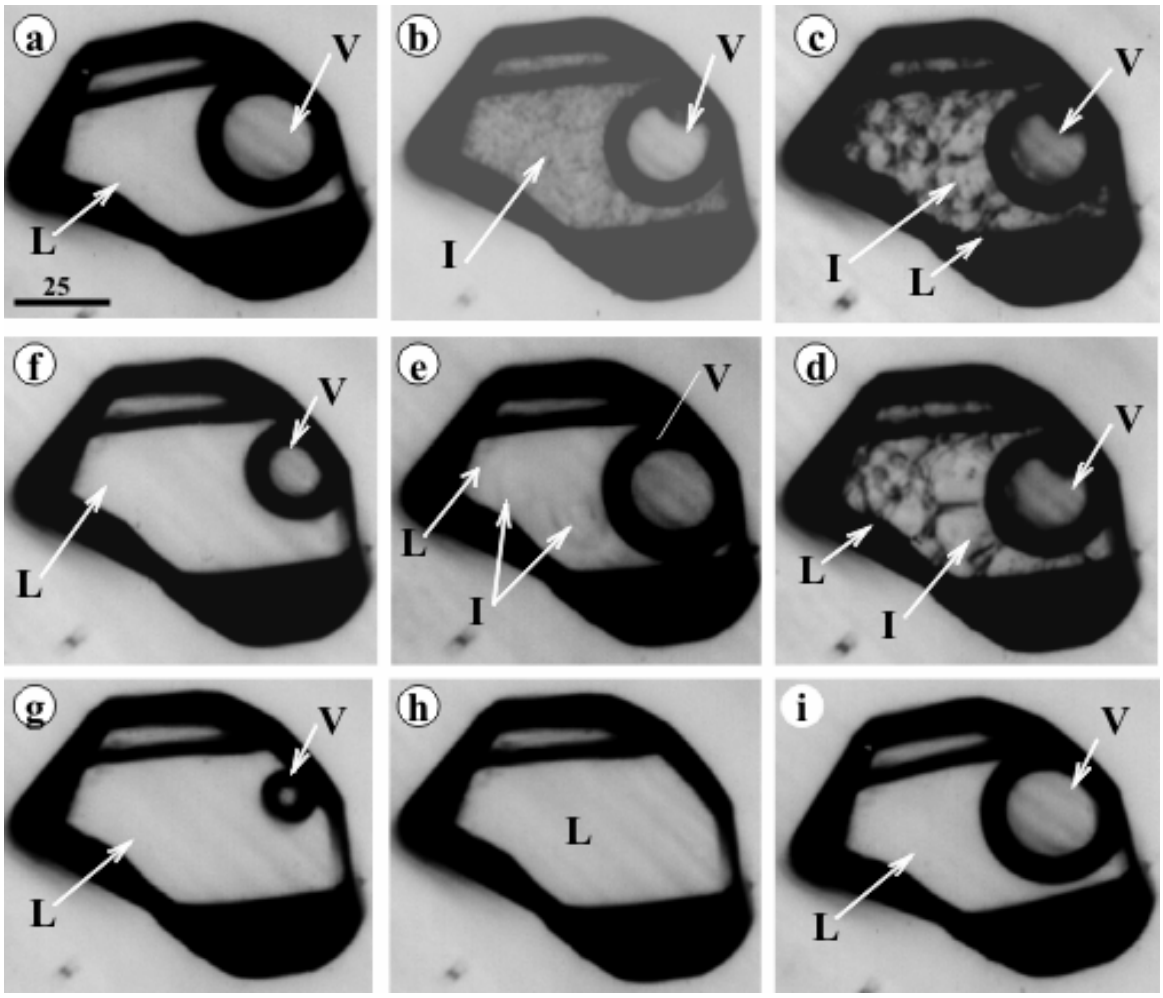

Fig. 96. Aqueous biphasic fluid inclusion microthermometry from Cavnic-Bolduţ sphalerite (Baia Mare mining district); **a**.+25°C, **b**.-70°C, **c**.-22.5°C, **d**.-14°C, **e**.-11oC, (Tmi= -9°C, salinity = 12.85 wt% NaCl eq), **f**.+162°C, g.+20°C, **h**. Th= +214°C. Scale bar in µm (Pintea, 1995a; 1996b). Scale bar in µm.

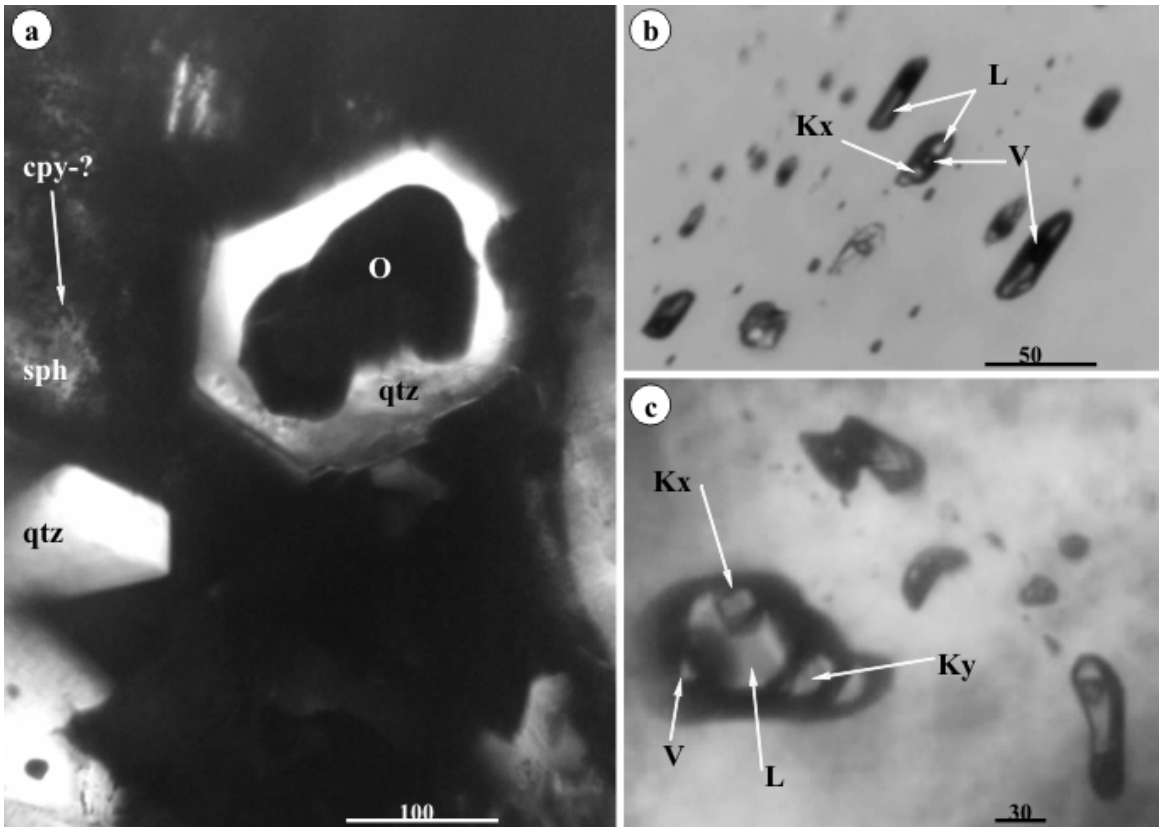

Fig. 97. Solid and multiphasic fluid inclusions in sphalerite quartz paragenese from Cavnic-Bolduț (Kelemen vein) epithermal Pb-Zn-Cu ore deposit; **a**. quartz containg an opaque grain coprecipitated with sphalerite; **b**, **c** – aqueous biphasic and multiphase fluid inclusions (the rounded solid phase suggest a soluble included salt, but halite daughter phase was not identified yet, by microthermometry- Pintea, 2012); L- liquid, V-vapor, kx- solid (soluble-?) entrapped or daughter pahases(?), ky- silicate, carbonate grains. Scale bar in μm.

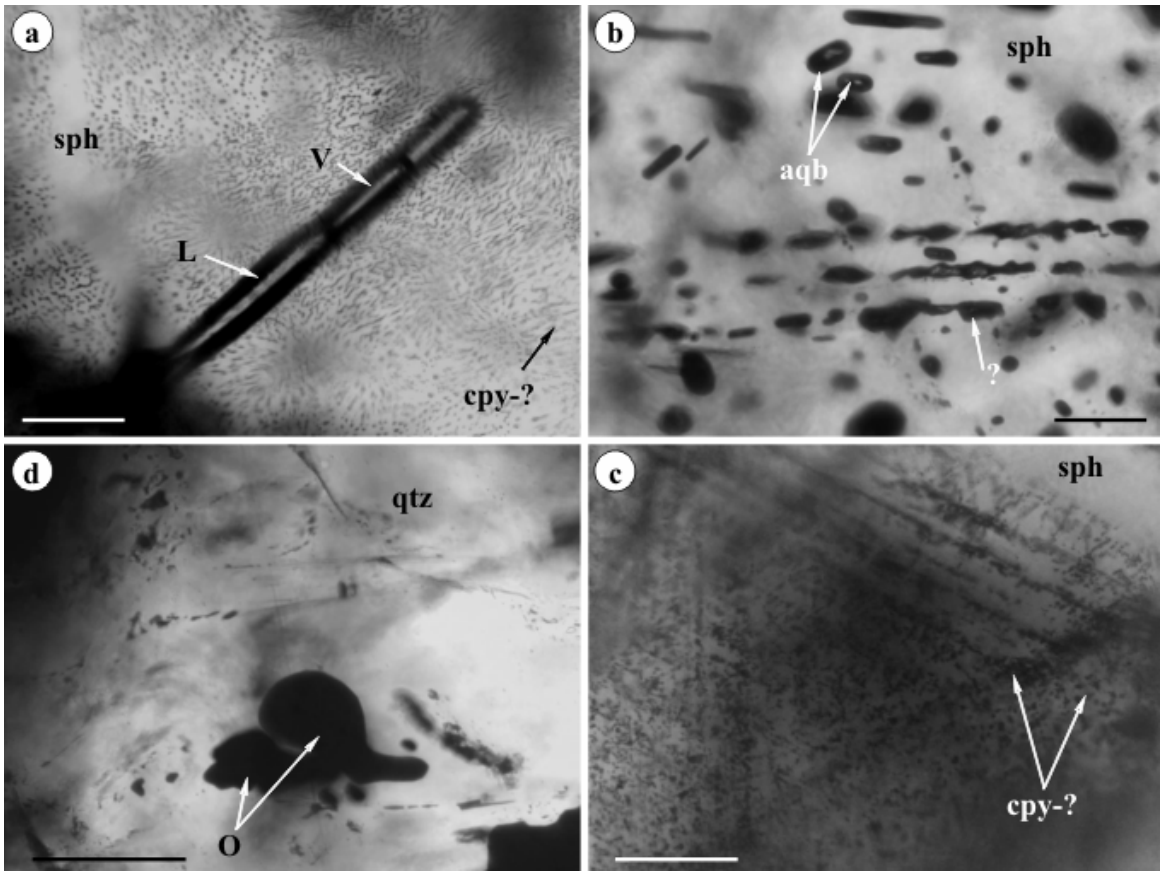

Fig. 98. Chalcopyrite "disease" in sphalerite and fluid and solid inclusions in paragenetic epithermal quartz crystal; **a**. tubular fluid inclusion trapped in a typical dusty "chalcopyrite disease" microtexture in sphalerite; contemporaneous fluid inclusions and opaque sulphides in **b** sphalerite and **d** in paragenetic quartz; **c**. coprecipitated microtexture of chalcopyrite in sphalerite. Coprecipitation was suggested during experimental work by Kojima (1990) to explain the intimate association of chalcopyrite in sphalerite. It was noticed that "it is likely that the typical "chalcopyrite disease" textures are generated from a comparatively high temperature solution following a typical solvation reaction such as (Kojima, 1990):

$CuFeS_2 + H^+ + 1/4O_2 + Cl^- = FeS_2 + 1/2H_2O + CuCl$;

$CuFeS_2 + 4H^+ + (n+1)Cl^- + 1/2H_2O = FeCl_n^{2-n} + CuCl + 1/4O_2 + 2H_2S$;

$ZnS + 2H^+ + nCl^- = ZnCl_n^{2-n} + H_2S$.

Notations: sph- sphalerite, cpy-chalcopyrite, L-liquid, V- vapor, ?-unknown, O-opaque, aqb- aqueous bipasic (L+V) fluid inclusions. Scale bar: 100 µm.

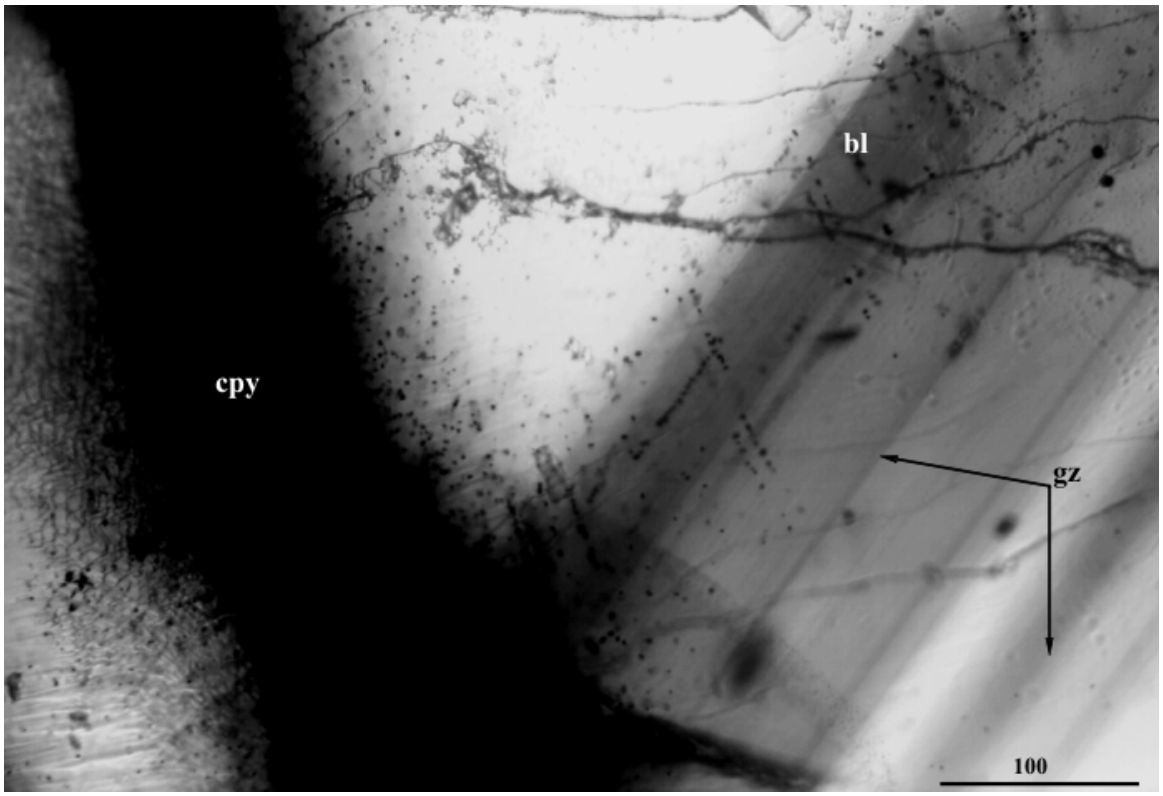

Fig. 99. Bimodal chalcopyrite "disease" in sphalerite from Cavnic-Boldut (Kelemen vein) Pb-Zn-Cu epithermal ore deposit suggesting a replacement process (Barton and Bethke, 1987) through a fracture dusted with chalcopyrite, cross-cutting a primary oscillatory growth zone in sphalerite. Replacement process in chalcopyrite disease microtexture was introduced by Barton and Bethke, 1987 and further discussed by Sugaki et al., 1987; Bortnikov et al., 1991. Replacement of the FeS from sphalerite with $CuFeS_2$ was suggested by Barton (1987) and Eldrige et al., (1988) showed experimentally that the process is characterized by such reactions:

$Zn_{0.80}Fe_{0.20}S + 0.20Cu^{+} + 0.20H^{+} = 0.60ZnS + 0.20CuFeS_2 + 0.20Zn^{+2} + 0.10H_2$

$FeS_2 + Cu^{+} + 0.5H_2O = CuFeS_2 + H^{+}$

$FeS_2 + 2ZnS + Fe^{+2} + 2Cu^{+} = 2CuFeS_2 + 2Zn^{+2}$

The presence of copper in sphalerite Cavnic samples is suggested for example in Fig. 95e by the triangular opaque daughter phase formed inside the aqueous epithermal fluid and also by some isolated rounded blebs from Fig. 95a,b,c in sphalerite or in paragenetic quartz in Fig. 97a and Fig. 98d. Notations: cpy-chalcopyrite, bl-sphalerite, gz-growth zones. Scale bar in µm.

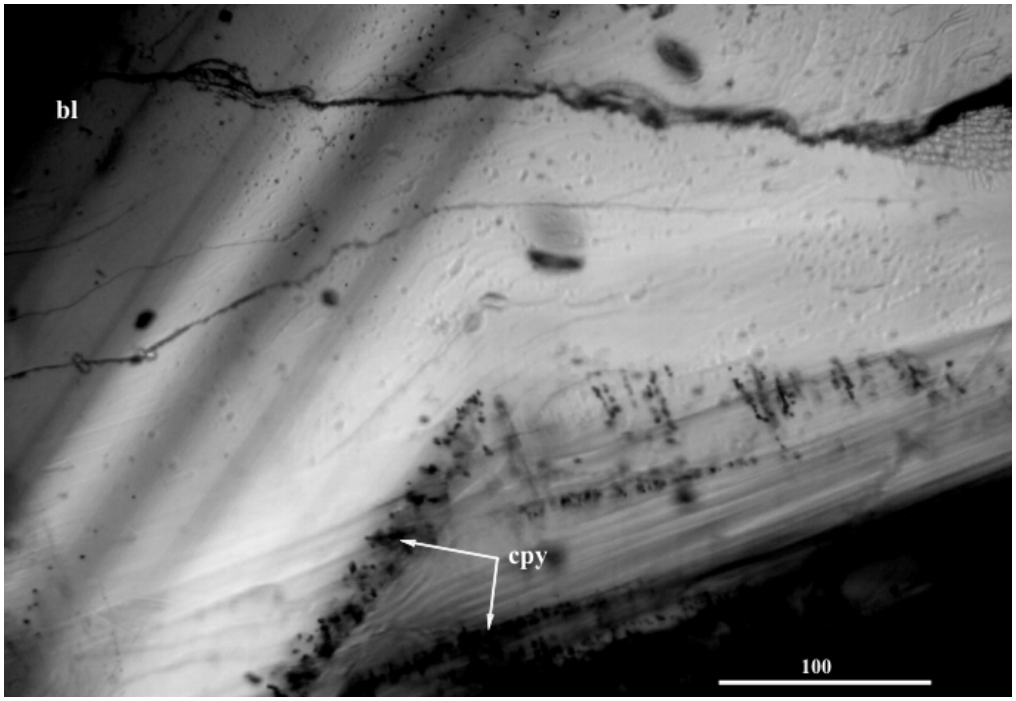

Fig. 100. Chalcopyrite "disease" partially oriented (coprecipitated) parallel to the oscillatory growth zone in sphalerite up to complete replacement (right down side of the picture); bl- sphalerite, cpy-chalcopyrite. Scale bar in µm.

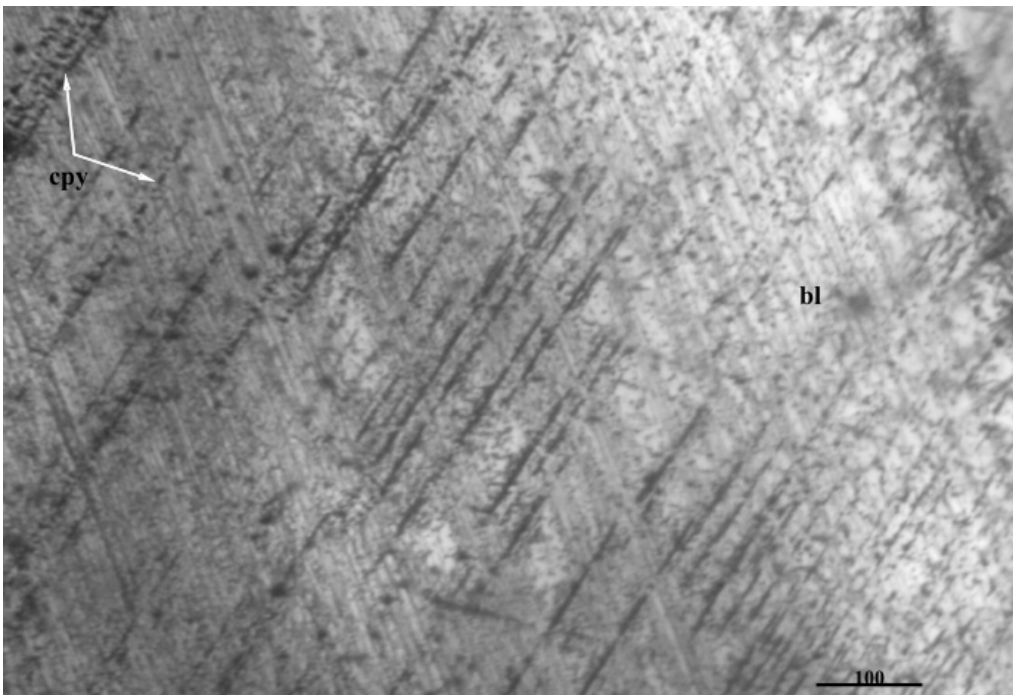

Fig. 101. Intimate chalcopyrite "disease" microtexture by coprecipitation (?) in the yellow-brown sphalerite from Coranda-Hondol epithermal ore deposit (Metaliferi Mountains). Scale bar in µm.

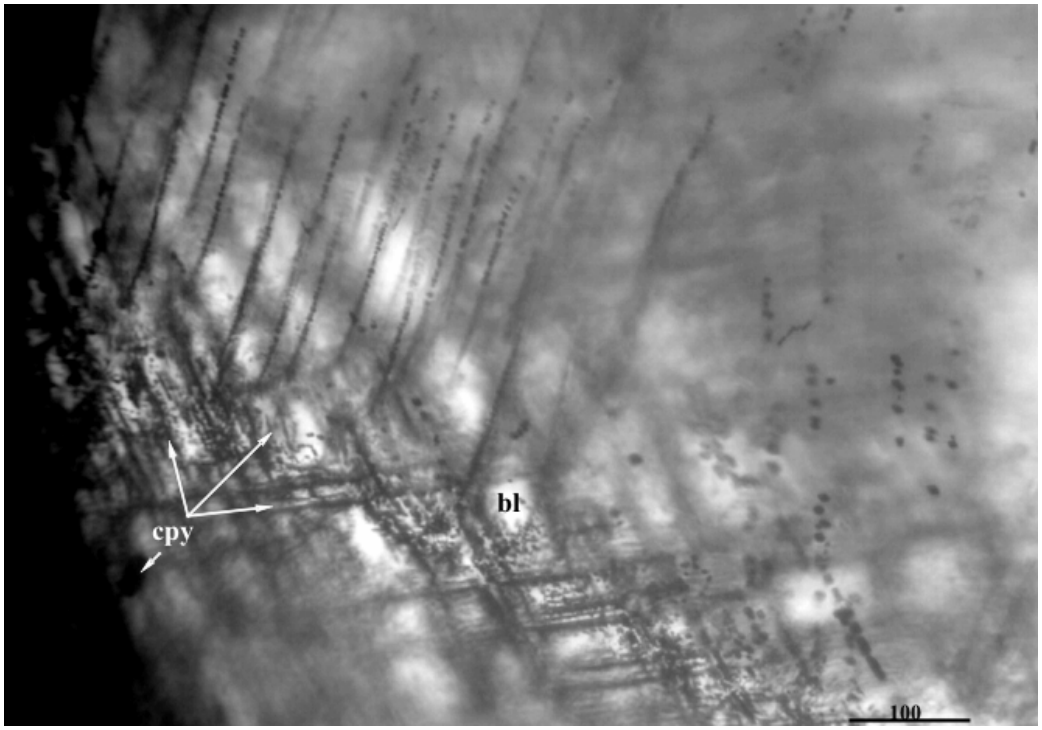

Fig. 102. Pseudo-3D image feature in sphalerite by lattice coprecipitation or replacement with chalcopyrite tiny blebs. Coranda – Hondol epithermal ore deposit (Metaliferi Mountains). cpy-chalcopyrite, bl-sphalerite. Scale bar in µm.

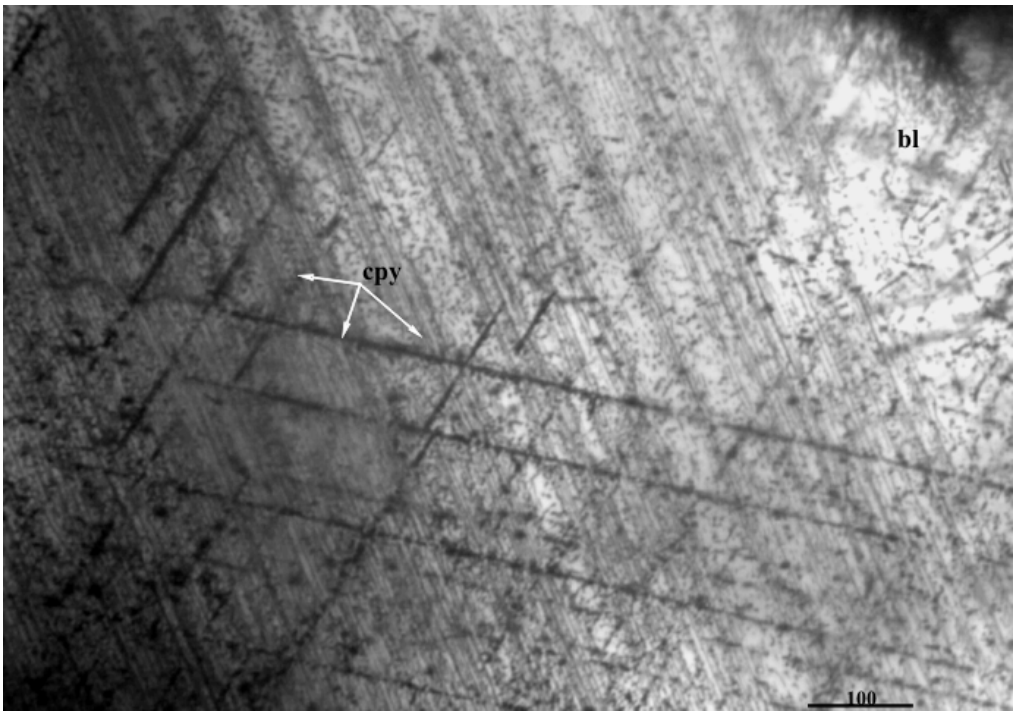

Fig. 103. Discontinuous coprecipitation or replacement of chalcopyrite blebs in sphalerite from Coranda-Hondol epithermal ore deposit (Metaliferi Mountains); cpy-chalcopyrite, bl- sphalerite. Scale bar in µm.

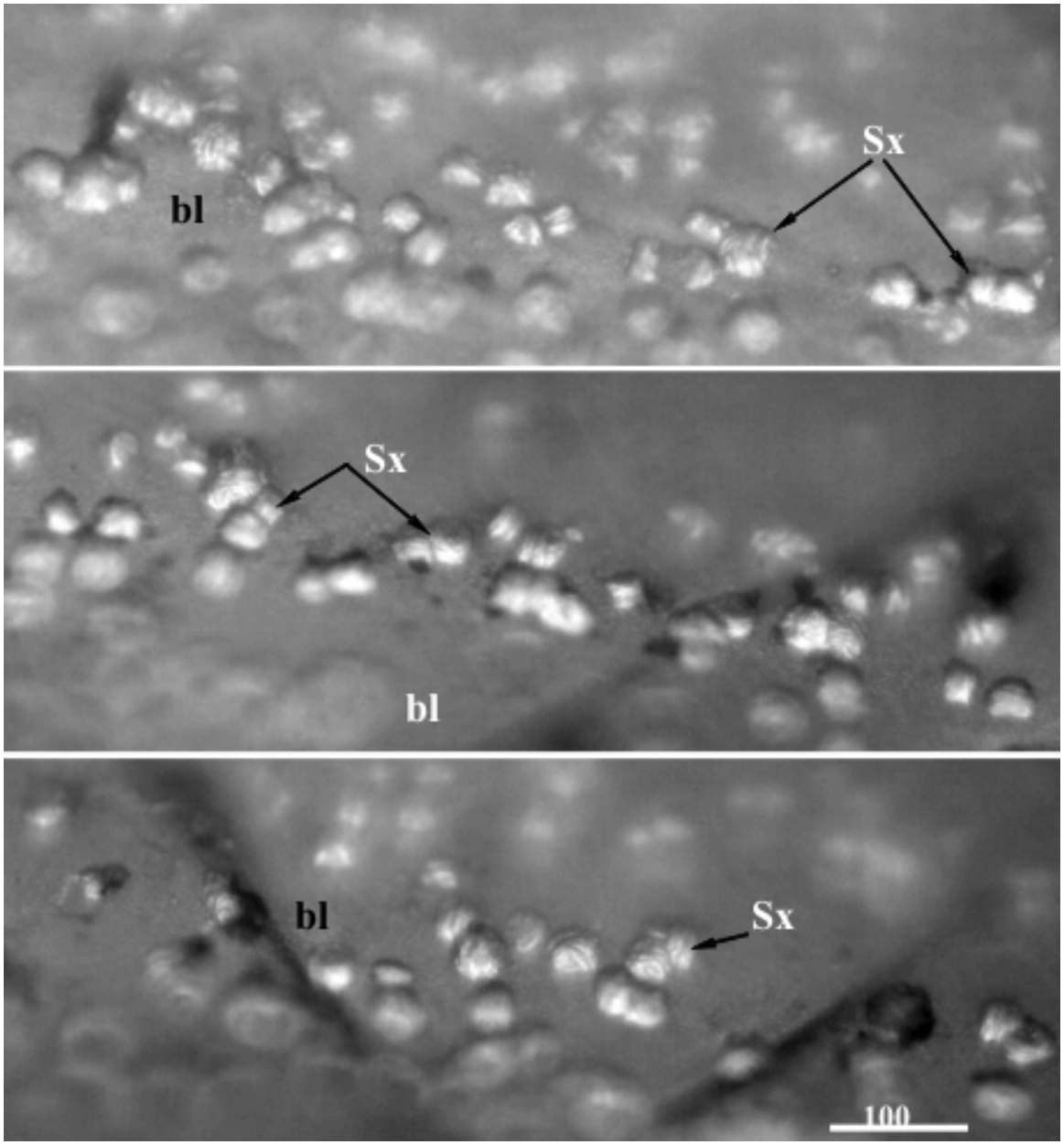

Fig. 104. Various focuses of transmited light microscopy onto the natural growing face of sphalerite from Coranda-Hondol epithermal ore deposit, showing the real half- shaped precipitated chalcopyrite blebs. The "lamellar-colomorphic" microtexture of chalcopyrite blebs is suggestive for precipitation in free voids in sphalerite already formed perhaps by resorption with reaction of acidic Cu- rich fluid related a mafic influx inside the magma chamber below. Coranda-Hondol ore deposit formation is caused mainly by the fluid escaped during the subvolcanic intrusion event in the Cretaceous sedimentary formations, and several magmatic successive events (even a porphyry- type mineralization was suggested by the presence of enargite-luzonite association on the "Avram brook" zone) (Udubaşa et al., 1979). Sx- chalcopyrite blebs (?), bl-sphalerite. Scale bar in μm.

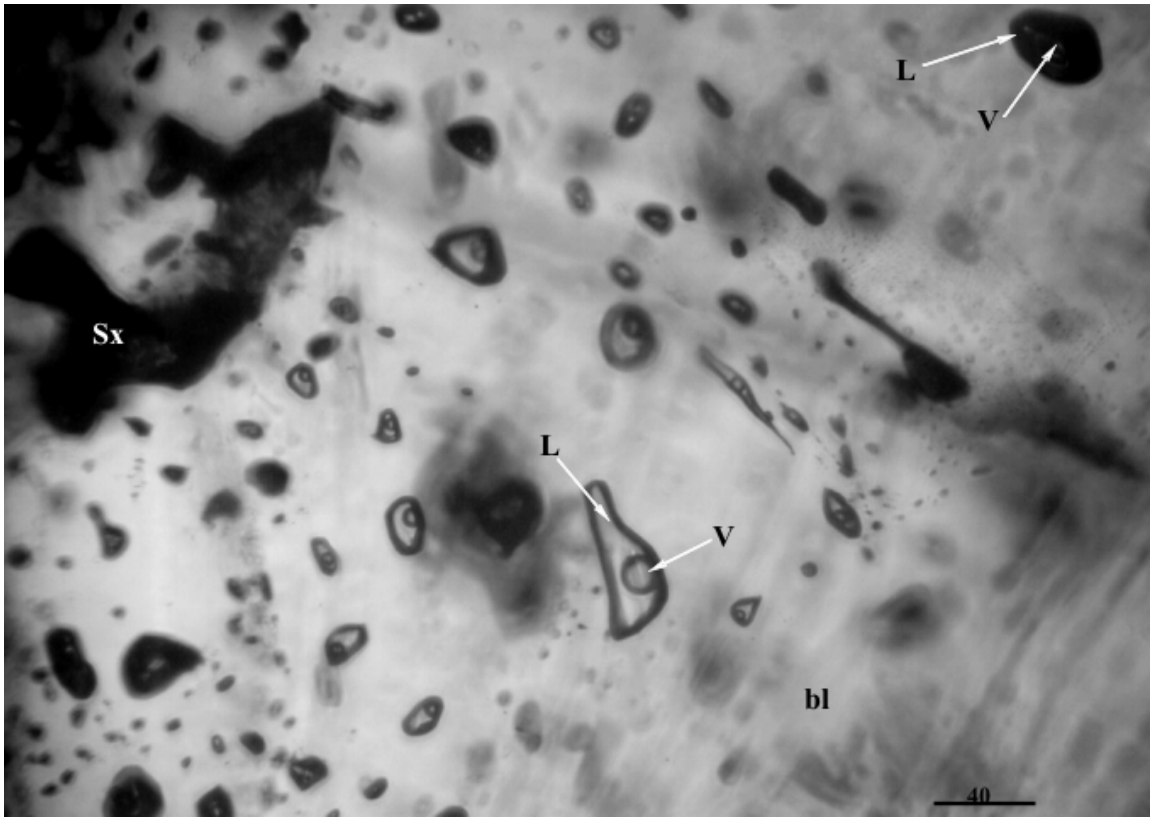

Fig. 105. Aqueous biphasic fluid inclusions trapped in a yellowish growth zone of sphalerite from Coranda-Hondol ore deposit, associated with isolated sulphides blebs (chalcopyrite-?). Sx- sulfide blebs (chalcopyrite-?), L-Lichid, V-vapor. Scale bar in µm.

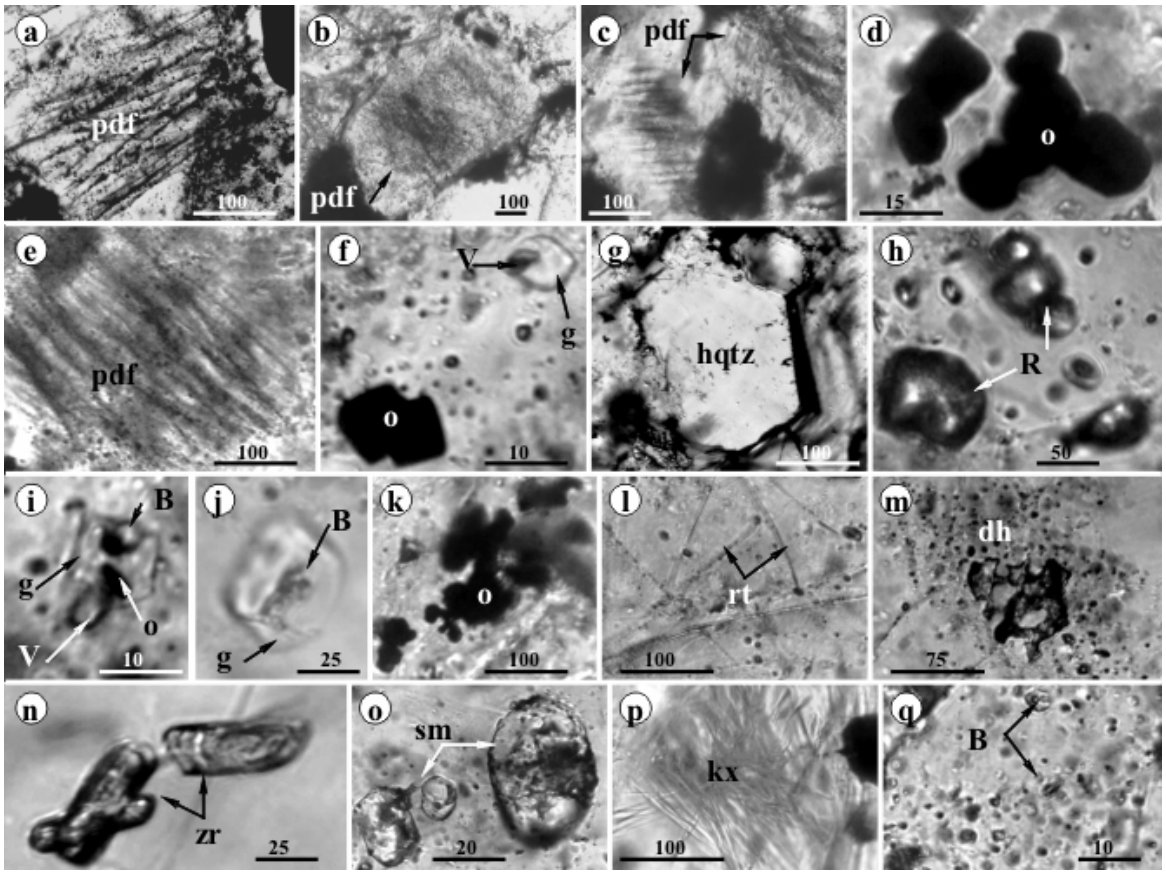

Fig. 106. Plan deformation features, solid-, melt and fluid inclusions types in the brecciated subvolcanic rock fragment pervasive hydrothermally altered from Coranda-Hondol open pit (Metaliferi Mountains); **a**, **b**, **c**, **e** - plan deformation paralel fractures (pdf) in quartz grain (pdf) similar to the features described in high pressure impact rocks (shocked quartz), **e**.**g**. Langenhorst (2002); Trepman and Spray (2003). They are very characteristic also in quartz from veinlets of porphyry copper deposit from Eastern Carpathians (e.g. Tibles massif) and Metaliferi Mountains, probably related to a strong decompression during exhumation (see also Fig. 22 and Fig. 109); **d**, **f**, **k**- opaque solid microcryst (O) isolated or agglutinated grain association; **h**, **l**, **n**, **p**- restitic solid mineral probably apatite (R-?) and rutile (R-?, rt), kx- silicate remnants or new dentritic; **i**, **j**, **o**- silicate melt inclusions containing brine (B), vapor (V) amd glass (g); g.- recrystallized quartz phenocrysts (hqtz); **m**- decrepitated silicate melt inclusion (dh); **q**- brine inclusion association (B). Scale bar in µm.

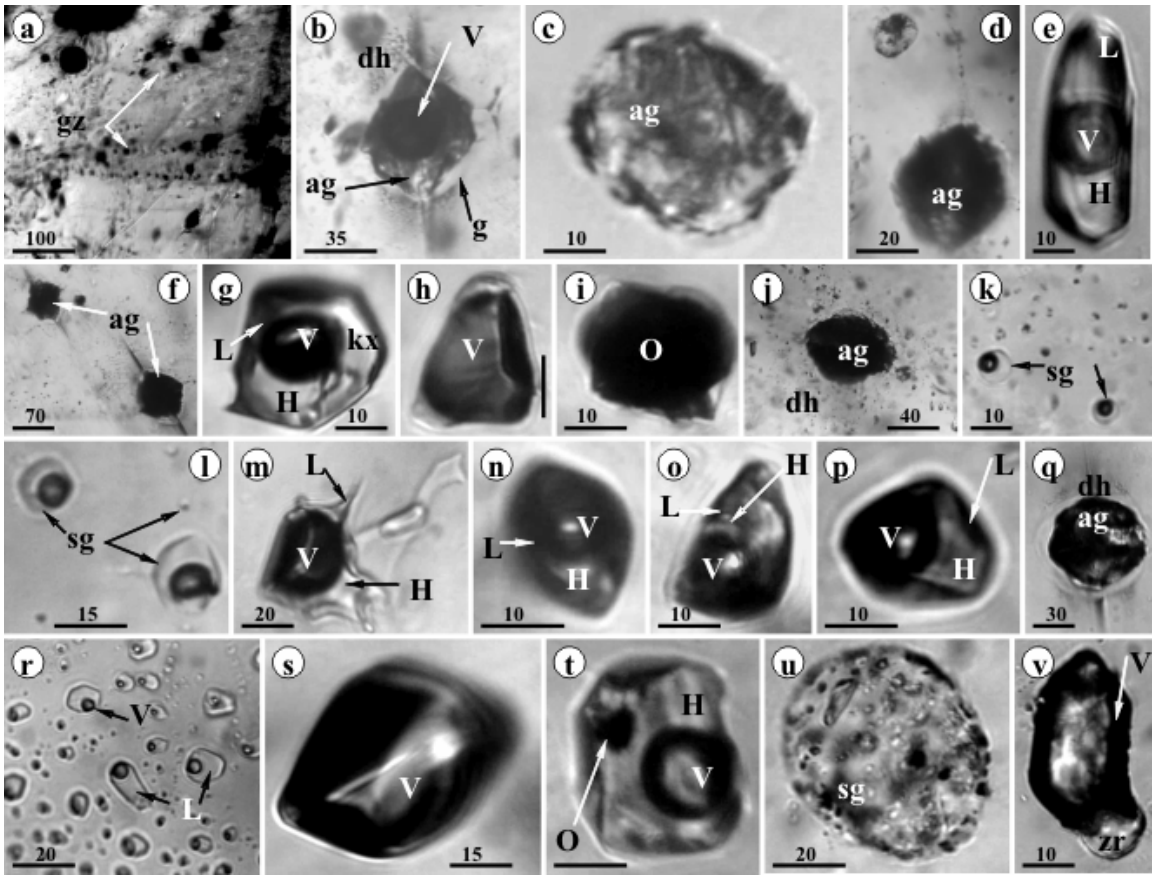

Fig. 107. Silicate melt and fluid inclusions types from β-quartz phenocrysts (2-3 mm) from quartz andesite (Săcărâmb type, e.g. Udubaşa et al., 1976) from Bocşa epithermal ore deposit (Metaliferi Mountains); **a**..- growth zoning in β-quartz phenocrysts; **b**, **c**, **d**, **f**, **j**, **q**, **u**- hydrothermally altered silicate melt inclusions; **e**. **g**. **m**. **n**. **o**. **p**. **t.**- brine inclusions; **h**, **s**, **v**- vapor rich inclusions; **k**, **l**- silicate glass inclusions; **i**- opaque inclusion; **r** secondary aqueous biphasic fluid inclusions; gz- growth zone, dh- decrepitated halo, ag.- altered silicate glass; L-liquid, H-halite, V- vapor, kx- other daughter(?) solid phase, zr- zircon. The microthermometry of the brine inclusions (L+H+V) suggested salinity between 30 and 50 wt% NaCl eq., and final homogenization temperature of ≥ 400° and 600°C. Their metallogenetic signification is very hard to be interpreted because many of them are secondary (and pseudosecondary) and perhaps formed "in situ" as alteration product of former silicate melt inclusions (Pintea, 2000- IGR unpubl. report). Scale bar in μm.

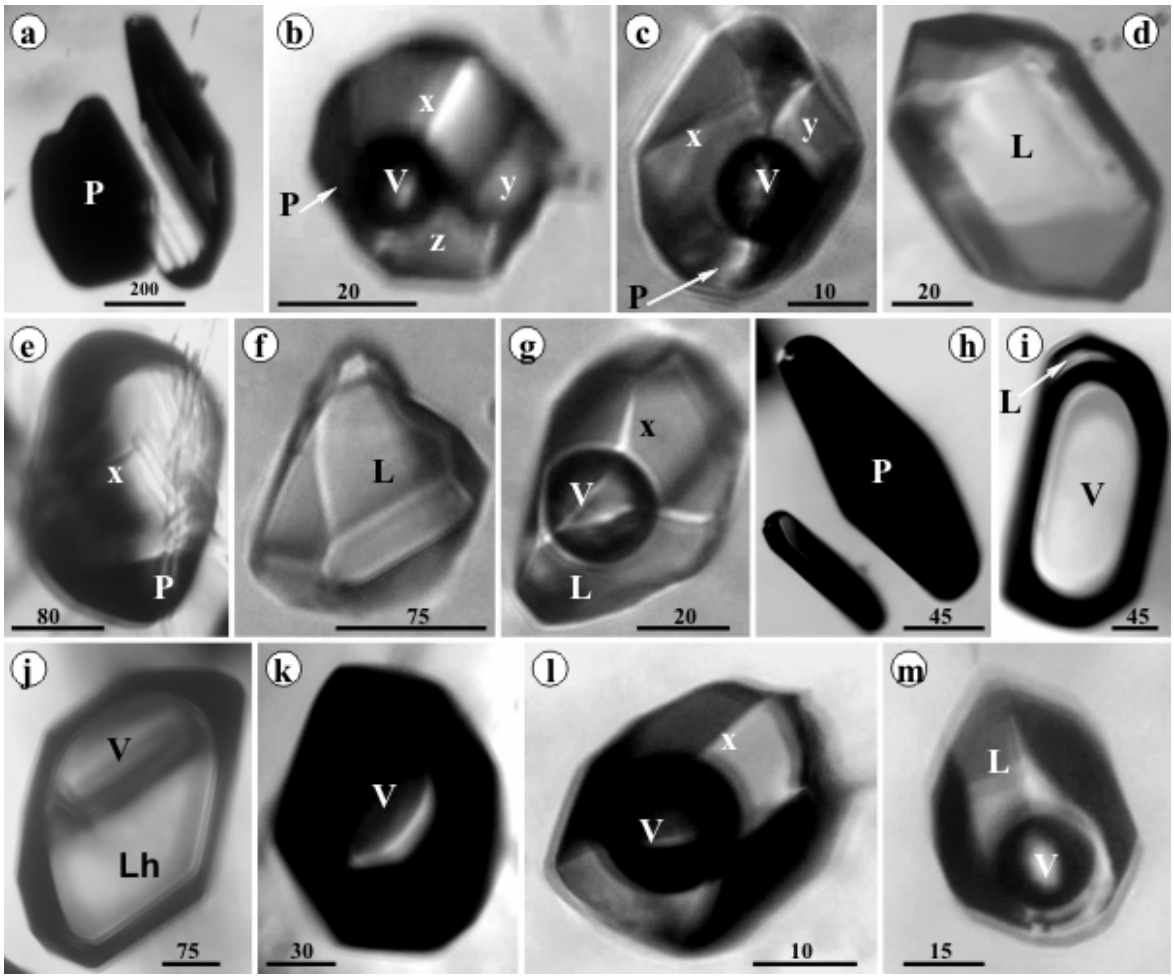

Fig. 108. Fluid inclusion types in epithermal quartz from Leopold upper level from Bocşa epithermal ore deposit (N Săcărâmb, Metaliferi Mountains); a. l. h. j.- possible hydrocarbons inclusions with pyrobitumen (?); **b**, **c**, **g**, **l**- multiphasic fluid inclusions; **d**, **f**- monophasic aqueous liquid inclusions; **i**, **k**- vapor rich inclusions; P-pyrobitumen(?), x, y, z,- unknown solid phases, L-Liquid, Lh- liquid hydrocarbons, V- vapor. Scale bar in µm.

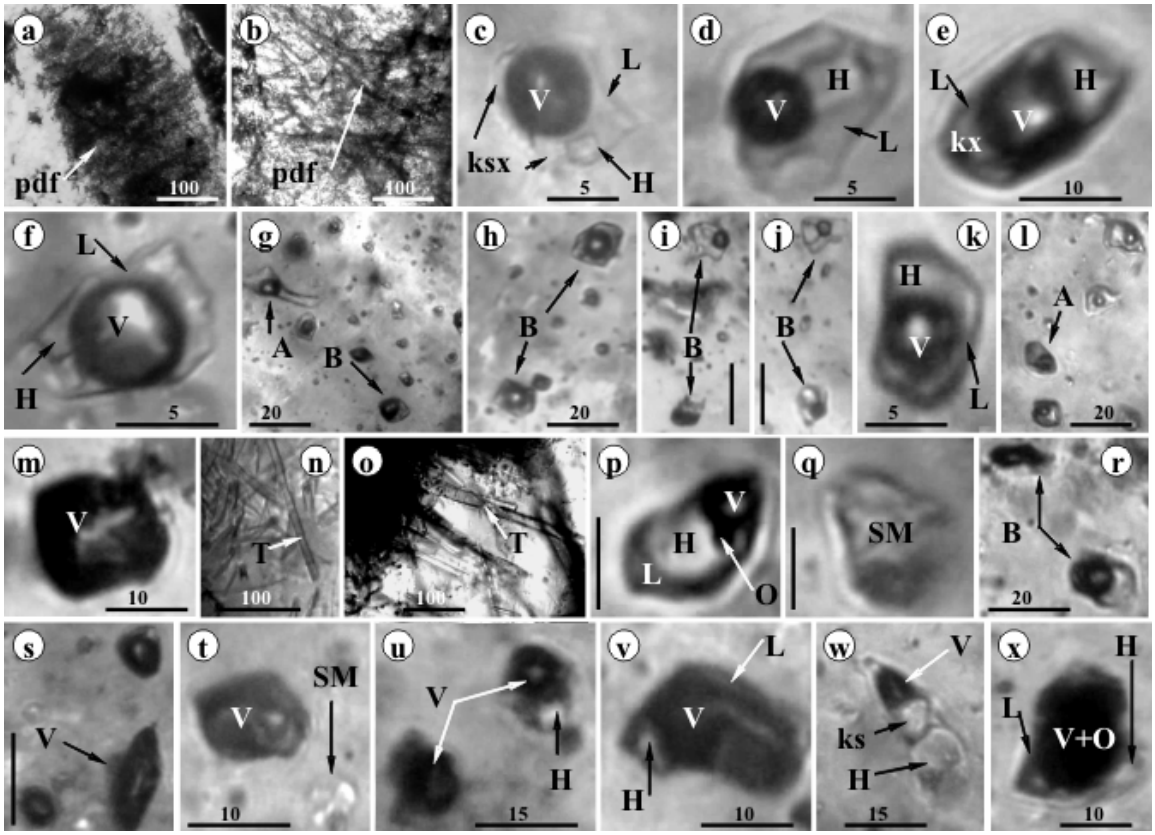

Fig. 109. Microtexture features, solid and fluid inclusions types in aplitic quartz veins from Toroioaga massif (Maramureş Mountains); **a**, **b**- plan deformation microcracks system in quartz grains; **c**, **d**, **e**, **f**, **h**, **j**, **k**, **p**, **r**, **w**- brine inclusions; g. l.- biphasic fluid inclusions; **m**, **s**, **t**, **v**, **x**- vapor rich inclusions; **u**- coeval vapor-rich and brine inclusions; **q**, **t**- silicate melt inclusions; n. o. recrystallized acicular phase (tourmaline-?); V- vapor, L-liquid, H- halite, ksx- another soluble solid daughter phase, kx- unknown solid phase, A- aqueous fluid inclusion, B- brine inclusiosions, T- tourmaline, o- opaque, SM- silicate melt (glass ±crystals). Silicate melt inclusion microthermometry showed Th ≥ 951°C and coeval brine inclusions indicated 50-52 wt % NaCl eq. and Th between 827°-974°C suggesting magmatic immiscibility (Pintea, 2014-PN 09210501 - IGR unpubl.). Scale bar in µm.

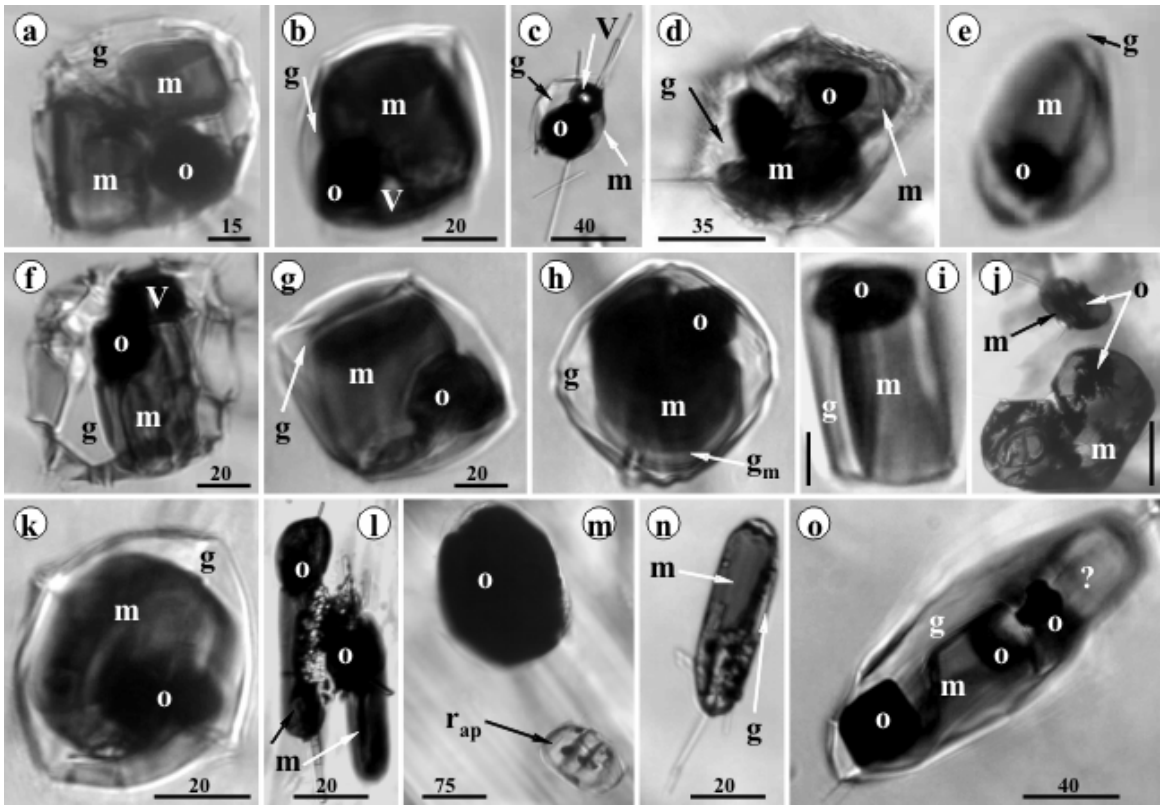

Fig. 110. Presumably magma mixing/mingling process suggested by the crystallized silicate melt inclusion containing brownish-dark mafic microminerals in acidic (white) silicate melt (now glass) in quartz and plagioclase phenocrysts from "Laleaua Albă" dacite (Baia Mare mining district); **a**, **b**, **d**, **e**, **f**, **g**, **i**, **o**- multiphasic silicate melt inclusions; **d**. **h**. **k**. **l**. - probable two contasting melt as a result of heterogeneous trapping (better evidentiated in complex silicate melt inclusions from Roşia Montană β-quartz phenocrysts showed in Fig.29 A, which homogenized around 1050°C- Pintea and Iatan, 2013); **m**- isolated Fe-S-O melt globule in plagioclase; Magma mixing/mixing was argued from Laleaua Alba dacite based upon the presence of sive microtexture in feldspar phenocrysts and xenocrysts, coronas with orthopyroxene around quartz (Kovacs, 2002) and also by recent EMPA analyses of isolated mafic solid minerals (biotite, amphibole) inclusions in quartz and plagioclase or K-feldspar and analyses of acidic silicate melt inclusions which shown distinctive ranges of SiO_2 content (Naumov et al., 2014). Notations: m- mafic minerals, o- opaque, V-vapor, g- glass, r- restitic apatite, ?- unknown. Scale bar in µm.

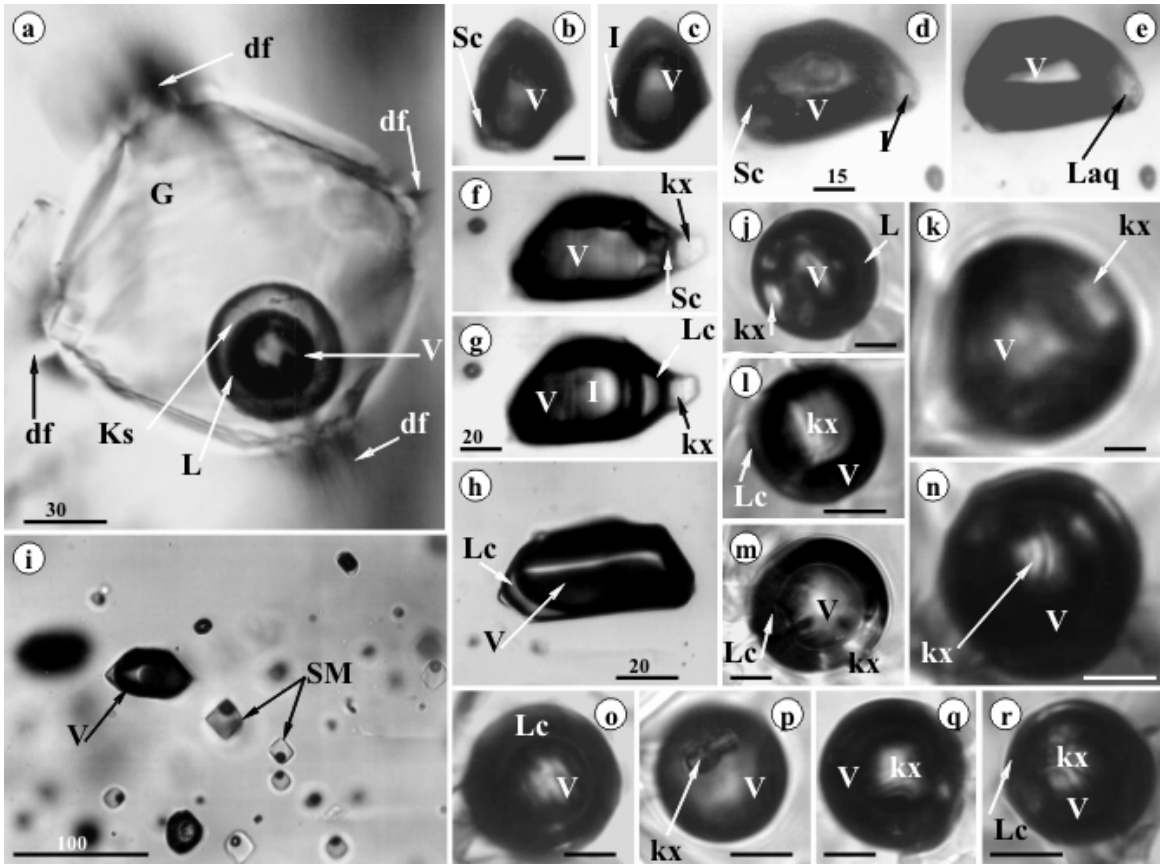

Fig. 111. Magmatic vapor phases in the contraction vapor bubbles from silicate melt inclusions in quartz and plagioclase from "Laleaua Albă" dacite (Baia Mare mining district); **a**. three-phasic aqueous fluid bubble in silicate glass inclusion. Biphasic inclusions (L+V) in the same silicate melt inclusion types measured by Naumov et al., 2014 showed salinity of 0.5 wt% NaCl eq, density of 0.84 g/cm^3 and Th=225°C, the author suggesting a minimum trapping pressue of about 8kbars for 800°C formation temperature; **b**. (-122°C), **c**.(-50°C), **d**.(-56.2^{o}C), **e**.(25°C), **f**.(-90°C), **g**.(-55°C), **h**.(-55.3^{o}C)- CO_2-rich secondary and pseudosecondary fluid inclusions at indicated temperatures; **j**, **k**, **l**, **m**, **n**, **o**, **p**, **q**, **r**-contraction vapor bubbles in silicate melt inclusions sometimes with solid and a tiny film of liquid CO_2 at room temperature conditions; **i**-association of silicate melt and vapor-rich inclusions in a secondary or pseudosecondary microcrack in quartz. Note: CO_2 rich inclusion pictured in **b** and **c** homogenized in vapor phase at +25.3^{o}C, from **f** and **g** Th= +23.6^{o}C, from **d** and **e** Th= +21.2^{o}C (Pintea, 1998 unpubl; Pintea, 2014b). The calculated trapping pressure, based upon CO_2 density value of about 0.2 g/cm^3 give around 0.4 kbars which means ≤1.5 km depth formation conditions, which suggest that the "Laleaua Alba" dacite was re-crystallized very close to the surface being brought out by hot magma influx (1100°-1200°C) from initial deep source (20-30 km). The vapor bubble content (soluble minerals and silicate, carbonate, sulfate solid phases) for unaltered silicate melt inclusions could be used successfully in magmatic vapor characterization and exploration purposes as it was documented elsewhere by Kamenetsky et al., 2002. Notations: df- decrepitation microfissure system oriented parallel to the C-axis of quartz, ks- soluble daughter pase (?), V-vapor, L-liquid, Sc- solid CO_2, kx- other daughter (?) solid phase (silicate, carbonate), Lc- CO_2- liquid film, SM- silicate melt inclusions. Scale bar in µm (b, c, j, k, l, m, n, o, p, q, r- 10µm).

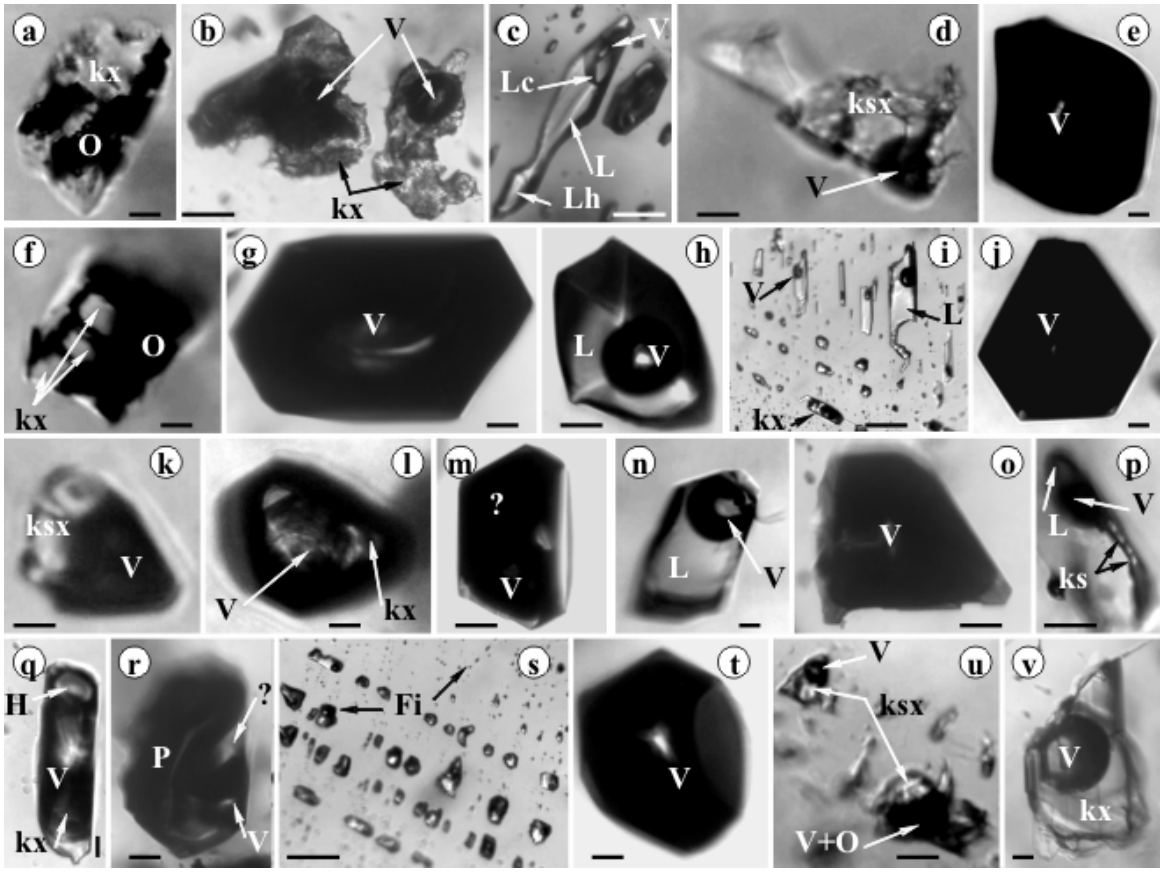

Fig. 112. Fluid and "melt" inclusions types in epithermal quartz crystals collected during "Field application" of the Geol. Soc. of Romania, Baia Mare branch (22-23 09.1990), from Hudin massif, near Arcer peak (Ţibleş Mountains); **a**, **b**, **d**, **f**, **i**, **k**, **l**, **m**, **p**, **u**, **v**- multiphasic inclusions with various ratio between solid, liquid and vapor phases; **c**, **r**.- hydrocarbons fluid inclusions (pyrobitumen-?); **e**, **g**, **j**, **o**, **t**- vapor-rich inclusions; **h**, **i**, **n**, **s**- aqueous biphasic fluid inclusions; **q**- brine inclusion (?); Fi- fluid inclusions, o-opaque, kx, ks- unknown solid daughter(?) phases, L-liquid, Lc- CO_2-liquid rim, Lh- liquid hydrocarbon, P-pyrobitumen-?, ?- unknown, V- vapor, H-halite(?). Scale bar: 10µm; **i**. **s**.- 100µm.

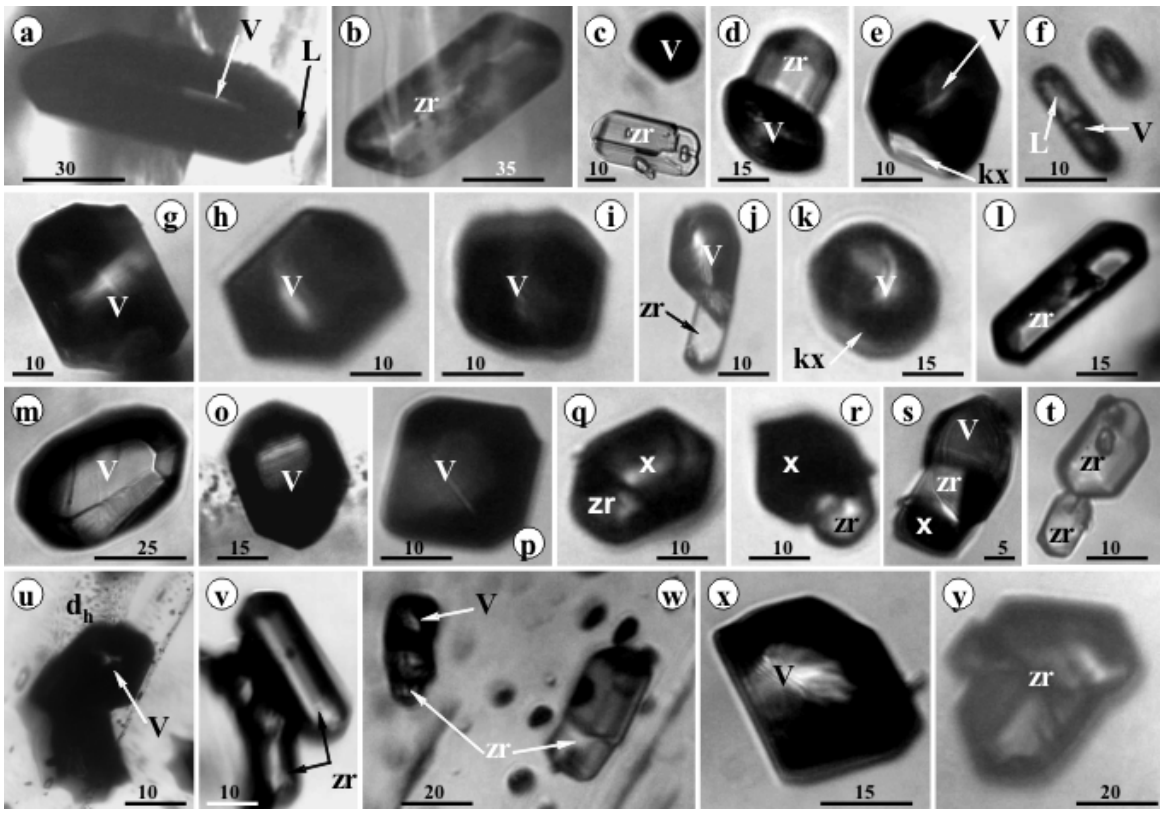

Fig. 113. Microsolid-, and fluid inclusions in remelted sphalerite (i.e. low-Fe yellow sphalerite-Udubaşa et al., 1983) from metamorphic upper Precambrian Rodna-Guşet Pb-Zn mineralization (Făget adit); **a. f**.- aqueous biphasic fluid inclusions; **c**, **d**, **g**, **h**, **i**, **k**, **m**, **o**, **u**, **x**-vapor rich inclusions; **b**, **c**, **d**, **j**, **l**, **q**, **r**, **s**, **t**, **v**, **w**, **y**- solid microinclusions (Pintea et al., 2021 - preliminary Raman analyses- Rruff data base- sugested the presence of Fizelyite-$Ag_5Pb_{14}Sb_{21}S_{48}$, Germanite- $Cu_{13}Fe_2Ge_2S_{16}$), Corkite-$PbF_3(SO_4)(PO)_4(OH)_6$ and possible zircon- $ZrSiO_4$ microcrysts, noted in the pictures undiferentiated by **zr**); **m**, **q**, **r**, **s**, **w**- others solid daughter (?) phases. Other notations: V-vapor, L-liquid, x-unknown, d_h-decrepitated halo. Scale bar in µm.

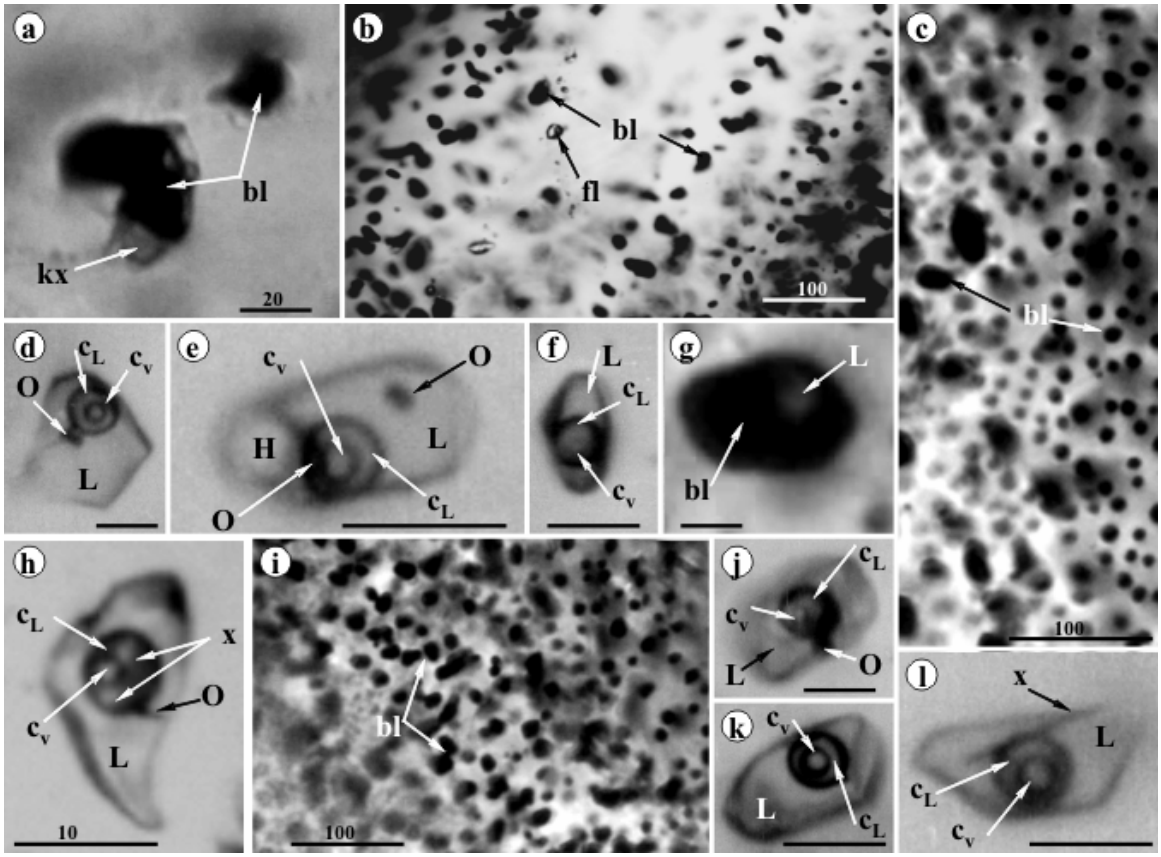

Fig. 114. Sphalerite globules (remelted) and CO_2- rich aqueous fluid inclusions in quartz from Blazna-Guşet metamorphic Pb-Zn mineralization (Faget adit); **a**, **g**, solid sphalerite globules (flakes) trapped together with liquid and others microsolid phases; **b**, **c**, **i**- sphalerite and fizelyite (?) flakes and blebs in trails of the recicatrized microcracks in quartz; **d**, **e**, **f**, **h**, **k**, **l**- CO_2- rich multiphasic fluid inclusion types in the same quartz samples; fl- fluid inclusions; bl- sphalerite, kx- other solid phases, H- halite, c_L- CO_2-liquid, c_V-CO_2 gas, L- aqueous liquid, O-opaque, x- unknown; (modified from Pintea 2012). Remobilization of sulphides as remelted product during metamorphism is a critical feature encountered in many metamorphic Pb-Zn ore deposits (e.g. Frost et al., 2002). Scale bar in µm; d, e, f, g, j, k, l,-ca 10µm.

Fig. 115. Two types of FIAs of the system H_2O-CO_2-NaCl trapped in (re)crystallized quartz veins from the REE-MoS_2 mineralizations of the NW Ditrău massif (Mesozoic) of the Jolotca mining prospect; **a**, **b**, **c**, **j**, **i**, **h**, **g**, **k**, **l**, **n**, **o**, **p**, **q**, **r**, **s**, **t**, **u**, **v**, **w**, **x**, **y**, **z**, **b'**, **c'**, **e'**, **f'**, **g'**, **k'**, **m'**- complex carbonic - rich type; **d**, **e**, **f**, **m**, **d'**, **h'**, **g'**, **l'**- brine type. Firstly, described by I. Pintea in the Jolotca epithermal prismatic euhedral quartz (750 Jolotca- main adit) and presented by Pomârleanu et al., 1984 (unpubl.) and further data from 21 Jolotca - adit, presented by Pintea, 1991a,1995a, 1996b; Pintea and Diamond, 1994 (unpubl.), mentioned in Fall et al., 2007; Notations: L_1- aqueous liquid, L_2- CO_2- liquid, Kx- unknown (KCl-?), H-halite, V- gas. Pictured at $\leq +10^oC$ in the microthermometric stage, under the microscope. Scale bar in µm.

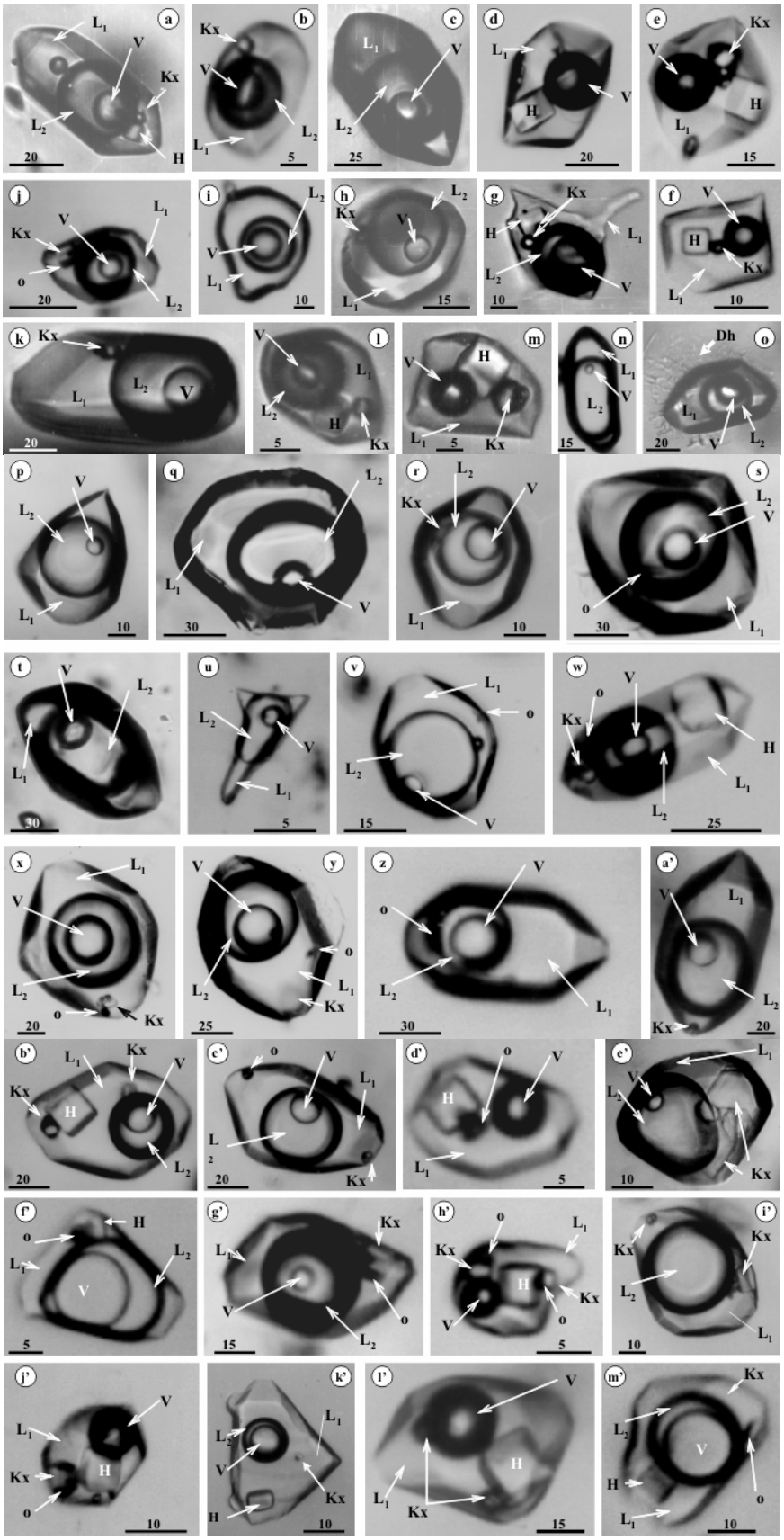
a
L1
V
Kx
L2
H
20
b
Kx
V
L2
L1
5
c
L1
V
L2
25
d
L1
H
V
20
e
Kx
V
H
L1
15
j
V
L1
Kx
o
L2
20
i
L2
V
L1
10
h
L2
Kx
V
L1
15
g
Kx
H
L1
L2
V
10
f
V
H
Kx
L1
10
k
Kx
L1
L2
V
20
l
V
L1
L2
H
Kx
5
m
V
H
L1
5
Kx
n
L1
V
L2
15
o
Dh
L1
V
L2
20
p
V
L2
L1
10
q
L2
L1
V
30
r
L2
Kx
V
L1
10
s
L2
V
o
L1
30
t
V
L2
L1
30
u
L2
V
L1
5
v
L1
o
L2
V
15
w
V
o
Kx
H
L1
L2
25
x
L1
V
L2
o
Kx
20
y
V
o
L2
L1
Kx
25
z
V
o
L2
L1
30
a'
V
L1
L2
Kx
20
b'
L1
Kx
V
Kx
H
L2
20
c'
o
V
L1
L2
Kx
20
d'
o
V
H
L1
5
e'
L1
V
L2
Kx
10
f'
H
o
L1
L2
V
5
g'
Kx
L1
V
o
L2
15
h'
o
L1
Kx
H
Kx
V
o
5
i'
Kx
Kx
L2
L1
10
j'
V
L1
Kx
H
o
10
k'
L1
L2
V
Kx
H
10
l'
V
H
L1
Kx
15
m'
Kx
L2
V
H
o
L1
10

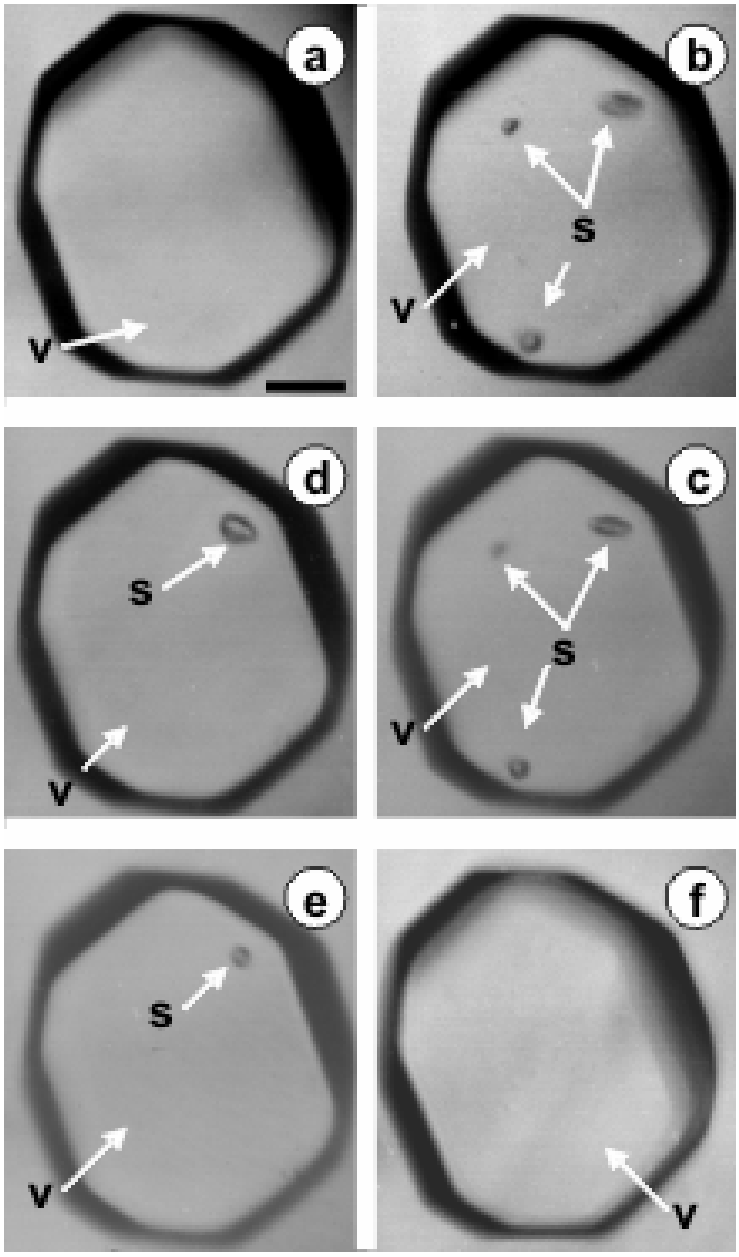

Fig.116. Microthermometric cycle in a gaseous inclusion (presumably empty at Troom), trapped in epithermal quartz. At temperature room condition in **a.** the microcavity look like empty but when was cooled down to -170°C, in **b.** three grains of solid were sublimated (s) . The first solid grain melted in **c.** between -112° and -94°C (H_2S) , **d.** the second melted around -84°C (CH_4) and in **e.** the ultimate grain melted sharply at -56.6°C (CO_2) , in **f.** back to room temperature the fluid inclusion contain a presumably pure and invisible gas mixture of CO_2-CH_4-H_2S, no liquid phase was detected by microthermometry in this fluid inclusion type (modified from Pintea and Iatan, 2013); V- vapor, S- sublimated gas mixture; Scale bar: 30 µm.

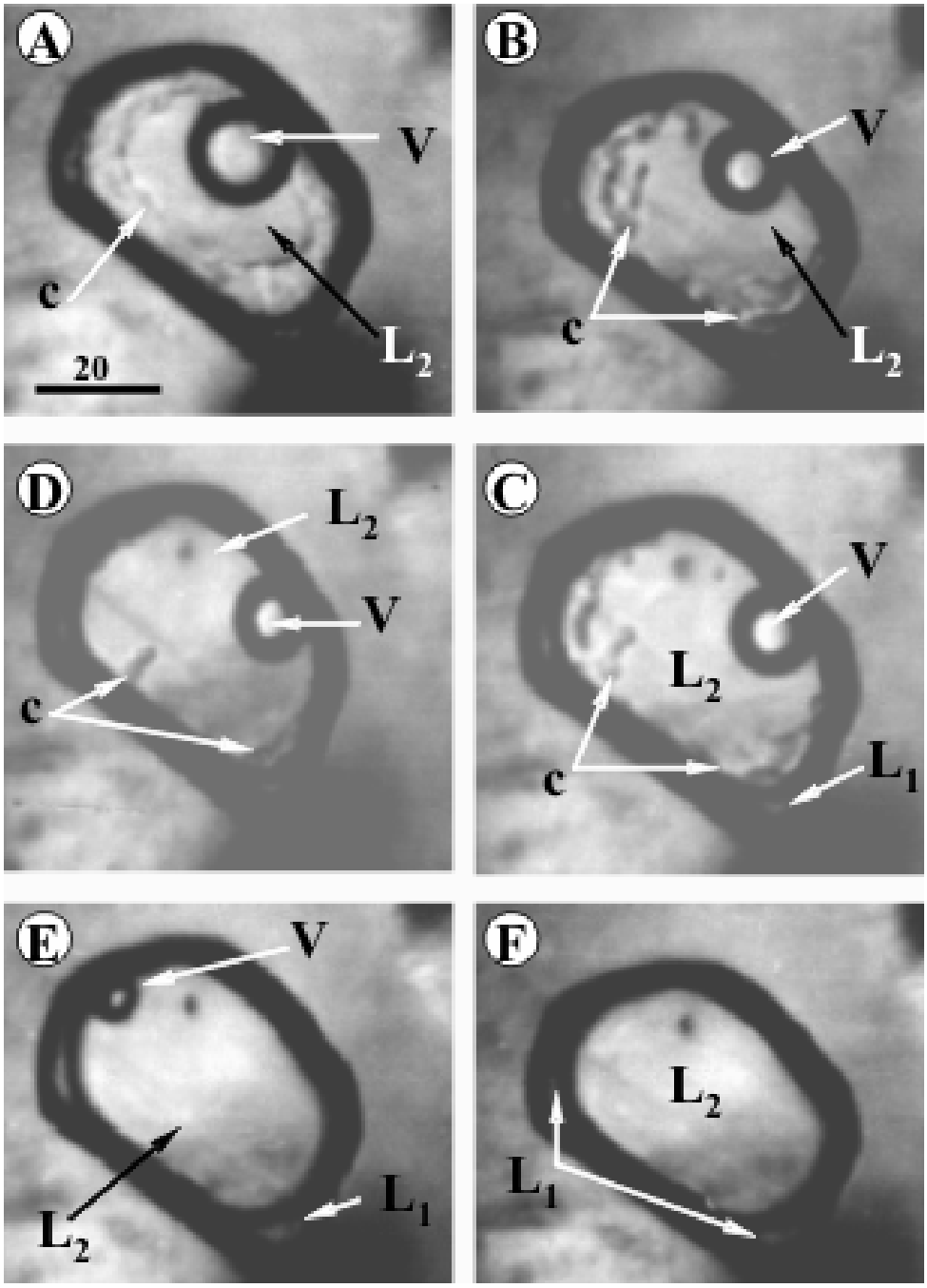

Fig. 117. Clathrate ($CO_2 5¾ H_2O$) microthermometry in CO_2-H_2O-(CH_4) fluid inclusion trapped in epithermal quartz from Jolotca REE-MoS_2 mineralization (Mesozoic Ditrau alkaline massif); Complete freezing was noted at -91.3°C, and during reversal heating the solid CO_2 melted at -57.6°C and clathrate melted at +11.8°C. On further heating the complete CO_2 homogenization was recorded at +19.7°C; c-clathrate, L_1- aqueous liquid rim, L_2- CO_2-liquid, V-gas. (Pintea, 1991a, 1995a, 1996b). Scale bar in µm

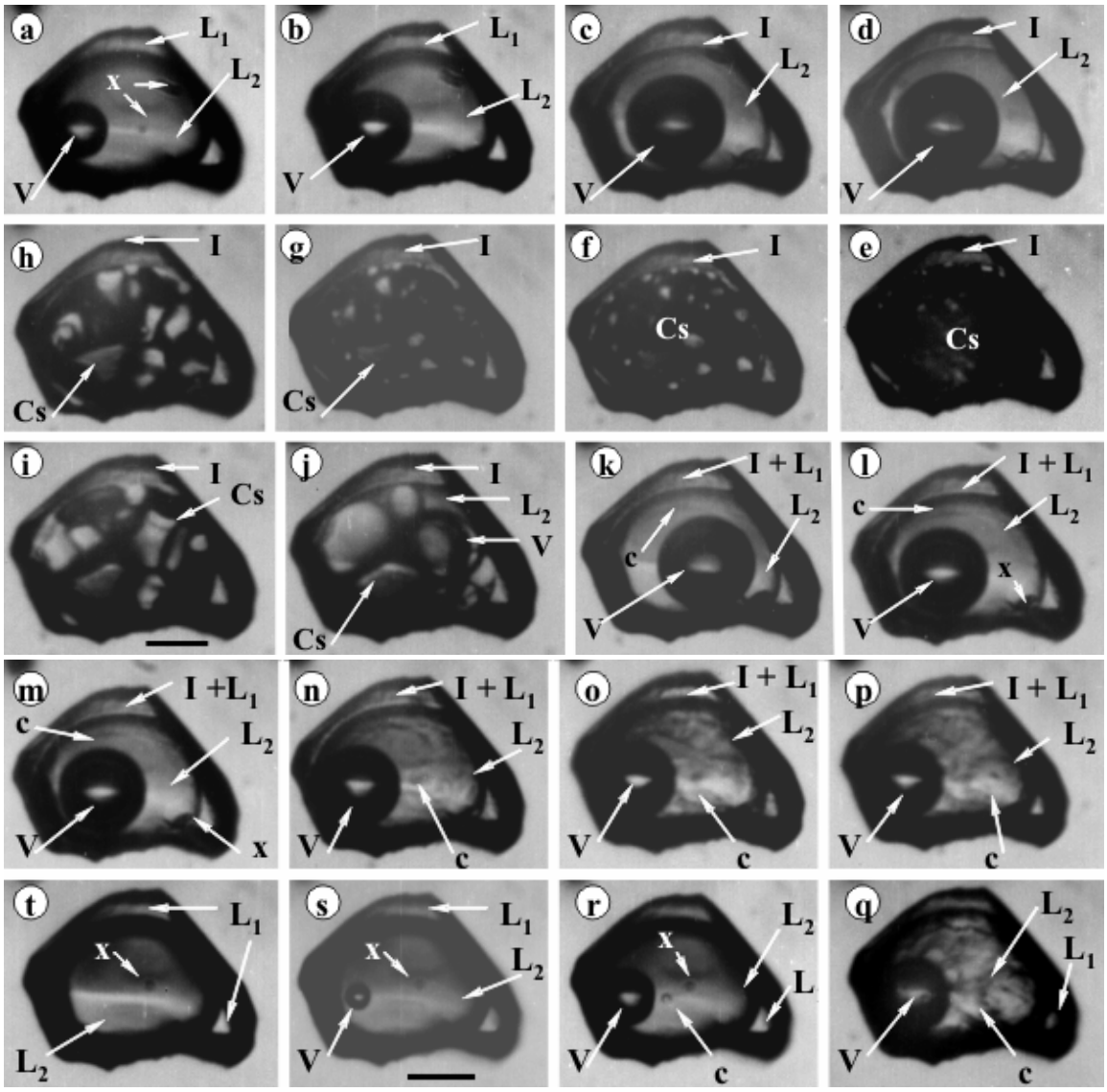

Fig. 118. Complete microthermometric cycle of CO_2-H_2O-(CH_4) fluid inclusion trapped in the epithermal quartz from Jolotca REE-MoS_2 mineralization (Mesozoic Ditrău alkaline massif); Complete freezing was noted between -96.6°C and -121.9°C, and during reversal heating the $TmCO_2$ solid = -57.7°C, Tm clathrate recorded at +10.1°C and Th CO_2 = +16.1°C; **a**. +9.8°C, **b**. -17.8°C, **c**. -35.7°C, **d**.-77.8°C, **e**. -121.9°C, **f**. -84.8°C, **g.** -73.4°C, **h. -**72.2°C, **i**. -67.2°C., **j**.-65.2, **k**. -57.7°C, **l**. -43.3°C, **m**. -36.8°C, **n**. -19°C, **o**. -8.6°C, **p**. -3.3°C, **q**. +3.5°C-, **r**. +9°C, **s**. +15.6°C, **t**. +17.7°C; L_1- aqueous liquid rim, L_2- CO_2-liquid, V-gas, Cs- solid CO_2, c- clathrate, x- unknown. (Pintea, 1991a, 1995a, 1996b); Scale bar in µm.

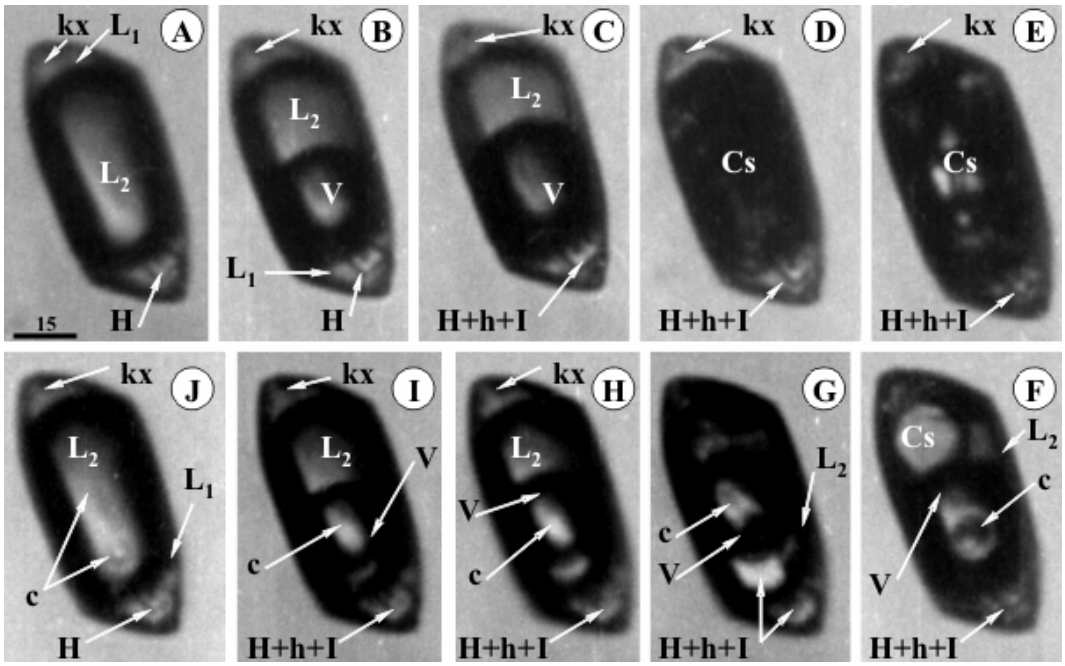

Fig. 119. Microthermometry of the carbonic-brine fluid inclusion containing more than one solid phase (daughter-?) in the euhedral hydrothermal quartz from Jolotca mining district (Mesozoic Ditrău massif); **A**.+25°C, **B**.-intermediate, **C**.-70°C, **D**.-101.9°C, **E**.-intermediate, **F**.-74.5°C, **G**.-59.8°C, **H**.-17°C, **I**.-2.5°C, **J**.+9.7°C ; kx-unknown, H-halite, L_1- aqueous liquid, L_2-CO_2 liquid, V- gas, h- hydrohalite (?), c-clathrate, Cs- solid CO_2.(compiled from Pintea, 1991a, 1995a,1996b). Scale bar in µm.

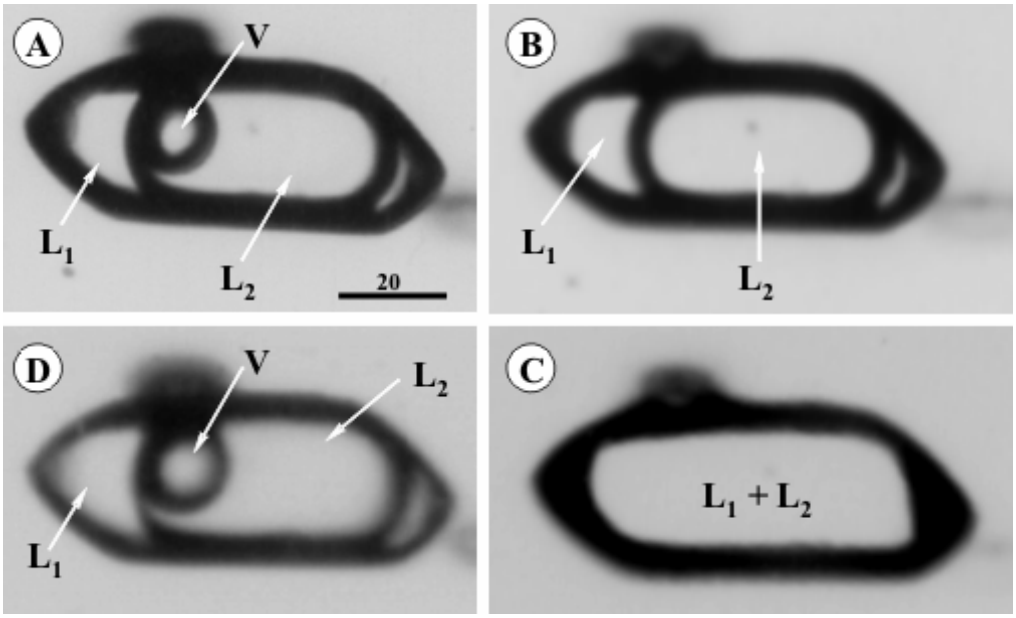

Fig. 120. Total homogenization temperatures in CO_2-H_2O fluid inclusions trapped in euhedral quartz crystals from Jolotca REE-MoS_2 mineralization (Mesozoic Ditrău massif). **A**. +13°C, **B**. ≥ 40°C ($ThCO_2$= -2° to = +31.5°C), **C**. Th= 275°-280°C, **D**. +10°C (n=38, Pintea, 1991a, 1995a, 1996b); L_1- aqueous liquid, L_2- CO_2 liquid, V- vapor. Scale bar in µm.

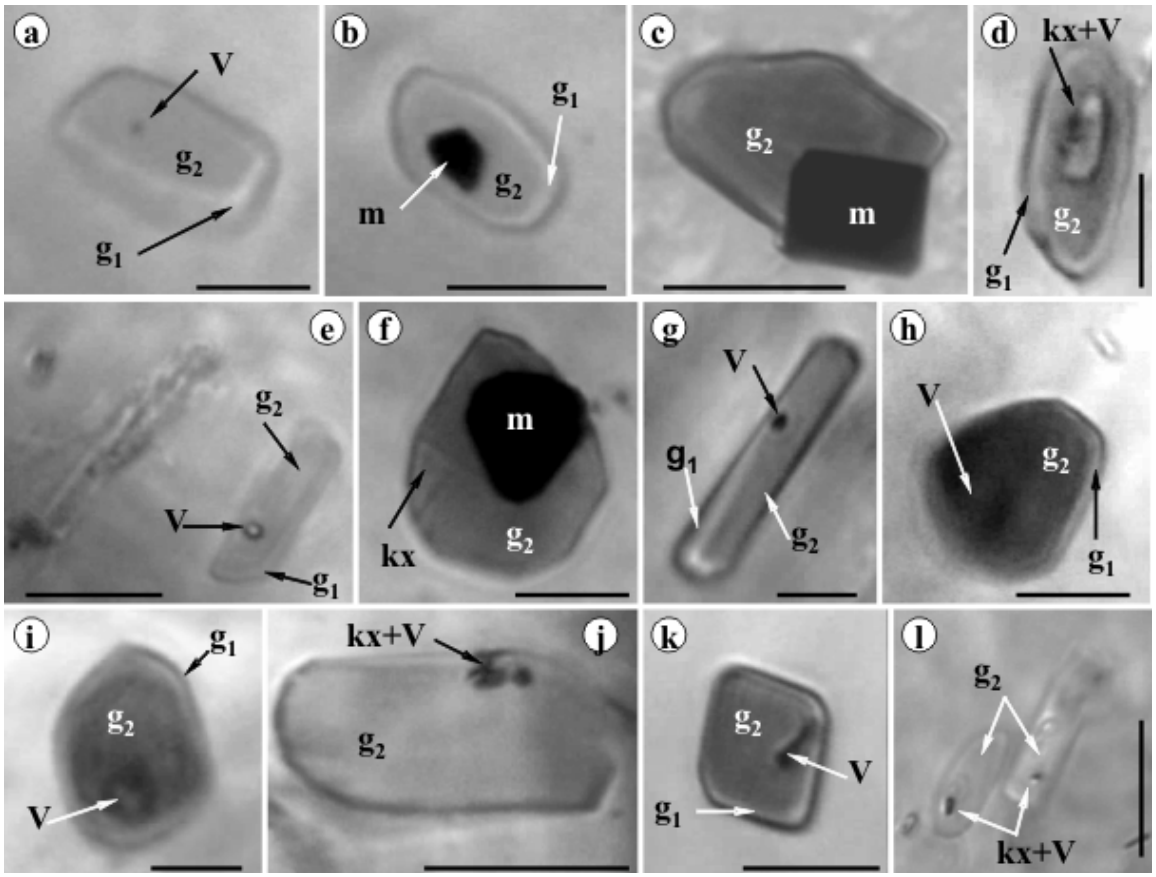

Fig. 121. Two immiscible silicate melt (now glass) trapped in heterogeneous silicate melt inclusions from nefeline syenite from Ditrău Mesozoic alkaline massif; **a**, **e**, **g**, **h**, **i**, **k**- immiscible silicate glass inclusions; **b**, **c**, **d**, **f**, **j**, **l**- multiphasic silicate glass inclusions; V- vapor, g_1- white glass (syenitic melt); g_2- dark gray glass (mafic silicate melt); m- mafic daughter microminerals; kx- unknown; Two or three magmatic events were envisaged to interact each others during Triassic/Jurassic time reprezented by syenitic and ultramafic rocks (gabbroic) and their interaction formed complex petrologic products during the genesis of the Ditrău massif (e.g. review in Fall et al., 2007). Such kind of heterogeneous silicate melt inclusions pictured in this figure are pristine samples to study silicate melt unmixing or magma fractionation processes. Scale bar 10μm.

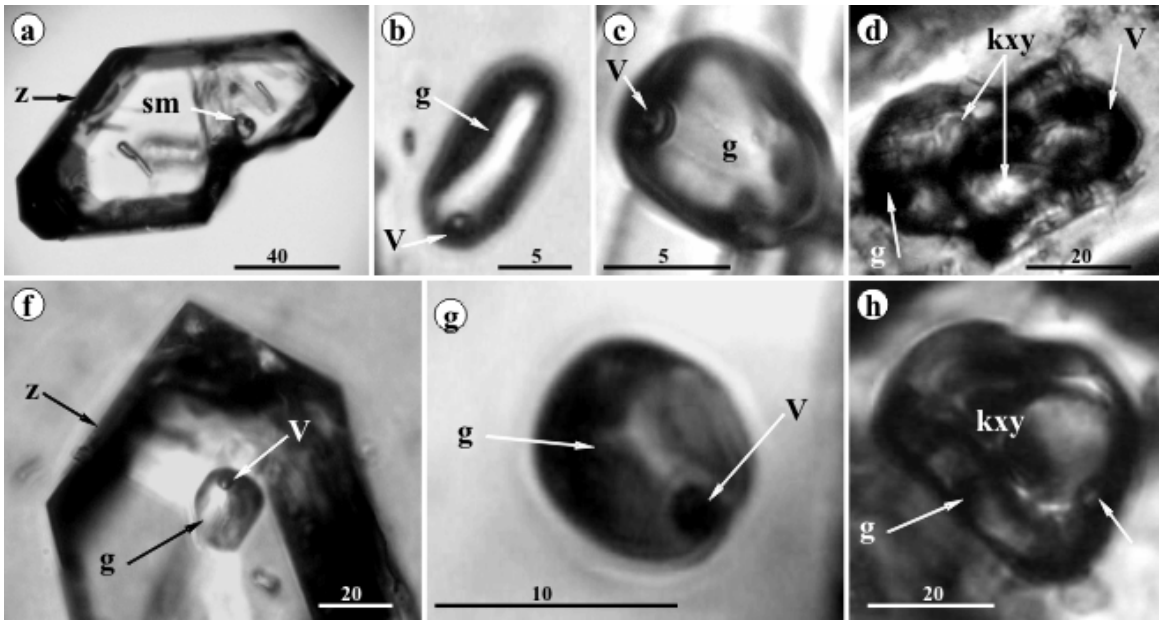

Fig. 122. Silicate melt inclusion types in zircons from granitoidic rocks from South Carpathians (zircons courtesy T.Berza); **a**, **b**, **c**, **f**, **g**- biphasic silicate glass inclusions; **d**, **h**- Partially remelted (unhomogenized) silicate melt inclusions; z- zircon, sm- silicate melt inclusion, g-glass, Kxy- remelted daughter microcrystals (partially); V-vapor. More microthermometry in Table 3 (Pintea in Berza et al., 2007- unpubl.). Scale bar in µm.

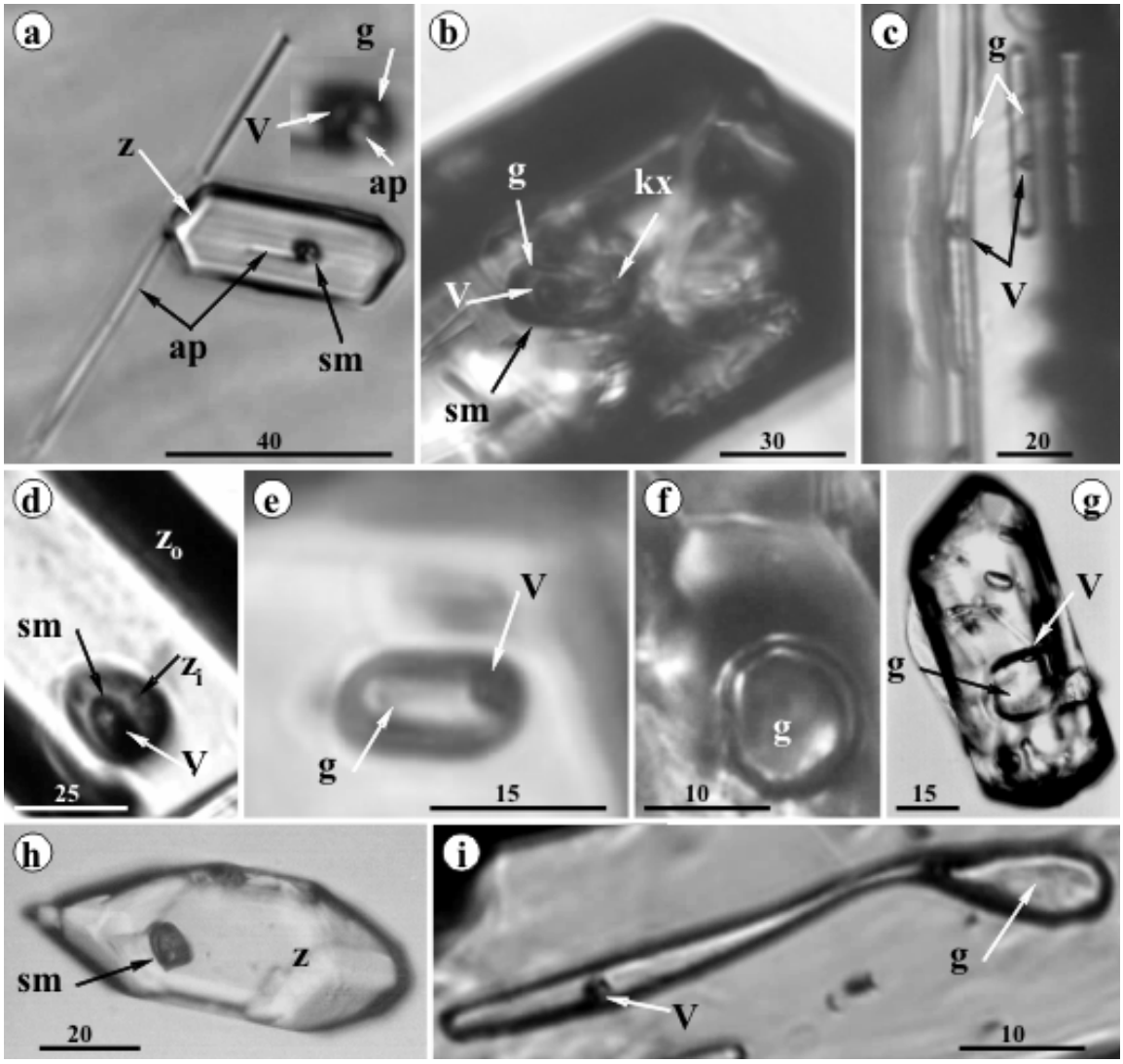

Fig. 123. Silicate melt inclusions in zircons from Neogene volcanic rocks (Dej Tuff, Dăneşti and Laleaua Albă dacite; Roşia Montană and Săcărâmb dacite and andesites (somes sample courtesy L.Robu); **a**, **b**, **d**, **h**- multiphasic silicate melt inclusions; **c**, **e**, **g**- biphasic glass inclusions, **f**- monophasic silicate glass inclusion; z, z_o- zircons, z_i- inherited zircon, ap- apatite, sm- silicate melt inclusion, g- glass, kx- microcrystal(s), V- vapor. Microthermometry: **a**. Th= 923°C and **g**. Th= 783°C, generally homogenization temperatures in silicate glass inclusions ranged between 552°C-990°C (Pintea in Berza et al., 2007- unpubl.). Scale bar in µm.

Fig. 124. Fluid inclusion types in volcanic - exhalative native sulfur from Gura Haitii open pit from Călimani caldera (sample courtesy I. Seghedi, 1982); **a**, **b**, **c**, **d**, **e**, **j**, **m**, **n**, **v**, **w**, **x**, **y**, **b'**, **c'**- vapor rich inclusions; **f**, **g**, **h**, **i**, **l**, **o**, **p**, **r**, **z**, **a'**- decrepitation features of the vapor rich inclusions; **q**, **s**, **t**, **a'**- sulfur melt-like inclusions (?); V- vapor, S- unknown; Pristine droplets of immiscible subcritical fluid sulfur were described as globular inclusions in plagioclase from Petricelu andesitic apophysis (Balintoni, 1970) and worldwide as spherules in acidic crater lakes (e.g. Mason et al., 2001). Our crushing experiments on Călimani volcanic sulfur, under the microscope, shown mainly H_2O vapor in the vapor-rich inclusion type (Pintea, 2007- unpubl.). Scale bar in µm.

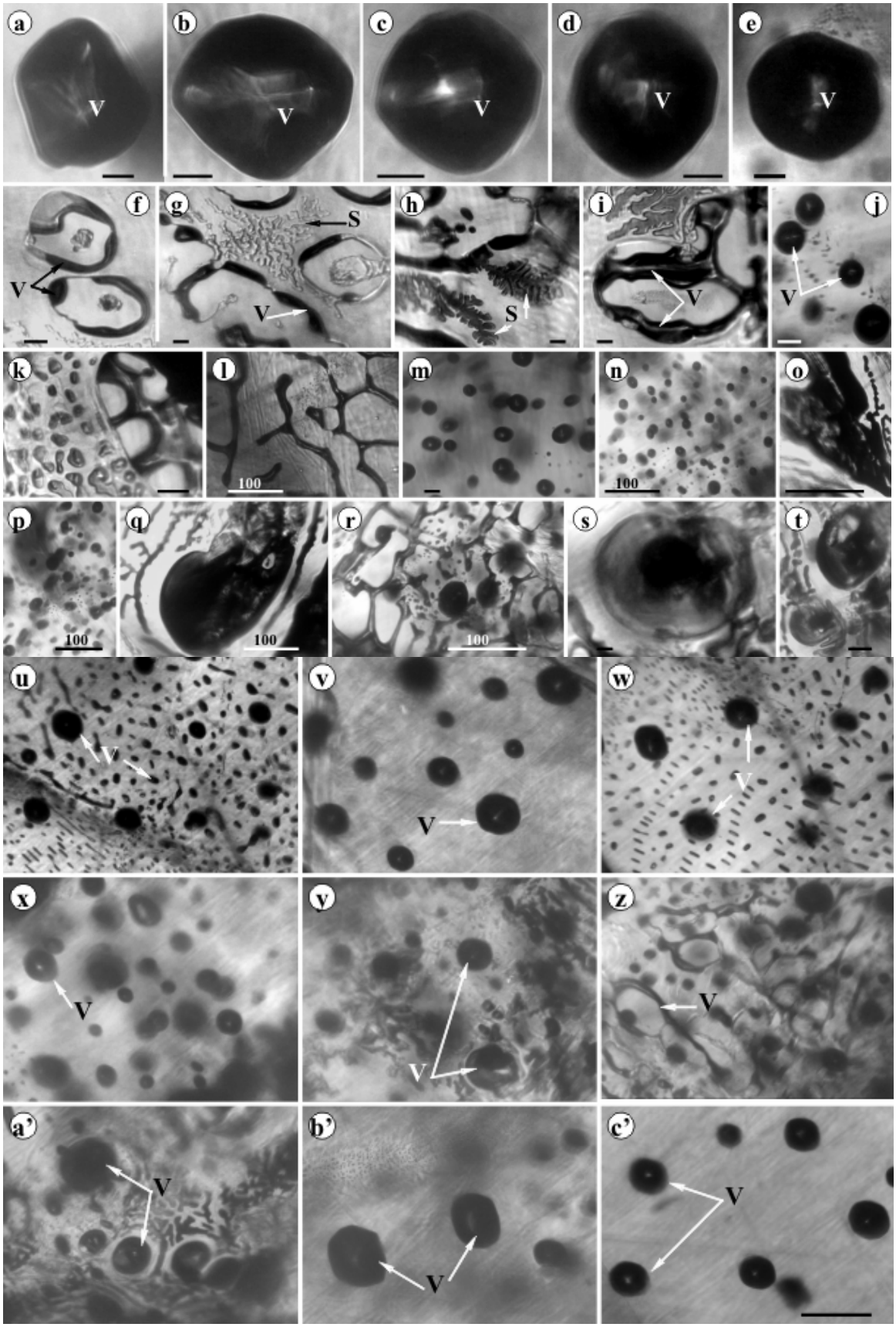
a
V
b
V
c
V
d
V
e
V
f
V
g
S
V
h
S
i
V
j
V
k
l
100
m
n
100
o
p
100
q
100
r
100
s
t
u
V
v
V
w
V
x
V
y
V
z
V
a'
V
b'
V
c'
V

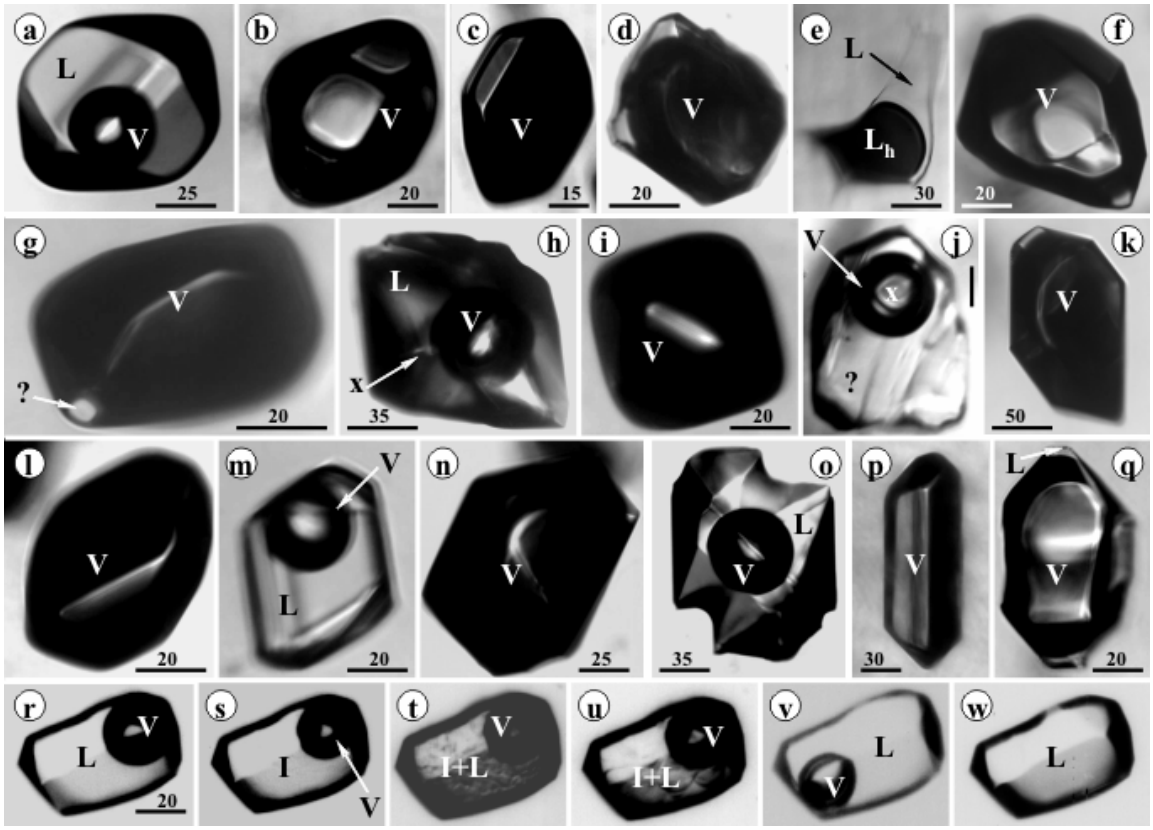

Fig. 125. Fluid inclusion types in the epithermal (geothermal) quartz crystals from Cucu and Vârghiş volcanic environments (Harghita Mountains- sample courtesy I. Seghedi, 1992); **a**. **h**. **m**. **o**. **r**.- aqueous biphasic fluid inclusions; **b**, **c**, **d**, **f**, **g**, **i**, **k**, **l**, **n**, **p**, **q**- vapor-rich inclusions; **e**. heterogeneous liquid inclusion(?); **j**.- multiphasic fluid inclusion(?); L-liquid, V- vapor, Lh- liquid hydrocarbon(?), x- undetermined solid, ?- unknown. Microthermometric cycle (Pintea, 1992- unpubl.): **r.** +25°C; **s**. -70°C; **t**. -21°C; **u**.-15°C; **v**. +200°C; **w**. +230°C (Th); Tmi=-9.5^{o}C (salinity = 13.4 wt% NaCl eq., P= 26 bar). Frequently, the vapor bubbles from biphasic liquid-rich inclusions seem to have a CO_2-liquid rim around its. This could be a feature of the magmatic fluids trapped in geothermal quartz. Blamey and Norman (2001) noticed that the most primitive or most magmatic fluid contain: 7-8 wt% NaCl eq., 5-6 mol % CO_2, 0.5 – 1 mol% CH_4, 0.01-0.02 mol % H_2S and N_2/Ar>400. Nevertheless, it seems that the fluid phases trapped in the Cucu and Vârghiş quartz crystals have mixed origin being contaminated with meteoric fluids containg also liquid hydrocarbons and/or pyrobitumen, otherwise a characteristic feature in the majority of the Neogene epithermal ore deposits from Carpathians. More data on petrography and microthermometry from Harghita Mountains (Sântimbru-Băi) in Pintea and Laczko, 2005). Scale bar in µm.

Fig. 126. Silicate melt remnants and fluid inclusions types in olivine and pyroxene peridotitic nodules brought out by Plio-Pleistocene alkali basaltic volcanism from the Perşani Mountains (Bogata Valley, SE Transylvania Basin); **a**, **h**, **k**, **p**, **a'**, **b'**, **h'**- dark-brown silicate glass inclusions vs. spinel like microinclusions (primary); **f**. **g**. **i**. **q**. **s**. **j'**.- immiscible silicate glass and sulfide globules (secondary); **b**, **c**, **e**, **j**, **l**, **m**, **n**, **o**, **r**, **t**, **u**, **v**, **w**, **x**, **y**, **z**, **c'**, **d'**, **f'**, **g'**, **j'** - carbonic fluids ± silicate glass ± sulfide (multiphasic, mainly secondary); g_1- dark-brown (ultramafic) silicate glass vs spinel microcrystal, g, g_2- white silicate glass(alkali basaltic), c_L- liquid CO_2, c_V- gas CO_2, c- carbonic fluid phases, V- vapor, dh- decrepitation halo, kx- silicate daughter phases, sg- silica globules, s- sulfide; Reequilibration features of the pure carbonic (sometimes dark sulfide globules) and multiphasic carbonic ± silicate were described at ca 3-4 kb (12-15 km) and 1100°-1200°C in the volcanic conduit (Pintea and Mârza, 1989). Immiscibility between calciocarbonatitic and silicate melts in veinlets cross-cutting the peridotitic nodules from Persani Mountains basaltic andesites were documented by Chalot-Prat and Arnold, 1999. Scale bar in µm. ⇨

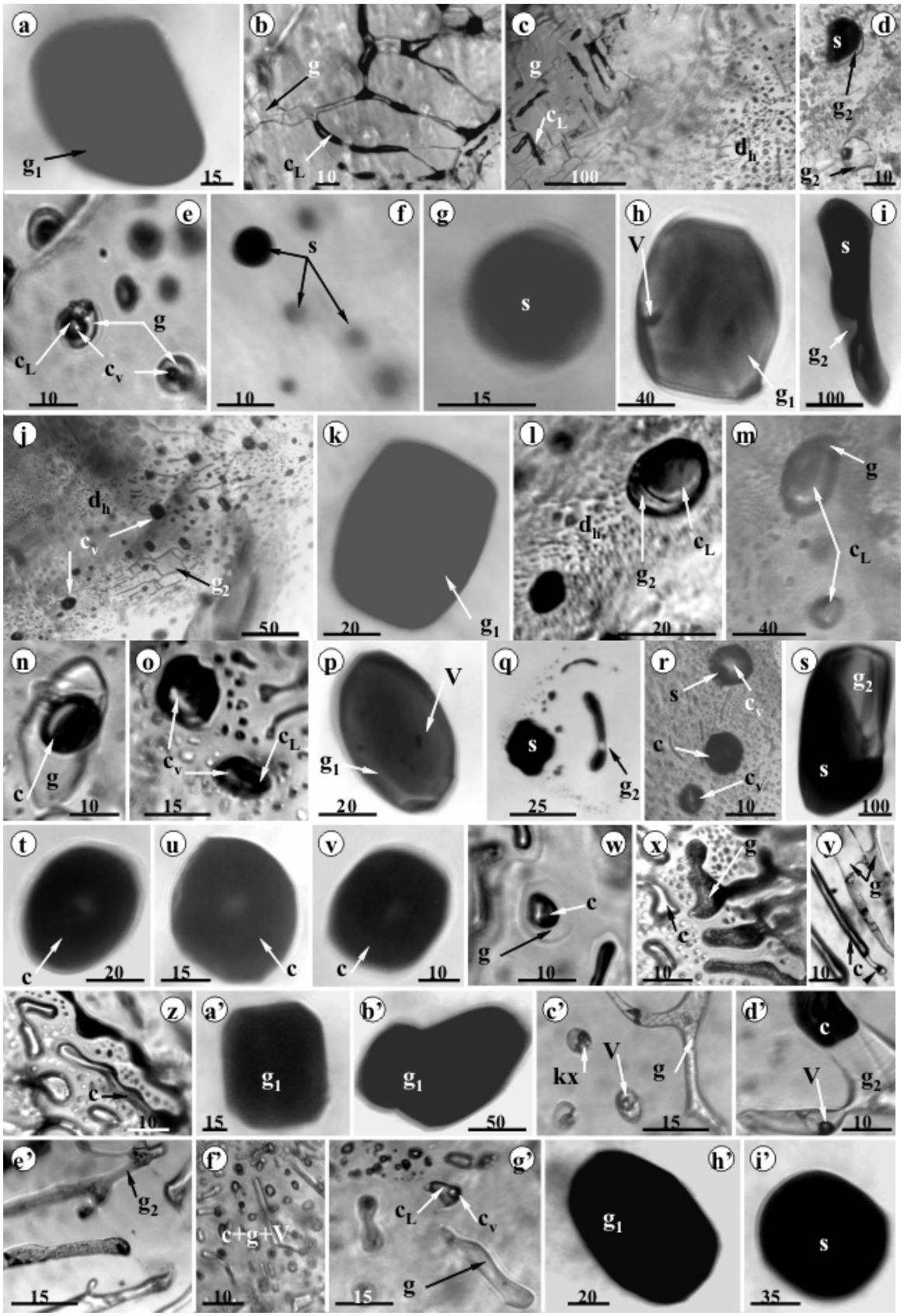
a
g1
15
b
g
cL
10
c
g
cL
dh
100
d
s
g2
g2
10
e
cL
cv
g
10
f
s
10
g
s
15
h
V
g1
40
i
s
g2
100
j
dh
cv
g2
50
k
g1
20
l
dh
cL
g2
20
m
g
cL
40
n
c
g
10
o
cv
cL
15
p
V
g1
20
q
s
g2
25
r
s
cv
c
cv
10
s
g2
s
100
t
c
20
u
c
15
v
c
10
w
c
g
10
x
g
c
10
y
g
c
10
z
c
10
a'
g1
15
b'
g1
50
c'
kx
V
g
15
d'
c
V
g2
10
e'
g2
15
f'
c+g+V
10
g'
cL
cv
g
15
h'
g1
20
i'
s
35

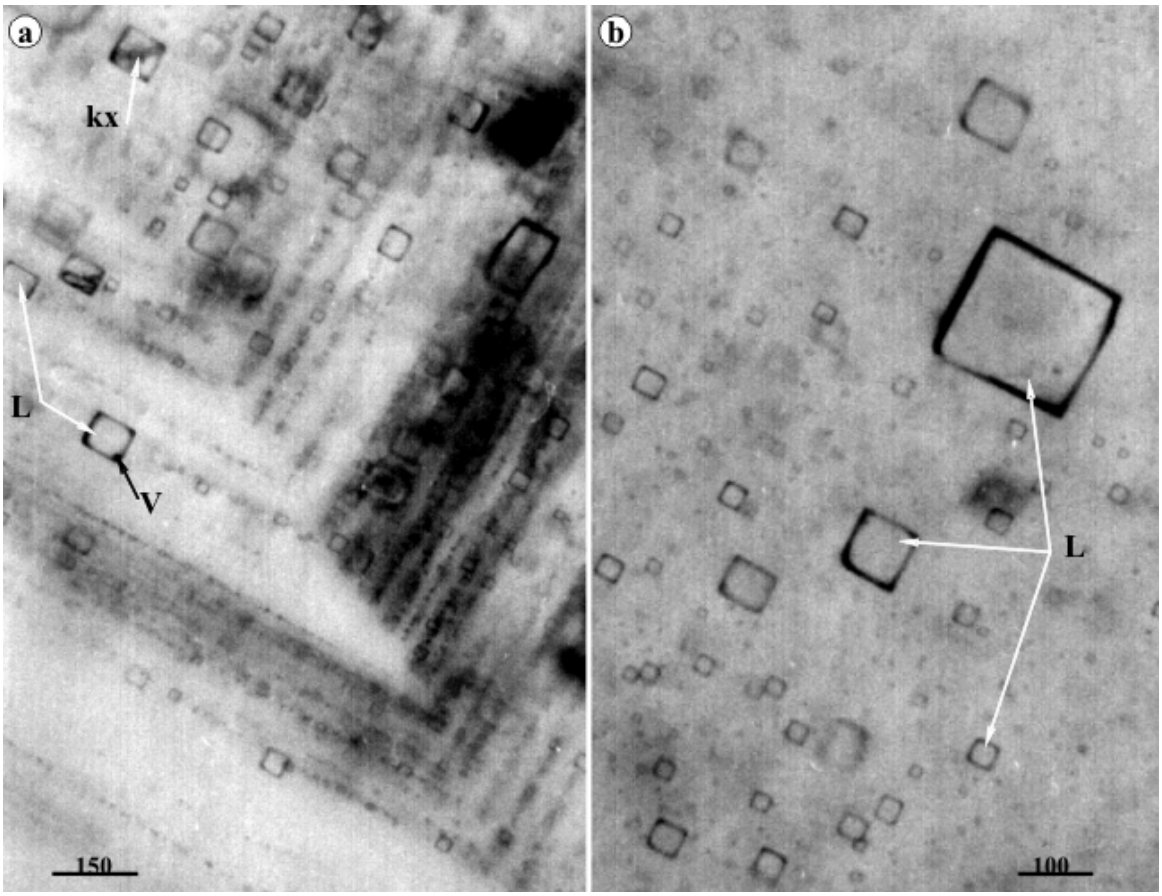

Fig. 127. Primary "en chevron" relict microtexture in Badenian halite from Slănic Prahova (Băile Baciului mining prospect); **a**. internal dihedral zonation growth bands decorated with monophase and biphasic liquid - rich inclusions; **b**.- distribution of monophase liquid inclusions in the growth zone; L- liquid, V- vapor, kx- diagenetic solid phase (recrystallized). New hypothesis on the genesis of the halite from Transylvania Basin, petrography and microthermometry of fluid inclusions in halite from Ocna Dej and Slănic Prahova were published by Balintoni and Petrescu, 2002; Pomârleanu and Mârza, 2003; Har et al., 2006, respectively. Scale bar in µm.

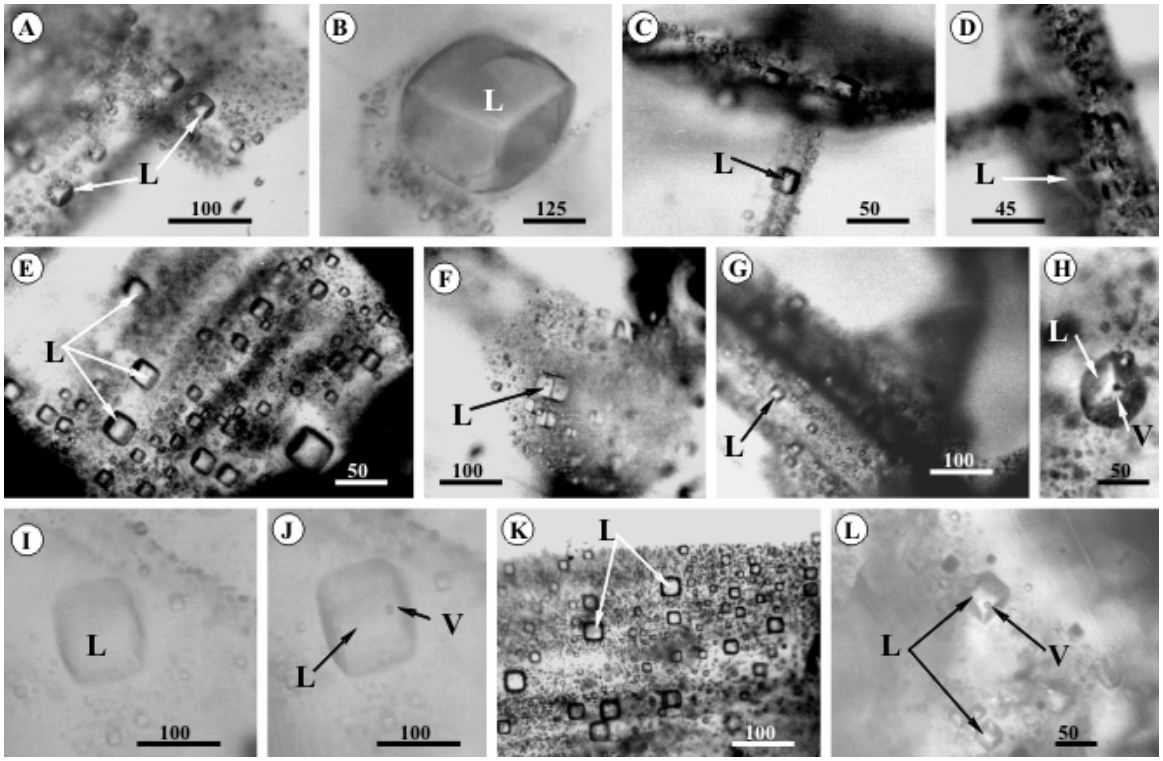

Fig. 128. Sedimentary microtexture remnants of monophase fluid inclusion associations in the Badenian recrystallized (partially) halite from Ocna Dej and Slanic Prahova salt mining prospects. **A**. **C**. **D**.- rectangular sedimentary relicts = primary growth zones in halite; **E**. **F**. **G**. **K**. **L**.- isolated groups of former rectangular growth zones in halite; **B**. **E**. **I**. **J**.- isolated liquid - rich liquid inclusions surrounded by halos. L- liquid, V- vapor (compiled from Pintea, 2005; 2008). The rounded corners of the primary "negative crystal" cavities is suggestive for equilibrium internal zones of the halite during recrystallization (in accord with NaCl equilibrium shape simulated by G. Barkema and M.Holzer, http://www.lassp.cornell.edu/-unpubl),and generally they contain the "unique" mother sample of the seawater (as liquid inclusions) used for paleotemperature estimation and chemistry evaluation of the precipitation marine/lagunar conditions (e.g. Petrichenko, 1977; Roedder, 1984a; Goldstein and Reynolds, 1994; Zimmermann, 2001; Kovalevich and Vovnyuk, 2010). Scale bar in μm.

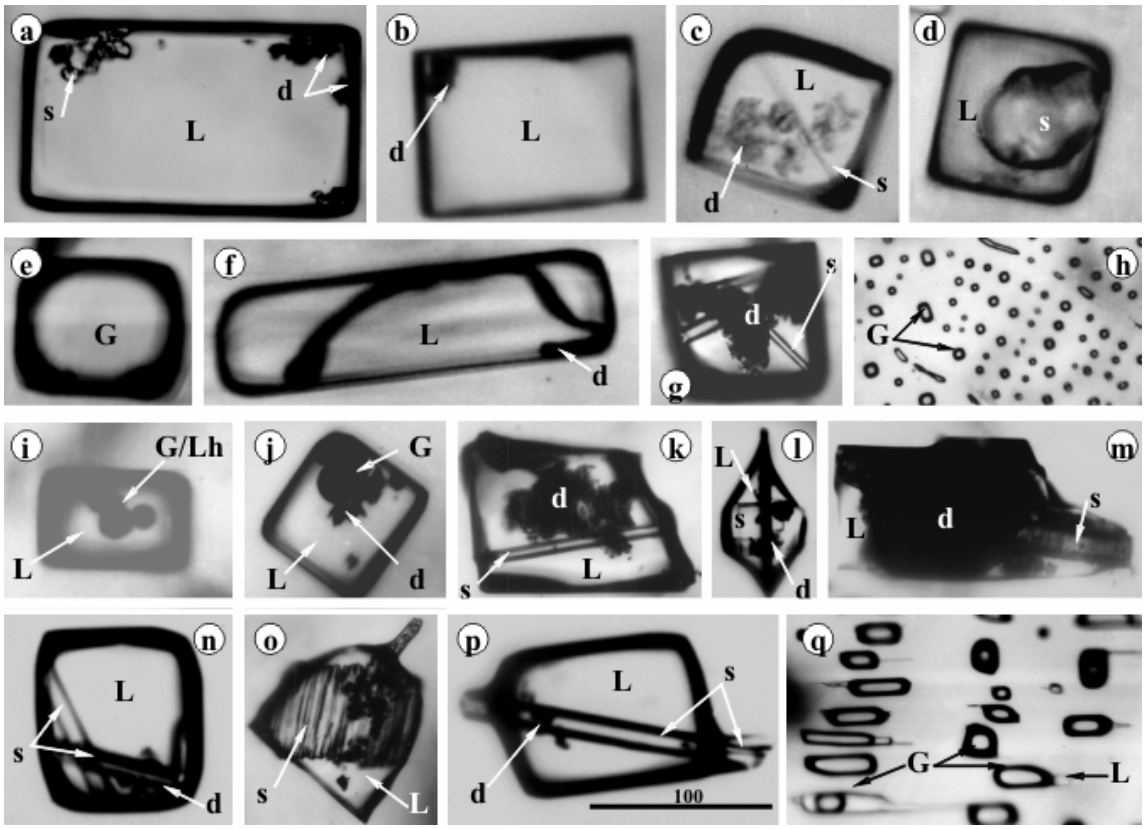

Fig. 129. "Diagenetic" fluid inclusion types in Badenian halite from Ocna Dej and Slănic Prahova mining prospects; **a**, **b**, **c**, **d**, **f**, **g**, **i**, **j**, **k**, **l**, **m**, **n**, **o**, **p**- liquid rich inclusions with solid(s) and immiscible liquid (?)or gas droplets/bubbles; **e**, **h**, **q**- vapor (gas)- rich fluid inclusions; L- aqueous liquid, s- sulphate minerals (mainly anhydrite) and other crystallized microcrystals, d- dendritic (argilleous) grains (agglutinated), Lh- droplets or bubbles of liquid/gas hydrocarbons (?). Scale bar: 100µm for all.

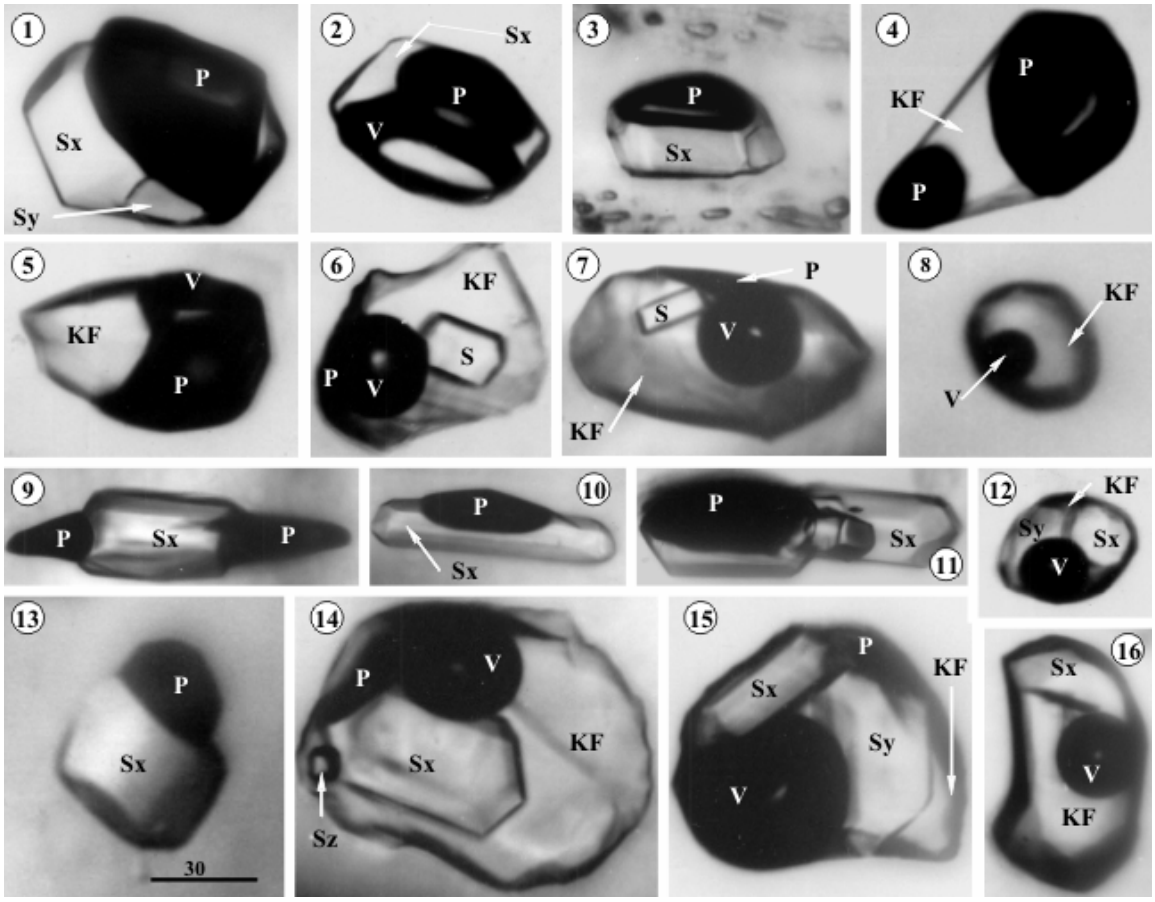

Fig. 130. Multiphase fluid (melt) inclusions in langbeinite from Tazlău potassium and magnesium salt deposit prospect; **1**, **3**, **4**, **9**, **10**, **11**, **13**- multisolid(s) with bitumen droplets; **2**, **5**, **6**, **7**, **8**, **12**, **14**,**15**, **16**- multisolids(s) with vapor (gas) ± bitumen droplets, Sx, Sy, Sz- salt/sulfate microminerals, S- sylvite (?), P- bitumen droplets, KF- potassium-magnesium dominant solid phase (?), V- vapor/gas. Host mineral description and genesis of K-Mg salt from Tg - Ocna - Găleanu -Tazlău were made by Rădulescu, 1960, Paucă, 1966, Stoica and Gherasie, 1981 and others. Scale bar in μm.

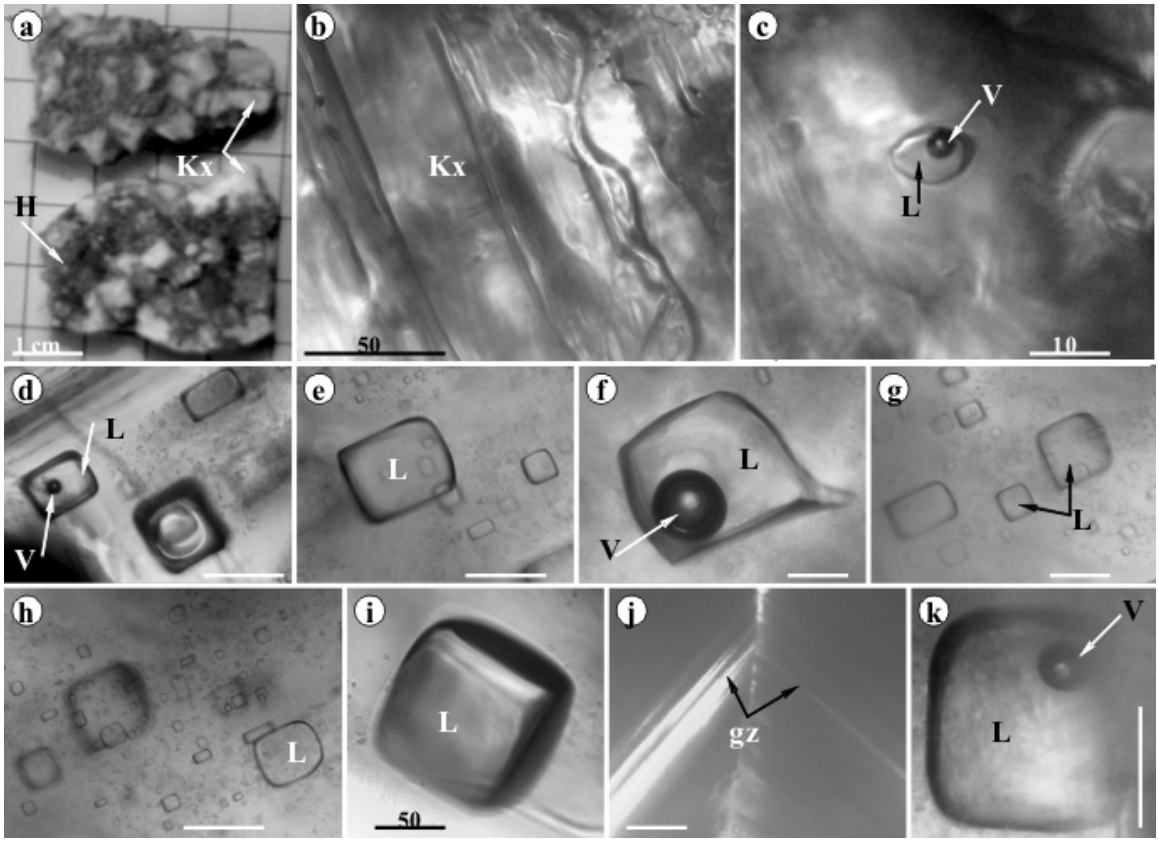

Fig. 131. Microtexture features and fluid inclusion types in recrystallized salt at laboratory conditions (pure H_2O, T_{room} and ambiental pressure) from Tazlău mining prospect (Pintea, unpubl); **a**- recrystallized mineral association containing halite (H) and probably langbeinite (Kx); **b**, **j**- microtexture in langbeinite (?) and dihedral zonation in halite, respectively; **c**- biphasic fluid inclusion in recrystallized langbeinite (?); **d**, **e**, **f**, **g**, **h**, **i**, **k**- liquid dominated fluid inclusions in the associated recrystallized halite; Scale bar in µm; d. e. f. g. h. j. k.- 100µm.

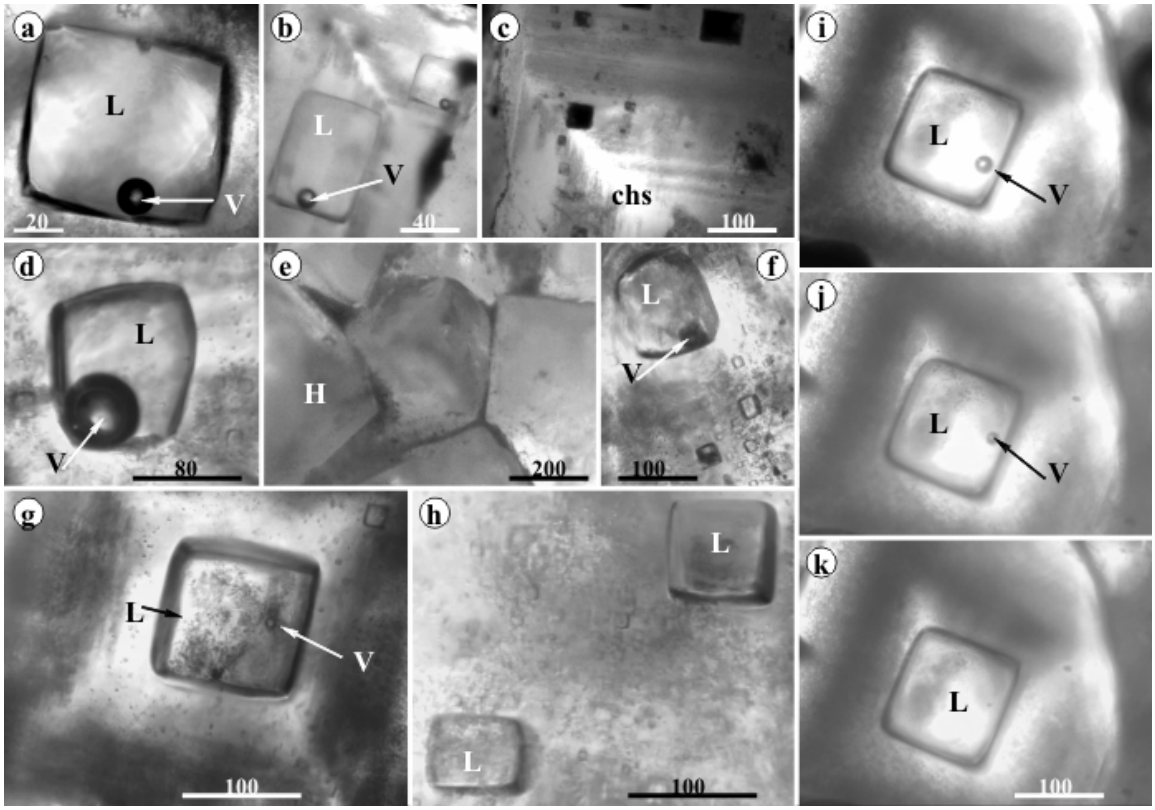

Fig. 132. Fluid inclusion types and microtexture features of the recrystallized halite crust around Cojocna old mining district (sampled by I. Pintea at 30.09. 2003); **a**, **b**, **d**, **f**, **g**, **h**- monophase and biphasic liquid-rich inclusions; **c**. **e**.- microtextural features; L-liquid, H-halite, V-vapor, chs- dihedral growth zone ("chevron" microtexture); Microthermometry: **i**. +29.5°C; **j**. intermediate; **k**. +31.5°C = Th (Pintea, 2003 and unpubl.). Scale bar in µm.

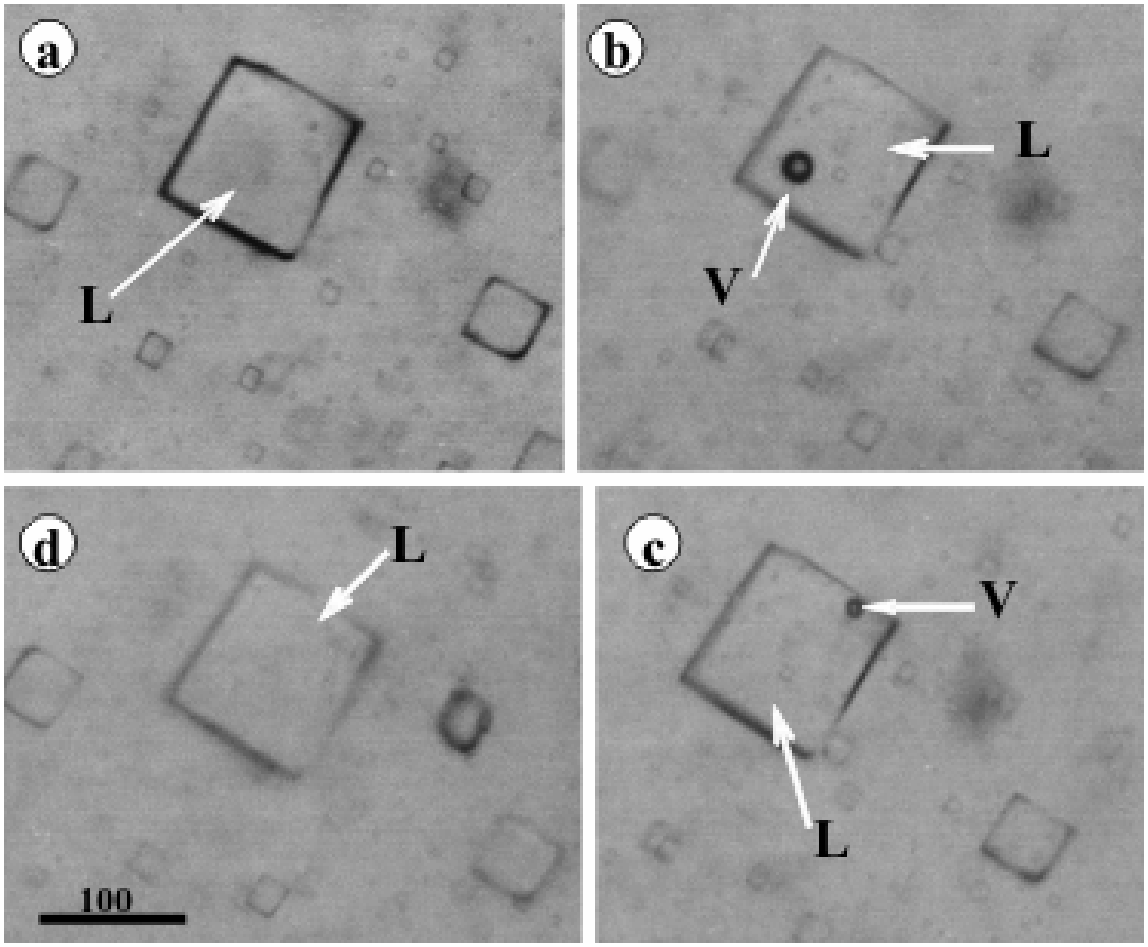

Fig. 133. The trapping temperature estimation by vapor bubble nucleation and homogenization, directly under the microscope (Pintea, 2005b; 2008b) in primary fluid inclusion in halite from Slănic Prahova mining prospect (Băile Baciului);**a**.-5.5°C, **b**.-20.4°C, **c**.+2.3°C, **d**.+10.1°C; L-liquid, V-vapor. Homogenization by vapor bubble recovery in monophasic liquid inclusion in evaporate minerals (Roedder, 1971; Petrichenko, 1973), was revised and applied for paleotemperature estimation in sedimentary basins by Golstein and Reynolds, 1994, Roberts and Spencer, 1995; Lowenstein and Brown 1998, among others. An ultimate high-tech method using laser pulse is used to generate vapor bubble in monophase metastable liquid inclusions in various minerals (Krüger et al., 2007). Scale bar in µm.

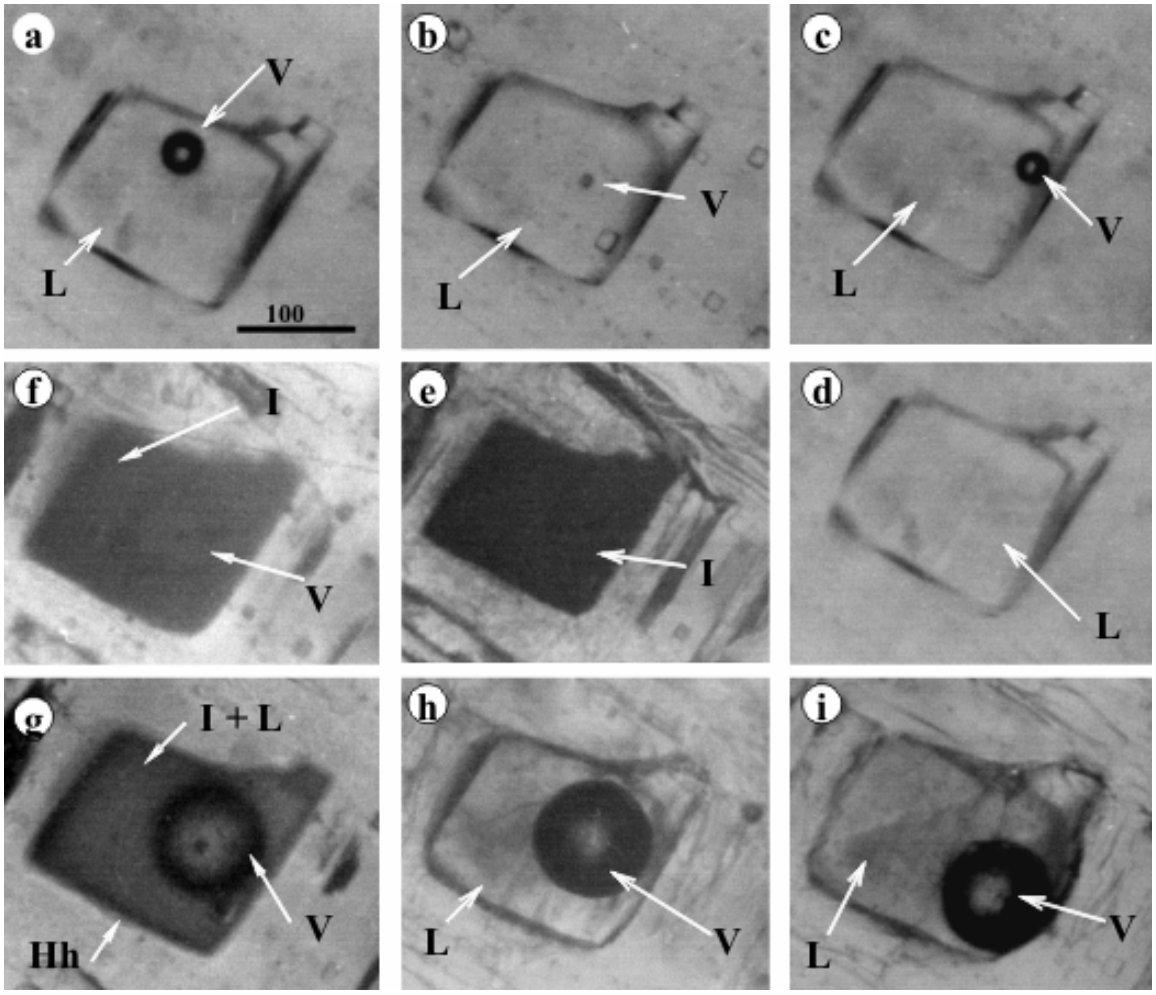

Fig. 134. Microthermometric cycle of primary monophase liquid inclusion showing decrepitation after second homogenization in halite from Slanic Prahova salt mining prospect; **a**.-12°C, **b**.+14.3°C (Th_1), **c**.-4.5°C, **d**.+5.3°C, **e**.-90°C, **f**.-70°C, **g**.-25°C. **h**.+25°C, **i**.+ 25°C after final homogenization at +101.8°C (Th_2); hydrohalite melted around ±0.1°C; L-liquid, V-vapor, Hh-hydrohalite. Completed microthermometry on several chloride salts-water systems from laboratory-grown halite was presented by Davis et al., 1990. Scale bar in µm.

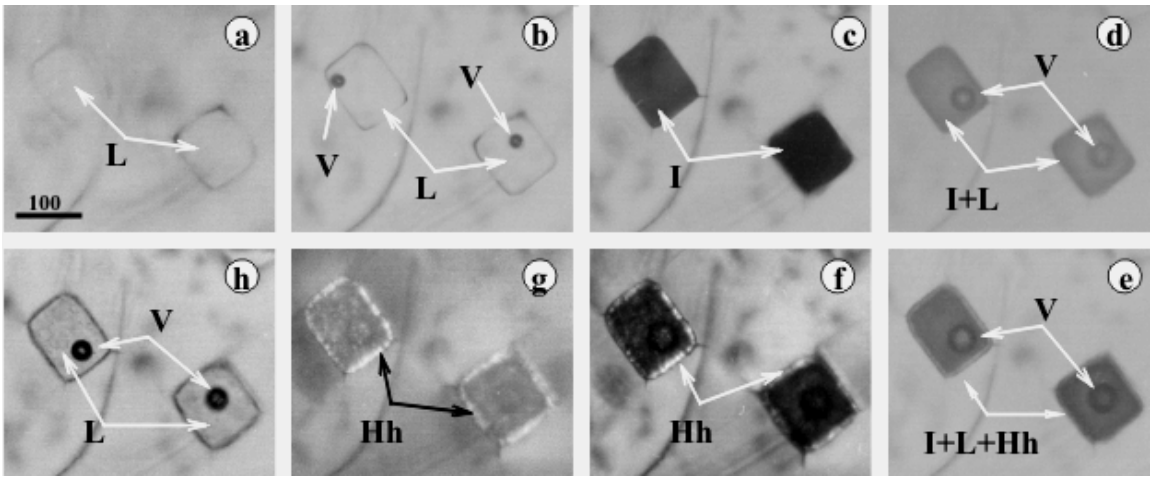

Fig. 135. Completed microthermometric cycle of the monophase liquid inclusions in the recrystallized halite around a fossilized tree (Sequoia sp.- I. Petrescu comm. pers. - 1988) from Ocna Dej mining prospect (Transylvania Basin); **a**.-4.3°C, **b**.-8.5°C, Th= +14.1°C (upper left); Th= +16.9°C (down right); **c**.-44°C, **d**.-22.4°C, Tmi= -21.8°C, **e**.-12°C, **f**.-8.6°C, **g**.-2.2°C, TmHh= ± 0.1°C, **h**. +4.3°C; L- liquid, V-vapor, I-ice, Hh- hydrohalite (compiled from several cycles - Pintea, 2005b; 2008b). Scale bar in µm.

Fig. 136. Fluid inclusion types in the Marmarosh diamond" quartz crystals from Bocicoiul Mare (Maramures district, Romania) from Neocomian-Albian argillaceous black shales from the Transcarpathian flysch (quartz sample courtesy V.Ghiurcă in Pintea and Ghiurcă,1991 unpubl., Pintea, 1995a); **a**, **b**- quartz crystal host; **c, g, h**- monophasic liquid hydrocarbon inclusions, **i**. **a'**. **b'**.- carbonic gas-rich inclusions; **d**, **e**, **f**, **j**, **m**, **n**, **p**, **r**, **s**, **t**, **u**, **v**, **w**, **x**, **y**, **z**, **c'**- multiphase hydrocarbon inclusions; **k**.- aqueous biphasic liquid-rich inclusions; Symplified microthermometry (example): **c**.'+25°C, **d'**. to **e'**.- around +300°C, **f'**.-120°C ($TmCH_4$= -82.4°C), **g'**.+25°C; generally hydrocarbon liquid- rich inclusions containg CH_4 bubble homogenized between +60 to +600°C and CH_4 solid melted between -66° and -82,1°C (Pintea, 1995a). Coeval aqueous rich inclusions shown Te= -21°C, Tmi=- 4.5 to -5.6°C (7-9 wt% NaCl eq.), Th= 150°-250°C ; Pt(corrected)= 0.5-1.0 kbars (Pintea, 1995); Banerjee and Ghiurcă (1997) identified in the "Marmarosh Diamond" quartz crystals by FTIR absorption spectroscopy the presence of H_2O, CO, CO_2, H_2S, CH_2, CH_3 and CH_4; dq- quartz specimen, Fi- fluid inclusions, Lh-liquid hydrocarbons, cg- carbonic gas, b- bitumen, V- vapor, L-liquid, I-ice, sc- solid CH_4. Experimentally work on synthetic oil-water mixtures at high P and T shown similar behavior between 180°-500°C and 1-150MPa (e.g. Balitsky et al., 2009). Microthermometry of liquid hydrocarbon-CH_4 gas + H_2O are useful for hydrocarbon identification and eventually for study oil migration and maturation during burial history of the country rocks, but not for determining fluid inclusions trapping conditions. For that purpose, the coeval aqueous-rich inclusions seem to be a good geobarometer in conjuction with external data offered by the geothermal gradients (e.g. Pintea, 1995) or tectonobarometers and (re)equilibration features of fluid inclusions (e.g. Vityk et al., 1996); More data about "Marmarosh diamond" quartz crystals and their fluid inclusions in Jarmolowicz-Szulc, 2003; Jarmolowicz-Szulc et al., 2006, among others. Scale bar in µm.

⇨

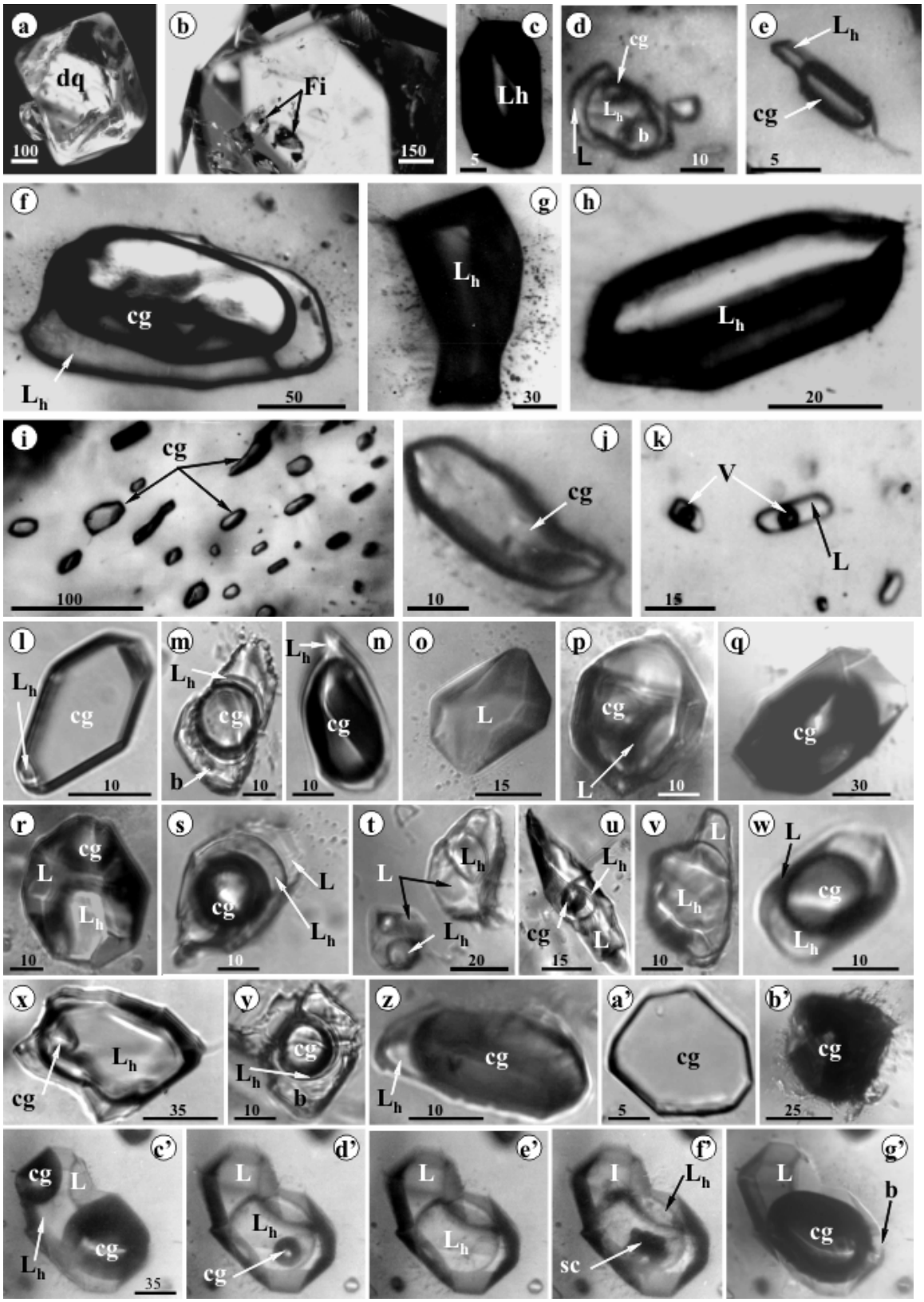
a
dq
100
b
Fi
150
c
Lh
5
d
cg
Lh
b
L
10
e
Lh
cg
5
f
cg
Lh
50
g
Lh
30
h
Lh
20
i
cg
100
j
cg
10
k
V
L
15
l
Lh
cg
10
m
Lh
cg
b
10
n
Lh
cg
10
o
L
15
p
cg
L
10
q
cg
30
r
cg
L
Lh
10
s
cg
L
Lh
10
t
L
Lh
Lh
20
u
Lh
cg
L
15
v
L
Lh
10
w
L
cg
Lh
10
x
Lh
cg
35
y
cg
Lh
b
10
z
cg
Lh
10
a'
cg
5
b'
cg
25
c'
cg
L
Lh
cg
35
d'
L
Lh
cg
e'
L
Lh
f'
I
Lh
sc
g'
L
b
cg

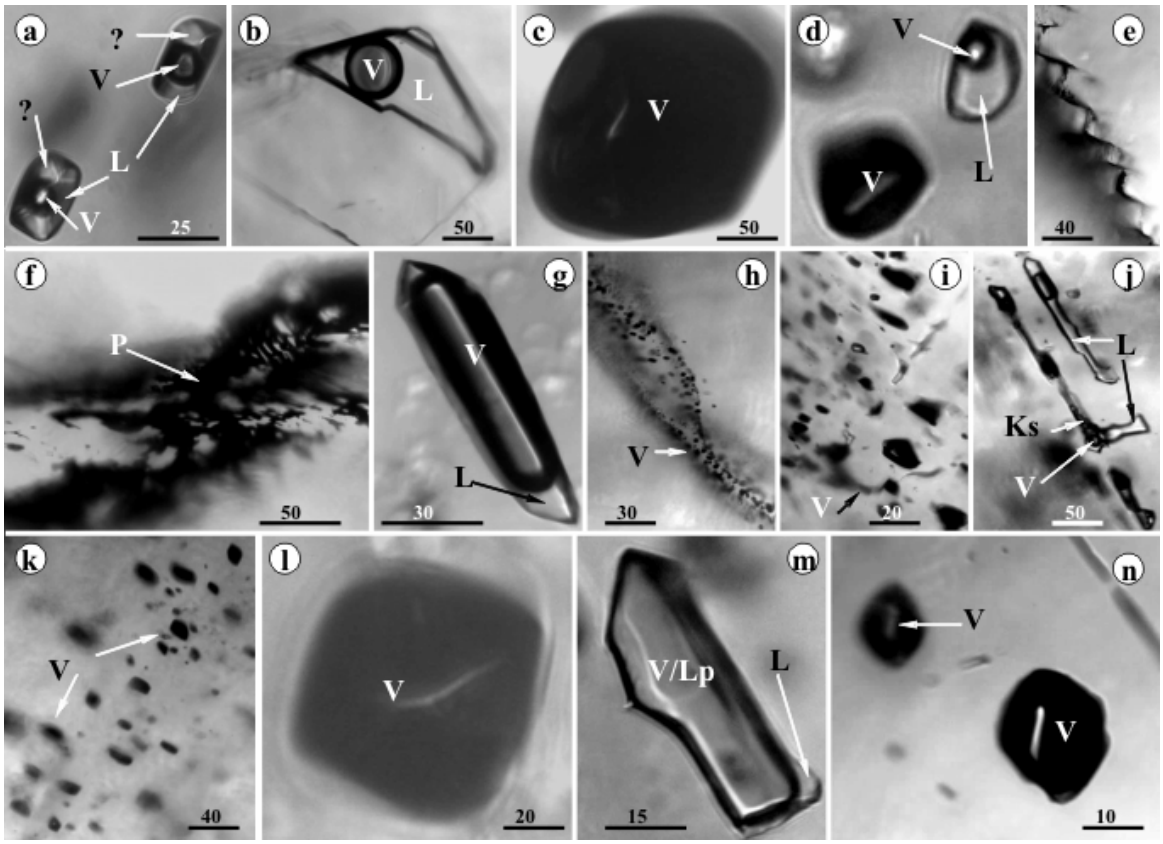

Fig. 137. Fluid inclusion types in quartz from Măgura Ţebei epithermal ore deposit (Caraci-Măgura Ţebei volcano-subvolcanic structure (Jude, 2012; sample courtesy S. Boştinescu); **a**. **b**. **j**.- liquid- rich fluid inclusions; **c, g**, **h**, **i**, **k**, **l**, **n**- vapor- rich inclusions; **d**. boiling assemblage; **m**.- vapor- rich vs. liquid hydrocarbon inclusion; **e**, **f**.- microcrack types in quartz,; L-liquid, V-vapor, P- pyrobitumen (?), Ks,?- unknown solid phases, Lp- liquid hydrocarbon (?). Scale bar in µm.

Fig. 138. Oscillatory zoning in β-quartz phenocrysts from Măgura Sturzii dacite-rhyolite subvolcanic structure from Bârgau zone (Bistriţa Năsăud county); **a**, **j**- oscillatory growth zones; **b**, **c**, **d**, **e, f**, **i**, **h**, **g**, **j**, **k**- altered silicate melt inclusions (ag); **l**, **m**, **n**, **o**, **p**, **r**- secondary fluid inclusions associated with altered silicate melt inclusions; q.- vapor - rich inclusions; dg- hydrothermally altered silicate melt inclusions, fc- microfissures oriented to c quartz axis, G- glass, mf- decrepitation microcracks, x- micromineral inclusion, PS- pseudosecondary, sh- "sweet" silicate glass halo, g- silicate glass globule, L- liquid, H- halite,V- vapor, kx- unknown solid. Scale bar in µm.

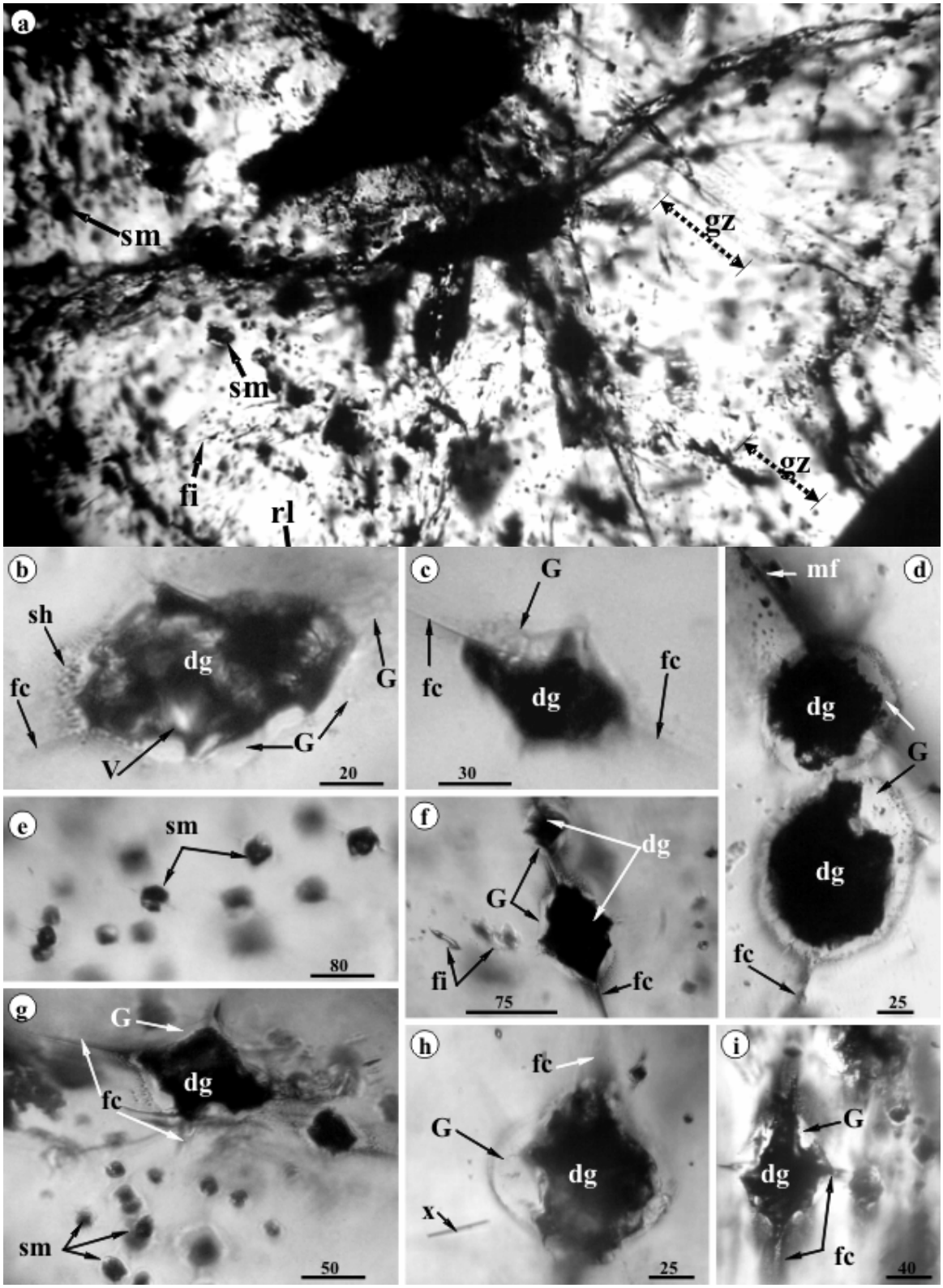
a
sm
sm
fi
rl
gz
gz
b
sh
fc
dg
G
G
V
20
c
G
fc
dg
fc
30
d
mf
dg
G
dg
fc
25
e
sm
80
f
dg
G
fi
fc
75
g
G
dg
fc
sm
50
h
fc
G
dg
x
25
i
G
dg
fc
40

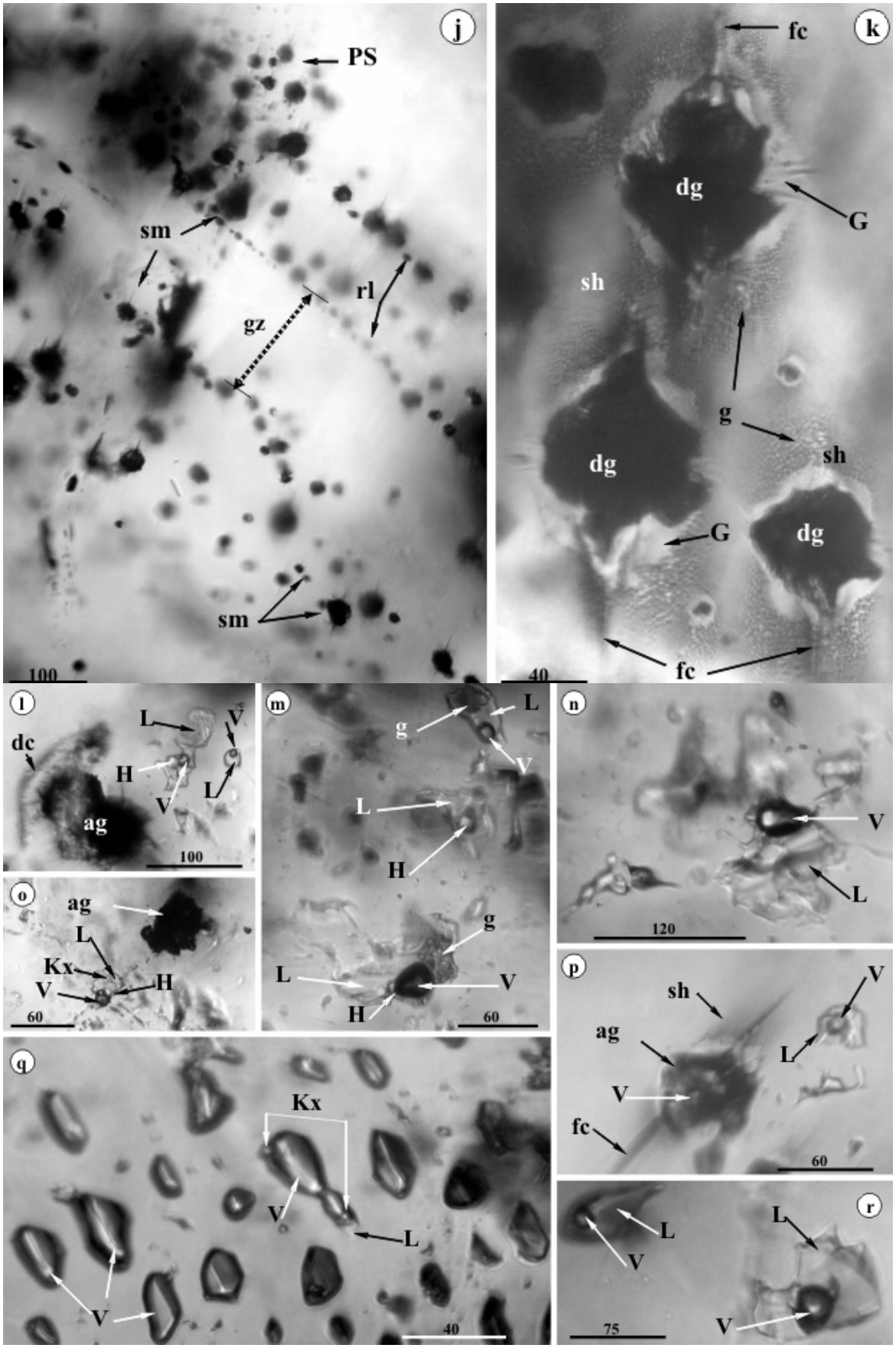
j
PS
sm
rl
gz
sm
100
k
fc
dg
G
sh
g
sh
dg
G
dg
fc
40
l
L
V
dc
H
V
L
ag
100
m
g
L
V
L
H
g
L
V
H
60
n
V
L
120
o
ag
L
Kx
V
H
60
p
sh
V
ag
L
V
fc
60
q
Kx
V
L
V
40
r
L
L
V
V
75

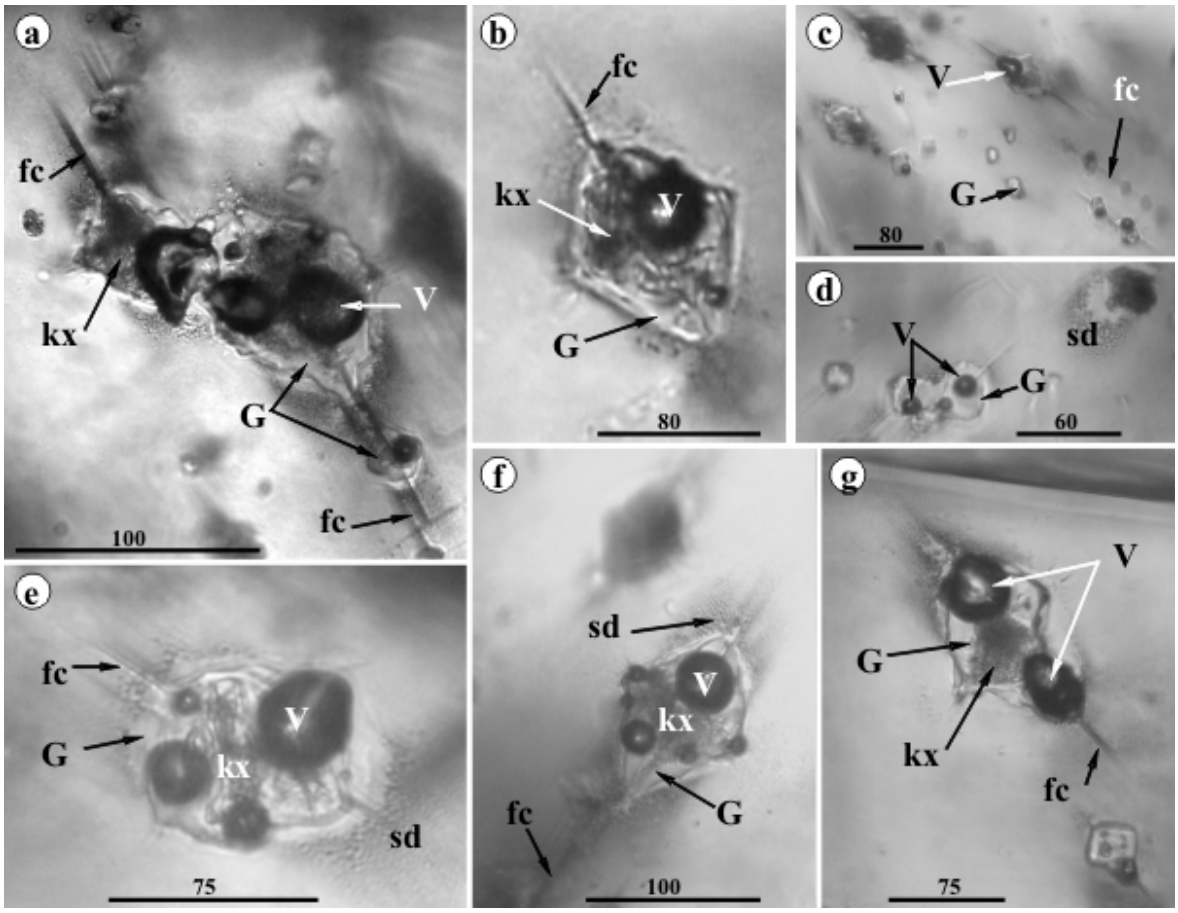

Fig. 139. a, **b**, **c**, **d**, **e**, **f**, **g**- Partially remelted features in silicate melt inclusions like those pictured in Fig 138, heated up to 1050°C in the stage under the microscope, at 1 bar pressure (Pintea, unpubl.) in β-quartz phenocrysts from Măgura Sturzii subvolcanic dacite-rhyolite structure (Bârgau Mountains); V-vapor bubbles, G- glass, fc- microfissures oriented along the c axis of β-quartz phenocrysts, kx- recrystallized microminerals, sd- "sweet" decrepitation halo. Fluid inclusion microthermometry in Papp et al. (2003). Scale bar in μm.

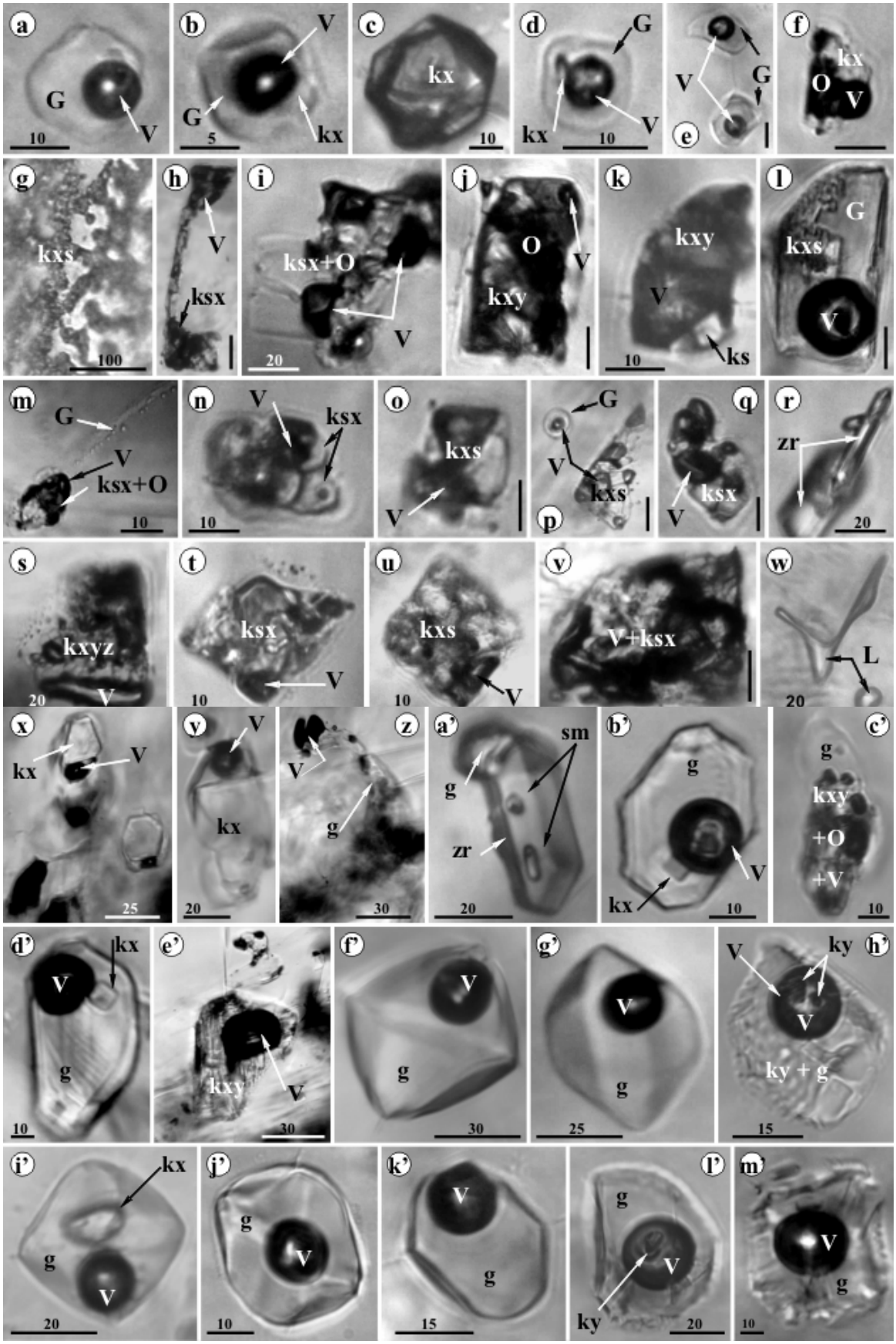
a
G
V
10
b
V
G
kx
5
c
kx
10
d
G
kx
V
10
e
V
G
f
kx
O
V
g
kxs
100
h
V
ksx
i
ksx+O
V
20
j
O
V
kxy
k
kxy
V
ks
10
l
G
kxs
V
m
G
V
ksx+O
10
n
V
ksx
10
o
kxs
V
p
G
V
kxs
q
ksx
V
r
zr
20
s
kxyz
V
20
t
ksx
V
10
u
kxs
V
10
v
V+ksx
w
L
20
x
kx
V
25
y
V
kx
20
z
V
g
30
a'
sm
g
zr
20
b'
g
V
kx
10
c'
g
kxy
+O
+V
10
d'
kx
V
g
10
e'
kxy
V
30
f'
V
g
30
g'
V
g
25
h'
V
ky
V
ky + g
15
i'
kx
g
V
20
j'
g
V
10
k'
V
g
15
l'
g
V
ky
20
m'
V
g
10

Fig. 140. Variety of silicate melt inclusions in plagioclase phenocrysts from andesitic (white) volcanic rocks (lava flow) from Cetăţeaua Hill (Dumbrava village, Cluj county); **a**, **b**, **d**, **e**, **f',g',j',k',l',m'**- silicate glass inclusions (mostly biphasic); **f**, **h**, **i**, **j**, **k**, **l**, **m**, **n**, **o**, **q**, **s**, **t**, **u**, **v, x, y, z, b', c', d', h', j',** - multiphase crystallized melt inclusions; **e**, **r**, **a'**- micromineral inclusions; **g**- secondary solid granular inclusions; **p**- coeval (immiscibility) silicate glass inclusion and crystallized melt inclusion; **w** - secondary liquid(?) inclusions; G- glass, V-vapor, kx, kxs, ksx, kxy, kxyz- unknown solid phases, O-opaque, zr- zircon. Petrologic data from Ştefan et al., 1985. Scale bar in µm.

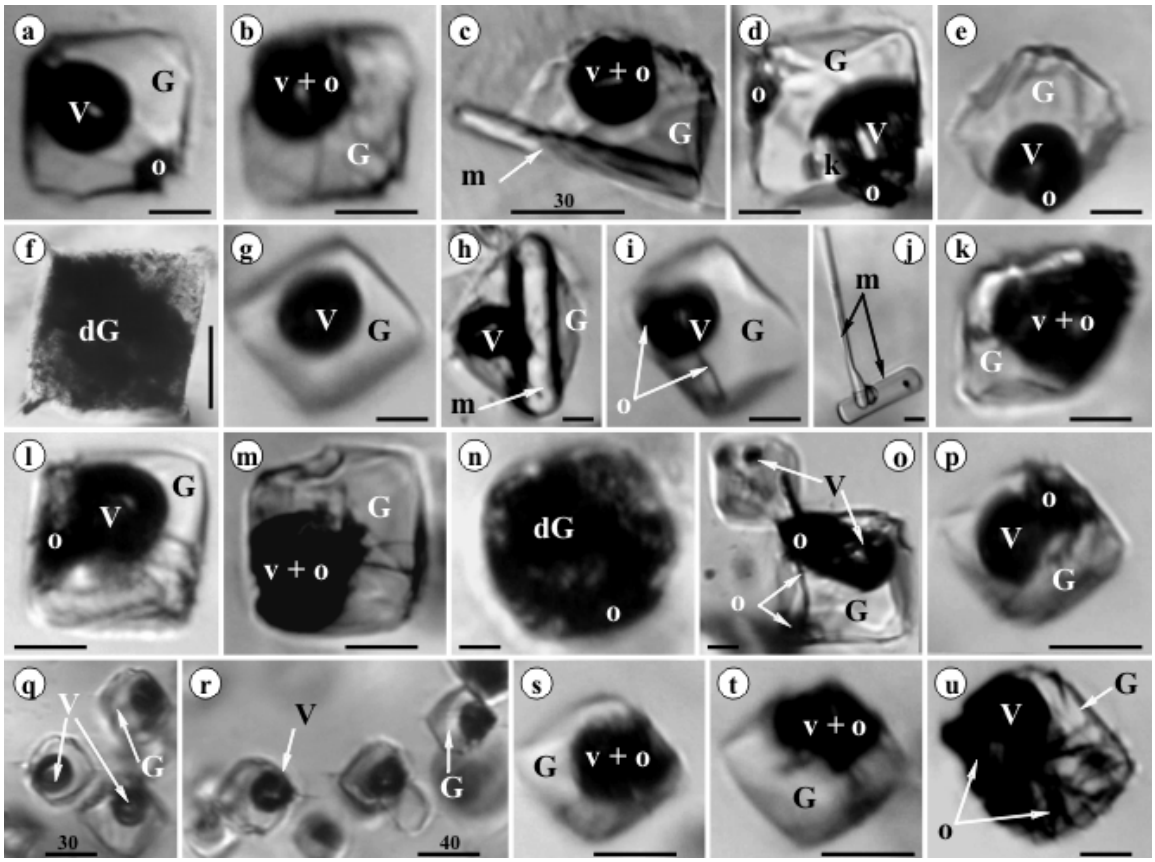

Fig. 141. Silicate melt inclusions types trapped in quartz (**a, b, c, d, e, f, g, h, i, j, k, l, n, o, p, q, r, s, t, u**) and feldspar (**m**) from Ulmoasa dacite collected from Ulmoasa Valley close to the confluence with Baita Valley on the right side (Baia Mare region, Maramureş county). Notations: V-vapor, G-silicate glass, dG-devitrified silicate glass, O – opaque, m- mocrosolid (mainly apatite). Scale bar in µm.

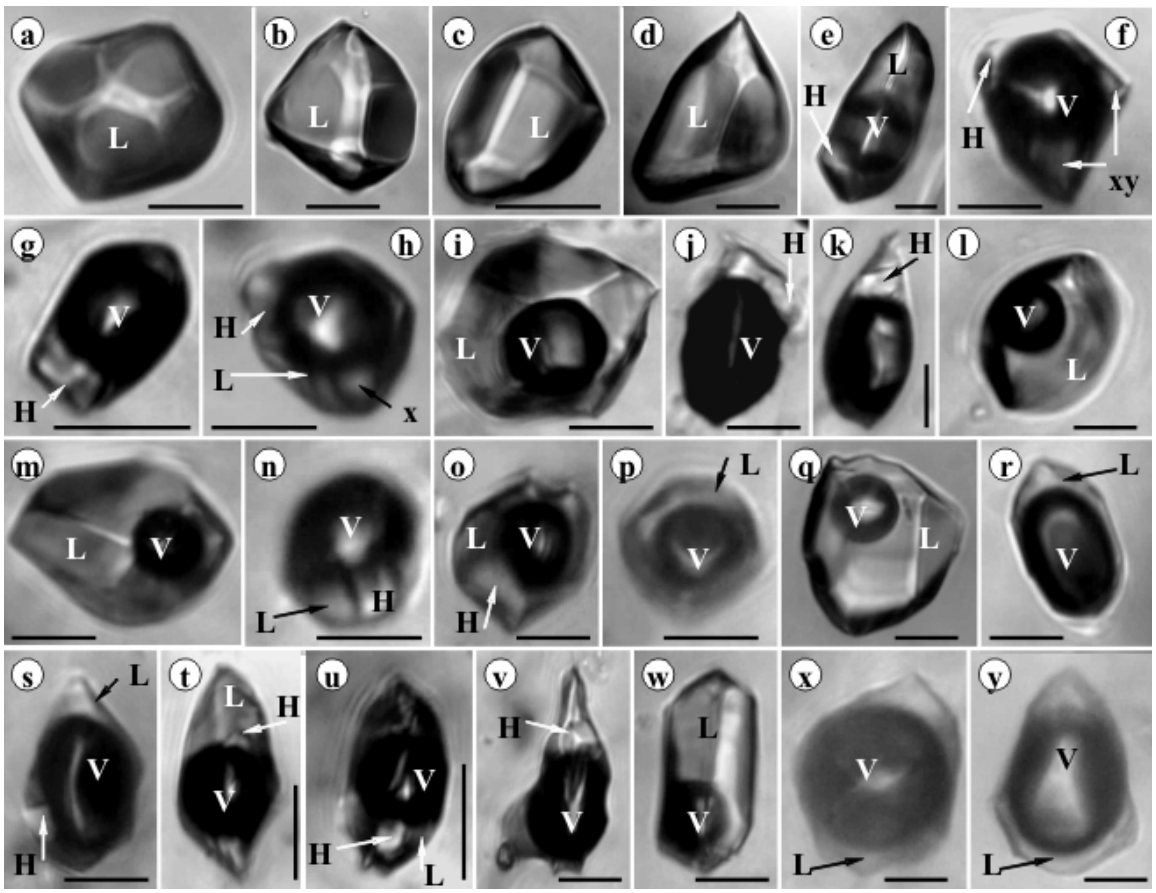

Fig. 142 Liquid monophase-, (**a**, **b**, **c**, **d**) – biphasic-, (**i, l**, **m**, **p**, **q**, **r**, **w**, **x**, **y**) and triphase-, (**e**, f, **g**, **h**, **j**, **k**, **n**, **o**, **s**, **t**, **u**, **v**) fluid inclusions in barite nodules from the bentonite Valea Chioarului mining prospect (geol. V. Todoran, 1997 - sample courtesy). Notations: L-liquid, H- halite, V- vapour. Homogenization temperature in un-stretched biphasic fluid inclusions ranged between 154° and 240°C (n = 30). Rarely, triphase fluid inclusions (n=4) showed Th= 263-330°C, with estimated salinity of 30-34 wt% NaCl eq., and formation pressure between 28 and 96 bars from a boiling fluid vent evolved under seawater down to 1000m. Scale bar: 10µm (Modified from Pintea, 2016).

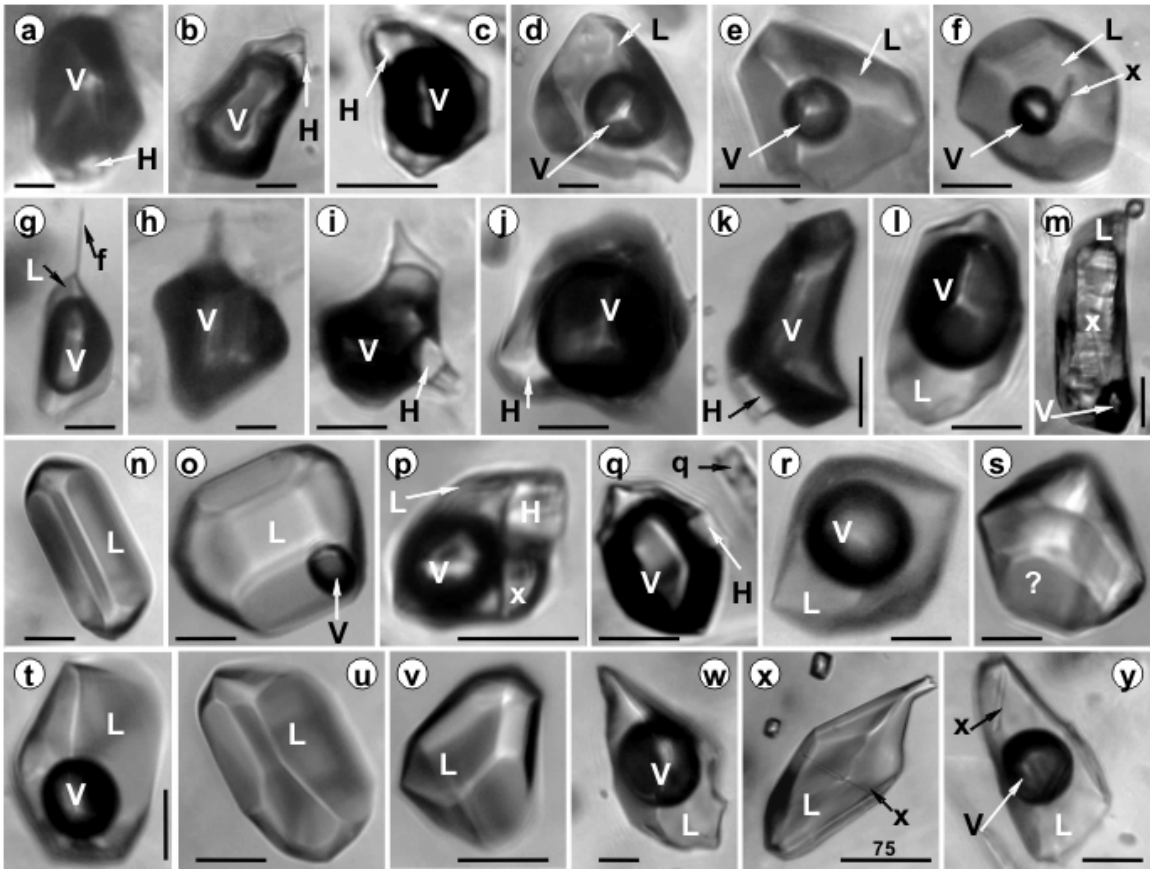

Fig. 143. Various filling ratio in fluid inclusions trapped in barite nodules from Valea Chioarului mining district suggesting heterogeneous mixtures of the trapped boiling fluid.Vapor-rich +liquid ± halite ± unknown solid phases: **a, b, c, g, h, i, j, k, l, q;** Biphasic**: d, e, f, o, r, t, w, y;** Monophase liquid**: n, u, v, x;** Liquid + unknown solid (s): **m, s.** Scale bar in μm.

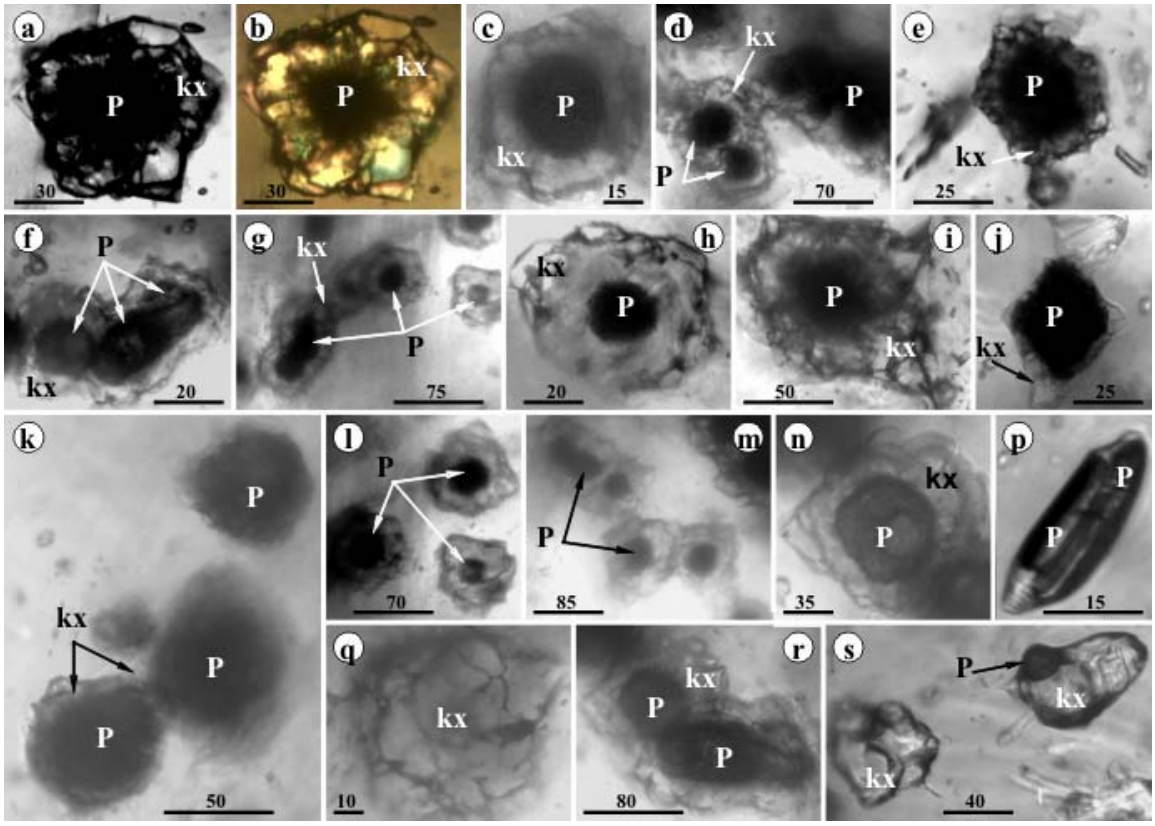

Fig. 144. Presumable recrystallized (solidified) multiphasic (?) fluid inclusions during barite diagenesis and bentonite formation in the Valea Chioarului mining district.
P, kx - unknown solid phases. Scale bar in µm.

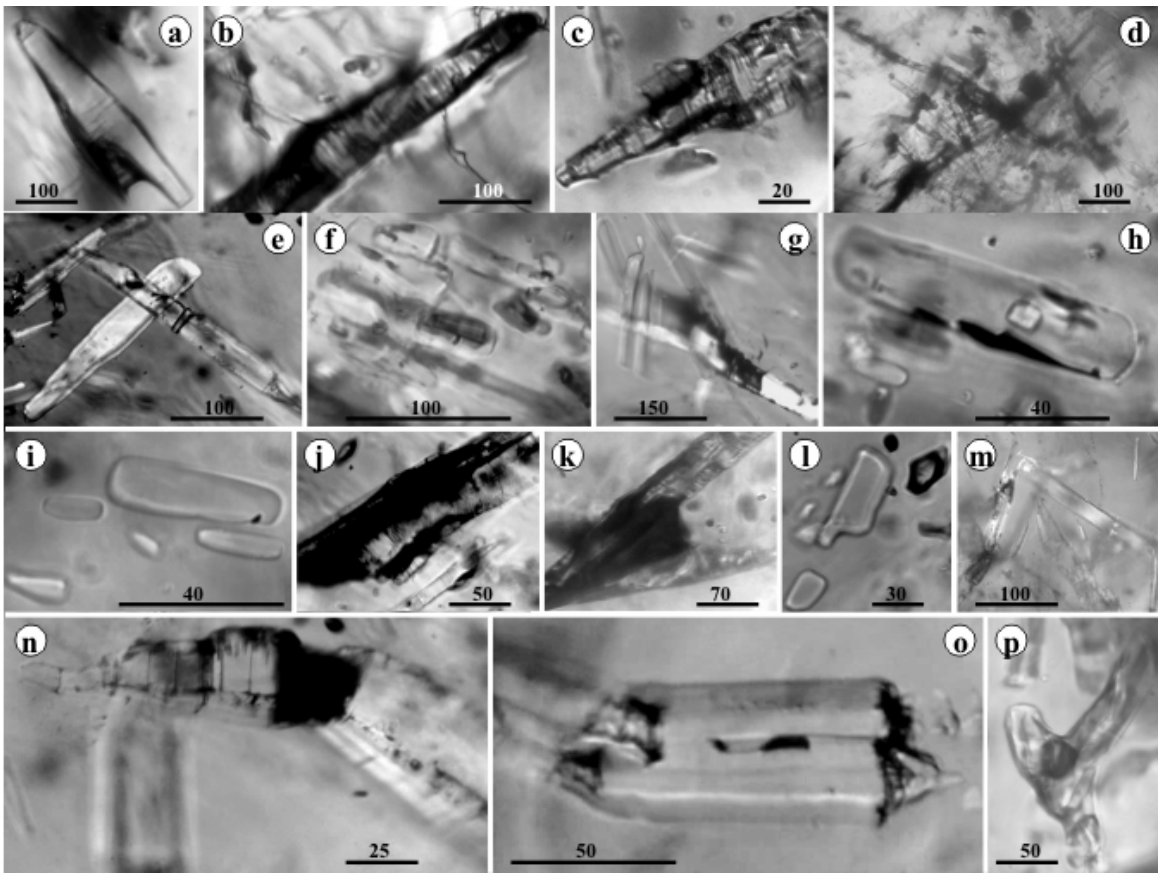

Fig. 145. Crystalline and amorphous solid microinclusions trapped accidentally in the barite nodules from Valea Chioarului mining district. They are also trapped in fluid inclusion as pictured in **p.** Scale bar in µm.

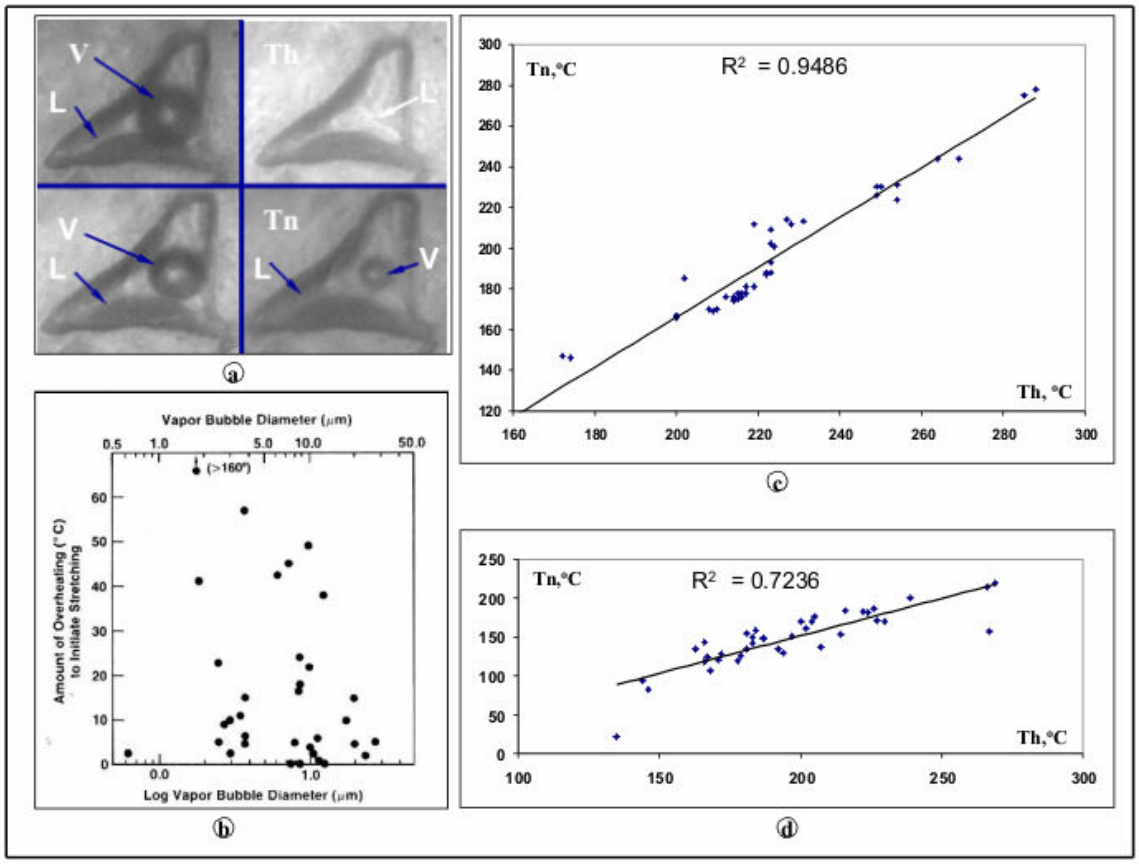

Fig. 146. Validation of homogenization temperature in presumable unstretched fluid inclusions from barite nodules from Valea Chioarului by using final liquid homogenization temperature value (Th) *versus* renucleation temperature value (Tn) of the vapour bubble during normal quenching in the microthermometric stage under the microscope (**a**). The stretching of fluid inclusions during microthermometry was tested by Ulrich and Bodnar (1988) by calculating the overheating amount necessary to induce stretching of fluid inclusion in barite at 1 atm confining pressure (**b**). Our data set (**c**) shown a very good correlation between Th and Tn comparable with similar measurements made in synthetic fluid inclusions in quartz measured by Schmulovich et al., 2009 (**d**). Tentatively, it is considered that based upon such data consistency the fluid inclusions in barite were unstretched during microthermometry and the homogenization temperature are the minimum formation temperature of the barite nodules from Valea Chioarului (Pintea, 2016). Notations: L-liquid, V-vapor.

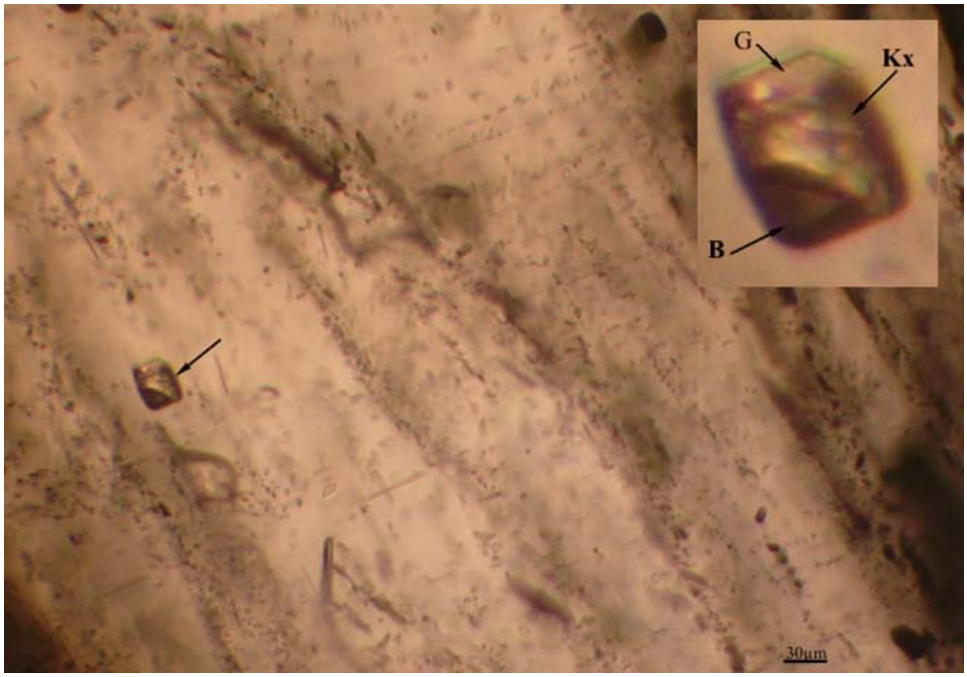

Fig. 147. Multisolid inclusion in oriented exsolution microtexture in almandine garnet from Lotru Metamorfic Suite (sample courtesy G. Săbău), unlocalized; arrowed inclusion in medalion: G-glass, B-vapor bubble, Kx – crystallised phases.

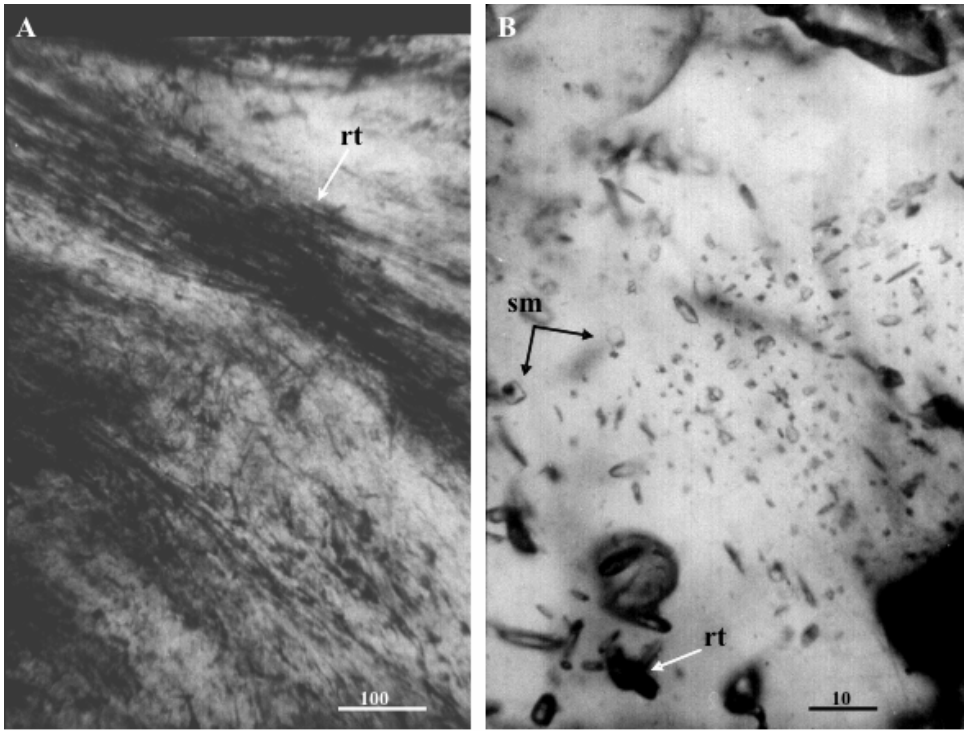

Fig. 148. Two microtextural features in almandine garnet from Lotru Metamorphic Suite (unlocalized, sample courtesy G. Săbău. A. liniation with rutile elongated microcrystal and B. central sieve texture with multiphase solid inclusions. Scale bar in µm.

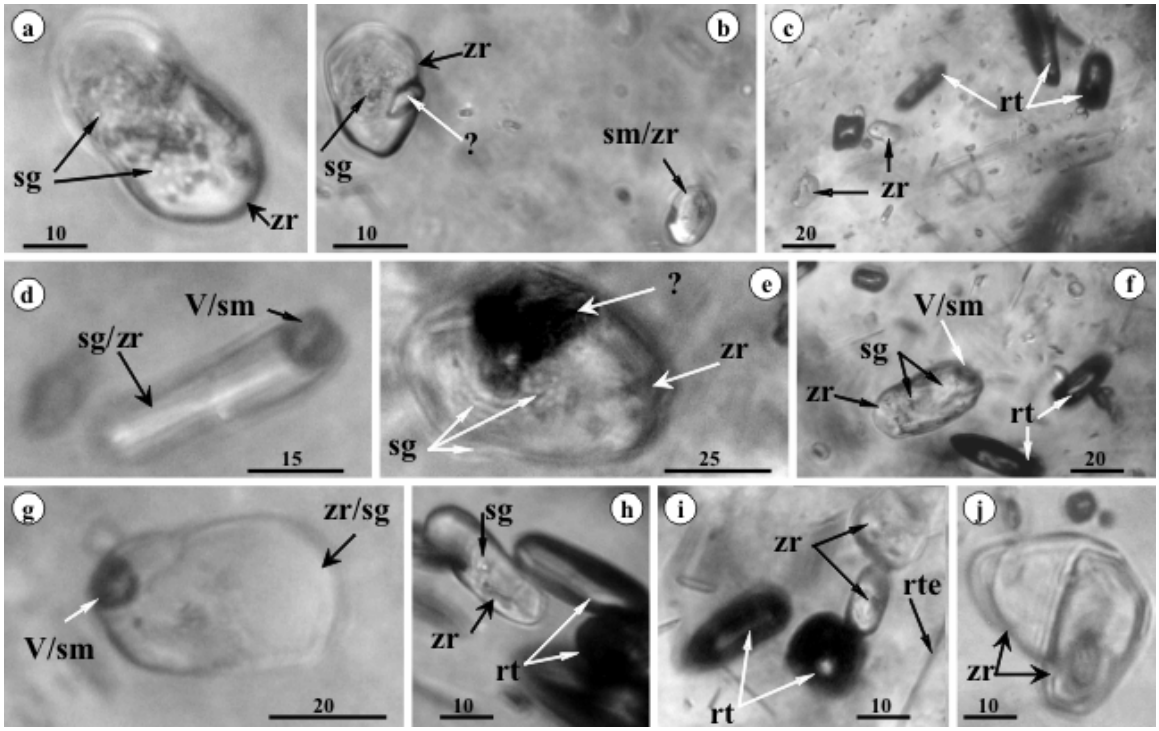

Fig. 149. Remelted features of zircon inclusions in almandine garnet from Lotru Metamorphic Suite (unlocalized), sample courtesy G. Săbău. Notations: zr. – zircon, sg- silicate glass, V- vapor bubble, sm- silicate melt, rt- restitic rutile, rte- exsolved rutile rod. Scale bar in µm.

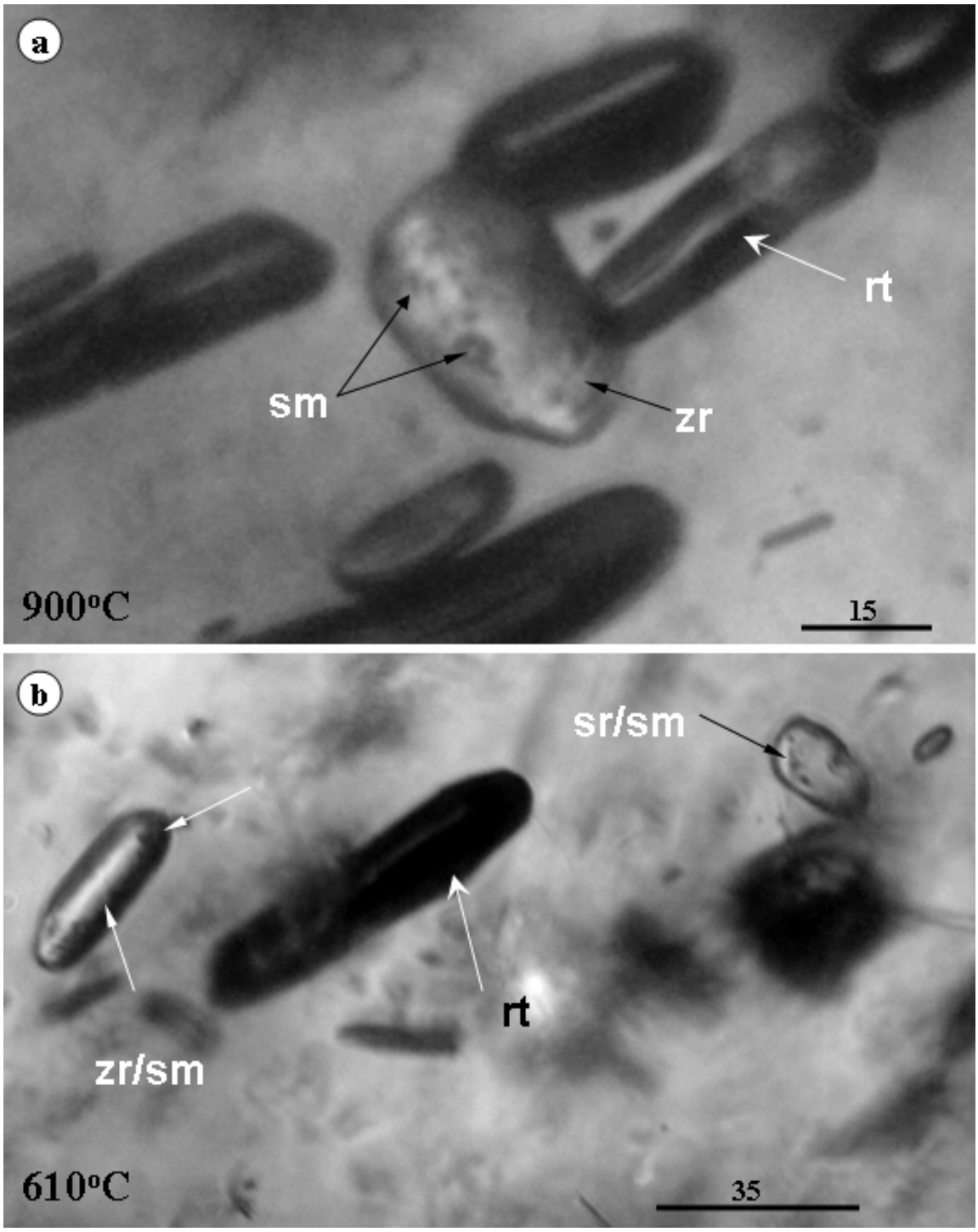

Fig. 150. Rounded (partially dissolved) rutile rods and zircon "xenocrysts" in garnet at indicated temperatures. Some of them have silicate melt (glassy) inclusions-?. Preliminary data (one recorded measurement indicated bubble homogenization between 875-939°C (not shown in the pictures). Notations: rt- rutile rods, zr-zircon, sm- silicate melt. The microthermometry data are similar with the P-T estimation of Săbău and Massone, (2003) from coexisting garnet-clinopyroxene. Unlocalized almandine, sample courtesy G. Săbău).

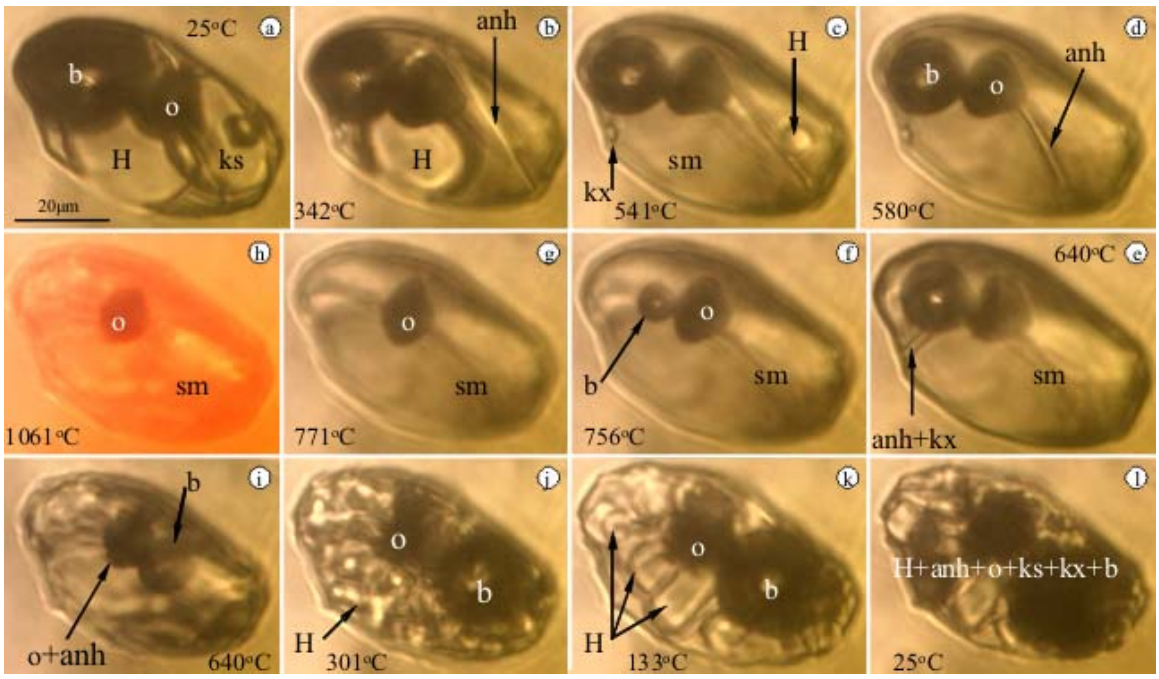

Fig. 151. Anhydrite microthermometry of brine inclusions in quartz from Roşia Poieni porphyry Cu-Au-(Mo)- Pintea et al., 2019. **a.** 25°C, **b.** 342°C, **c.** 541°C, **d.** 580°C, **e.** 640°C, **f.** 756°C, **g.** 71°C, **h.** 1061°C, **i.** 640°C, **j.** 301°C, **k.** 133°C, **l.** 25°C; Tm1= 66-238°C, TmH= 543°C, Tmanh= 723°C, Th= 770°C, Tmax= 1062°C; Tmo> 1062°C, T= 770, P= 907.48 bar, Ws= 66.0109 wt % NaCl eq., d= 1.064, x=0.4, single phase state; Notations: b-bubble, o-opaque, H-halite, ks-other salt daughter minerals, anh-anhydrite, kx-unidentified; scale bar in microns; Tm-anhydrite almost fitted to the experimental data in the Albite-Quartz-Anhydrite-H_2O system (Ducea et al., 1999).

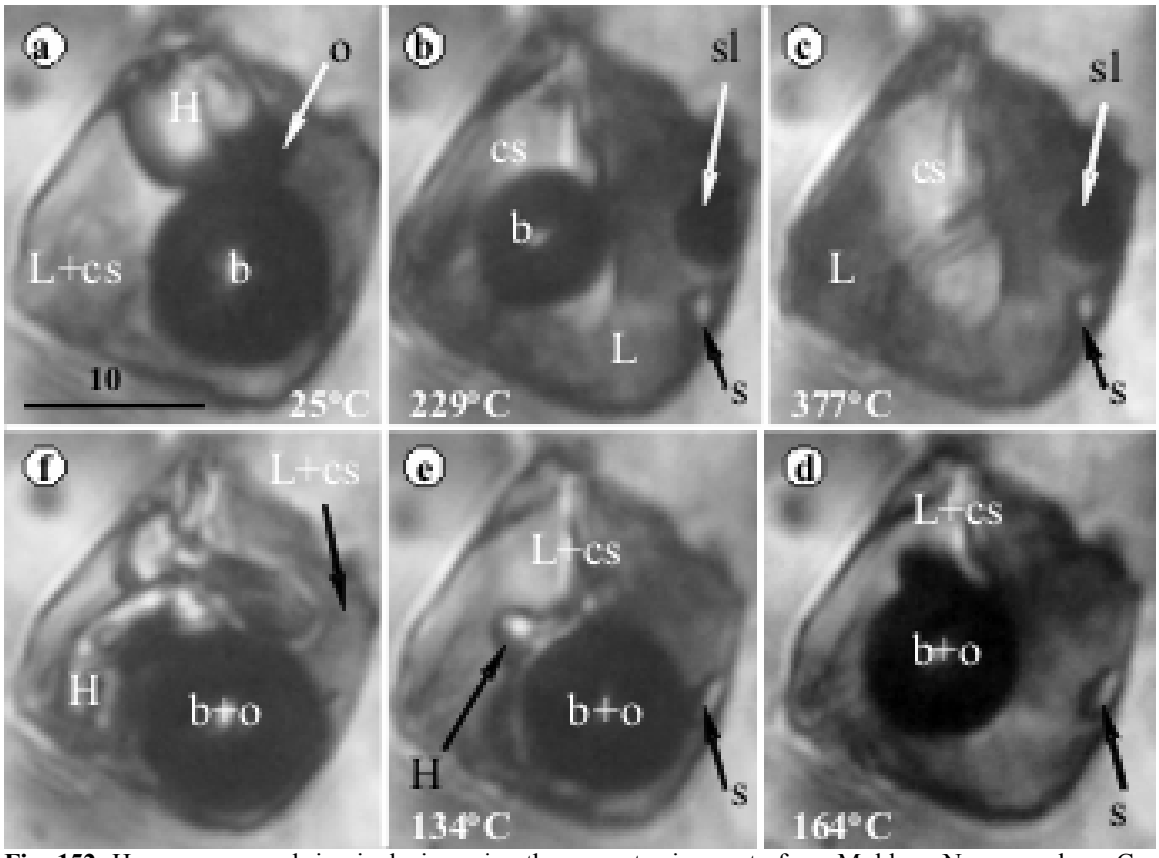

Fig. 152. Homogeneous - brine inclusion microthermometry in quartz from Moldova Noua porphyry Cu-Mo-(Au). **a.** 25°C, **b.** 229°C, **c.** 377°C, **d.** 164°C, **e.** 134°C, **f.** 25°C; TmH=298°C, Th=363°C, P=136.265 bar, Ws=37.5702 wt% NaCl eq., d=1.02705g/ccm, x=0.16, single phase state; Notations: L-liquid, H-halite, cs- clathrasil, b- vapor bubble, o-opaque (chalcopyrite ?), sl- liquid sulphide globulae, s-unknown solid; scale bar in microns (Pintea et al., 2019).

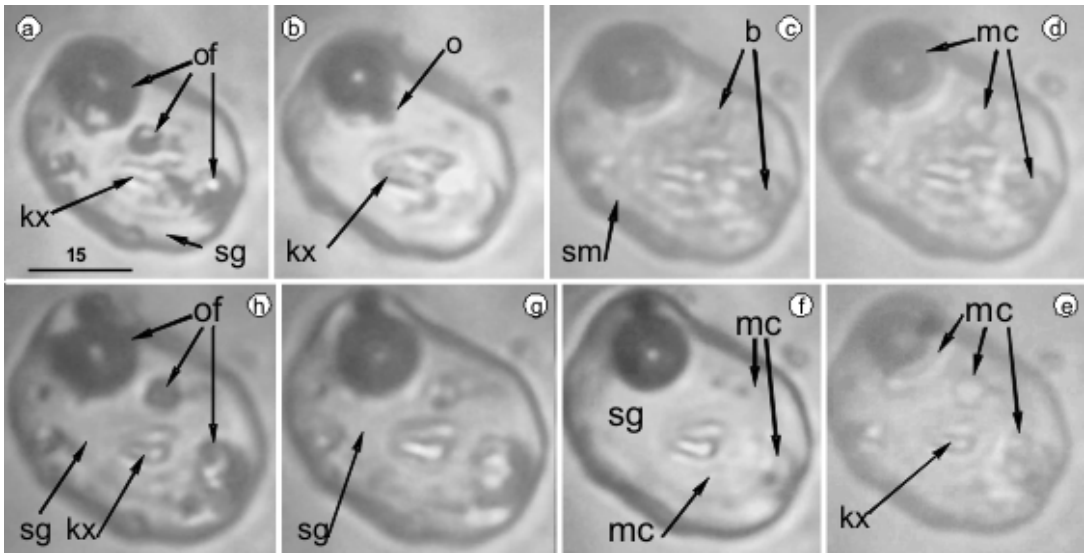

Fig. 153. Hydrosaline melt – silicate melt immiscibility in quartz from Bolcana porphyry Cu-Au-Mo deposit. (Pintea et al., 2019). **a.** 25°C, **b.** 517°C, **c.** 897°C, **d.** 943°C, **e.** 1048°C, **f.** 547°C, **g.** 265°C, **h.** 25°C; notations: of-ore fluid, kx- solid, sg- silicate glass, sm- silicate melt, mc- salt melt, b- bubble, o-opaque; scale bar in microns.

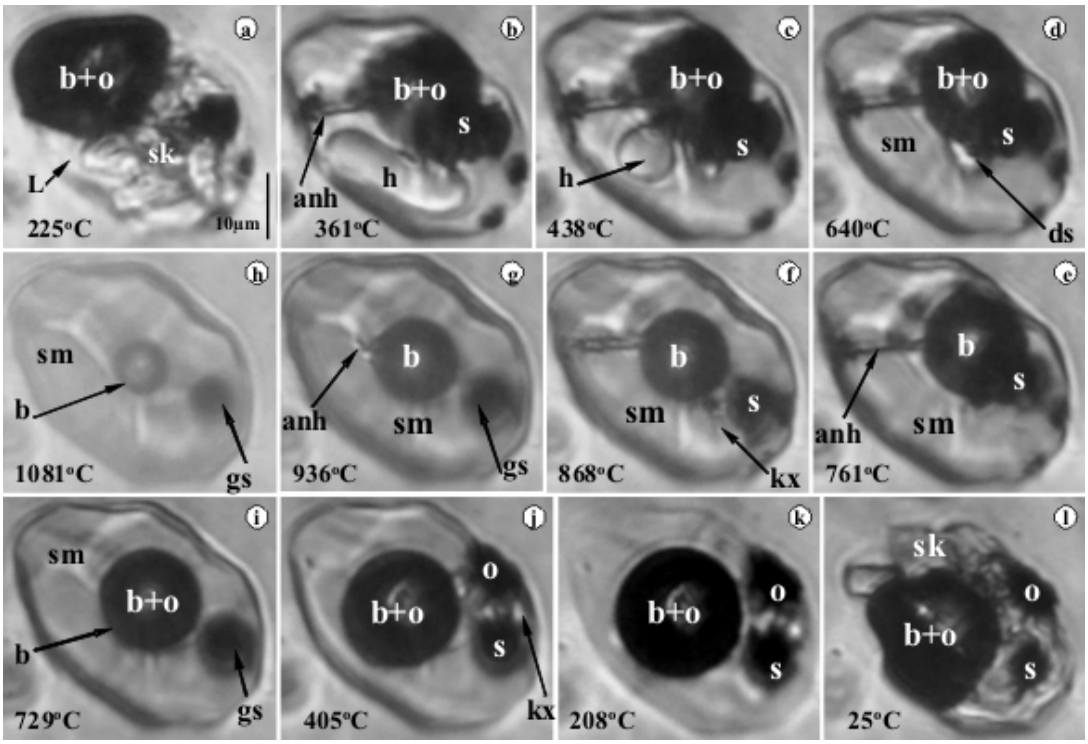

Fig. 154. Hydrosaline melt inclusion microthermometry, Bolcana porphyry Cu-Au-Mo deposit (B4-3). **a.** 25°C, **b.** 487°C, **c.** 539°C, **d.** 569°C, **e.** 735°C, **f.** 908°C, **g.** 925°C, **h.** 1095°C, **i.** 882°C, **j.** 756°C, **k.** 208°C, **l.** 25°C; TmH= 575°C, Tmkx= 645°C; Tnky= 902°C, Tmky= 1028°C, Tnxo= 786°C; Th≥ 1095°C, P= 1897.36 bars, Ws= 70.6299, d= 1.05291, single phase state; Notations: ks- saline minerals, b+O= bubble + opaque, kx,ky,kz- unidentified solids, xo- oxide (magnetite or hematite), sm-salt melt, gs-globular sulfide; s-sulfide; Tm-melting temperature, Tn- nucleation temperature; Th- homogenization temperature; P= pressure, Ws-salinity; scale bar in microns.

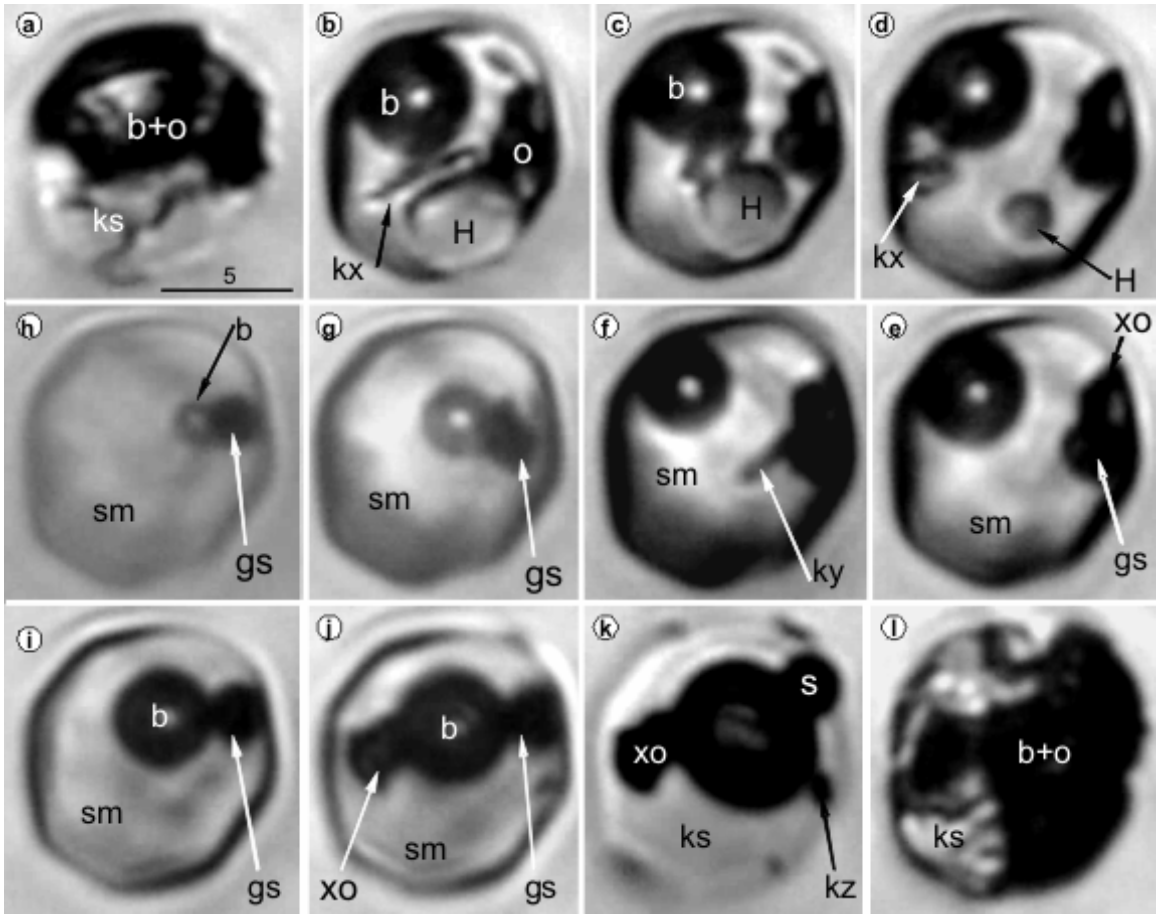

Fig. 155. Hydrosaline melt inclusion microthermometry from Bolcana porphyry Cu-Au-Mo (Pintea et al., 2019). **a.** 225°C, **b.** 361°C, **c.** 438°C, **d.** 640°C, **e.** 761°C, **f.** 868°C, **g.** 936°C, **h.** 1081°C, **i.** 729°C, **j.** 405°C, **k.** 208°C, **l.** 25°C; Tmh= 464°C, Tmds= 716°C, Tmo= 936-1025°C, Tno= 644°C, Tnds= 609°C; T≥ 1081°C, P= 2331.66 bar, Ws= 55.0043 wt% NaCl eq., d= 0.883646 g/ccm, xNaCl= 0.27, V+L phase state. Notations: L-interstitial liquid phase, sk-salt crystals, b-bubble, anh-anhydrite, s-sulphide, o-oxide (magnetite and or hematite), sm-salt melt, gs-globular liquid sulfide, kx-unknow solid, scale bar in microns.

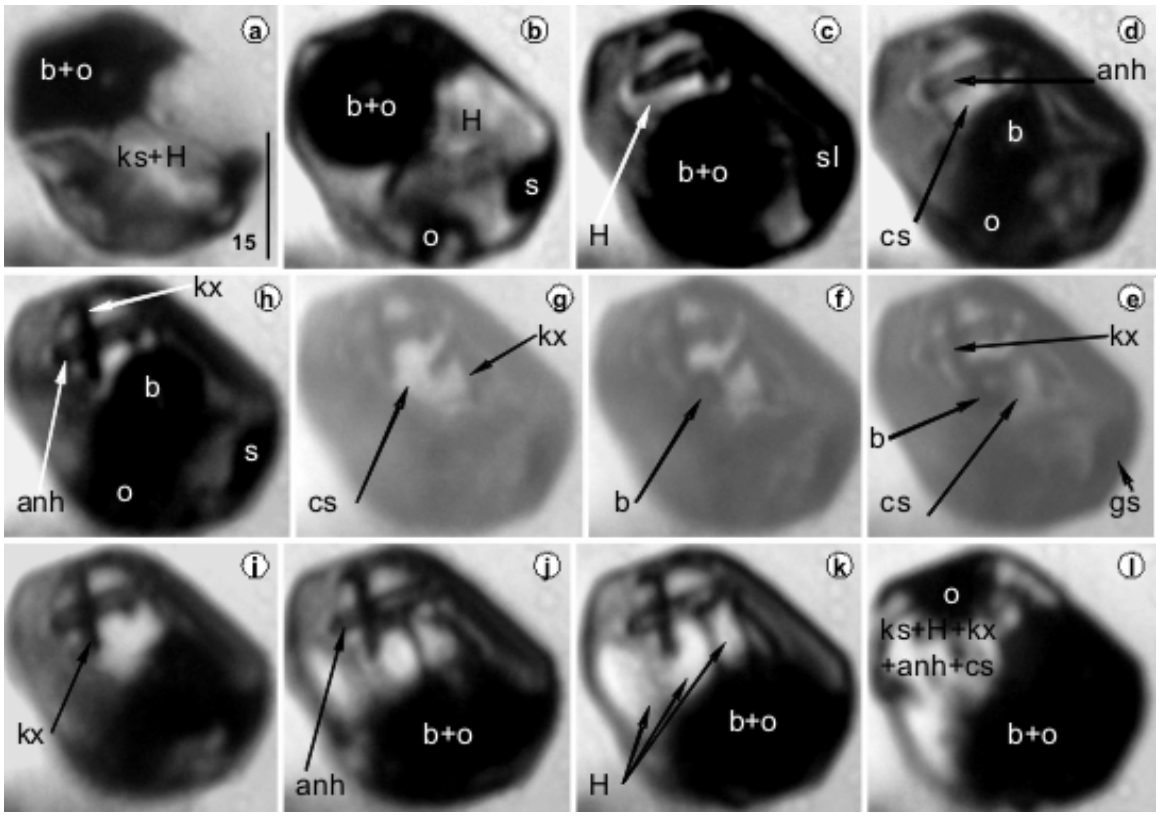

Fig. 156. Hydrosaline melt inclusion microthermometry. Valea Morii porphyry Cu-Au-Mo deposit (Pintea et al., 2019). **a.** 25°C, **b.** 366°C, **c.** 545°C, **d.** 753°C, **e.** 863°C, **f.** 881°C, **g.** 891°C, **h.** 658°C, **i.** 556°C, **k.** 507°C, **l.** 27°C; TmH= 554°C, ThV= 889°C, TnV= 778°C, TnH= 538°C, Tnfinal= 207°C; T=889°C, P=1246.21 bar, Ws=67.5962 wt% NaCl eq., d= 0.773078 g/ccm; single phase state; Notations: B+O bubble + opaque, ks-saline daughter phases, s-sulfide, sl-liquid sulfide, anh-anhydrite, kx – unknown phase, clathrasil (?), gs-globular sulfide; scale bar in microns.

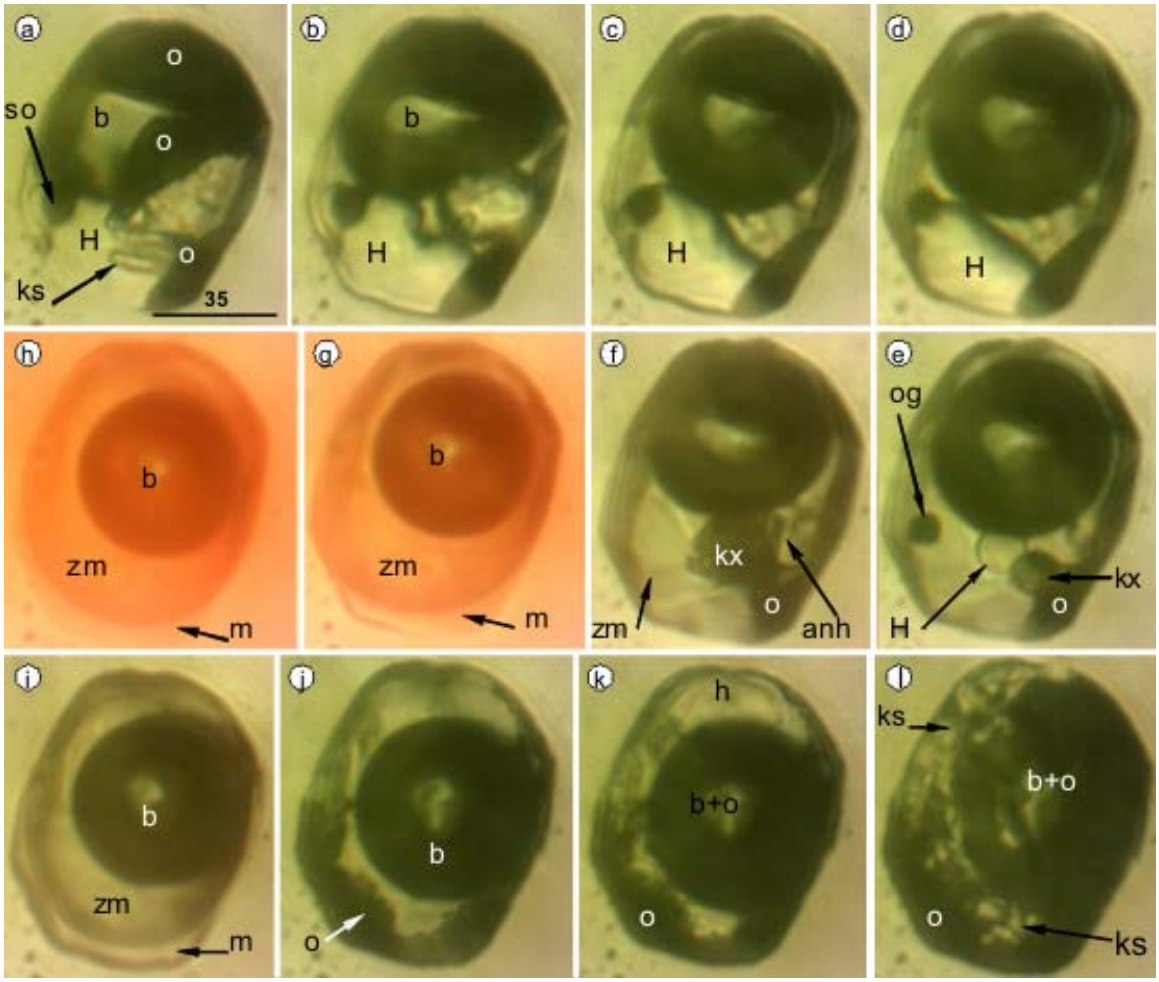

Fig. 157. Hydrosaline melt inclusion microthermometry. Valea Morii porphyry Cu-Au-Mo deposit (Pintea et al., 2019). **a.** 25°C, **b.** 285°C, **c.** 443°C, **d.** 553°C, **e.** 609°C, **f.** 828°C, **g.** 1003°C, **h.** 1033, **i.** 870°C, **j.** 560°C, k. 319°C, **l.** 25°C. Microtermometry: TmH= 612°C, Tmog= 786°C, Tmo= 1000°C, Th >>1037°C; Tfmenisci=1000°C, Tno=574°C; if Tf= 1037°C P= 1312.53 bar, Ws= 75.9472 wt% NaCl eq., d= 1.102 g/ccm, xNaCl= 0.5. Notations: so-solid opaque, H-halite, o-another opaque, b- bubble, ks- soluble minerals,og-globular opaque (liquid),anh-anhydrite, zm- hydrosilicate liquid, m- silicate melt,. Scale bar in microns.

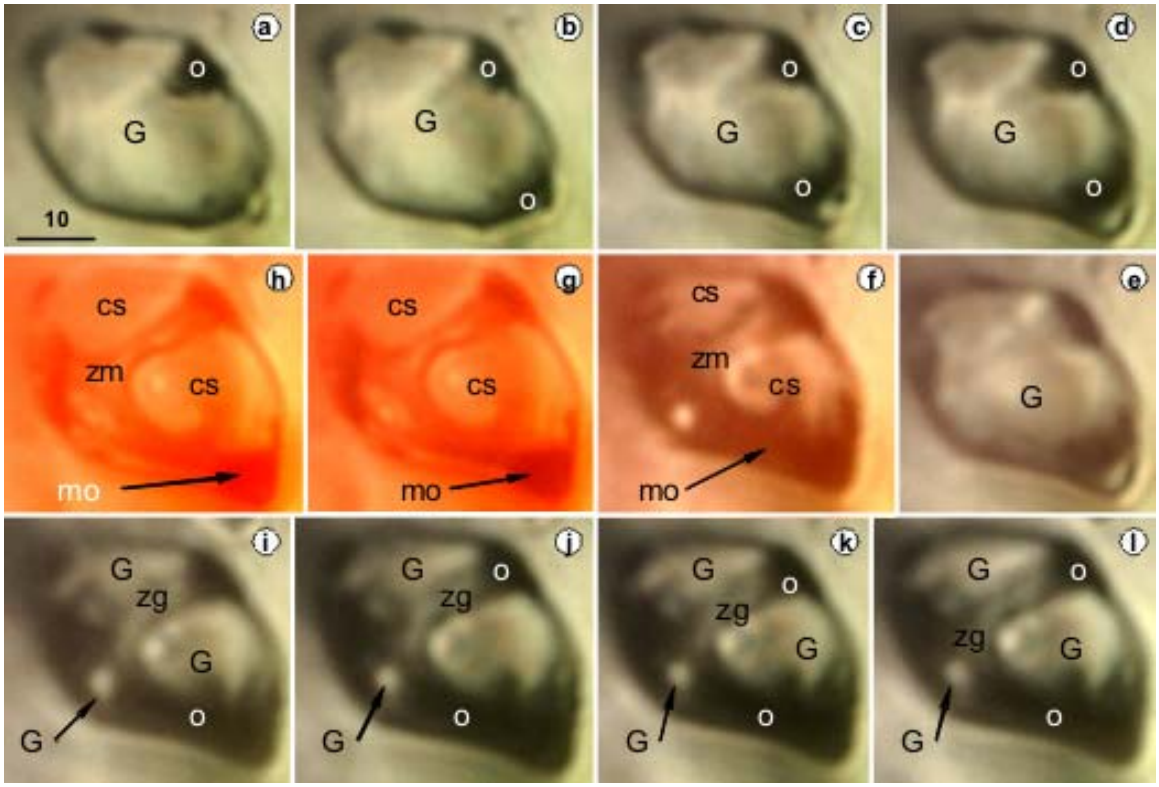

Fig. 158a. Hydrosilicate glass inclusion microthermometry. Valea Morii porphyry Cu-Au-Mo deposit. **a.** 25°C, **b.** 266°C, **c.** 537°C, **d.** 584°C, **e.** 837°C, **f.** 931°C, **g.** 1007°C, **h.** 1015°C, **i.** 760°C, **j.** 502°C, **k.** 206°C, **l.** 25°C; TmG= 546°C (start melting), Ti~ 808°C (immiscibility); Notations: G-glass, o-opaque, cs- other salt, zm- hydrosilicate melt (clathrasil), mo- opaque melt; scale bar in microns.

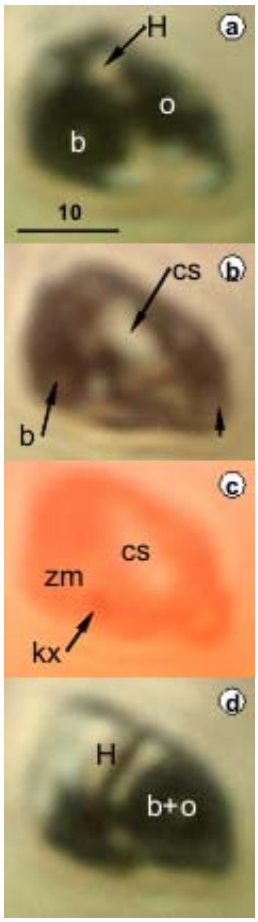

Fig. 158b. Coeval hydrosaline melt inclusion microthermometry.
a. 429°C, **b.** 827°C, **c.** 1015°C, **d.** 206°C;
Microthermometric data: TmH= 573°C, Th=992°C, P=1482.11 bars, Ws= 70.341 wt% NaCl eq., d= 1.05842 g/ccm, xNaCl=0.41, Tmk= 1011°C, Tnb= 832°C, Tno= 712°C, TnH=344°C, Tnks=159°C; Notations: H-halite, o-opaque, b-bubble, cs- salt melt (or other melt?), zm- hydrosilicate melt (cathrasil), kx-anhydrite; sacale bar in microns.

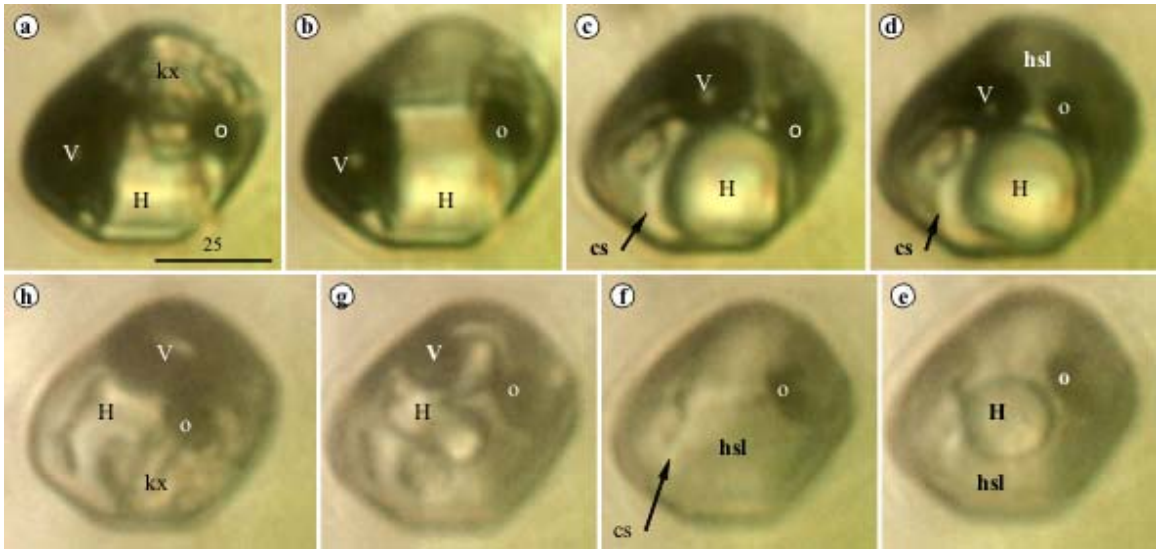

Fig. 159. Hydrosaline melt inclusion microthermometry from Vlădeasa miarolitic quartz pegmatite (Zarna Valley). **a.** 25°C, **b.** 164°C, **c.** 274°C, **d.** 360°C, **e.** 450°C, **f.** 507°C, **g.** 362°C, **h.** 41°C; Microthermometry: Th(L+H)= 451°C, Th (L)= 511°C, P= 807.231 bar, Ws= 61.152 wt% NaCl eq., d= 1.2168, xNaCl= 0.32, Tn(V+H)= 375°C, Tnkx= 43°C, single phase state. Notations: V- vapor, kx- unidentified solid(s), H-halite, o-opaque, hsl- hydrosaline melt, cs- clathrasil, scale bar in µm.

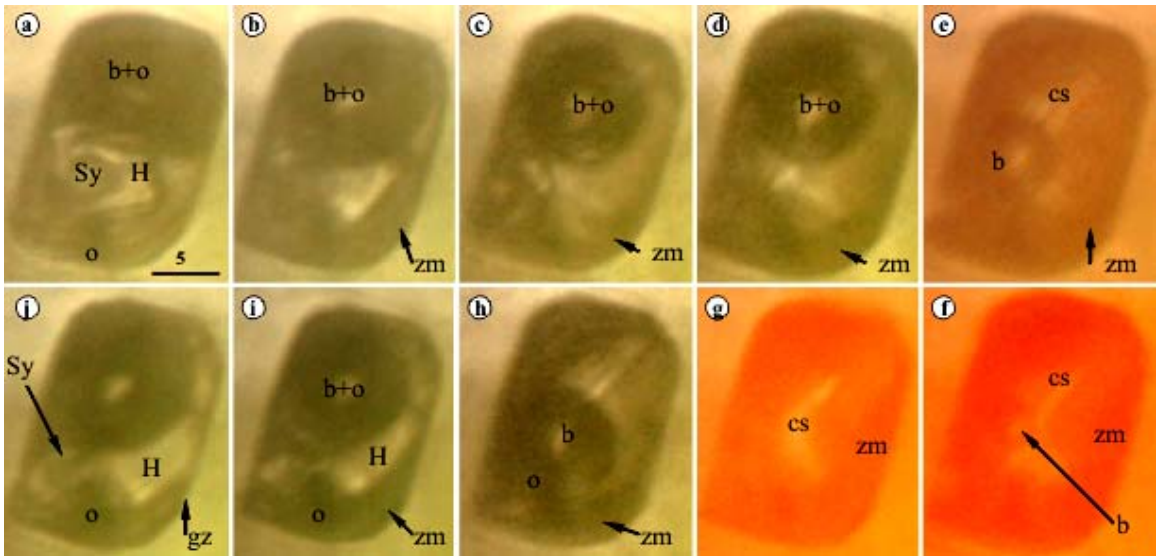

Fig. 160. Hydrosaline melt inclusion microthermometry in quartz from Vladeasa miarolitic pegmatite. (Zarna Valley). **a.** 40°C, **b.** 157°C, **c.** 465°C, **d.** 683°C, **e.** 935°C, **f.** 992°C, **g.** 1004°C, **h.** 650°C, **i.** 190°C, **j.** 25°C; Tm1= 100°-149°C, TmH=450°C, Th=1004°C, TnV=953°C, P=2099.57 bar, Ws=53,177 wt% NaCl eq., d=0.8769 g/ccm, xNaCl=0.26, single phase state; Notations: Sy-sylvite, b-bubble, o-opaque, H-halite, cs-clathrasil, zm- hydrosilicate liquid, gz- hydrosilicate glass; scale bar in microns.

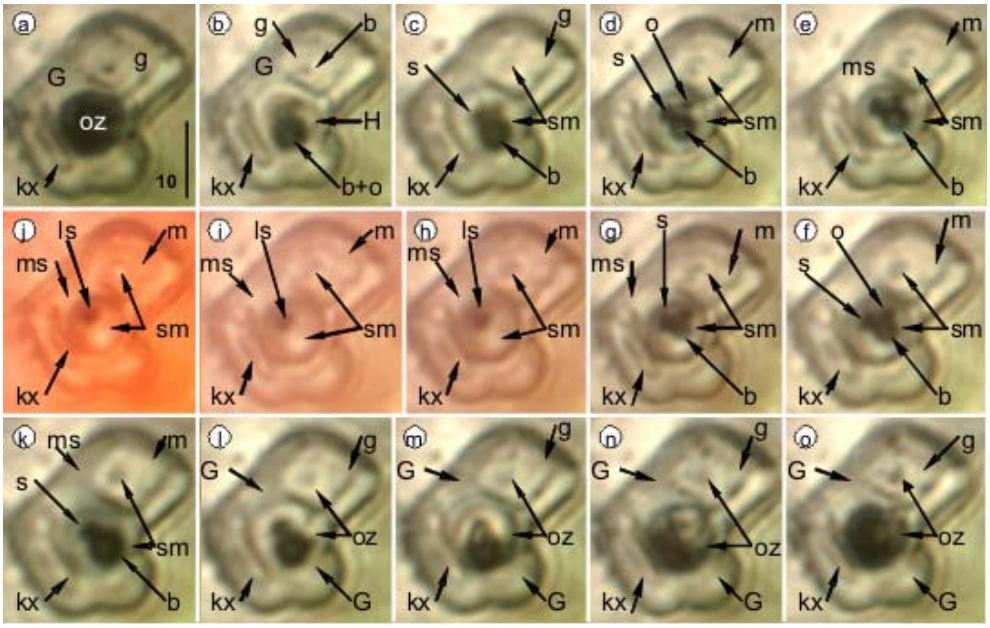

Fig. 161. Hydrosilicate-hydrosaline melt inclusion from Moldova Noua porphyry Cu-Mo-Au deposit (Pintea et al., 2019). **a.** 25°C, **b.** 337°C, **c.** 405°C, **d.** 689°C, **e.** 708°C, **f.** 775°C, **g.** 830°C, **h.** 918°C, **i.** 939°C, **j.** 988°C, **k.** 661°C, **l.** 369°C, **m.** 259°C, **n.** 187°C, **o.** 25°C; Microthermometry: TmH= 401°C, Th= 892°C, P= 1784.59 bar, Ws= 47.2345 wt% NaCl eq., d= 0.831571 g/ccm, xNaCl=0.21, single phase state: (L+V); Notations: ks-solid, xg-glass, sg-silicate glass, of-ore fluid, sm-silicate melt, mc- salt melt, s- solid sulfide, gs- liquid sulfide, m- magnetite, h-halite, hs- hydrous salt crystal; scale bar in microns.

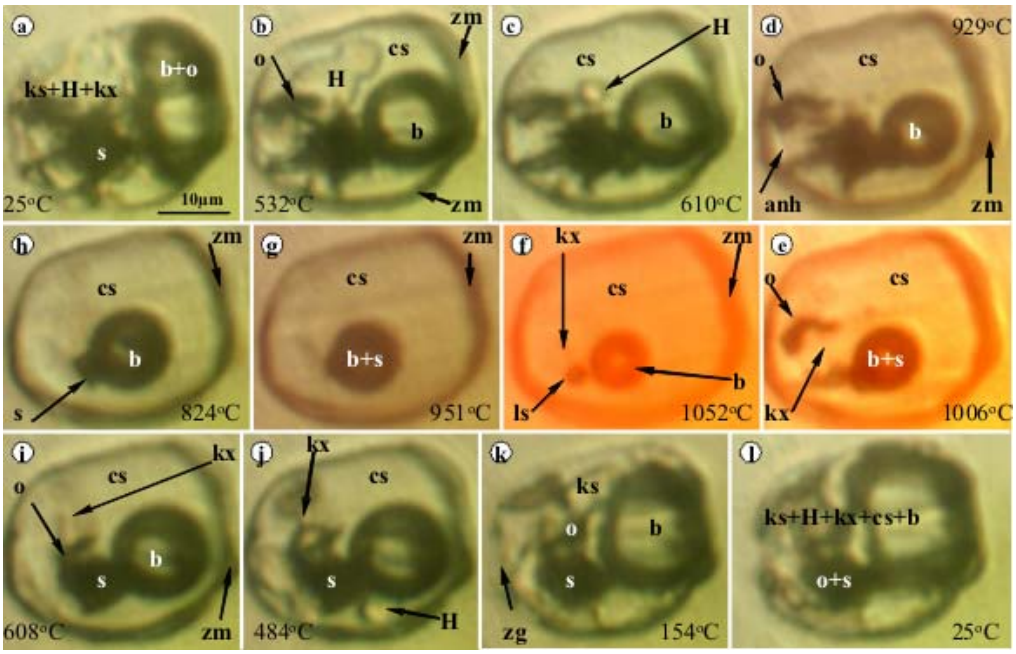

Fig. 162. Hydrosaline melt inclusion microthermometry. Valea Morii porphyry Cu-Au-Mo deposit (Pintea et al., 2019). **a.** 25°C, **b.** 532°C, **c.** 610°C, **d.** 929°C, **e.** 1006°C, **f.** 1052°C, **g.** 951°C, **h.** 824°C, **i.** 608°C, **j.** 484°C, **k.** 154°C, **l.** 25°C; Microthermometry: TmH=611°C, Tmo= 1017°C, Th ≥1052°C, Tno= 657°C, TnH= 495°C, (Tm anhydrite = 987°C in the followed cycle), Tmkx≥1040, Tf≥1052°C, P=1364.37 bar, Ws=75.8046 wt% NaCl eq., d=1.09793, xNaCl= 0.5; Notations: s-sulfide (chalcopyrite?), liquid sulfide, H-halite, ks-other salt, b-bubble, cs– cathrasil (?), zg- hydrosilicate glass, o-opaque; scale bar in microns.

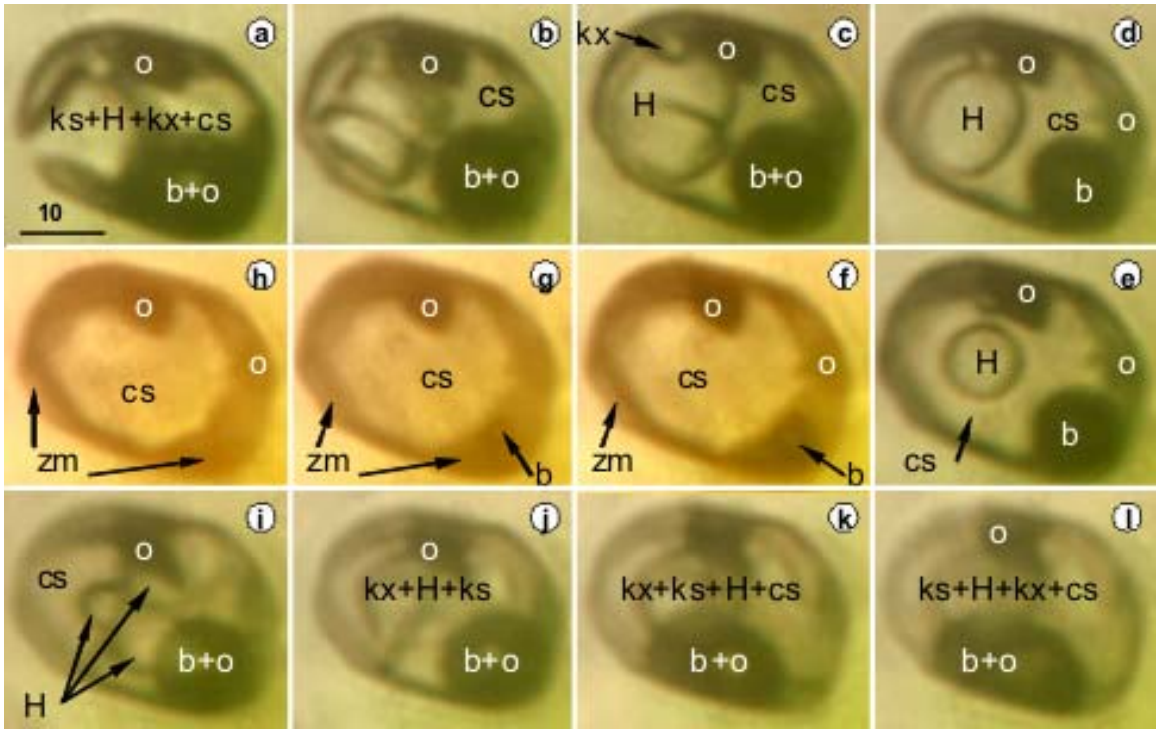

Fig. 163. Hydrosaline melt inclusion microthermometry. Rovina porphyry Cu-Au-Mo deposi.(ROV- 1A). a. 25°C, b. 348°C, c. 402°C, d. 507°C, e. 545°C, f. 789°C, g. 816°C, h. 828°C, i. 433°C, j. 238°C, k. 155°C, l. 101°C; Tm1=258°C, TmH=562°C, Th=825°C, P=1009.37 bar, Ws=68.7515 wt%NaCl eq., 1.07986 g/ccm, x=0.41, single phase state. Notations:H-halite, kx-other salt, kx-anhydrite (?), b-bubble, o-opaque undiferentiated, cs-clathrasil, zm- hydrosilicate liquid; scale bar in microns.

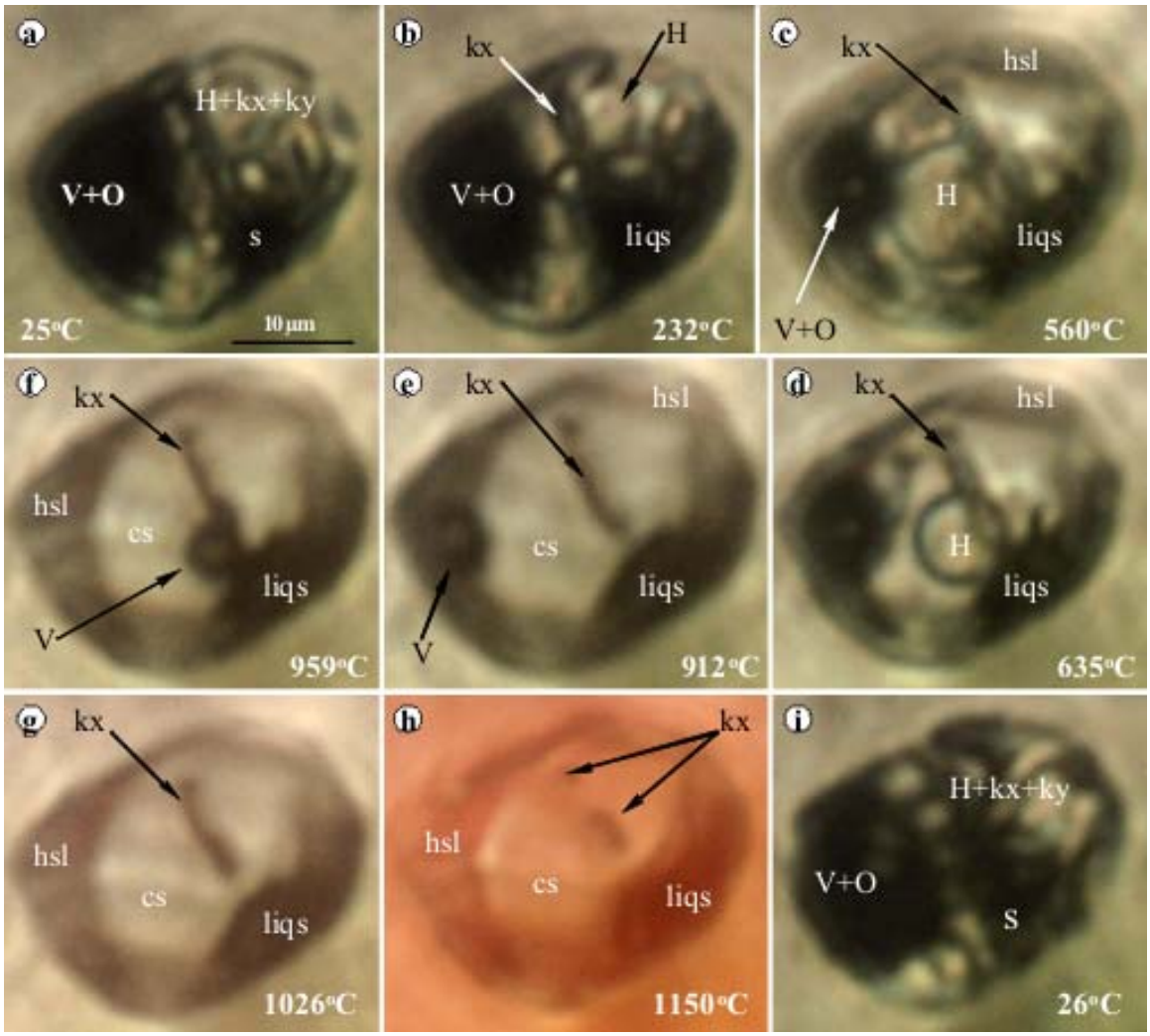

Fig. 164. Hydrosaline melt inclusion microthermometry. Rovina porphyry Cu-Au-Mo deposit, the same in **Fig 163**, after two years, modified by stretching(?). Microthermometry: TmH= 659°C, Th (L)= 989°C, P= 863.021 bar, Ws= 82.5287 wt% NaCl eq., d= 1.18199, xNaCl= 0.60, single phase state. Notations: V-vapor, H-halite, kx, ky- unknown, hsl- liquid hydrosaline, cs- clathrate, liqs- liquid sulfide, s- sulfide, o-opaque.

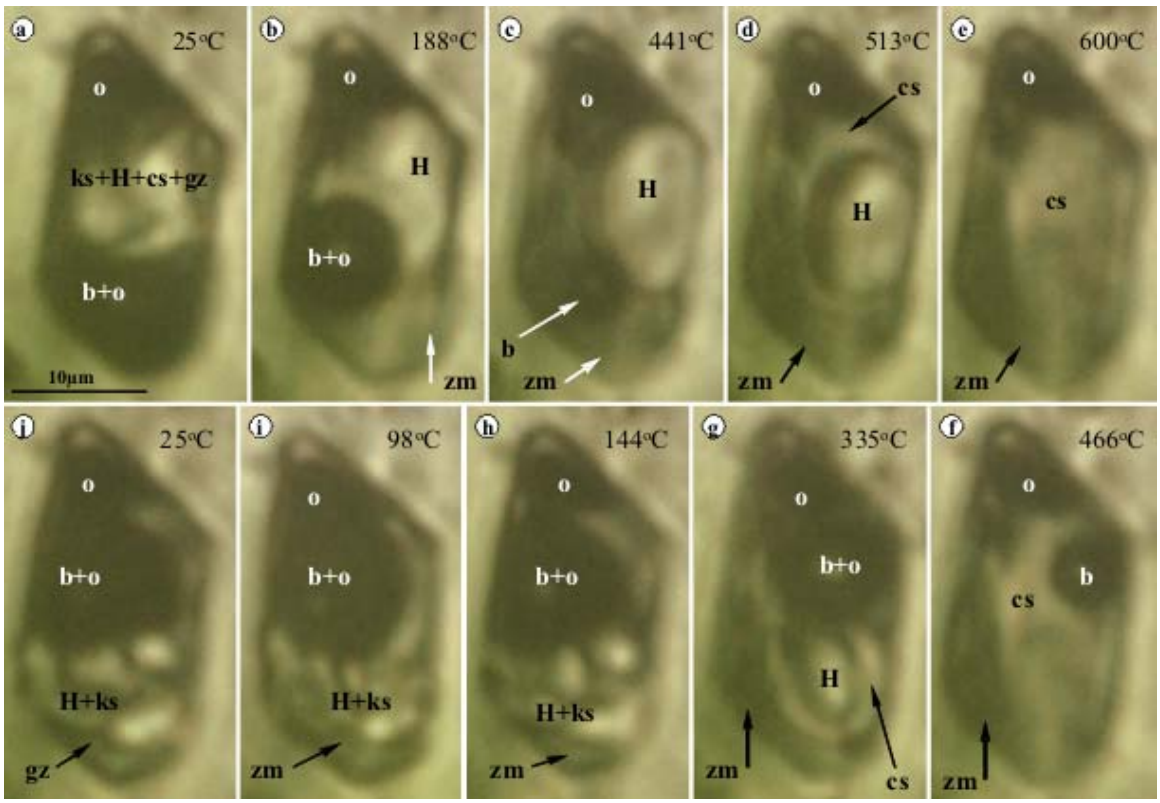

Fig. 165. Hydrosaline melt inclusion from Tălagiu porphyry Cu-Au-Mo deposit (Pintea et al., 2019). **a.** 25°C, **b.** 188°C, **c.** 441°C, **d.** 513°C, **e.** 600°C, **f.** 466°C, **g.** 335°C, **h.** 144°C, **i.** 98°C, **j.** 25°C; Microthermometry by halite homogenization: Tmks= 161°C, ThV= 512°C, TmH= 599°C (formation temperature), P= 1628.25 bar, Ws=72.5583 wt% NaCl, d= 1.33906 g/ccm, xNaCl= 0.4, single phase state; Notations: ks- soluble salt, H- halite, cs- clathrasil, b-bubble, o-opaque, zm- hydrosilicate liquid (melt), gz-transparent glassy crust-?; scale bar in microns.

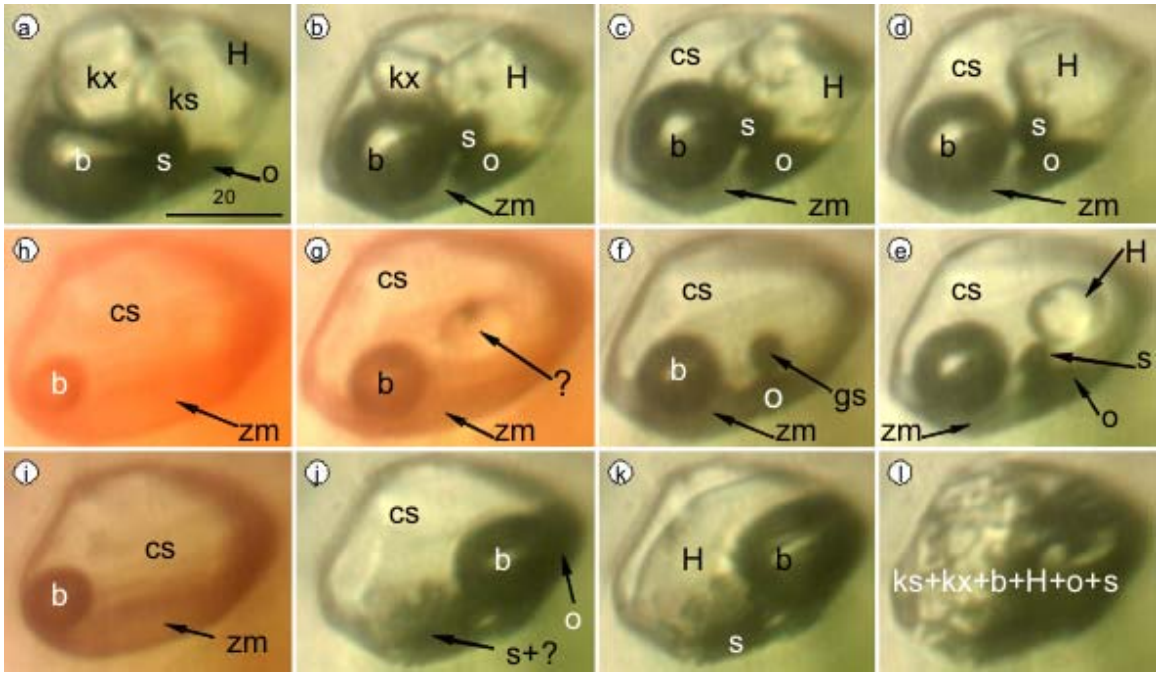

Fig. 166. Hydrosaline melt inclusion microthermometry. Valea Morii porphyry copper Cu-Au-Mo deposit (VM520-1-1). **a.** 25°C, **b.** 284°C, **c.** 377°C, **d.** 523°C, **e.** 650°C, **f.** 863°C, **g.** 1006°C, **h.** 1083°C, **i.** 997°C, **j.** 594°C, **k.** 237°C, **l.** 25°C; Microthermometry: TmH= 652°C, Tmo= 1031°C, Th≥1083°C, P= 1077.71 bar, Ws= 81.5662 wt%NaCl eq,, d= 1.1409, xNaCl= 0.6; Notations: b- bubble, s-sulphide, H-halite, ks-other salt;o-opaque, cs-clathrasil (?), zm- hydrosilicate melt, ?-unknown, scale bar in microns.

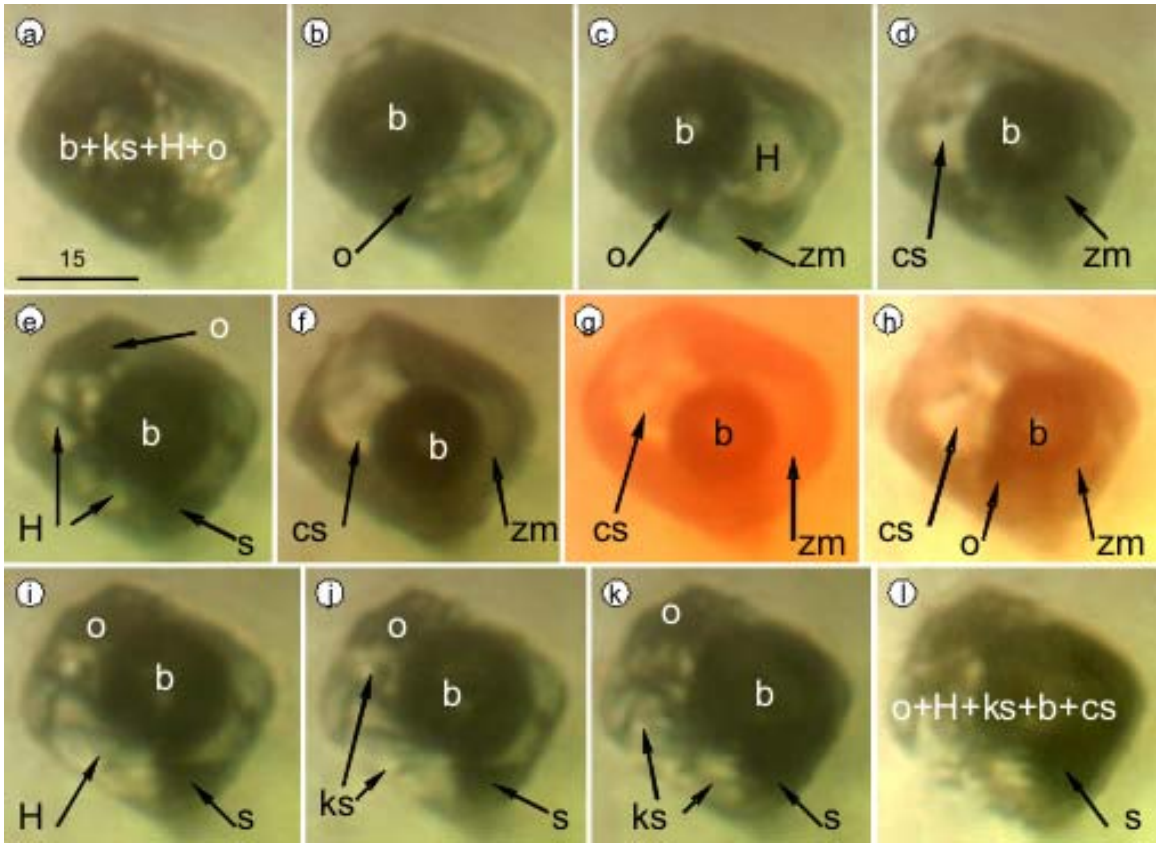

Fig. 167. Hydrosaline melt inclusion microthermometry. Valea Morii porphyry Cu-Au-Mo deposit (VM-520-1-3). **a.** 25°C, **b.** 149°C, **c.** 297°C, **d.** 466°C, **e.** 737°C, **f.** 971°C, **g.** 1060°C, **h.** 880°C, **i.** 443°C, **j.** 216°C, **k.** 150°C, **l.** 106°C, Tm1= 206°-365°C, TmH=662°C, TnH= 456°C, Tnz= 107°C, Th≥1060°C, P=1141.65 bar, Ws=79.7607, d=1.13109, x=0.6,Notations: b-bubble, H-halite, Ks-other salt daughter phases, o-opaque, cs-clathrasil (?), zm-hydrosilicate gel., s-sulphide, scale bar in microns.

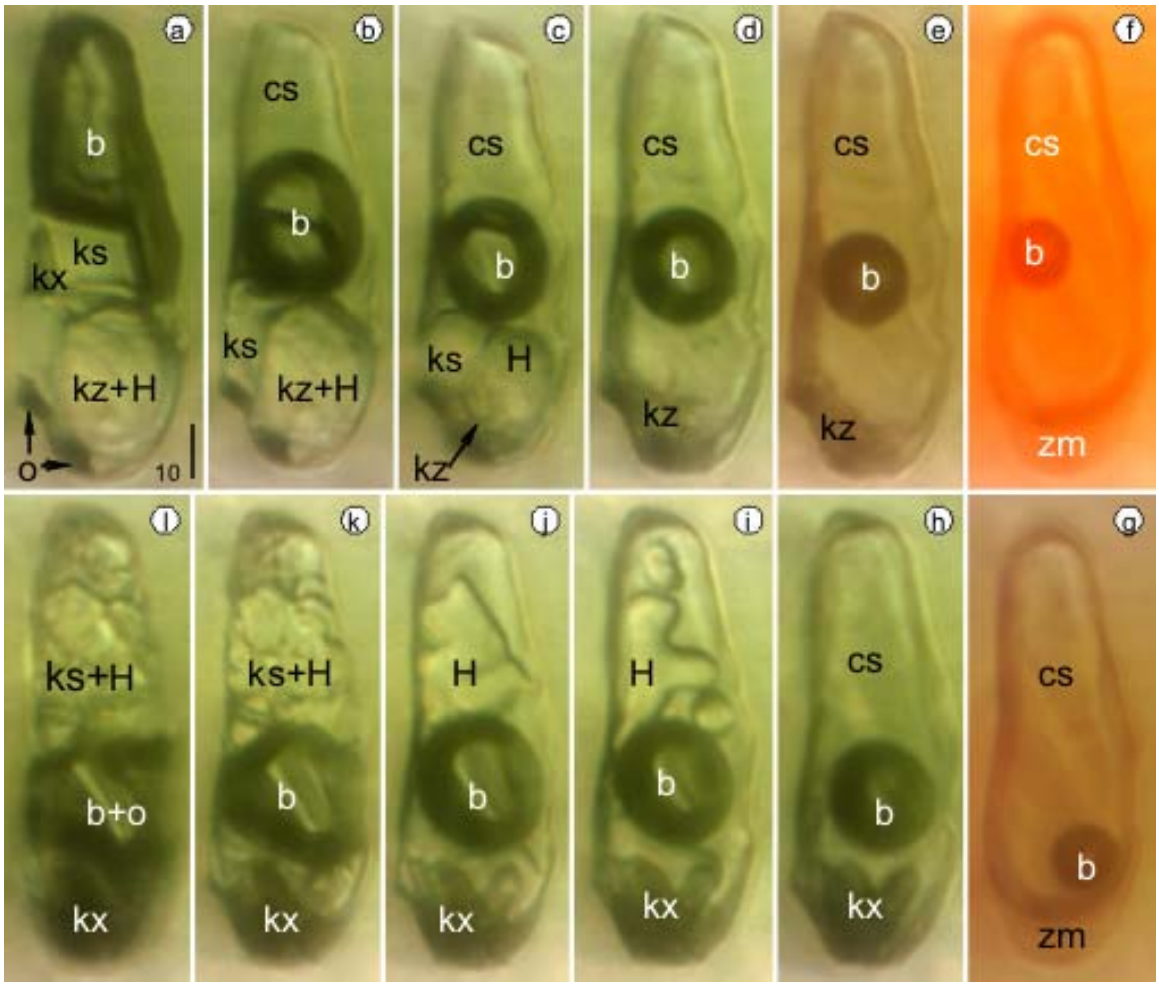

Fig.168. Hydrosaline melt inclusion microthermometry. Valea Morii porphyry Cu-Au-Mo deposit (VM-520-2-1). **a.** 25°C, **b.** 373°C, **c.** 553°C, **d.** 651°C, **e.** 934°C, **f.** 1047°C, **g.** 997°C, **h.** 644°C, **i.** 495°C, **j.** 248°C, **k.** 152°C, **l.** 54°C; Tmks= 366°C, TmH= 624°C, Tmkx= 989°C, Tnh= 526°C, Tmax≥1050°C, P= 1245.21 bar, Ws= 77.6515 wt% NaCl eq., d= 1.11454, xNaCl= 0.52; Notations: H-halite, Kx-anhydrite?, ks-other salt, o-opaque, cs-clathrasil (?), zm-hydrosilicate liquid, b-bubble; scale bar in microns.

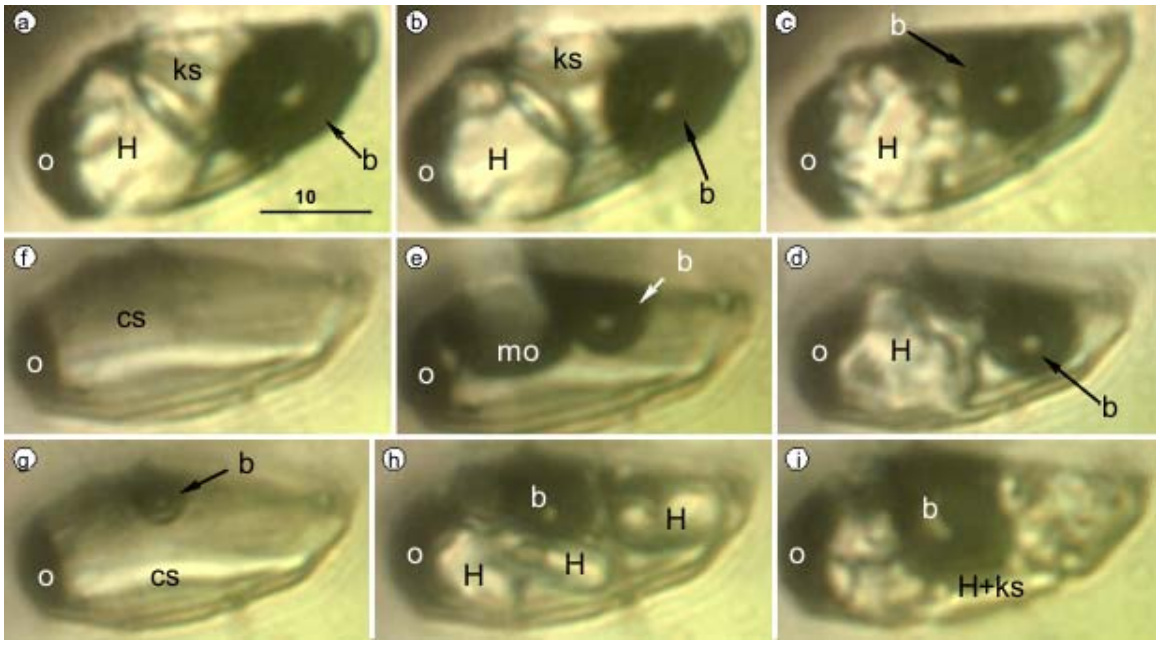

Fig. 169. Hydrosaline melt inclusion microthermometry. Valea Morii porphyry Cu-Au-Mo deposit (VM-520-6). **a.** 25°C, **b.** 131°C, **c.** 278°C, **d.** 354°C, **e.** 502°C, **f.** 567°C, **g.** 629°C, **h.** 430°C, **i.** 25°C; TmH=550°-562°C; Tmo~600°C, Th=618°C, TnV=573°C, TnH=431°C, T=618°C, P= 497.215 bar, Ws= 68.7515 wt% NaCl eq., d= 1.19284, xNaCl=0.41, single phase state; Notations:H-halite, ks- other salt, b- bubble, o-opaque, cs- clathrasil (?) , mo-opaque globulae; scale bar in microns.

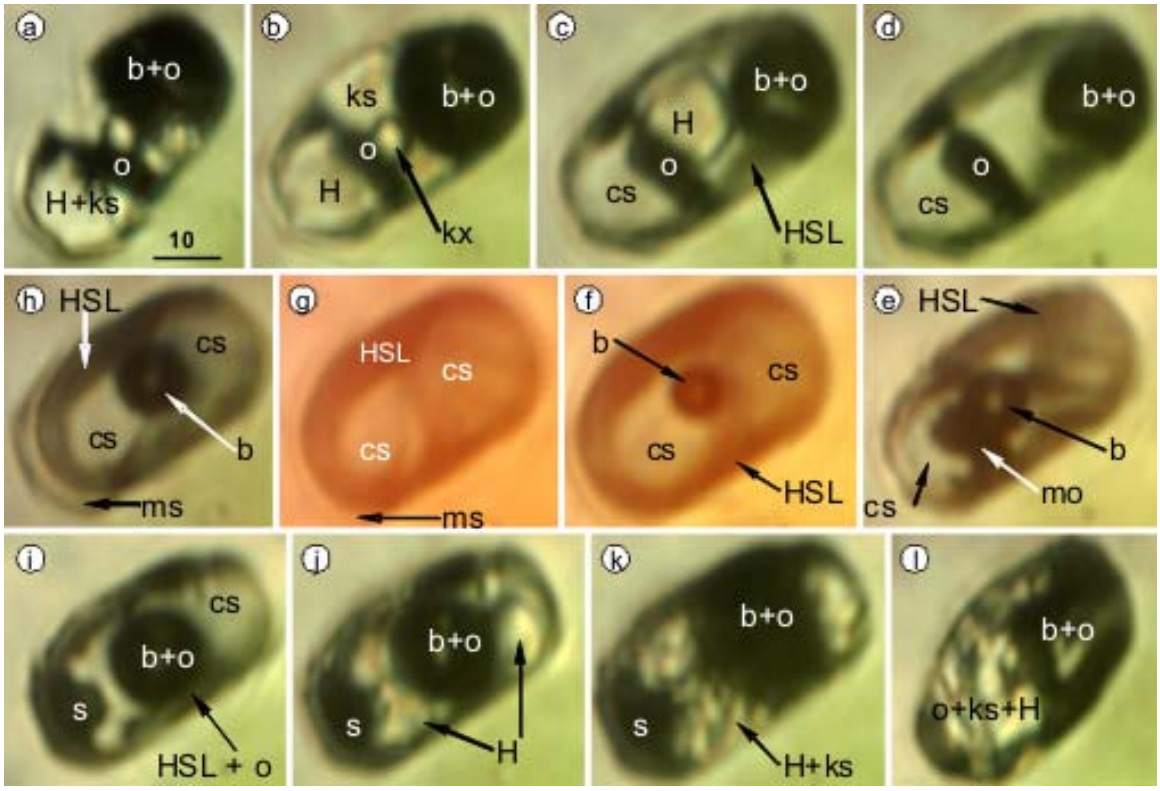

Fig. 170. Hydrosaline melt inclusion microthermometry. Valea Morii porphyry Cu-Au-Mo deposit (VM-520-20-4bis). **a.** 25°C, **b.** 193°C, **c.** 438°C, **d.** 562°C, **e.** 840°C, **f.** 979°C, **g.** 1083°C, **h.** 842°C, **i.** 541°C, **j.** 378°C, **k.** 213°C, **l.** 25°C; TmH=577°C, Tmkx (anhydrite?)= 982°-988°C, Tmo~1050°C,Th=1077°C, P=1790.97 bar, Ws= 70.9187 wt% NaCl eq., d= 1.05572 g/ccm,xNaCl= 0.43, single phase state; Tnb=977°C, Tno=705°-583°C, TnH=402°C, TnKs=100°-95°C; Notations: Tm- melting temperature, Tn-renucleation temperature, b- bubble, o- opaque, H-halite, ks, kx, ky- other salt including anhydrite, s-sulphide (chalcopyrite ?), cs-cathrasil (?), zm-hydrosilicate melt, ms- silicate melt; scale bar in microns; Note: salt melt is floating in zm coated with silicate melt; (zm- hydrosilicate-carbonate-sulphate-chloride-fluoride liquid).

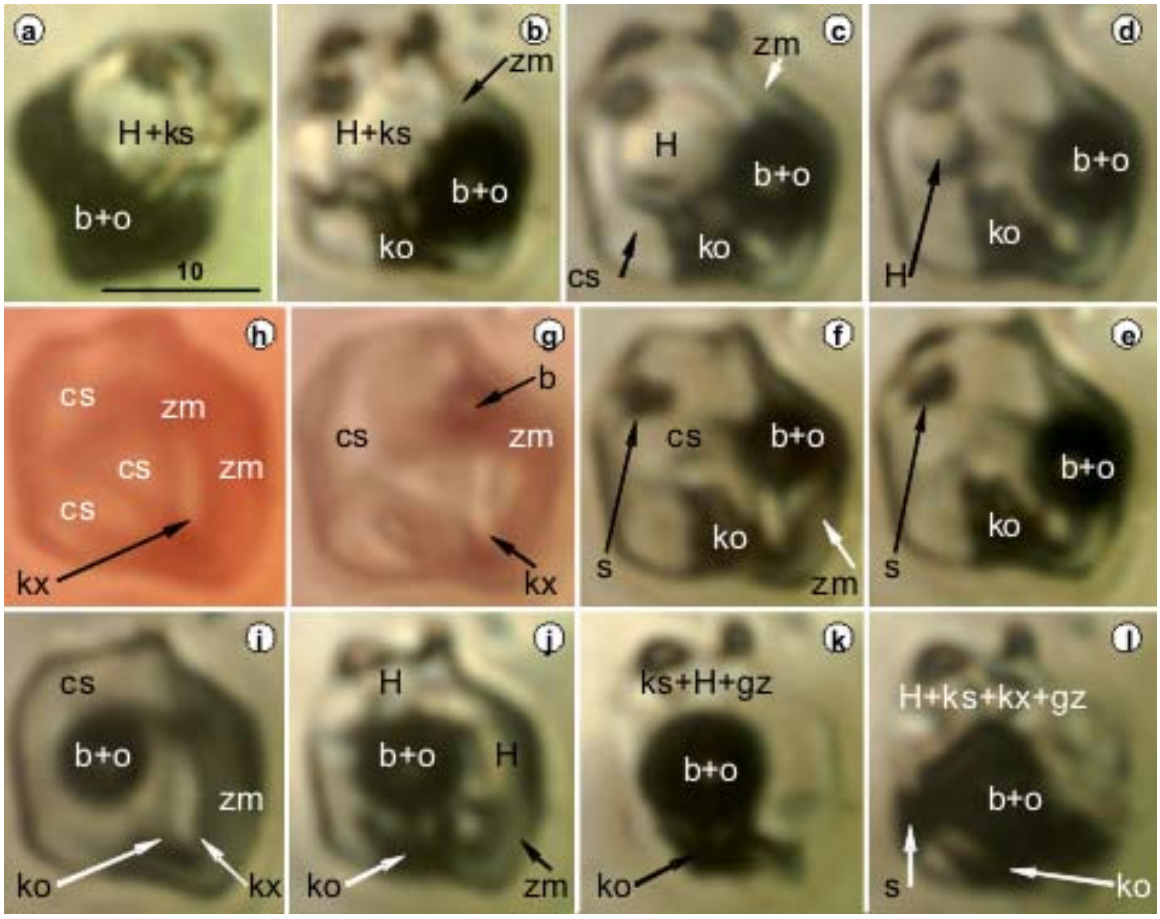

Fig. 171. Hydrosaline melt inclusion microthermometry. Valea Morii porphyry Cu-Au-Mo deposit (VM-520-20-5bis- second cycle). **a.** 25°C, **b.** 220°C, **c.** 344°C, **d.** 531°C, **e.** 616°C, **f.** 813°C, **g.** 1006°C, **h.** 1083°C, **i.** 780°C, **j.** 429°C, **k.** 109°C, **l.** 25°C; Microthermometric data: TmH= 553°C, Tms= 980°C, TnH= 451°C, Th= 1076°C, P= 2002.72 bar, Ws= 67.4519 wt% NaCl eq., d= 1.0255 g/ccm, xNaCl=0.38, Tnb=1039°C, Tmko= 1017°C, Tnko= 690°C; first cycle microthermometric data: Tmks= 207°-248°C, Tmgz= 393°C,Tmkx= 1004°C, Tnks= 109°C; Notations: H-halite, ks-other salt, b-bubble, o-opaque, ko-another opaque, zm- hydrosilicate liquid, cs-clathrasil (?), s- sulphide, kx-anhydrite(?), gz-glassy zm, s-sulphide (chalcopyrite?), scale bar in microns.

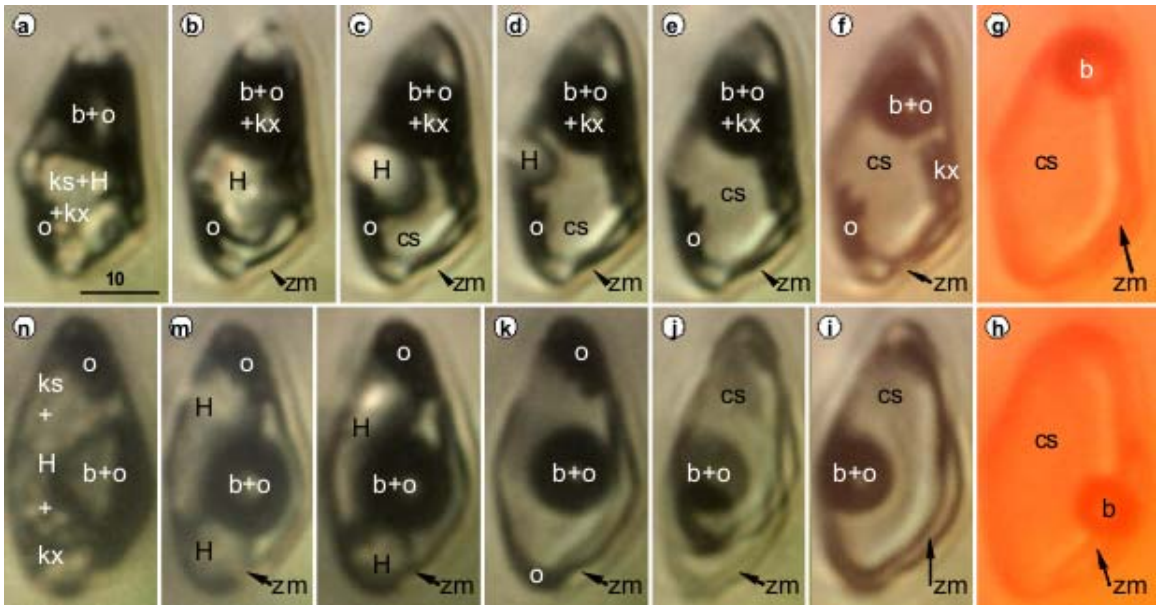

Fig.172. Hydrosaline melt inclusion microthermometry. Valea Morii Cu-Au-Mo deposit (VM-520-26-4). **a.** 25°C, **b.** 289°C, **c.** 565°C, **d.** 604°C, **e.** 613°C, **f.** 871°C, **g.** 1049°C, **h.** 1101°C, **i.** 826°C, **j.** 695°C, **k.** 561°C, **l.** 413°C, **m.** 205°C, **n.** 25°C; Microthermometric data: TmH= 613°C, Tmkx= 1007°C, Tmo= 1001°C, Th≥1001°C, P=1499.67 bar, Ws= 76.0892 wt% NaCl eq., d= 1.09311 g/ccm, xNaCl= 0.5; TnH= 422°C, Tnks=151°C; Notations: b- bubble, o-opaque, H-halite, ks-other salt, kx- anhydrite, cs- clathrasil (?), zm-hydrosilicate melt; scale bar in microns.

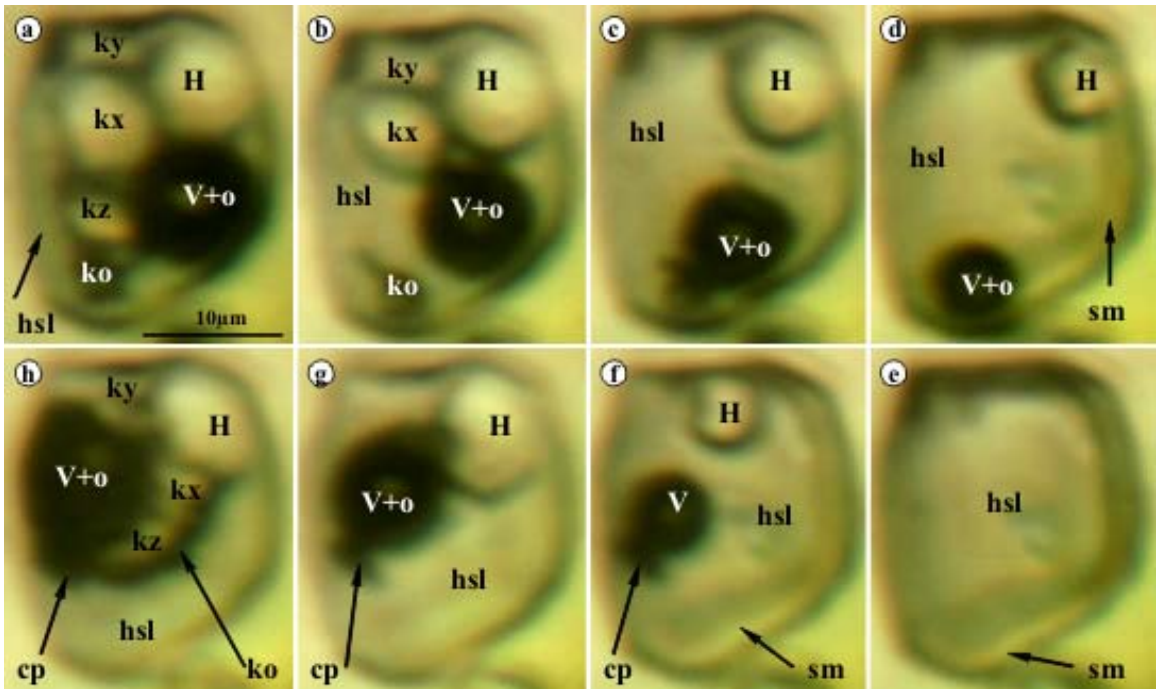

Fig. 173. Hydrosaline melt inclusion microthermometry. Pseudosecondary assemblage. Rovina porphyry Cu-Au deposit. (ROV Ia pseudosecondary) **a.** 27°C, **b.** 135°C, **c.** 200°C, **d.** 312°C, **e.** 424°C, **f.** 309°C, **g.** 129°C, **h.** 60°C; Microthermometric data: Tmkz= 89°C, Tmky= 180°C, Tmkx= 302°C, TmH= 363°C, Th(L)= 416°C, T= 416°C, P= 219, 154 bar, Ws= 43.033 wt% NaCl eq., xNaCl= 0.19, single phase state. Notations: kx, ky, kz, - undetermined salt, H-halite, V-vapor, o, ko-opaque, cp- chalcopyrite, hsl-hydrosaline melt, sm- hydrosilicate melt.

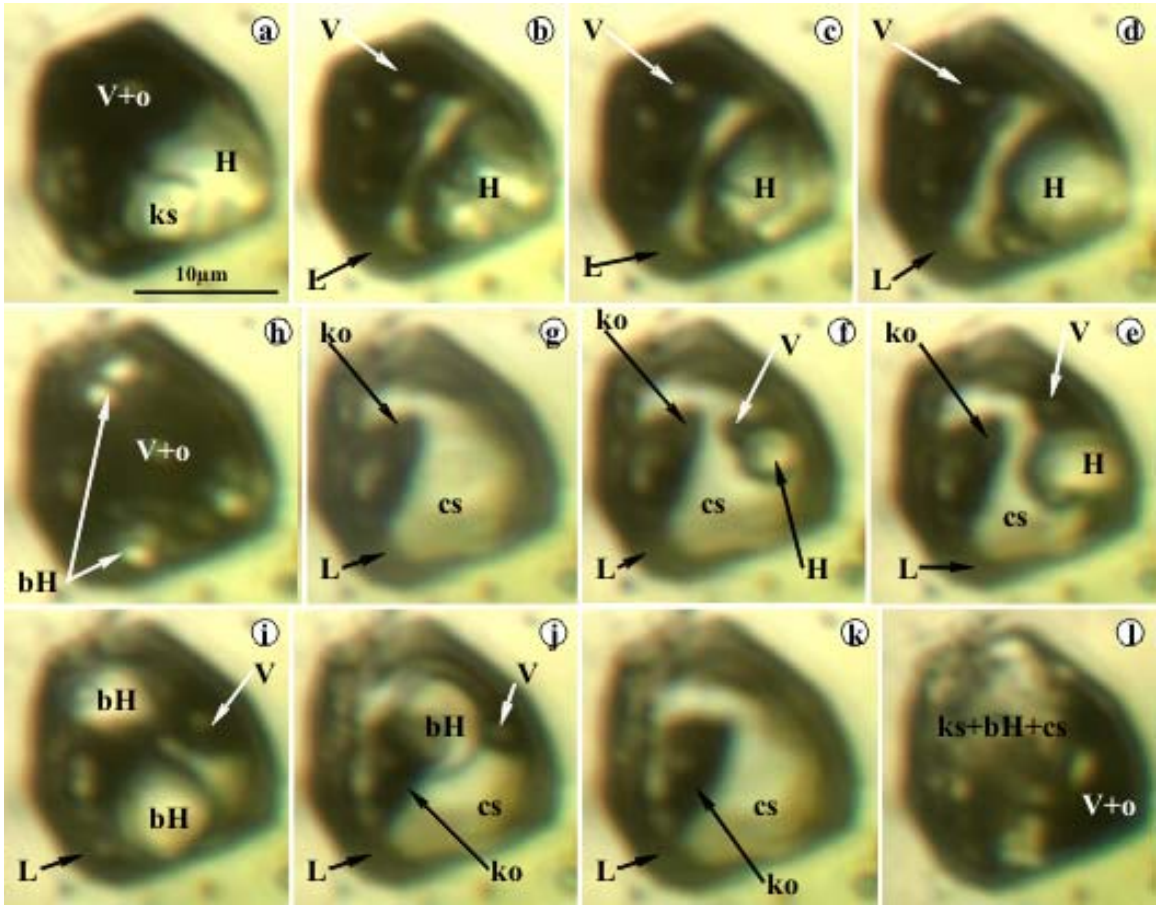

Fig. 174. Hydrosaline melt inclusion microthermometry, double cycled by halite homogenization. Tarnița porphyry Cu-Au. (T-Ta-I-8-1a), Pintea et al., 2020. **a.** 23°C, **b.** 408°C, **c.** 426°C, **d.** 485°C, **e.** 528°C, **f.** 542°C, **g.** 561°C, **h.** 365°C, **i.** 477°C, **j.** 525°C, **k.** 550°C, **l.** 29°C; Microthermometric data- (1 cycle): Th(L+H)= 545°C, Th(L)= 549°C. TnV= 508°C, TnH= 396°C), d= 1.21804 g/ccm, Ws= 66.2987 wt% NaCl eq., - (2cycle): TmbH= 499°C, Th(L+H)= 544°C, Th(L)= 549°C, TnV= 508°C, TnH= 429°C, Tnks= 211°C, Tnko= 371°C; d= 1.21681 g/ccm, Ws= 66.1548wt% NaCl eq., Notations: V- vapor (Fe-rich phase), opaque, ko- another opaque (pyrrothite), H-halite, ks- another salt, bH- bursted halite, cs- clathrasil, L- hydrosaline melt.

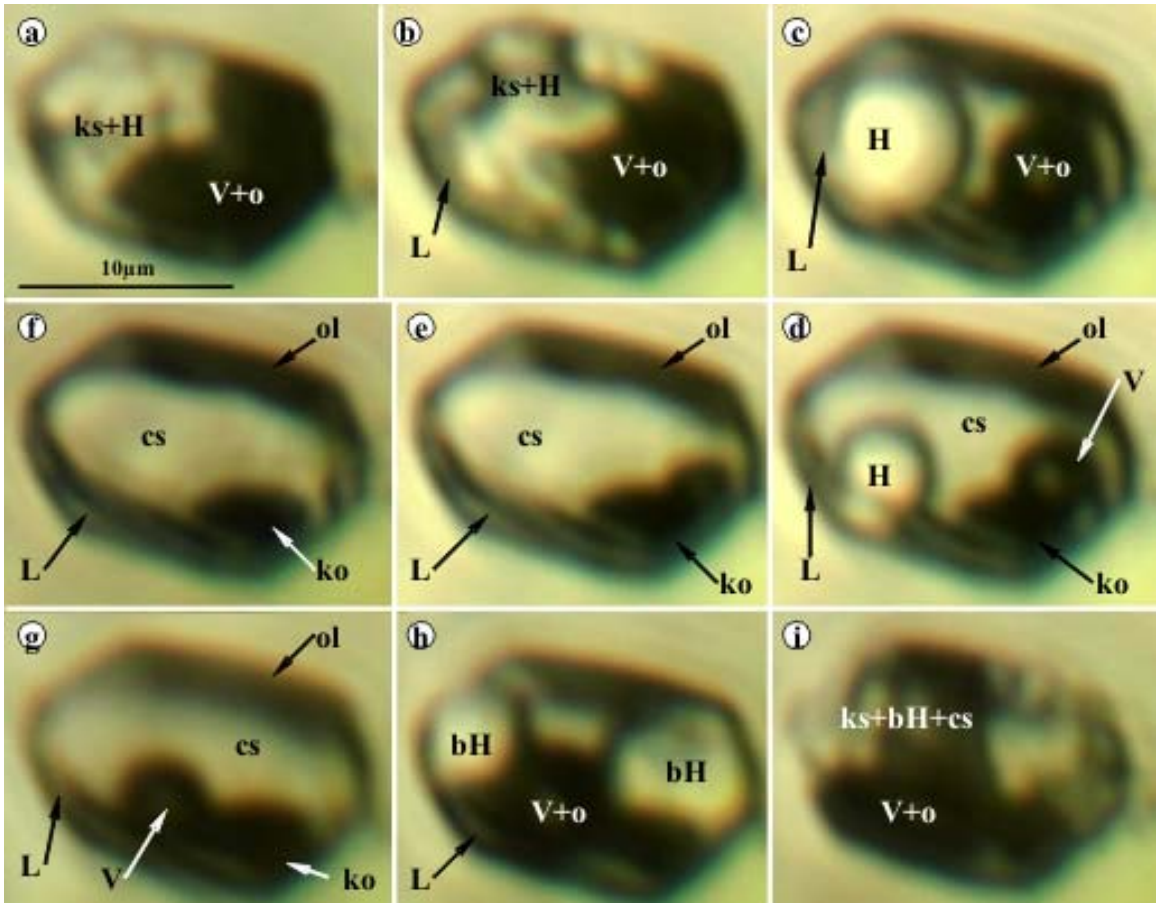

Fig. 175. Hydrosaline melt inclusion microthermometry, double cycled. Tarnița porphyry Cu-Au-Mo deposit.(T-Ta-I-6g). Pintea et al., 2020. **a.** 24°C, **b.** 243°C, **c.** 517°C, **d.** 590°C, **e.** 636°C, **f.** 696°C, **g.** 535°C, **h.** 307°C, **i.** 27°C. Microthermometric data: Tmks= 103°C; 242°C; 286°C, TmH= 611°C, Th(L)= 683°C, TnV= 657°C (**1 cycle**); 612°C (**2 cycle**), TnH 489°C **(2 cycle)**: Tnks= 94°C, T= 683°C (**2 cycle**), P=505.773bar, Ws= 75.8046 wt% NaCl eq., d= 1.24775 g/ccm, xNaCl= 0.5, single phase state. **Notations**: H-halite, ks- anotther salt, V-Fe-rich vapor "melt" phase, o- opaque undiferentiated (oxide, sulfide), cs-clathrasil, L-hydrosaline melt, ko- opaque sulfide, ol- opaque liquid, bH- bursted halite.

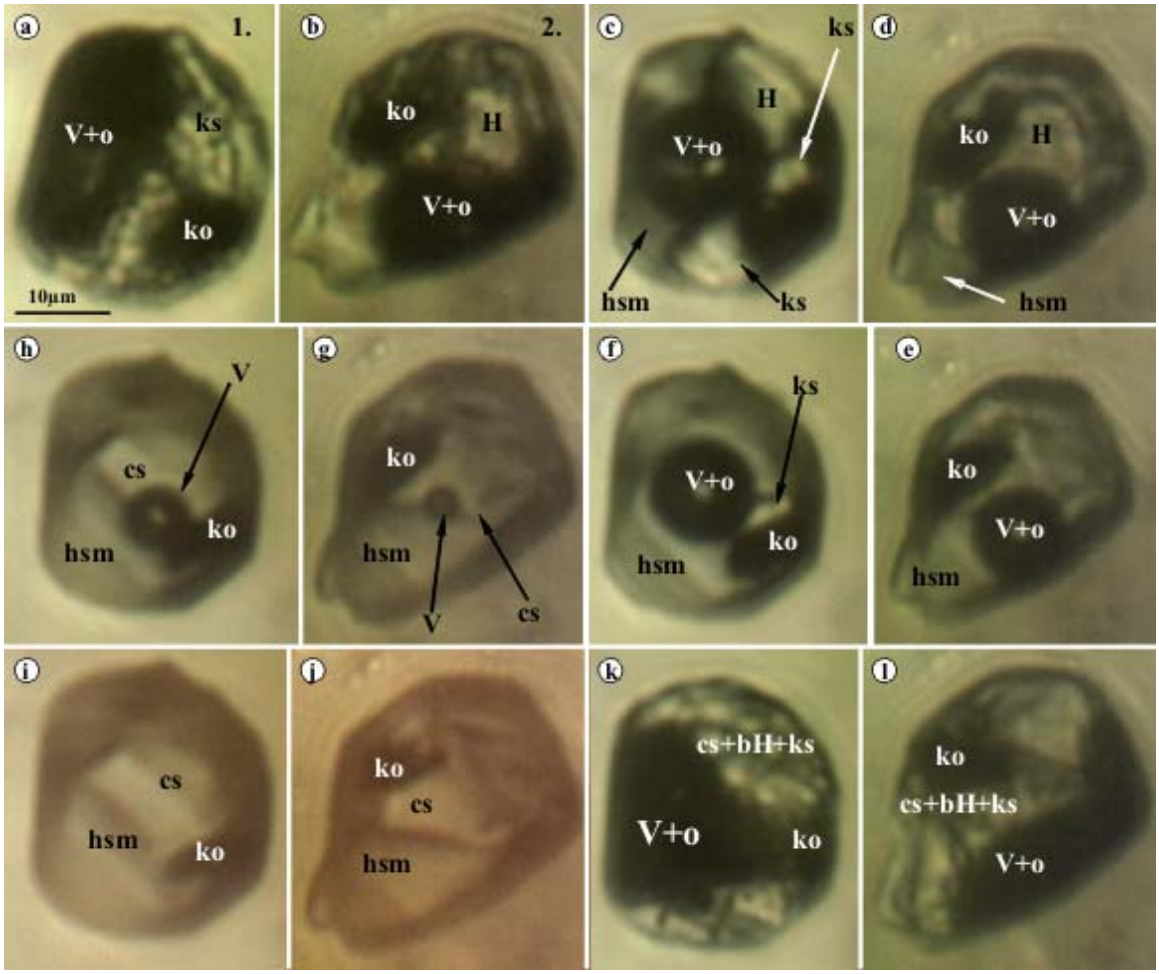

Fig. 176. Two Hydrosaline melt inclusion microthermometry, cycled in tandem.(Rovina porphyry Cu-Au-Mo deposit. (Ro-H4-2c). **a,b**. 23°C, **c,d.** 326°C, **e,f.** 409°C, **g,h.** 857°C, **i,j.** 931°C, **k,l.** 24°C; Microthermometric data: **1.** Tm1= 252°C, Tm2= 489°C, TmH= 599°C, Tms=591°C (anhydrite), Th(L)= 922°C, TnV= 839°C, Tq= 573°C-567°C, TnH= 383°C; P=1329.96bar, Ws= 68.318 wt% NaCl eq., xNaCl= 0.40, d= 1.0513g/ccm, single phase state. **2.** Tm2= 422°C,TmH= 522°C, Tms= 603°C (anhydrite) Th(L)= 866°C, TnV= 779°C, TnH= 471°C; P= 1180.54 bar, Ws= 67.3076 wt% NaCl eq, d= 1.0513 g/ccm, xNaCl= 0.38, V+L state; Notations: V- vapor (Fe-rich phase), o opaque, ko- another opaque, H-halite, bH- bursted halite, ks-another salt (anhydrite and others), hsm- hydrosaline melt, cs-clathrasil.

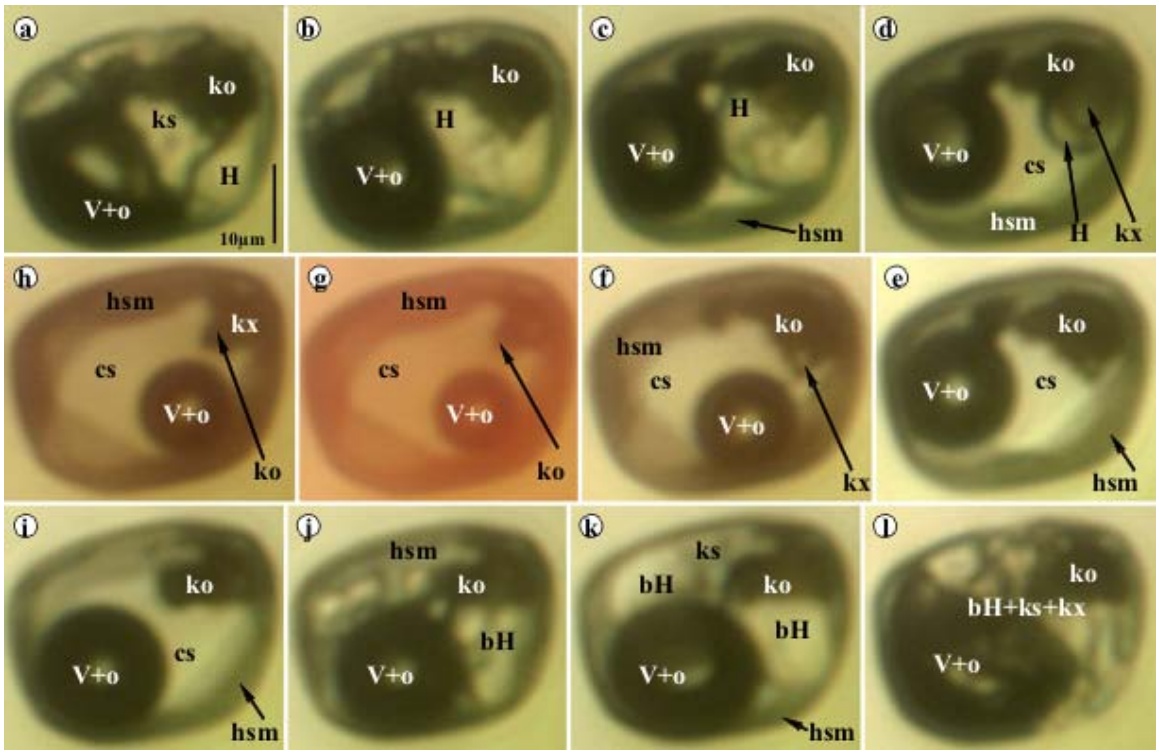

Fig. 177. Homogeneous hydrosaline melt inclusion microthermometry in quartz from Rosia Poieni porphyry Cu-Au-Mo deposit.(RP18new-9f). **a.** 36°C, **b.** 196°C, **c.** 351°C, **d.** 538°C, **e.** 678°C, **f.** 939°C, **g.** 1071°C, **h.** 995°C, **i.** 325°C, **j.** 303°C, **k.** 159°C, **l.** 27°C; Microthermometric data: TmH= 566°C, Th(L) ≥ 1071°C, P= 1869.38 bar, Ws= 69.3295 wt% NaCl eq., d= 1.04274 g/ccm, xNaCl= 0.41, TnbH= 318°C, Tns= 74°C, single phase state; Notations: V-vapor, o- opaque (Fe- rich phase), Ko- another opaque (oxide, sulfide), kx- anhydrite?, H-halite, ks- another salt, hsm- hydrosaline melt, cs- clathrasil, bH- bursted halite.

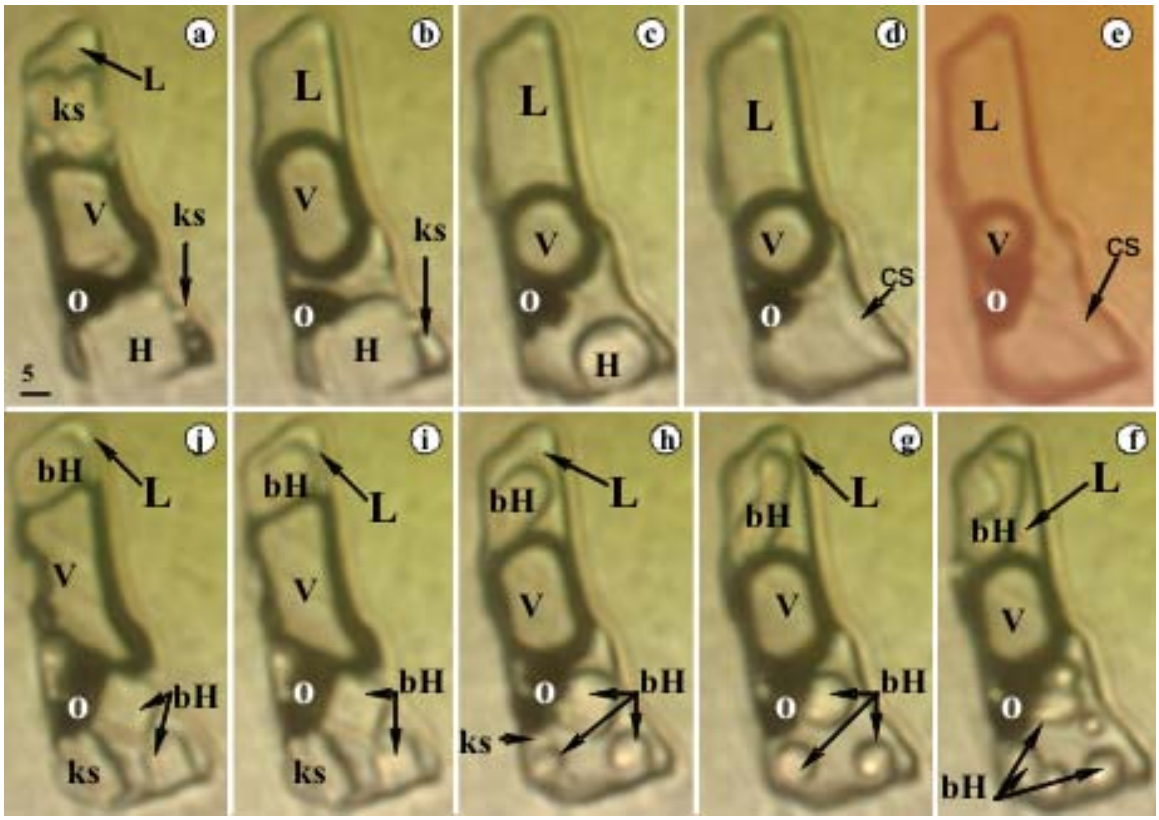

Fig. 178. Hydrosaline melt inclusion microthermometry. Rosia Poieni porphyry Cu-Au-Mo deposit.(RP-18re-3-4). **a.** 25°C, **b.** 172°C, c. 542°C, **d.** 656°C, **e.** 1014°C, **f.** 313°C, **g.** 294°C, **h.** 94°C, **i.** 50°C, **j.** 30°C; Microthermometric data: Tmks=145°C, TmH= 572°C, Th(L)≥ 1014°C, P= 1572.1 bar, Ws= 70.1965 wt% NaCl eq., d= 1.05434 g/ccm, xNaCl= 0.4, (V+L) phase state; Notifications: H-halite, Ks-other salt, o-opaque, V-vapor, bH- bursted halite, L-hydrosaline liquid, cs-clathrasil.

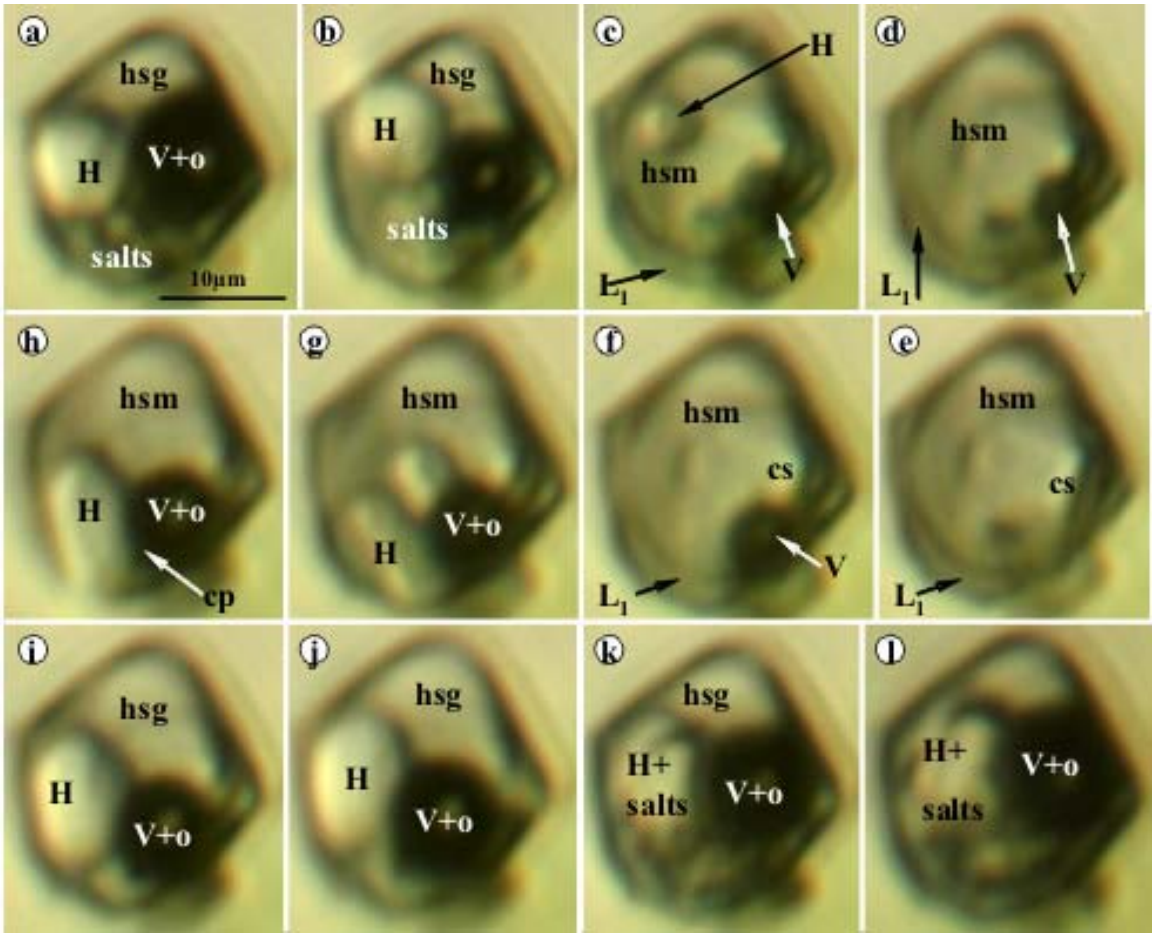

Fig. 179. Hydrosaline melt inclusion microthermometry. Rovina porphyry Cu-Au-Mo deposit. (Rov-Ih pseudosecondary). **a.** 27°C, **b.** 139°C, **c.** 334°C, **d.** 358°C, **e.** 423°C, **f.** 309°C, **g.** 238°C, **h.** 185°C, **i.** 158°C, **j.** 100°C, **k.** 70°C, **l.** 28°C; Microthermometric data: Tm1= 115°C, TmH= 353°C, TH(L)= 401°C, TnV= 322°C, TnH= 253°C, Tnsalt= 78°C, T= 401°C, P= 192.137bar, Ws= 42.2285 wt% NaCl eq., d= 1.03857 g/ccm, xNaCl= 0.18, single phase state. Notations: H-halite, hsg-hydrossilicate (carbonate-sulphate-phosphate) glass?, salts-unidintified salt phases, hsm- hydrosaline melt, V-vapor, o-opaque, cp-chalcopyrite, cs-clathrasil, L1- silicate-(carbonate-sulphate-phosphate) liquid phase.

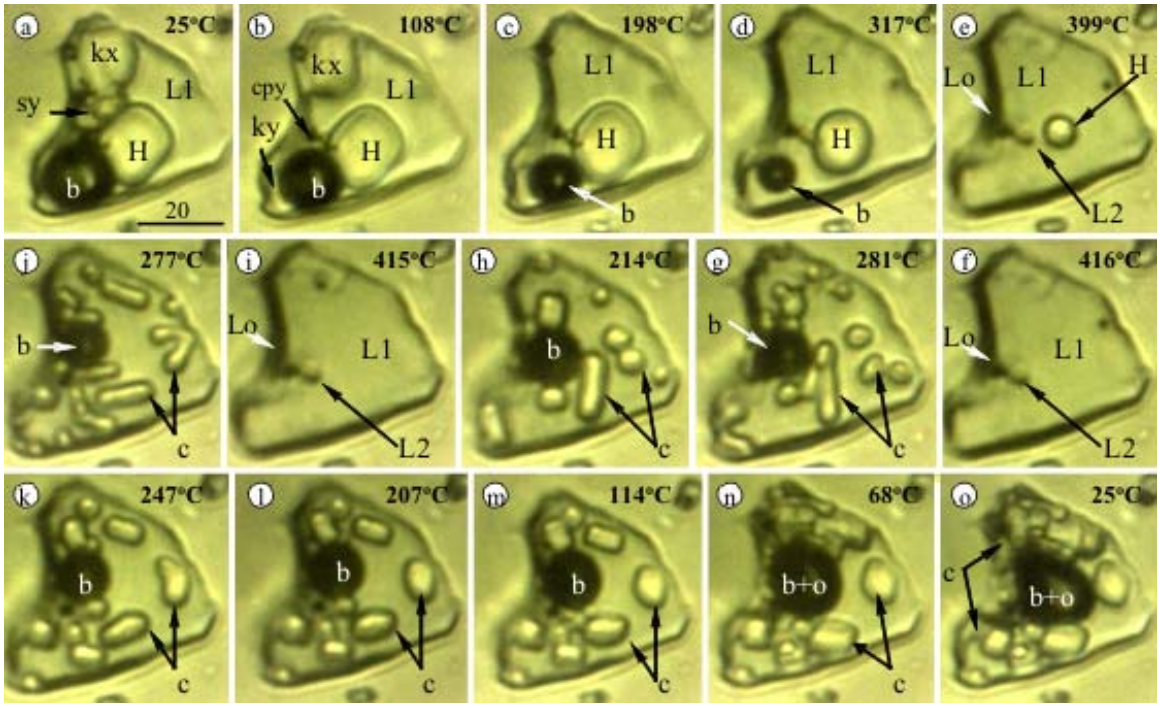

Fig 180. Hydrosaline melt inclusion microthermometry. Rovina porphyry Cu-Au-Mo deposit, double cycled with formation of second liquid salt phase (Ro-H1).Pintea et al., 2021. Microthermometric data: ***Cycle 1***: ThV=375°C;TmH= 410°C,Tn (H+b)= 306°C; ***Cycle 2***: ThV= 377°C, TmH= 406°C, Tm intemediate = 274°C; 324°C; 349°C; 382°C;Tn (H+b)= 303°C, Tnlast= 101°C; 81°C;
Notations: sy-sylvite, kx-second salt unknown, ky-third salt unknown, cpy-chalcopyrite, b-bubble, H-halite, L1- liquid salt, Lo- opaque liquid, o-opaque solid, c- "conglomerate salt"; scale bar in µm.

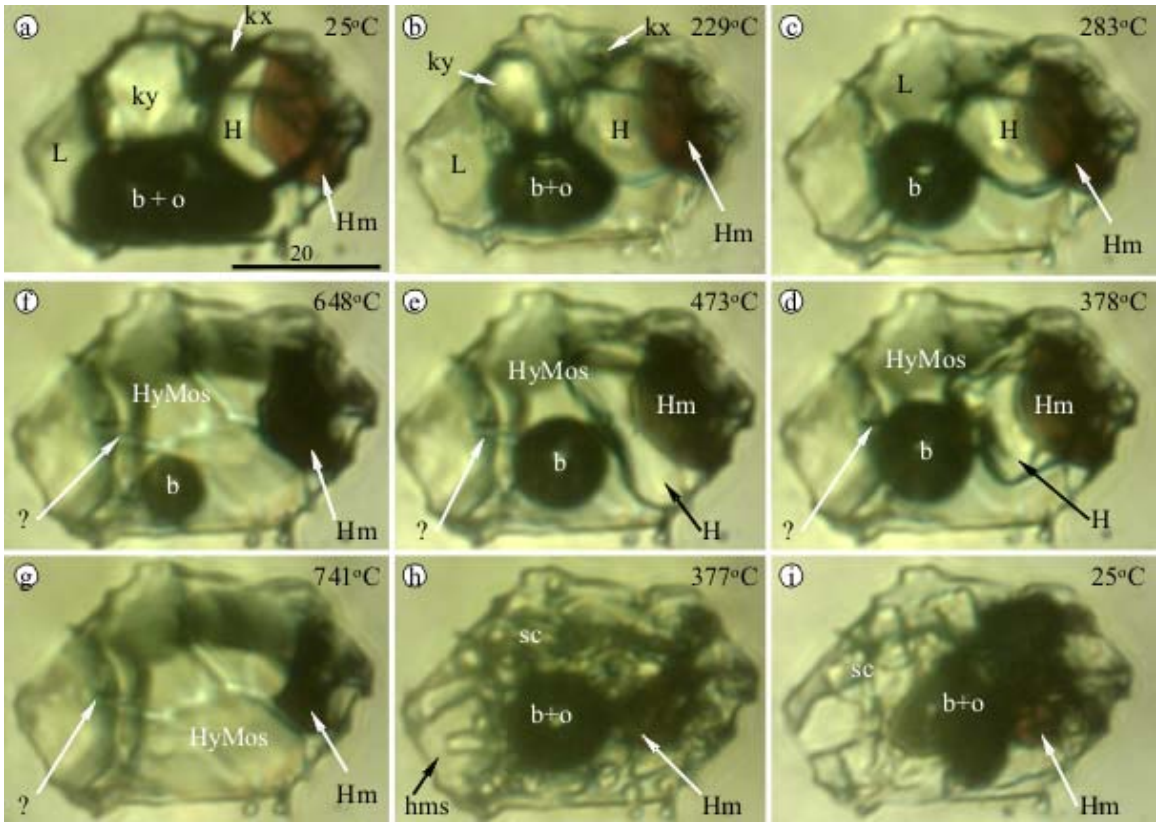

Fig. 181. Hydrosaline melt inclusion microthermometry with specularitic hematite. Rovina porphyry Cu-Au-Mo deposit. (Ro-H8-1); Pintea et al., 2021. TmH= 555°C, Th(L)= 717°C, P= 724.398 bar, Ws= 67.7405 wt% NaCl eq., d= 1.10995 g/ccm, xNaCl= 0.4, single phase state. Notations: L-saline aqueous solution (brine), b-bubble, o- opaque, kx,ky-unknown, H-halite, Hm-hematite, HyMos- hydrous molten salt, sc- "conglomerate"- salt. Scale bar in microns.

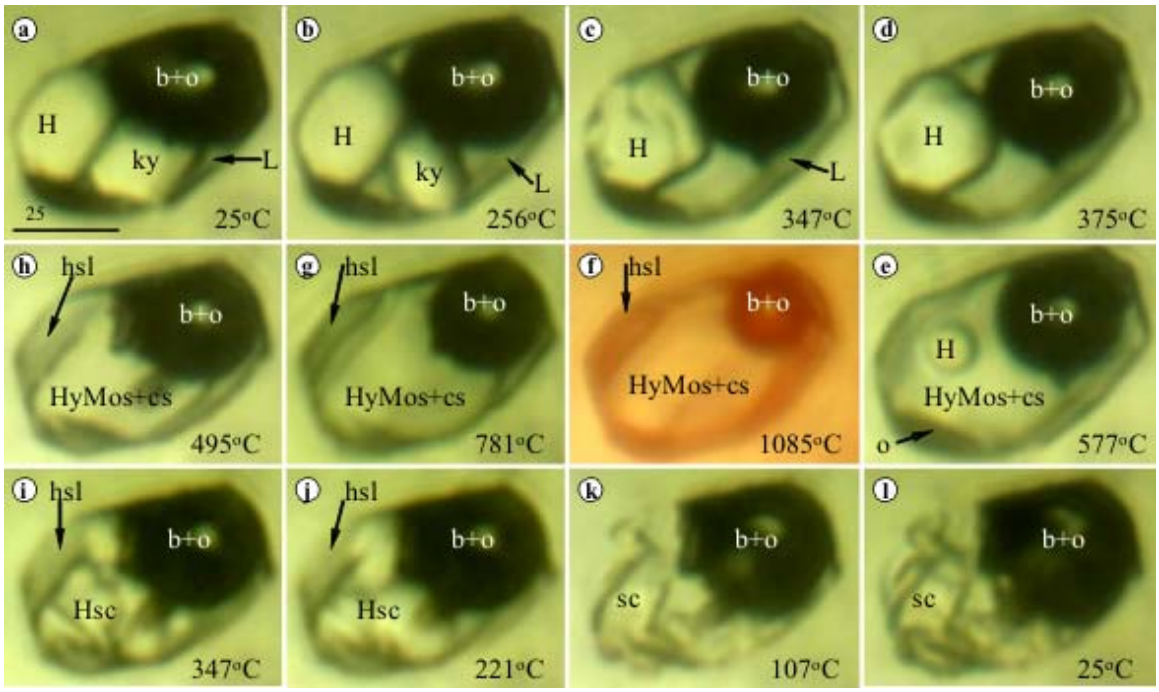

Fig. 182. Hydrosaline melt inclusion microthermometry. Rovina porphyry Cu-Au-Mo deposit (Ro-H19-1), Pintea et al., 2021. Microthermometric data: Tm H= 585°C, Th(L)≥ 1085°C, P= 1743.83 bar, Ws= 72.0732 wt% NaCl eq., d= 1.06448 g/ccm, xNaCl= 0.4, V+L phase state, TnH= 392°C, Tmnew= 966°C (crystalised from around 642°C probably by reaction of mixed salt liquid and opaque Fe- rich phase initially adhering to the wall inclusion, not shown in the pictures), Tn2 (zeolite?)= 105°C. Notations: H- halite, ky- unknown, b- bubble, o- opaque, L- brine, cs┐ clathrasil, HyMos- hydrothermal molten salt, Hsc- conglomerate halite mixed salt, sc- whole salt conglomerate, Tn- renucleation temperature, scale bar in microns.

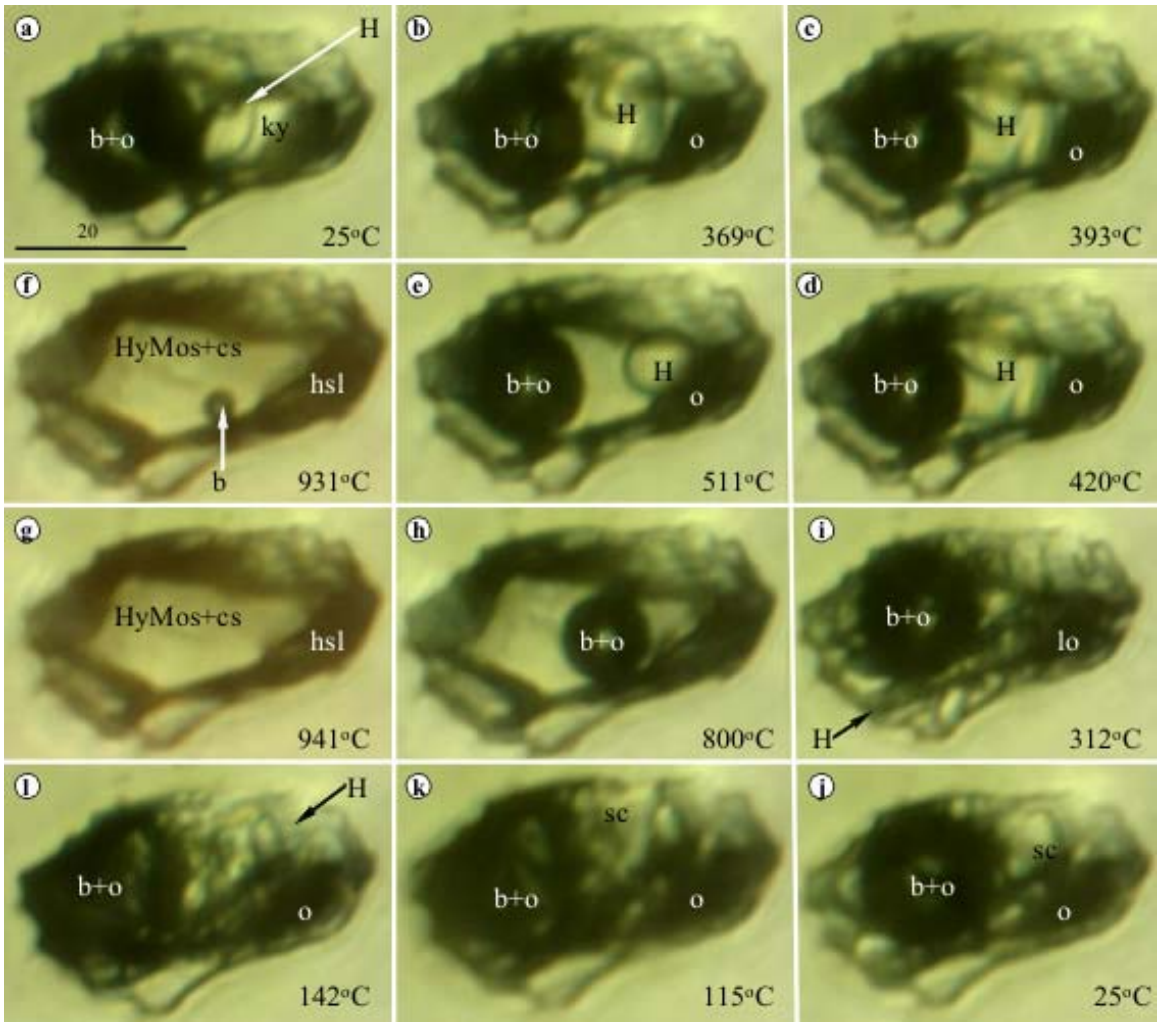

Fig. 183. Hydrosaline melt inclusion microthermometry. Rovina porphyry Cu-Au-Mo. (Ro-H10). Pintea et al., 2021. Halite retrograde solubility in **b-c**. Microthermometric data: TmH=522°C, Th(V)= 936°C, P=1596.84 bar, Ws= 63,0048, d= 0.995068 g/ccm, xNaCl= 0.34, V+L phase state. Notations: H-halite, b-bubble, o-opaque, HyMos-hydrothermal molten salt, hsl-Fe-rich hydrosilicate liquid, cs-clathrasil, cs-conglomerate salt. Scale bar in microns.

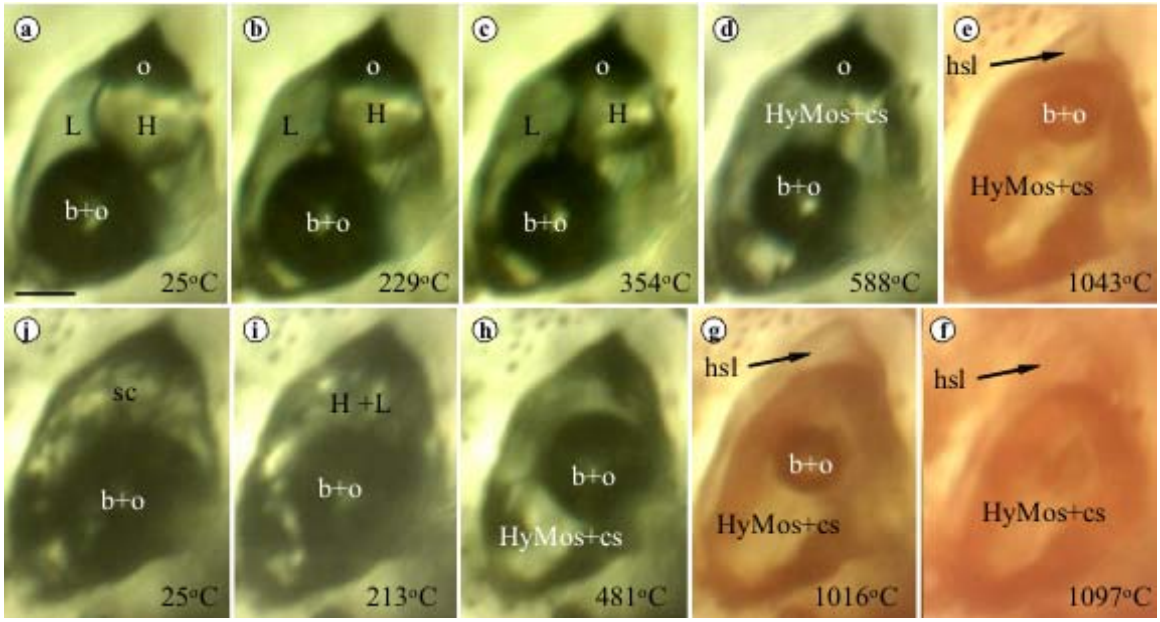

Fig. 184. Hydrosaline melt inclusion microthermometry.Rovina porphyry Cu-Au-Mo deposit. (Ro-H12-1). Pintea et al., 2021. Microthermometric data: TmH= 509°C, Th(V)≥ 1096°C, P= 2298.22 bar, Ws= 61.165 wt% NaCl eq., XNaCl= 0.33, d= 0.954659 g/ccm. Notations: L-aqueous liquid, H-halite conglomerate, b-bubble, o- opaque, hsl- hydrosilicate liquid, HyMos-hydrothermal molten salt, sc- conglomerate salt. Scale bar: 10µm.

Note: Immiscible fluxing fluids penetrates already crystallized quartz microfissures at ≥ 1097°C generating heterogeneous pseudosecondary trail of hydrosaline melt inclusions; ones are single phase others V+L or L+H even V+H sugesting large range of temperatures but they trapped various quantity of the fluid phases; Decreasing P and T are very fast and the differences of trapping condition are very large, apparently. In such cases Roedder, 1992, suggested to take the minimum P-T-X values from such assemblages, for further interpretations.

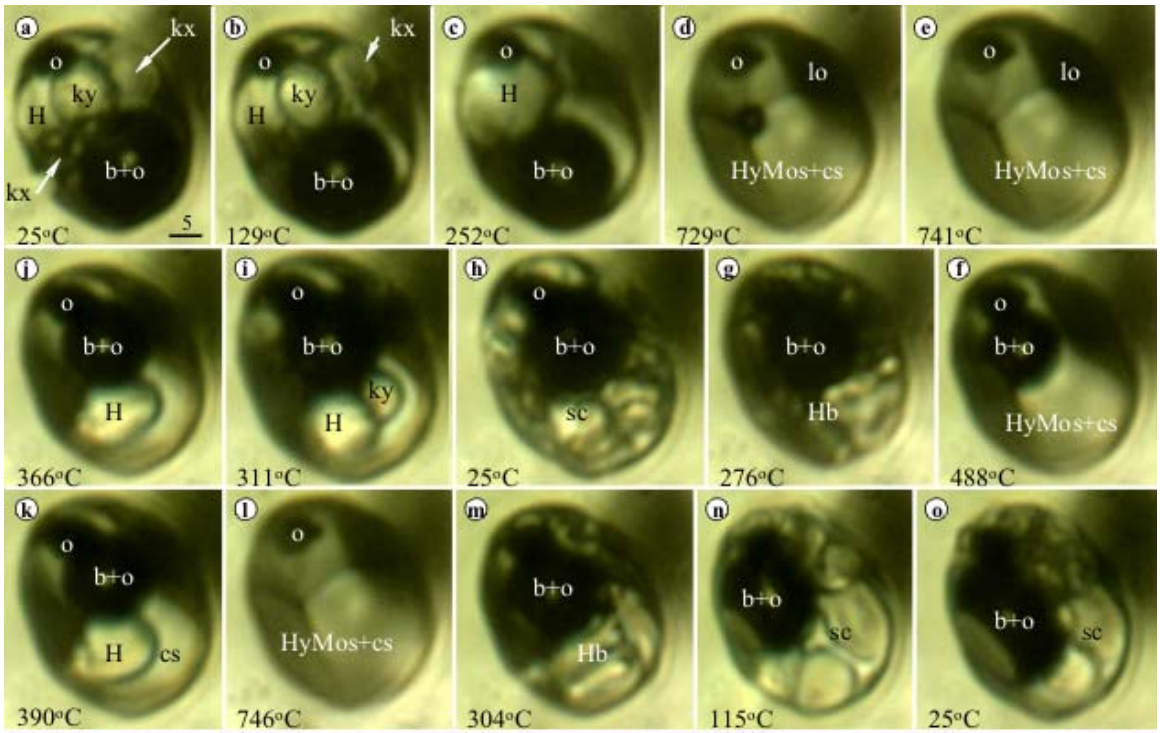

Fig. 185. Hydrosaline melt inclusion microthermometry. Double cycled. Rovina porphyry Cu-Au-Mo deposit. (Ro-H12-3). Pintea et al., 2021. Microthermometric data: **cycle 1**: Tm1= 69°C, 87°C; Th= 572°C (overestimated?), Th(L)= 740°C, TnV= 672°C, TnH= 278°C, Tnkx= 70°C, P= 729.457bar, Ws= 70.1965 wt%, d= 1.13032 g/ccm, xNaCl= 0.4 V+L phase state; **cycle 2**: Tmky= 106°C, Tm bursted halite= 313°C, 348°C, 358°C, 450°C; Th(L)= 741°C, TnV= 673°C, TnH= 314°C, Tnkx= 81°C, T= 741°C, P= 1091.64 bar, Ws= 53.177 wt% NaCl eq., xNaCl= 0.23; V+L phase state.. Notations: (**a-h** cycle **1**; **h-o** cycle **2**), H-halite, Hb-bursted halite conglomerate, b-bubble, o-opaque, lo-liquid opaque, kx-sylvite + unknown, ky-unknown, HyMos-hydrothermal molten salt, cs-clathrasil, sc- salt conglomerate; scale bar in microns.

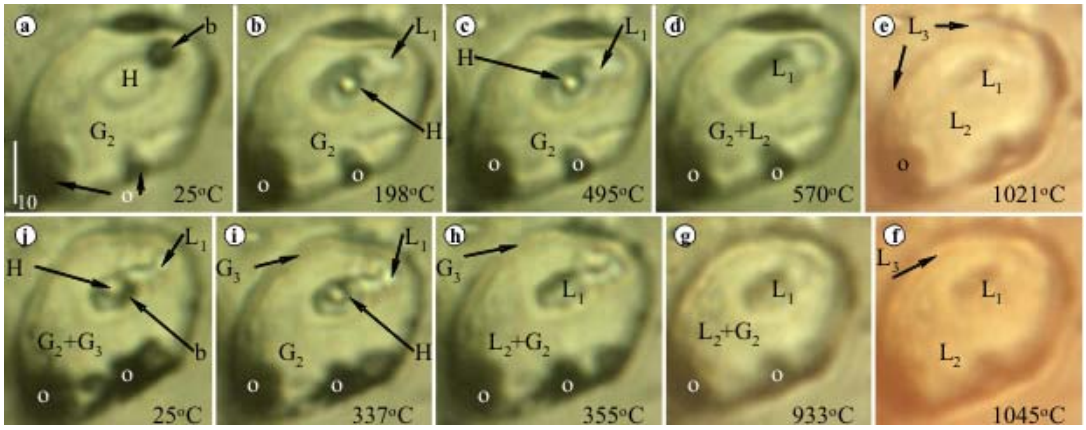

Fig. 186. Complex hydrosilicate (carbonate-sulphate-phosphate) - hydrosaline melt inclusion microthermometry. Rovina porphyry Cu-Au-Mo deposit. Ro-H17-1. Secondary magmatic fluids. Notations: H- halite, G2- sulphate – silicate glass, L1- hydrous salt melt, L2-sulphate- silicate liquid, L3-hydrosilicate liquid, G3- silicate glass, o- opaque (oxide, sulphide)

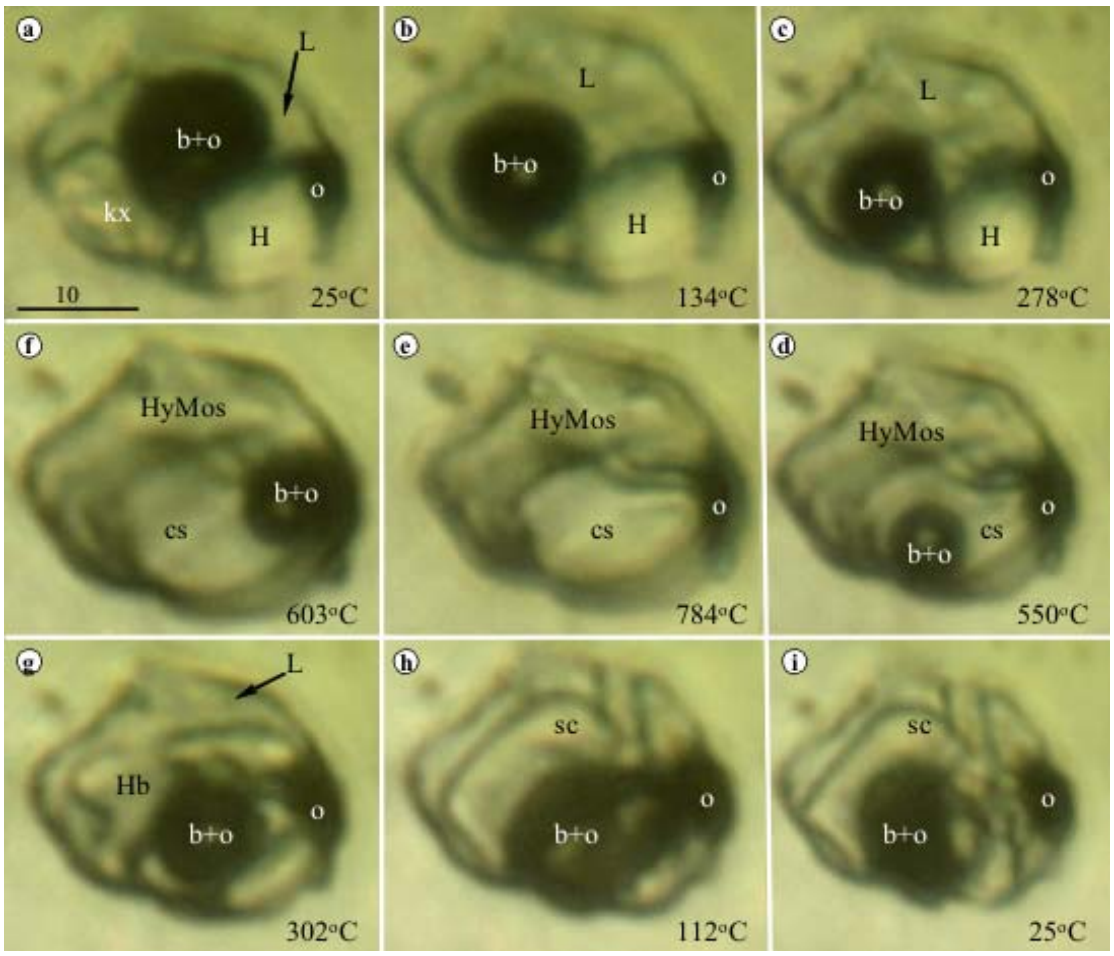

Fig. 187. Hydrosaline melt inclusion microthermometry. Rovina porphyry Cu-Au-Mo deposit. Ro-H18. Microthermometric data: TmH= 511°C, Th(L)= 713°C, P= 834.754 bar, Ws= 61.4467 wt% NaCl eq., d= 1.03153 g/ccm, xNaCl= 0.33, single phase state, TnV= 632°C, TnH= 315°C. Notations: Kx-unknown, H, halite, b-bubble, o-opaque (Fe oxide, sulfide),L-brine, HyMos-transparent hydrothermal molten salt, cs-clathrasil, Hb-bursted halite, sc-conglomerate salt, scale bar in µm.

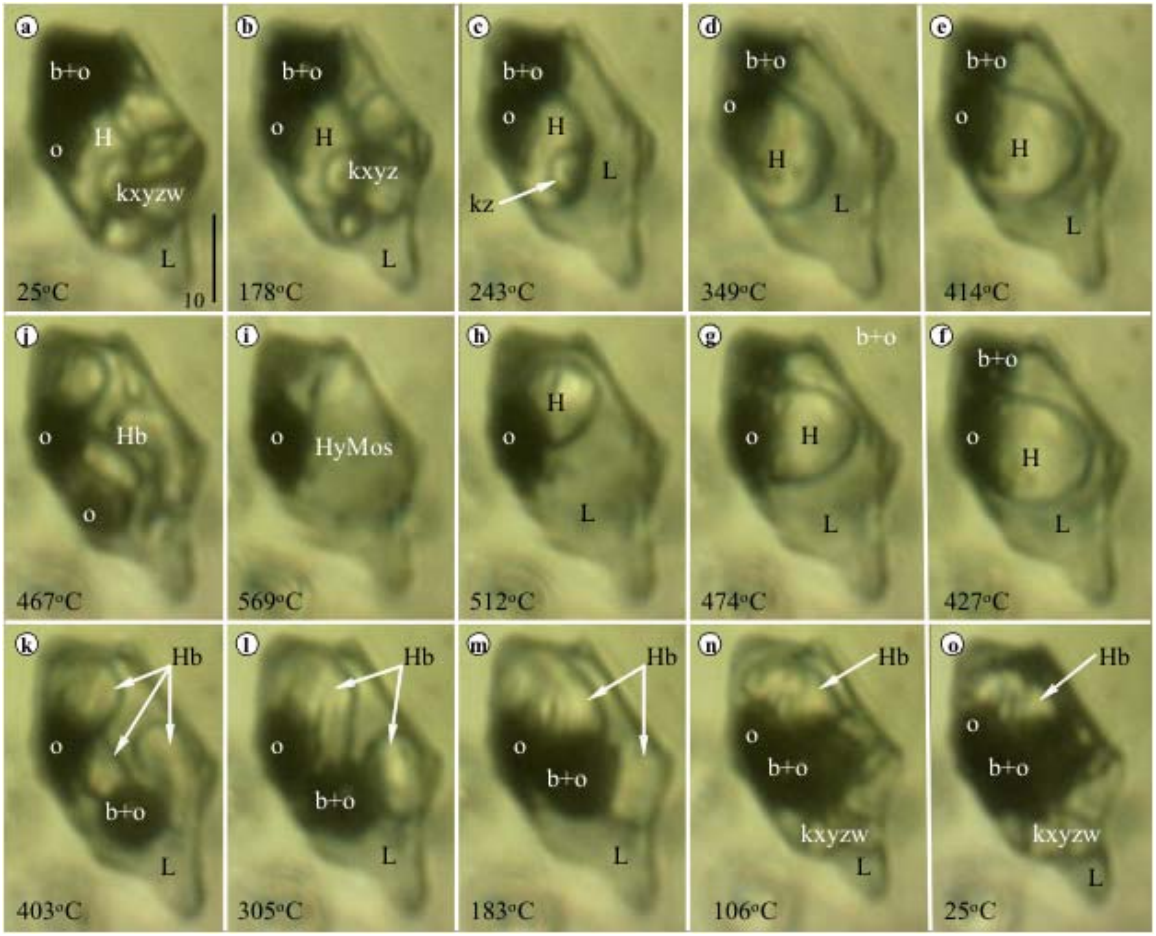

Fig. 188. Hydrosaline melt inclusion microthermometry by halite homogenization. Rovina porphyry Cu-Au-Mo. (Ro-H19-1). Pintea et al., 2021. Microthermometric data: Tm1= 98°C, 112°C; Th(L+H)= 508°C, Th(L)= 566°C, TnH= 452°C, Tn2= 263°C, 108°C; T= 566°C, P= 947,428 bar, Ws= 68.7552 wt% NaCl eq, , XNaCl= 0.41, d= 1.28198 g/ccm,fluid is in the (L+H) state. Notations: H-halite, o-opaque (Fe oxide, sulfide), Kxyzw- sylvite + unknown, L-brine (aqueous molten salt or a hydrosilicate brine liquid or solidified metastable crust), HyMos-hydrothermal molten salt, Hb- bursted halite, scale bar in µm.

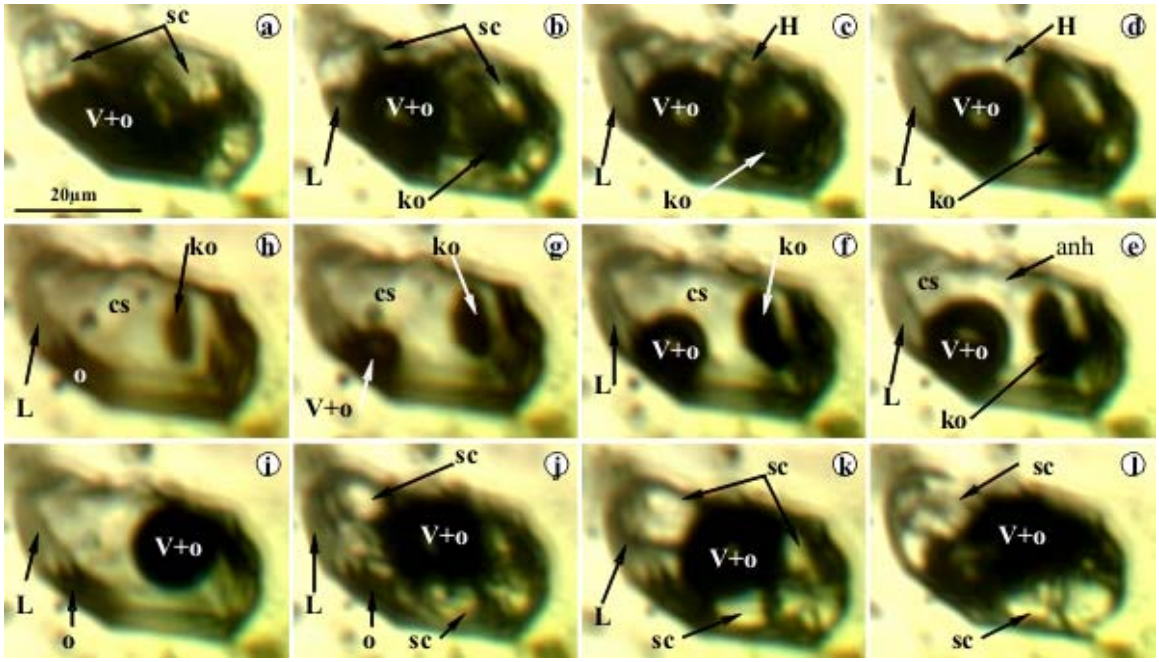

Fig. 189. Replicated (after one year) hydrosaline melt inclusion microthermometry from Rosia Poieni porphyry Cu-Au-Mo deposit.(RP18-rep). **a.** 25°C, **b.** 420°C, **c.** 560°C, **d.** 755°C, **e.** 932°C, **f.** 969°C, **g.** 861°C, **h.** 567°C, **i.** 567°C, **j**. 218°C, **k.** 118°C, **l.** 25°C; Microthermometric data: Tm (sc)= 126°C, 312°C, 370°C, 446°C, Tm last H= 580°C, Tm anh?= 836°C, Th(L)= 965°C, TnV= 926°C, TnH= 369°C, Tn (sc)= 234°C, 161°C, 83°C; T= 965°C, P= 1339.56 bar, Ws= 71.3519 wt% NaCl eq., xNaCl=0.42, (V+L) state. Notations: v-vapor-o-opaque (oxide, sulfide), bH- bursted halite, L-hydrosaline melt, H- last halite grain, sc- salt conglomerate, cs- clathrasil, lo- liquid opaque.

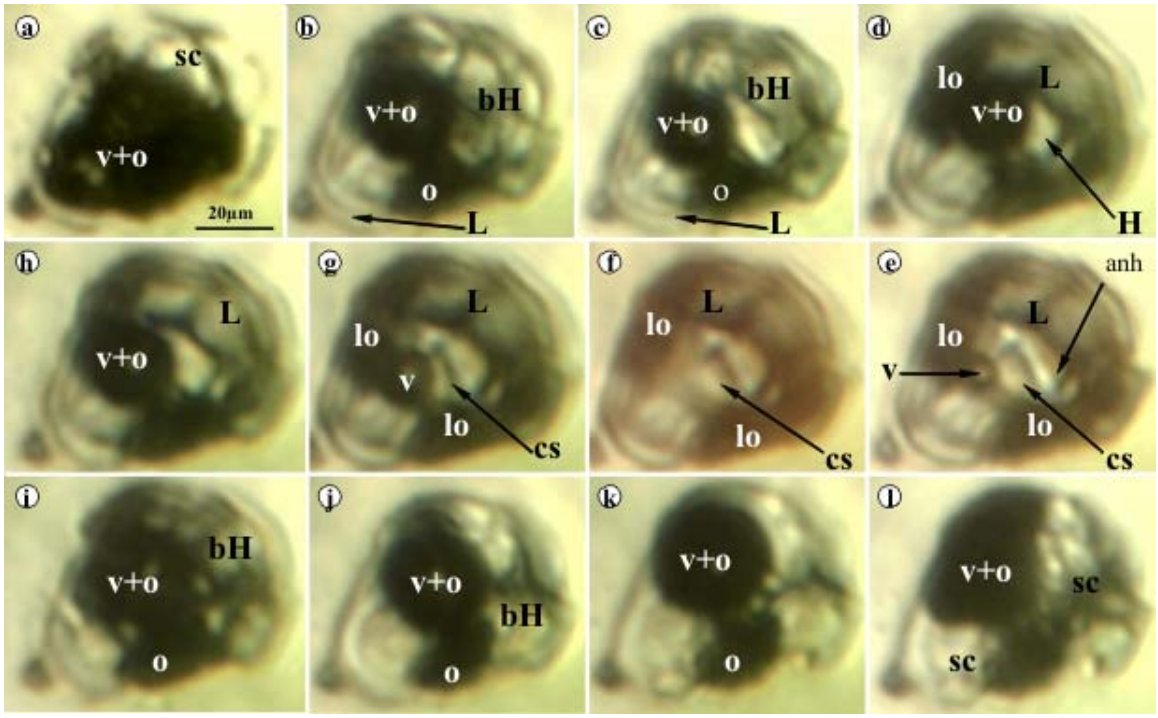

Fig. 190. Complex hydrosilicate – chloride – sulphate – phosphate – fluoride - bromide inclusion from Tarnita porphyry Cu-Au-Mo deposit. (T-Ta-T-8). Pintea et al., 2020. Microthermometric data: Tmsalt=313°C, 391°C, 443°C; TmH=592°C, Tm anh(?)= 711°C, Th(L)= 1078°C, TnbH=379°C, Tnsalt(zeolite-?)= 138°C; T= 1078°C; P=1639.51 bar; Ws= 73.0815 wt%NaCl eq; d= 1.0726 g/ccm, xNaCl= 0.45, (V+L) phase state inside hydrosaline melt. Notations: V- vapor, o- opaque, hsm- hydrosaline melt, hsl- hydrosilicate liquid, sc- conglomerate salt, G- silicate glass, CL- chloride melt.

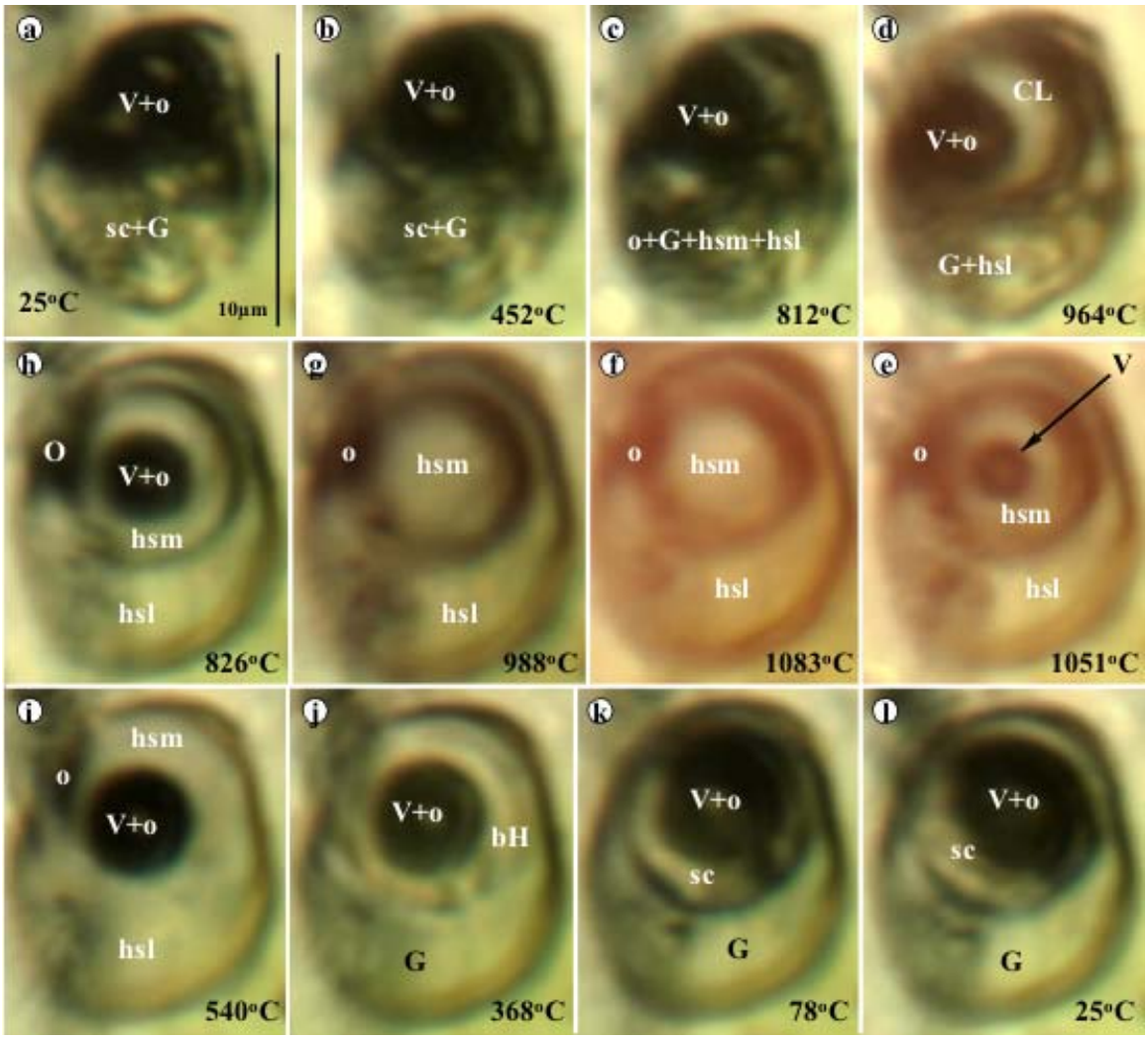

Fig. 191. Complex hydrosilicate – chloride – sulphate – phosphate – fluoride - bromide inclusion from Tarnita porphyry Cu-Au-Mo deposit. (T-Ta-T-8). Pintea et al., 2020. Microthermometric data: Tmsalt=313°C, 391°C, 443°C; TmH=592°C, Tm anh(?)= 711°C, Th(L)= 1078°C, TnbH=379°C, Tnsalt(zeolite-?)= 138°C; T= 1078°C; P=1639.51 bar; Ws= 73.0815 wt%NaCl eq; d= 1.0726 g/ccm, xNaCl= 0.45, (V+L) phase state inside hydrosaline melt. Notations: V- vapor, o- opaque, hsm- hydrosaline melt, hsl- hydrosilicate liquid, sc- conglomerate salt, G- silicate glass, CL- chloride melt.

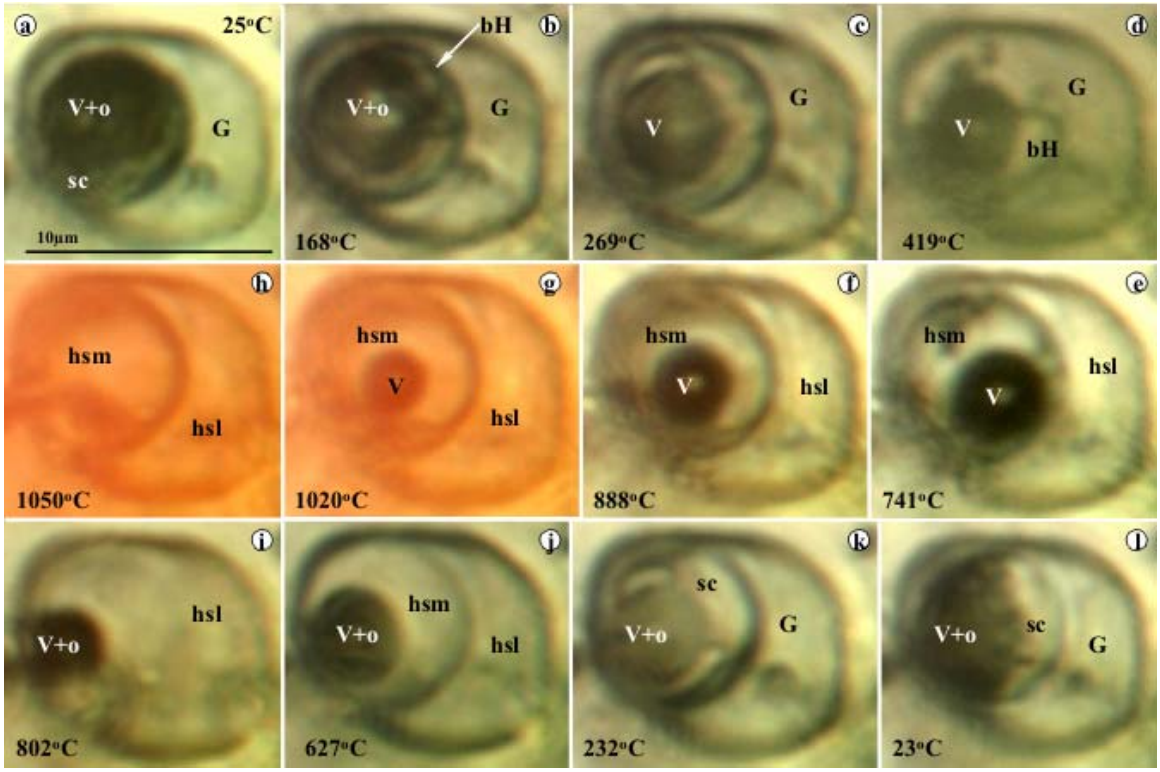

Fig. 192. The same complex hydrosilicate-salts inclusion from **Fig. 191**, replicated microthermometry after one year.(T-Ta-I-8, third cycle), Pintea et al., 2020. Microthermometric data: Tmsalt= 229°C; 348°C; 478°C, TmbH=558°C; Tmglass (start)= 343°C,Tmo= 829°C, Th(L)= 1045°C, Tnmenisc= 642°C, TnbH= 407°C, Tnsalt= 330°C, 302°C; T= 1045°C, P= 1819°C, Ws= 68.1737 wt% NaCl eq., d= 10339 g/ccm, xNaCl=0.39, (V+L) – phase state. Notations: V-vapor, o-opaque, bH- bursted halite, sc- salt conglomerate, G-glass, hsl- hydrosilicate liquid, hsm- hydrosaline melt.

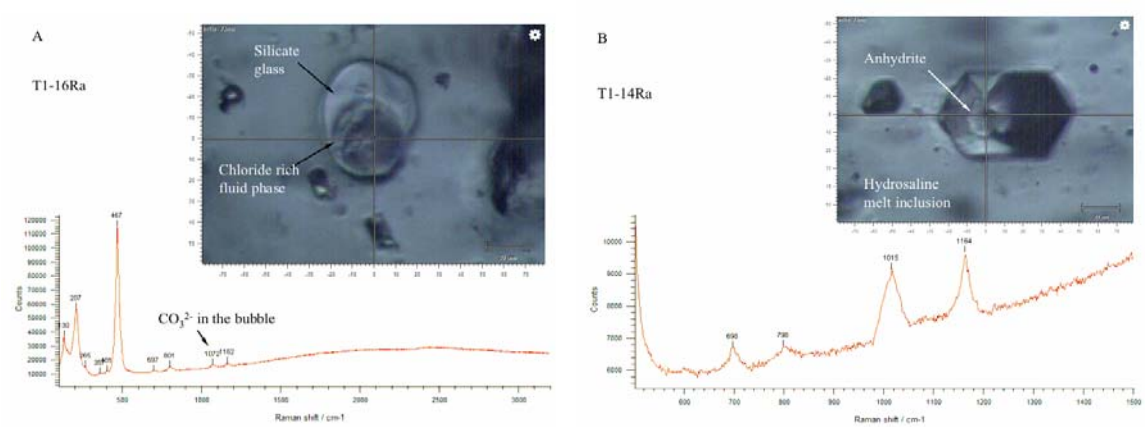

Fig. 193. Raman spectra of the same (left) complex silicate-hydrosaline melt inclusion pictured in **Fig. 191** and **Fig. 192** showing the presence of carbonate ion in the bubble of the salt melt phase surrounded by silicate glass (**A**) and anhydrite daughter phase (**B**) formed in hydrosaline melt inclusion (without liquid phase at room temperature) from the same quartz sample. Pintea et al., 2020.

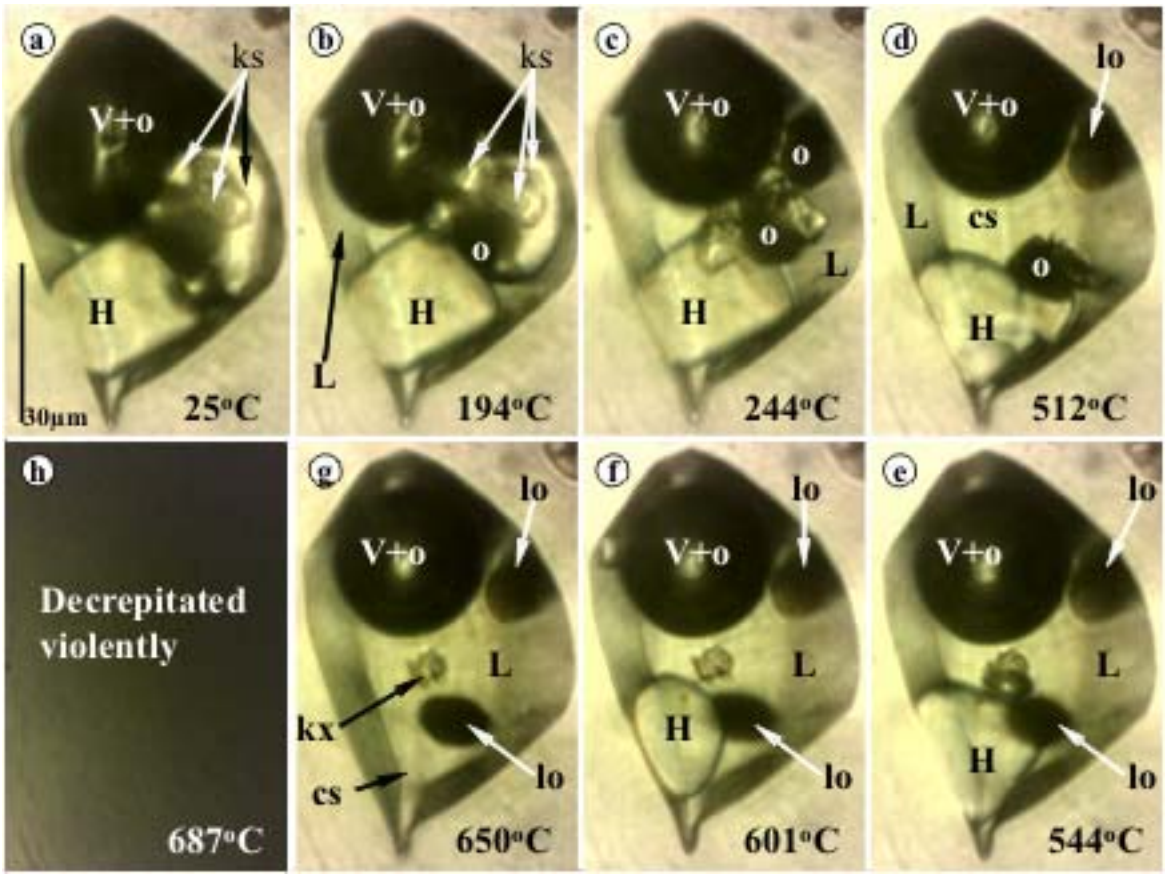

Fig.194. Hydrosaline melt inclusion microthermometry in quartz from Roşia Poieni porphyry Cu-Au-Mo deposit, decrepitated before final homogenization. (RPnew18-re3-4). Microthermometric data: TmKs=242°C, 253°C, 315°C; TmH= 638°C, Td=687°C, Th≥ 687°C, T≥ 687°C, P= 441.112 bar, Ws=79.6209 wt% NaCl eq., d= 1.30426 g/ccm; xNaCl= 0.56, Single phase state. Notations: V- vapor, o-opaque, H-halite, ks-other salts, L-hydrosaline melt, lo- liquid opaque , Kx-unknown, cs-clathrasil, Td-decrepitation temperature.

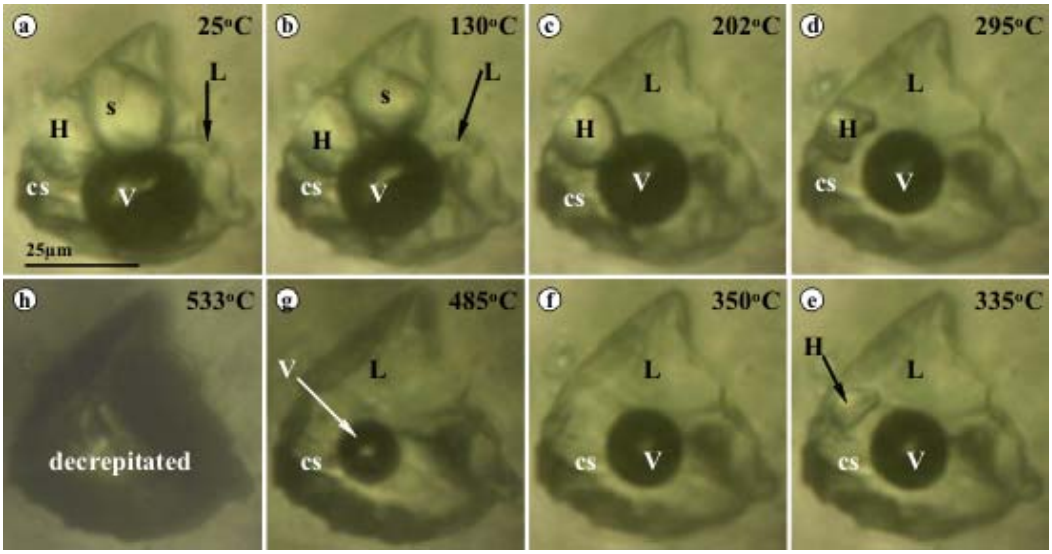

Fig.195. Hydrosaline melt inclusion microthermometry in quartz from Moldova Nouă porphyry Cu-Mo-(Au) deposit (Banat, Upper Cretaceous), decrepitated before final homogenization. (11W-1a-6a). Microthermometric data: Tms= 198°C,TmH= 349°C, Td=530°C, Th(L) ≥ 530°C; T≥530°C, P=548.786 bar, Ws= 41.8509 wt% NaCl eq., d= 0.910066 g/ccm, xNaCl= 0.18; Notations: H-halite, s- salt, L- hydrosaline melt, cs-clathrasil, Td- decrepitation temperature.

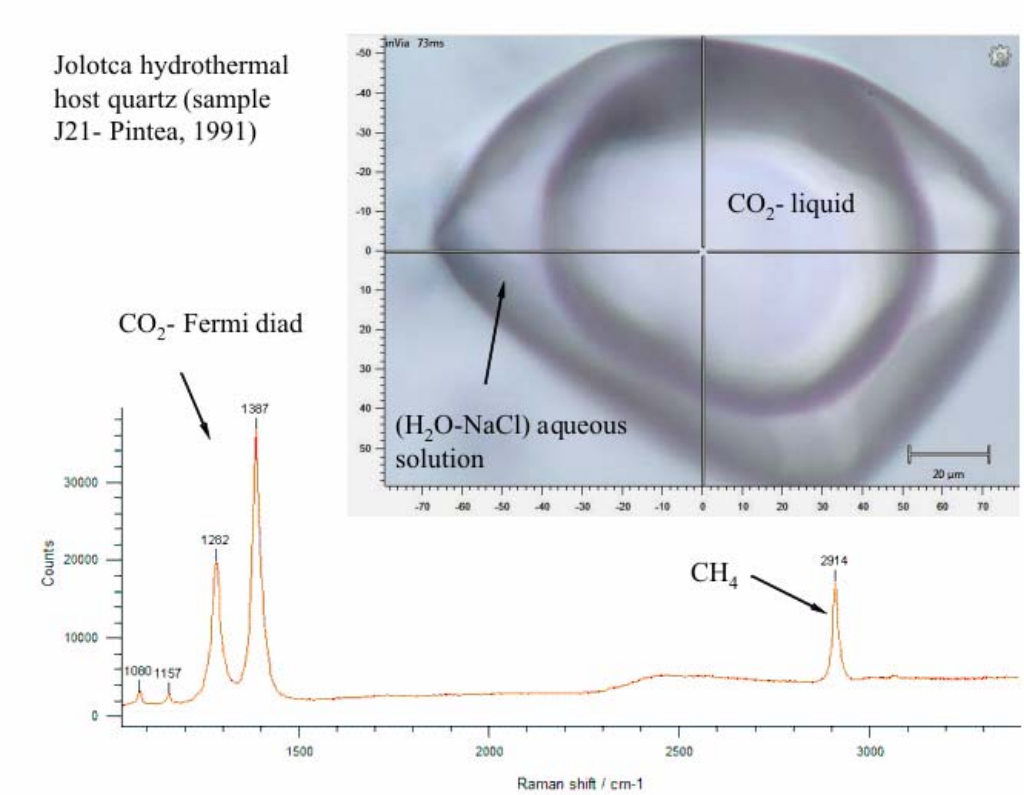

Fig. 196. Raman spectra of CO_2-H_2O-NaCl fluid inclusion in hydrothermal quartz from the complex hydrothermal REE-sulfide mineralization from Jolotca, Ditrău Massif (Eastern Carpathian). The presence of CH_4 in the carbonic part of the inclusion was inferred firstly by freezing microthermometry showing lower solid melting temperature of the CO_2-rich phase down to -57.7°C (e.g. **Fig. 118**). In Via Renishaw Raman spectrometer at IGR Bucharest (E. Ghinescu, operator- incident line 523 nm, lense x50, 1200l/mm, exposure 10s, accumulation 20.

Table 1. Characteristic microthermometry and related data obtained for a lot of brine inclusions from recrystallized quartz veins and pods from Ţibleş Massif (Magura Neagră – Suplai mining district and Mestecanului Valley zone). V- Vapor, L-liquid, D- density, Wt % NaCl eq. brine salinity based upon Tm NaCl daughter phase. Red numbers represent salinity values for homogenization measured values. The sowat calculation at that Th had shown the coexistence of liquid and vapor phase as boiling pairs. The differences indicated some disequilibrium condition because water loss at high temperature, partial decrepitation and stretching. But liquid composition is very close to the initial fluid and that inclusion must have a counterpart vapor - rich inclusion nearby (e.g., Fig 23l above). Data were calculated with SoWat PC program version 0.1/2007 (Driesner and Heinrich, 2007). Supplementary unpublished data on Figs 23, 24 and 25

Nr	T,°C	P, bar	wt% NaCl eq	d, g/ccm	Fluid phase state
1	838	778.586	77.51	1.1835	single phase state
2	758	604.722	77.51	1.2224	single phase state
3	973	1069.98	77.51	1.1331	single phase state
4	705	647.34	70.341 0.49756 V 70.3571 L	0.1749 V 1.15281 L	V+L
5	872	1709.01	47.8048	0.84265	single phase state
6	431	1037.16	51.6237	1.17291 L 2.0576 H	L+H
7	886	1556.36	58.1057 8.0111 V 58.106 L	0.36964 V 0.95206 L	V+L
8	886	1594.22	56.7434 9.0325 V 56.744 L	0.38539 V 0.93787 L	V+L
9	831	1336.53	58.1057 9.0325 V 56.744 L	0.33107 V 0.96116 L	V+L
10	902	1015.76	74.8042 2.0775 V 74.804 L	0.21136 V 0.96116 L	V+L
11	682	681.946	65.5795 0.62135 V 65.58 L	0.19625 V 1.1021 L	V+L

12	910	725.044	82.8023 0.85425 V 82.802 L	0.14371 V 1.2187 L	V+L
13	882	951.505	75.2334 1.7286 V 75.233 L	0.20171 V 1.1373 L	V+L
14	552	439.361	60.8838 0.18995 V 60.884 L	0.16303 V 1.1345 L	V+L
15	1035	1461.5	73.3692 5.1088 V 73.369 L	0.27226 V 1.0796 L	V+L
16	1070	1587.35	73.3692	1.0755	single phase state
17	830	1011.07	69.185 2.0221 V 69.185 L	0.23399 V 1.0796 L	V+L
18	458	376.642	31.3097 0.49891 V 31.31 L	0.22456 V 0.84732 L	V+L
19	932	1151.23	73.3692 2.89 V 73.369 L	0.23428 V 1.1008 L	V+L
20	985	1302.94	73.3692 3.9306 V 73.369 L	0.25273 V 1.0883 L	V+L
21	993	1691.61	66.2987 7.7234 V 66.299 L	0.34293 V 1.0208 L	V+L
22	1006	1746.85	66.2987 8.3167 V 66.299 L	0.3512 V 1.0196 L	V+L
23	1050	1941.49	66.2987	1.0161	single phase state

Table 2. Leachate analyses (modified from Pintea et al., 1999) shown a different composition vs. microthermometry.
Σ^{+}/Σ^{-} = + 0.26 which means that other ions could be present in solution, e.g. metallic cations and SO_4^{2-} etc.
As general observation the fluid was very rich in $CaCl_2$ and possible anhydrite phase was formed as daughter solid inside the brine inclusions. This is the same at Rosia Poieni porphyry Cu (Au-Mo) system from Metaliferi Mountains, which could be related to a special magma-fluid evolution regime during exhumation process in the postcollisional stage.

Sample/Cl µg/ml	Element	Cation concentration (µg/ml)	Total cations (wt%)	Cl needed to balance cations(µg/ml)	Total chlorides (wt%)
Quartz	Na	1.206	5.40	1.86	5.69
26.2	K	7.272	32.51	6.62	20.25
	Ca	11.1	49.62	19.70	60.26
	Mg	0.578	2.59	1.71	5.23
	Fe	2.21	9.88	2.80	8.57
Total		22.37	100.00	32.69	100.00

Table 3. Microthermometry of the silicate melt inclusions trapped in zirrcons from Fagetel gneiss, Petreanu and Tismana granitoids from South Carpathians. (Pintea in Berza et al., 2006, unpublished). Z- zoned zircon, NZ- unzoned zircon, R- inherited zircon relict, St-glass, K- crystallized silicate phases (micas, feldspar, quartz, glass remnant etc),V-vapor, Ts- silicate melt, Tfo- final observation temperature in the stage, Tm- melting temperature. Reference works in silicate melt inclusions from zircons worldwide were published by Li Zhaolin, 1994, Thomas, 2003, Thomas et al., 2003 among others. Size in µm.

Crt. no.	**Sample no.**	**Locality/ petrotype**	**Zircon type/size**	**Silicate melt inclusions content /size**	**Phases at Th (°C)**	**Th (°C)**	**Observations**
1	R126	Fagetel gneiss		St +V(10)	**Ts**	**835**	U-PB
			*NZ,250/120	St +V(10)	**Ts**	**904**	777 Ma
				St +V(10)	**Ts**	**678**	secondary?
2	R16	Tismana granite	*Z,250/90	St+V(10)	**Ts**	**826**	U-Pb 567Ma
			*Z,250/120	St+V(30)	**Ts**	**959**	
			*NZ,25/40	St+V(50)	**Ts**	**923**	
			*NZ,150/100	St+V(20)	**Ts**	**637**	secondary?

3	308	Petreanu granite	NZ,240/50	St+V(40)	**Ts**	**959**	U-PB 320 Ma
			*NZ,250/60	St+V(10)	**Ts**	**906**	
			NZ,220/90	St+V(20)	**Ts**	**977**	
4	T_1	Tismana granite	*NZ,150/50, R	St+V(10)	**Ts**	**642**	
5	T_2	Tismana granite	*NZ,230/100	St+V(40)	**Ts**	**951**	
6	T_8	Tismana granite	NZ,260/50	St+V(20)	**Ts**	**701**	
			NZ,240/110	St+V(20)	**Ts**	**835**	Complete opaque at Th
			NZ,250/80	St+V(20)	**Ts**	**881**	
7	3287I	Petreanu granitoide	NZ,250/70	St+V+K(30)	Ts+V(**941**)	**?**	**Tm = 905°C**
			NZ,130/50	St+V(20)	**Ts**	**923**	
8	3302III	Furcatura syeno-granite	Z,230/80	St?+V?+K (40)	Ts+K+V? (**1004**)	**?**	**Tm=607°C**

Table 4. Microthermometry of silicate melt inclusions fron zircon prismatic crystals from some Neogene volcanic rocks from Eastern Carpathians and Metaliferi Mountains (extracted from unpublished IGR report – Pintea in Berza et al., 2007, unpublished).NZ- unzoned prismatic zircons with length-wide ratio; G- glass, V-vapor; Kx- unidentified solid phases, Th-total homogenization temperature. Size in µm. Detalied data set of Fig 123.

Crt. no.	**Locality/ petrotype**	**Zircon type/size**	**Silicate melt inclusions content/size**	**Phases at Th (°C)**	**Th (°C)**	**Observations**
1	Dej tuff	NZ/1:3 to 1:5	Silicate glass (G +V) /5-20	Silicate melt	552°C(?); 636°C; 720°C; 830°C	Total homogenization
2	Dej tuff	NZ/1:3 to 1:5	silicate glass (G+V)/10-30	Silicate melt + vapors	850-900°C and > 1000°C	Partial homogenization

3	Dej tuff	NZ rarely Z, 1;3 to 1:5	Silicate melt (G+V +Kx)/20-30	Silicate melt + vapor + unmelted solid(s)	>750-1000°C	Partial homogenization
4	Danesti-Piatra Rosie dacite	NZ/1:3	Silicate glass (G+V)/20	Silicate melt	730°C; 783°C; 978°C;	Total homogenization
5	Danesti – Piatra Rosie dacite	NZ/1:3	Silicate glass (G+V)/10-60	Silicate melt + vapor	780-1041°C	Partial homogenization
6	Laleaua Alba dacite	NZ/1:3	Silicate glass (G+V)/5-10	Silicate melt	789°C 975°C 923°C(zircon embeded in quartz)	Total homogenization
7	Rosia Montana	NZ/1:3	Silicate glass (G+V)5	Silicate melt	894°C	Total homogenization
8	Sacaramb	NZ/1:3	Silicate glass (G+V)/5	Silicate melt	916-990°C	Total homogenization

ADDENDA

A. Up - to - date development of practical methodology and analytical protocols on fluid and melt inclusions in Romania.

No	Analytical method	Apparatus/Methodology	Analytical device and range	Applications	Authors
1	Microthermo-metry	Microthermo-metric stages (“custom-made”) Analitycal protocols	+20°C to +270°C; +20°C to +600°C	Homoge-nization temperature	Pomârleanu, 1958,1971
2	Microthermo-metry	Analytical protocol	“Boetius” Melting-point apparatus	Homoge-nization temperature	Borcoș, 1965; Manilici et al., 1965

3	Decrepitometry	Decrepitometer “custom-made” Analytical protocols	+1100°C	Decrepitation temperature	Pomârleanu, Filip,1966 ; Filip,1972 ; Pomârleanu, 1975 ; Pomârleanu, Filip,1976
4	Micro-thermometry	Analytical protocols	Leitz 1350°C Heating stage +20° to + 1350°C	Homoge- nization temperature	Borcoș,1970
5	Gas-Cromatography	Analytical protocol	gCO_2/ 100g H_2O; molCO_2/ 1000 gH_2O “Porapaq” column and “custom-made” heating device	Gas content liberated by heating	Pomârleanu, Neagu,1981
6	Microthermo-metry	Analytical protocol	“Heiz- Kammer-400”	Homoge-nization temperature	A.Götz, (personal communi-cation, 1985)
7	Decrepitometry	Decrepitometer “home made”	1400°C	Decrepitation temperature	Pintea, 1982 ; Pintea,1983 (arh IPEG Harghita)
8	Microthermo-metry	“Termoinc-01” Microthermo-metric stage “custom-made”	-190° to +750°C	Heating – cooling microthermo-metry	Pintea, 1988; Pintea in Udubașa et al,1989 (arch IGR) ; Pintea et al., 1992 ; Pintea, 1995b

9	Microtermo-metry	Analytical protocols	"Termoinc-01"; (IMTG-1); -190° to + 750°C Linkam THMSG600 -190°- to +600°C	Heating – freezing analyses	Pintea et al., 1992 ; Sava and Constanti-nescu (1992-unpublished); Panaiotu C, 2001; Fall, 2002; Cioacă, 2007; Iatan, 2008;
10	SEM-EDAX	Analitycal protocols	Scanning Electronic microscopy with X- ray analizor	Daughter phase identification an d semiquanti-tative analyses	Pintea et al., 1992,arh IGR Nedelcu et al.,1998 ; 2001
11	Coupled Gas Cromatography-Mass Spectrometry	Analytical protocols	"Custom-made"- in vacuum crushing device coupled to mass spectro-metry;	Gas analyses CO_2, SO_2, CH_4, H_2S, N_2; µg/g; 10^{-9}g	Palibroda et al.,(1990, unpublished) ; Cuna et al 1991; 1992, unpublished) ; C una et al., 2001
12	« Crush leach »	Analytical protocols	Atomic absorbtion spectro-metry, X-ray spectro-metry	Chemical micro-analyses of Na, K, Li, Rb, Cs, La, Mg, Fe, Mn, Zn, Cl, SO_4	Morar et al., (1990;1998, unpublished)
13	« Crush-leach »	Original Membrane-Selective ion « EMIS-Cl » Analytical protocols	Selective ion electrode 10^0 to 10^{-4}	Chloride determina-tion and chlorine isotopes analysis by Mass Spectrometry	Hopârtean et al., 1998 ; Pintea, 1998 ; Pintea et al., 1999b
14	« Crush-leach »	Analytical protocols	Capillary Electro-phoresis "Mili Q"	Micro-chemical analyses of SO_3^{2-}, $S_2O_3^{2}$, HS, Cl^-, SO_3^{2-} $HAsO_4^{2-}SeO_4^{2-}$, MoO_4^{2-}, NO_3^-	Halbauer, 1997; Forray, Halbauer, 2000

				,WO_4^{2},F^-, HCO_3^-, acetate, propionate; NH^+, K^+, Na^+, Ca_2^+, Sr^{2+},Mg^{2+}, Mn^{2+},Li^+, Zn^{2+}, Cu^{2+}, Co, Ni Cu, Ba, Be	
15	Micro-thermometry	Analytical protocols	USGS Heating-cooling stage; -190 la +750°C	Heating-cooling micro-thermometry	Pintea, 1996b
16	Micro-thermometry	"Home-made" heating device	+20° la +1100°C	High temperature micro-thermometry	Pintea,1998, Arh IGR
17	Coupled Raman spectroscopy-High temperature micro-thermometry	Analytical protocol for Renishaw inVia-Linkam TS1500 system	+20 to + 1500°C	Raman Heating-quenching micro-thermometry	Pintea et al., 2018 (unpublished protocol)

B. The up- to - date analytical methods used in Romania - still in "the embryonic state" (Pintea, 2019).

Deposit/ Formation	**Host mineral**	**Fluid/Melt inclusion association**	**Methods**	**Autor(s)**
Epithermal Dacites	Quartz Calcite Sphalerite wolframite	Aqueous Brine Silicate melt	**HF-M, HT-M, NIR-M,** **CL-OM, Raman,** **LA-ICP MS, LA-OES, SEM-EDS,** **EPMA, SIMS,** **CE (capillary electrophoresis)** **MS**	Alderton and Fallick, 2000; Bailly, et al., 2002; Gál, 2014; Grancea, 2002; 2003, Halbauer, 1997; Naumov et al., 2013; 2014; Nedelcu et al., 1995; Marias, 1996; Papp et al., 2003; Pintea, 1995a; Pintea et al., 2018; Pintea and Iatan, 2017; Wallier et al., 2006;

Porphyry Cu-(Au-Mo)	Quartz Enargite anhydrite pyrite	Aqueous Brine Hydrosaline melt Silicate melt	**HF-M, HT-M, NIR-M,** **SEM-CL** **LA-ICP-MS, PIXE,** **SEM-EDS,** **ISE, AAS, EPMA,** **MS,** **CG-MS**	André-Mayer et al., 2001; Bailly, com pers, 2002; Cioaca, 2007; 2011; Grancea, 2001; Heinrich et al., 2003; Iatan, 2008; Ivascanu et al., 2003; Kouzmanov et al., 2010; Nedelcu et al., 2003; Pintea, 1996b ; 2014a,
Ditrau alkaline massif	Quartz, nepheline	Aqueous Brine Carbonic	**HF-M, Raman,** **GC-MS**	Pintea and Diamond, 1994; Fall et al., 2007;
Pegmatite	Quartz Muscovite Garnets	Aqueous Brine Carbonic Hydrosaline melt Silicate melt	**HF-M** **HT-M** **GC, Decrepitometry** **Raman**	Pintea, 1993; 1996; 2014; Pintea et al., 2018;Pomârleanu & Filip, 1976; Pomârleanu & Pomârleanu, 1981
Low- and amphibolitic grade	Quartz	Aqueous Brine Carbonic	**HFM** **GC-MS**	Pintea, 1991,unpubl.; Udubaşa et al., 2003;
Sedimentary	Halite, calcite, gypsum baryte	Aqueous Gaseous	**HF-M** **GC-MS** **FTIR-spectrometry**	Banerjee & Ghiurca, 1997; Nutu- Dragomir M.L., 2012; Panaiotu, 2001; Pintea, 1989 unpbl.; 1995; 2008; 2016; Pomârleanu & Mârza, 2003;
Peridotite	Olivine Xenolits	Carbonic Calcicarbonate in silicate matrix veinlets	**HF-M** **SEM-CL** **EPMA**	Pintea & Mârza, 1989; Chalot-Prat & Arnold, 1999;

Notations: HF-M - heating-freezing microthermometry, **HT-M**- high temperature microthermometry, **NIR-M**- near infrared microthermometry, **CL-OM** – cathodoluminescence-optical microscopy, **LA-ICP-MS**- laser ablation- Inductively Coupled plasma – Mass Spectrometry, **LA-OES**- Laser ablation-optical emission spectroscopy, **SEM-EDS**- Scanning Electron Microscopy with Energy Dispersive Spectroscopy, **EPMA**- Electron Probe Micro

Analyses, **SIMS**- Ion Mass Spectrometry, **SEM-CL**-Cathodoluminescence Scanning Electron Microscopy, **PIXE**- Proton induced X-ray emission, **ISE**- Ion Selective Electrodes, **AAS**- Atomic Absorbtion Spectroscopy, **CG-MS**- Gz Cromatography-Mass Spectrometry, **FTIR**- Fourier – transform Infrared Spectroscopy

Note added in proof: Recent Raman spectra suggested that liquid hydrocarbons and pyrobitumen supposed to be present in the fluid inclusions from **Figs 38, 108, 112, 125 and 137** seem to be a complex hydrosilicate ± chloride ± carbonate ±phosphate ± CO_2±CH_4 vapor-rich "melt" inclusions or a clathrasil like component (Pintea et al., 2018; 2019).

REFERENCES

Alderton D.H.M., Fallick A.E., 2000. The nature and genesis of gold-silver-tellurium mineraliozation in the Metaliferi Mountains of western Romania. Econ. Geol., 95, 495-516.

Amorim D.L.E., Freitas M.E., Rios F.J., de Lima T.A.F., 2012. Melt inclusions: principas caracteristicas e tecnicas de estudo. Geonomes, 20, 2, 58-67.

Andersen T, Frezzotti ML, Burke E.A.J. eds., 2001. Fluid inclusions: phase relationships - methods- applications (special issue). Lithos 55 (1-4), 320 pp.

Anderson A.T., Jr., 1991. Hourglass inclusions: Theory and application to the Bishop rhyolitic Tuff. Am. Min. 76, 530-547.

Anderson A.J., Bodnar R.J., 1993. An adaption of the spindle stage for geometric analysis of fluid inclusions. Amer. Mineral., 78, 657-664.

André-Mayer, A.S., Leroy, J.L., Marcoux, E., Lerouge,C., 2001. Inclusions fluides et isotopes du soufre du gisement Cu-Au de Valea Morii (Monts Apuseni, Roumanie) : un télescopage porphyre-épithermal neutre? C. R. Acad. Sci. Paris, Sciences de la Terre et des planètes, 333 : 121-128.

Audétat A., Gunther D, Heinrich C.A., 1998. Formation of a magmatic-hydrothermal ore deposit: insights with LA-ICP-MS analysis of fluid inclusions. Science, 279, 2091–2094.

Audétat A., Günther D., 1999. Mobility and H_2O loss from fluid inclusions in natural quartz crystals. Contrib. Mineral. Petrol., 137, 1-14.

Audétat A., Simon A.C. 2012. Magmatic control on porphyry copper genesis.SEG.Spec.Publ., 16,21, 553-572.

Ayora C., Fontarnau R., 1990. X-ray microanalysis of frozen fluid inclusions. Chem .Geol., 89, 135-148.

Baker D.R., Barnes S.-J., Simon G., Bernier F., 2001. Fluid transport of sulfur and metals between sulfide melt and basaltic melt. The Canadian Mineral., 39, 537-546.

Bakker R.J., 1999. Optimal interpretation of microthermometrical data from fluid inclusions: thermodynaminc modeling and computer programming. Schriftliche Habilitationsleistung zum Thema. Ruprecht-Karls-Universität Heidelberg Geologisch-Paläontologisches Institut Im Neuenheimer Feld 234 D-69120 Heidelberg.

Bakker R.J., Brown P.E., 2003., Computer modelling in fluid inclusion research. In: Fluid Inclusions, Analysis and Interpretation (eds. Samson I, Anderson A, Marshall D), Short Course v. 32, Mineralogical Association of Canada, 175-212.

Bakker R.J., 2003. Package FLUIDS 1. Computer programs for analysis of fluid inclusion data and for modelling bulk fluid properties. Chemical Geology, v. 194 , 3-23.

Bakker R.J., Diamond L.W., 2006. Estimation of volume fractions of liquid and vapor phases in fluid inclusions, and definition of inclusion shape.Amer. Mineral., 91, 635-657.

Bailly L., Milési J.P., Leroy J., Marcoux E., 1998. The Au-Cu-Zn-Sb epithermal mineralization of the Baia Mare district (north Romania): new mineralogical and microthermometric results. C R Acad Sci Paris 327:385–390.

Bailly L., Grancea L., Kouzmanov K., 2002. Infrared microthermometry and chemistry of wolframite from the Baia Sprie epithermal deposit. Romania. Econ. Geol., 97, 415-423.

Balintoni I., 1970. New data and ideas on the genesis of the native sulfur ore deposit from Călimani Mountains and related of the adjacent geologic environments. D.S. IGG (IGR), LV (1967-1968), 1-22 (in Romanian).

Balintoni, I., Petrescu, I., 2002. A hypothesis on the Transilvanian halite genesis. Studia Universitatis Babeş-Bolyai, Geologia, Special issue, 1, 51- 61.

Balintoni I.C., 2000. Geologic and isotopic models for the Carpathian crystalline evolution.Stud. Univ. "Babes-Bolyai", Geol., XLV,1, 47-54.

Balitsky V,S., Bondarenko G.V., Balitskaya L.V., Novikova M.A., Bublikova T.M., Penteley S.V., 2009. Experimental study of phase transformation of hydrocarbons in water-oil mixes at elevated and high temperatures and pressures. Inf. Bull. Ann. Sem. and Exp. Mineral. Petrol. and Geochem.-2009, Vestnik otdelenia nauk o zemle RAN, 1997-2009.

Ballhaus C., Tredoux M., Späth A., 2001. Phase relations in the Fe-Ni-Cu-PGE-S system at magmatic temperature and application to massive sulphides ores of the Sudbury igneous complex. Jour. of Petrol., 42, 10, 1911-1926.

Banerjee A., Ghiurcă V., 1997. Investigation of fluid inclusions in quartz crystals from Romania by FTIR spectroscopy. ECROFI XIV, Abstracts, 29-30.

Banks D.A., Yardley B.W.D., 1992. Crush-leach analysis of fluid inclusions in small natural and synthetic samples. Geochim.Cosmochim.Acta, 56, 245-248.

Barton P. B. Jr., 1978. Some ore textures involving sphalerite from the Furutobe mine, Akita Prefecture,Japan. Mining Geol., 28, 293-300.

Barton P. B. Jr., Bethke P. M., 1987. Chalcopyrite disease in sphalerite: pathology and epidemiology. Amer. Mineral., 72, 451-467.

Bassett, W.A., Shen, A.H., Bucknum, M., Chou, I-M., 1993. A new diamond anvil cell for hydrothermal studies to 2.5 GPa and from -190 to 1200 ^{o}C. Rev. of Sci. Instr., 64, 2340–2345.

Becker S.P., 2008. Fluid inclusion characteristics in magmatic-hydrothermal ore deposits. PhD thesis, Virginia Polytechnic Inst. and State Univ., Blacksburg, VA, 138p.

Becker S.P., Fall A., Bodnar R.J., 2008. Synthetic fluid inclusions. XVII. PVTX properties of highsalinity H_2O-NaCl solutions (> 30 wt% NaCl): applications to fluid inclusions that homogenize by halite disappearance from porphyry copper and other hydrothermal ore deposits. Econ. Geol., 100, 539-554.

Blamey N.J.F., Norman D.I., 2001. Fluid inclusion evidence for a supercritical magmatic fluid modified by wall-rock interaction and mixing with meteoric waters. Proceed., 26th Workshop on Geothermal Reservoir Engineering Stanford University, Stanford, California, January 29-31, 2001 SGP-TR-168.

Blundy J., Cashman K., Humphries M., 2006. Magma heating by decompression-driven crystallization beneath andesite volcanoes. Nature, 443, 76-80.

Bodnar R.J., 1993. Revised equation and table for determining the freezing point depression of H_2O-NaCl solutions. Geochim. Cosmochim. Acta, 57, 683-684.

Bodnar R.J., Reynolds T.J., Kuehn C.A., 1985a. Fluid inclusion systematics in epithermal systems. In Society of Economic Geology., Review in Economic Geology, Geology and Geochemistry of Epithermal Systems, B.R. Berger and M. Bethke, eds., 73-98.

Bodnar R.J., Burnham C.W., Sterner S.M., 1985b. Synthetic fluid inclusions in natural quarlz. - III. Determination of phase equilibrium properties in the system H_2O-NaCl to 1000°C and 1500 bars. Geochim. Cosmochim. Acta 49, 1861-1873.

Bodnar R.J., Sterner, S.M., 1987. Synthetic fluid inclusions. In Hydrothermal Experimental Techniques, G.C. Ulmer and H.L. Barnes, eds., Wiley–Interscience, New York. p.423–457.

Bodnar R.J., 1989. Synthetic fluid inclusions: A novel technique for experimental water-rock studies.In Water-Rock interaction, Miles (ed), 99-102.

Bodnar R.J., 1993. Revised equation and table for determining the freezing point depression of H_2O-NaCl solutions. Geochim. Cosmochim. Acta, 57, 683-684.

Bodnar R.J., Vityk O.M., 1994. Interpretation of microthermometric data for H2O-NaCl fluid inclusions. In Fluid Inclusions in Minerals, Methods and Applications, B. De Vivo and M.L. Frezzotti, eds, published by Virginia Tech, Blacksburg,VA, 117-130.

Bodnar R.J., 1995. Fluid-inclusion evidence for a magmatic source of metals in porphyry copper deposits: Mineralogical Association of Canada Short Course Series, 23, p. 139-152.

Bodnar, R.J., 2003a. Introduction to fluid inclusions. *In* Fluid Inclusions: Analysis and Interpretation (I. Samson, A. Anderson & D. Marshall, *eds*.) Mineral. Assoc. Can. Short Course 32*,* 1–8.

Bodnar, R.J., 2003b. Reequilibration of fluid inclusions. *In* Fluid Inclusions: Analysis and Interpretation (I. Samson, A. Anderson & D. Marshall, *eds*.) Mineral. Assoc. Can. Short Course 32*,* 213–230.

Bodnar R.J., 2003. Introduction to aqueous fluid systems. In I. Samson, A. Anderson, & D. Marshall, eds.Fluid Inclusions: Analysis and Interpretation. Mineral. Assoc. Canada, Short Course 32, 81-99.

Bodnar R.J., 2005. Fluids in planetary systems. Elements, 1, 9-12.

Bodnar R.J., Student J.J., 2006. Melt Inclusions in plutonic rocks: petrography and microthermometry. Min. Assoc. Can. Short Course 36, Montreal, Quebec, 1-25.

Bodnar R.J., 2010. Magmatic fluid evolution associated with epizonal silicic plutons. ACROFI III and TBG XIV, p. 230-31, Novosibirsk, Russia.

Bodnar R.J., Mernagh T.P., Samson I.M., Manning C.E., 2013. Introduction to thematic issue on fluid and melt inclusions.Geofluids Spec. issue: Fluid and Melt inclusions 2012, 13, 4, 395-609.

Bodnar R., Lecumberri-Sanchez P., Moncada D., Steele – MacInnis M., 2014. Fluid inclusions in hydrothermal ore deposits. In: Holland H.D., Turekian K. K., (eds.)Treatise on Geochemistry,Second Edition, 13, 119-142.Oxford: Elsevier.

Borcoș M. (1965) Metoda omogenizarii fazelor in analiza mineralotermometrica pentru determinarea conditiilor termodinamice de formare a zacamintelor hidrotermale. Rev. Minelor, XV, 11, 448-452.

Borcoș M. (1970**)** Cercetari de microtermometrie geologică cu privire specială asupra unor procese metalogenetice si petrogenetice din România. Rez. tezei de doctorat, 36p.

Borcoş M., Vlad S., Udubaşa G. Gabudeanu B., 1998. Qualitative and quantitative metallogenetic analysis of the ore genetic units in Romania. Rom. J. of Mineral Dep., 78, spec iss., 158p.

Borcoş M., Udubaşa G., 2012. Chronology and characterization of mining development in Romania.Rom.Journ of Earth Sci., 86, 1, 17-26.

Bortnikov N.S., Genkin A.D., Dobrovolskaya M.G., Muratvitskaia G.N., Filimonova A. A., 1991. The nature of chalcopyrite inclusions in sphalerite: exsolution, coprecipitation, or "disease"? Econ.Geol., 86, 1070-1082.

Boştinescu S., 1984. Porphyry copper systems in the south Apuseni Mountains-Romania. Anuarul Inst. Geol. Geofiz. (IGR), LXIV, 163-174.

Bottrell S.H., Yardley B.W.D., Buckley F., 1988. A modified crush-leach method for the analysis of fluid inclusion electrolytes.Bull.Mineral. 111, 279-290.

Brown P., 1998. Fluid inclusions modeling for hydrothermal systems. In Rev. in Econ. Geol., "Techniques in hydrothermal ore deposits geology", 10, 7, 151-171.

Burnham C.W., 1979. Magmas and hydrothermal fluids. In: Barnes H.L.(ed.) Geochemistry of Hydrothermal Ore Deposits. John Wiley & Sons, New York, 2, pp.71 - 136.

Burruss R.G., Slepkov A.D., Pegararo A.F., Stolow A., 2012. Unraveling the complexity of deep gas accumulation with three-dimensional multimodal CARS microscopy.Geology, 40, 1063-1066.

Campos E., Touret J.L.R., Nikogosian I., Delgado J., 2002. Overheated, Cu-bearing magmas in the Zaldívar porphyry-Cu deposit, Northern Chile. Geodynamic consequences, Tectonophys. 345, 229-251.

Cesare B., Ferrero S., Salvioli-Mariani E., Pedron D., Casallo A., 2009. "Nanogranite" and glassy inclusions: the anatectic melt in magmatites and granulites.Geol., 37, 7, 627-630.

Chalot-Prat F., Arnold M., 1999. Immiscibility between calciocarbonatitic and silicate melts and related wall rock reactions in the upper mantle: a natural case study from Romanian mantle xenoliths. Lithos 46, 627-659.

Chi G., Chou I-M., Lu H-Z., 2003. An overview on current fluid – inclusion research and applications. Acta petrologica Sinica, 19 (2): 201-212.

Chou I.-M., 1987. Phase relations in the system NaCl-KCI-$H_2$0. Part III: Solubilities of halite in vapor-saturate&liquids above 445°C and redetermination of phase equilibrium properties in the system NaCl-$H_2$0 to 1000°C and 1500 bars. Geochim. Cosmochim. Acta 51, 1965-1975.

Cioacă M.E. (2007) Studiul mineralizatiei de cupru si aur tip « porphyry » de la Bolcana, Muntii Metaliferi, RTD (pdf) 168 p, Univ. Bucuresti.

Cioacă M.E., 2011. Fluid evolution in the Bolcana ore deposit, Metaliferi Romania. Carpath. Jour.of Earth and Environm. Sci., 6, 2, 215-224.

Clocchiatti R., 1975. Les inclusions vitreuses des cristaux de quartz. Étude optique, thermooptique et chimique. Applications geologiques. Memoires de la Société Géologique de France, LIV, 122, 1-96.

Cook N.J., Damian G.S., 1997. New data on "plumosite" and other sulphosalt minerals from the Herja hydrothermal vein deposit, Baia Mare district, Rumania. Geol. Carpath., 48, 6, 387-399.

Coveney R.M., Kelly C.W., 1971. Dawsonite as a daughter mineral in hydrothermal fluid inclusions. Contr. Mineral. and Petrol. 32, 334-342.

Craig J.R., 2001. Ore-mineral textures and the tale they tell.The Canadian Mineral., 39, 937-956.

Cuna S., Palibroda N., Cuna C., Pintea I., 2001. The mass spectrometric method for analysis of volatile species from fluid inclusions. Rom. Mineral Deposits, v. 79 suppl.2, ABCD-GEODE, 2001 Workshop Vaţa Băi, Romania. Abstract volume, 48-49.

Cuna S., Moldovan Z., Pintea I., 1991. Analiza gazelor din incluziunile fluide din minerale prin cromatografie in faza gazoasa si spectrometrie de masa. Contract de Cercetare (ITIM Cluj-Napoca-IGR Bucuresti) nr 760/1991.

Cuna S., Cuna C., Palibroda N., Pintea I., 1992. Elaborarea metodei de analiza individuala a gazelor din incluziunile fluide folosind spectrometrul de masa quadrupolar.Contract de cercetare (ITIM Cluj Napoca-IGR Bucuresti), 1226/1992.

Damian G., 2003. The genesis of the mase metal ore deposit from Herja. Studia Univ. "Babes-Bolyai", Geol., XVIII, 1, 85-100.

Damman A.H., Karis S.M., Touret J.L.R., Rieffe E. C., Kramer J.A.L.M., Vis R.D., Pintea I., 1996. PIXE and SEM analysis of fluid inclusions in quartz crystals from the K-alteration zone of the Roşia Poieni porphyry - Cu deposit, Apuseni Mountains, Rumania. Eur. J. Mineral. 8, 1081 - 1096. Stuttgart.

Danyushevski L.V., Mcneill A.W., Sobolev A.V., 2002. Experimental and petrological studies of melt inclusions in phenocrysts from mantle-derived magmas: an overview of techniques, advantages and complications. Chem. Geol. 183, 5-24.

Davidson P., 2004. A new methodology for the study of the magmatic hydrothermal transition in felsic magmas: applications to barren and mineralised systems. PhD thesis, University of Tasmania, 338p.

De Vivo B., Frezzotti M.L., 1994. Fluid inclusions in minerals: methods and applications. Short course of the working group (IMA) "Inclusions in Minerals" (Siena) Fluids Research Laboratory, Department of Geological Sciences, YPI, Blacksburg.

Deicha G., 1955. Les lacunes des cristaux et leurs inclusions fluids.Signification dans la genese des gites mineraux et des roches. Masson et CIE edit., Paris VI, 126p.

Dénes R., Márton I., Kiss G.B., Ivăşcanu P., Veress Z., 2014. Additional data regarding the petrography and geochemistry of the magmatic phases and hydrothermal vein types from Bolcana porphyry Cu-Au mineralization (Apuseni Mts., Romania). R. J. Min. Dep., 87, 1, 99-104.

Desborough G.A., Anderson A.T., Wright T.L., 1968. Mineralogy of sulfides from certain Hawaiian basalts.Eon.Geol., 63., 636-644.

Diamond L.W., 1994. Introduction to the phase relations of CO_2-H_2O fluid inclusions. In Fluid Inlusions in Minerals: Methods and Applications. Ed. by B. De Vivo and M. L. Frezzotti,Virginia Tech., 1994, 131-158.

Diamond L.W., 2003a. Systematics of H_2O inclusions. In Fluid Inclusions: Analysis and Interpretation, (I.M. Samson, A.J. Anderson, & D.D. Marshall eds.). Mineralogical Association of Canada, Short Course 32, 55-79.

Diamond L.W., 2003b. Introduction to gas bearing, aqueous fluid inclusions. In I. Samson, A. Anderson, & D. Marshall, eds. Fluid Inclusions: Analysis and interpretation. Mineral. Assoc. Can., Short Ser. 32, 101-158.

Driesner, T., and Heinrich, C. A., 2007. The system H_2O-NaCl. Part I: Correlation formulae for phase relations in temperature-pressure-composition space from 0 to 1000 degrees C, 0 to 5000 bar, and 0 to 1 X NaCl: Geochim. Cosmochim. Acta, v. 71, p. 4880-4901.

Driesner T., Geiger S., 2007. Numerical simulation of multiphase fluid flow in hydrothermal systems. Rev. in Min. and Geochem. 65, 187-212.

Dubessy J., Poty B., Ramboz C., 1989. Advances in C-O-H-N-S fluid geochemistry based on micro-Raman spectrometric analysis of fluid inclusions. Eur. J. Mineral. 1, 51 7- 534.

Dubessy J., 1994. Single component systems: phase diagrama and their application to fluid inclusions. In Fluid Inlusions in Minerals: Methods and Applications. Ed. by B. De Vivo and M. L. Frezzotti,Virginia Tech., 1994, 95- 115.

Dubessy J., 2004. Fluid inclusions in sedimentary basin: Theoretical basis, diagrams, analytical techniques. Acta Petrologica Sinica, 20, 6,, 1301-1318.

Ducea N.M., McInnes I.A.B., Wyllie P.J., 1999. Experimental determination of compositional dependence of hydrous silicate melts on sulfate solubility. Eur. J. Mineral., 11,33-43.

Eldridge C.S., Bourcier W.L., Ohmoto H., Barnes H.L., 1988. Hydrothermal inoculation and incubation of the chalcopyrite disease in sphalerite. Econ. Geol., 83, 978-989.

Ermakov N.P., Dolgov Yu.A.., 1979. Thermobarogeochemistry (In Russian), Ed. Nedra, Moscow.

Etschmann B., Pring A., Putnis A., Grguric B.A., Studer A., 2004. A kinetic study of the exsolution of pentlandite $(Ni,Fe)_9S_8$ from the monosulfide solid solution (Fe,Ni)S. Amer., Mineral., 39-50.

Esposito R., Klebesz R., Bartoli o., Klyukin Y.I., Moncada D., Dohertthy A.L., Bodnar R.J., 2012. Application of the Linkam TS1400XY heating stage to melt inclusion studies. Cent. Eur. J. Geosci., 4 (2), 208-218.

Eugster P.H., 1986. Minerals in hot water. Amer. Mineral., 71,655-673.

Fall A., 2002. Fluid inclusions in nepheline: the role of the fluids in the petrologic evolution of the nepheline syenites of the Ditrau Alkaline Massif, Department of Mineralogy, Univ. of Bucharest, Romania (MS dissertation topic, in Romanian, pp.39).

Fall A., Bodnar R.J., Szabó Cs., Pál-Molnár E., 2007. Fluid evolution in the nepheline syenites of the Ditrău alkaline massif, Transylvania, Romania. Lithos, 95, 331- 345.

Filip D. P., 1972. Measuring device for temperature and acoustic oscillation parameters. Anal. St. Univ. Al. I.Cuza, sect. 1B. Physics, T. XVIII fasc.1, 85-86.

Frezzotti M.-L., 1992. Magmatic immiscibility and fluid phase evolution in the Mount Genis granite (southeastern Sardinia, Italy), Geochim. Cosmochim. Acta 56, 21-33.

Frezzotti M. L., 2001. Silicate-melt inclusions in magmatic rocks: applications to petrology, Lithos 55, 273-299.

Frezzotti M.L., Ferrando S., 2007. Multiphase solid inclusions in ultrahigh-pressure metamorphic rocks: a petrographic approach. Per. Mineral., 76, 113-125.

Frezzotti M.-L., Tecce F., Casagli A., 2012. Raman Spectroscopy for fluid inclusion analysis.Journ. of Geoch. Expl., 112, 1-20.

Frost B.R., Mavrogenes J.A., Tomkins A.G., 2002. Partial melting of sulfide ore deposits during medium- and high-grade metamorphism. The Can. Mineral., 40, 1-18.

Forray F.L., Hallbauer D.K., 2000. A study of the pollution of the Aries River (Romania) using capillary electrophoresis as analytical technique. Env. Geol., 39, 1372-1384.

Gàl A., 2014. Epithermal processes related to the Neogene andesitic intrusions from Certej zone.(Apuseni Mts., Romania), PhD thesis summary, 34p (in Romanian).

Giuşcă D., 1960. Adularization of the neogene volcanites from Baia Mare region. Stud. cerc. geol.,geof., geogr., Ser. Geol.V, 3, Bucharest (in Romanian).

Goldstein R.H., Reynolds, T.J., 1994. Systematics of Fluid Inclusions in Diagenetic Minerals. Society for Sedimentary Geology Short Course 31, Tulsa, Oklahoma, 199 p.

Gondé C., Martel C., Pichavant M., Bureau H., 2011. In situ bubble vesiculation in silic magmas.Amer.Mineral., 96, 111-124.

Grancea L., Cuney M. Leroy J.L., 2001. Mineralized versus barren intrusions: a melt inclusion study in Romania's gold quadrilateral. C. R. Acad. Sci. Paris, Sciences de la Terre et des planets 333, 705-710.

Grancea, L., Bailly, L., Leroy, J.L., Banks, D., Marcoux, E., Milesi, J.P., Cuney, M., Andre´, A.S., Istvan, D., Fabre, C., 2002. Fluid evolution in the Baia Mare gold/polymetallic epithermal district (Inner Carpathians, Romania). Miner. Deposita, 37, (6-7), 630- 647.

Grancea, L., A. Fülop, M. Cuney, J. Leroy, Pironon J., 2003. Magmatic evolution and ore-forming fluids involved in the origin of the gold/base metals mineralization in the Baia Mare province, Romania. J. Geochem. Explor., 78/79, 627–630.

Guo J., Griffin W.L., O'Reilly Y., S., 1999. Geochemistry and origin of sulfide minerals in mantle xenoliths: Qilin Southeastern China. Jour. Petrol., 40, 7, 1125-1149.

Halbauer D.K., 1983. Geochemistry and fluid inclusions in detrital minerals as guides to their provenance and distribution. Spec. Publ. geol. Soc. S. Afr., 7, 39-57.

Halbauer D.K., 1997. The application of capillary ion analysis to the geochemistry of natural aqueous fluids and in particular to the analysis of fluid inclusions in minerals. Pei Rongfu (Ed.). Energy and Mineral Res. for the 21st Century, Geol. of Min. Dep., Min. Econ., Proceed. of the 30th Intern., Geol. Congr., volume 9, xii+514 pag; ISBN 90-6764-264-9, Intersci. Publ. (VSP), AH Zeist, The Netherlands, 1997, 409-424.

Hall D.L., Sterner S.M., 1993. Preferential water loss from synthetic fluid inclusions. Contrib Mineral petrol 114, 489-500.

Halter W.E., Heinrich C.A., Pettke T., 2004. Laser –ablation ICP-MS analysis of silicate and sulfide melt inclusions in an andesitic complex II: magmas genesis and implications for ore-formation. Contrib Mineral Petrol 147, 397-412.

Halter, W.E., Pettke, T., Heinrich, C.A., 2005. Magma evolution and the formation of porphyry Cu–Au fluids: evidence from silicate and sulphide melt inclusions. Mineralium Deposita, 39, 845–863.

Harlow D., 2014. The role of fluids in the lower crust and upper mantle: A tribute to Jacques Touret. Geosci. Frontieres, 5, 621-625.

Harris C.R., Pettke T., Heinrich C.A., Rosu E., Woodland S., Fry B., 2013. Tethyan mantle metasomatism creates subduction geochemical signatures in non-arc Cu-Au-Te

mineralizing magmas, Apuseni Mountains (Romania). Earth and Planet. Sci. Lett., 366, 122-136.

Hansteen T.H., Klügel A., 2008. Fluid inclusion thermobarometry as a tracer for magmatic processes. Rev. in Miner. and Geochem., 69, 143-177.

Har N., Barbu O., Codrea V., Petrescu I. (2006) New data on the mineralogy of the salt deposit from Slanic Prahova (Romania).Stud. Univ. "Babes-Bolyai", Geol., 51(1-2),29-33.

Harlow D., 2014. The fluids in the lower crust and upper mantle: A tribute to Jacques Touret. Geosci. Frontiers, 5, 621-625.

Hauri E., Wang J., Dixon J.E., King P.L., Mandenville C., Newman S., 2002. SIMS analysis of volatiles in silicate glases.1. Calibration, matrix effects and aomparison with FTIR. Chem. Geol., 183, 99-114.

Heinrich C.A., PettkeE, T., Halter W.E., Aigner-Torres M., Audétat A., Günther D., Hattendorf B., Bleiner D., Guillong M., Horn I., 2003. Quantitative multi-element analysis of minerals, fluid and melt inclusions by laser-ablation inductively-coupled-plasma massspectrometry. Geochim. Cosmochim. Acta 67, 3473-3496.

Heinrich C.A., 2005. The physical and chemical evolution of low-salinity magmatic fluids at the porphyry to epithermal transition: A thermodynamic study: Mineralium Deposita, 39, p. 864−889.

Heinrich C.A., Halter W., Landtwing M.R., Pettke T., 2005. The formation of economic porphyry(-gold) deposits: constraints from microanalysis of fluid and melt inclusions. From: Mcdonald, I., Boyce A. J., Butler, I. B., Herrington R. J. & Polya D.A. (eds) 2005. Mineral Deposits and Earth Evolution. Geological Society, London, Special Publications, 248, 247–263.

Heinrich C.A., 2006. From fluid inclusions microanalysis to large-scale hydrothermal mass transfer in the Earth's interior. Jour. of Mineral. and Petrol. Sci., 101, 1, 110-117.

Heinrich C.A., 2007. Fluid–fluid interactions in magmatic-hydrothermal ore formation: Reviews in Mineralogy and Geochemistry, 65, p. 363–387.

Hollister L.S., Crawford M.L. eds., 1981. Short course in fluid inclusions: application to petrology. 304 p. (Calgary, Mineralogical Association of Canada), 304 p.

Holloway J.R., 1973. The system pargasite-H_2O-CO_2: A model for melting of anhydrous mineral with a mixed-volatile fluid-1. Experimental results to 8 kbar. Geochim. Cosmochim. Acta, 37, 651-666.

Hurai V., Huraiova M., Slobodnik M., Thomas R., 2015. Geofluids-Development in Microthermometry,Spectroscopy,Thermodynamics and Stable Isotopes.Elsevier, 504 p.

Iatan L.E., 2008. Relatia dintre magmatism si metalolgeneza in aria zacamintelor Roșia Montana si Roșia Poieni, Muntii Metaliferi. RTD (pdf), 58 p. Univ. Bucuresti.

Ivăşcanu P., Petke T., H.C. Heinrich, Rosu E., Nedelcu L., Pintea I., 2001. Magmatic hydrothermal transition in porphyry environment, South Apuseni Mountains, Romania. Outline from single inclusion LA-ICP-MS. Geode, ABCD-Geode workshop Vaţa Băi, Romania, abstr. p. 111 – 112.

Ivăşcanu P.M., Pettke T., Kouzmanov K., Heinrich C.A., Pintea I., Roşu E., Udubaşa G., 2003. The magmatic to hydrothermal transition: Miocene Deva porphyry copper – gold deposit, South Apuseni Mts, Romania. In Proceedings of the 7th Biennial SGA meeting. Mineral Exploration and Sustainable Development (Eliopoulos et al., 9 eds), Athens, 24 – 28.

Jackson, S.E., 2008. Calibration strategies for elemental analysis by LA-ICP-MS In Laser Ablation ICP-MS in the Earth Sciences: Current Practices and Outstanding Issues (P. Sylvester, ed.). Mineral. Assoc. Can. Short Course Series 40, 169-188.

Jarmolowicz-Szulc K., 2003. The secrets of the Marmarosh diamonds. Min. Soc. of Poland. Spec. papers, Zeszyt, 22, 91-94.

Jarmolowicz-Szulc K., Karwowski L., Dudok I.V., 2006. Marmarosh diamonds the typical association with the organic matter in the outer Carpathians. Acta Min-Petr. Abstr, series, 5, Szeged, p. 51.

Jones D.M., Macleod G., 2000. Molecular analysis of petroleum in fluid inclusions: a practical methodology. Organic Geochem., 31, 1163-1173.

Jude R., 1977. La géologie et la pétrologie des volcanites néogènes du nord-ouest de la zone éruptive des monts Oas (région de Tarna Mare-Turţ). IGG (IGR) Stud. Tech. Econ., Ser. A, nr. 11, 165- 201.

Jude R., 2012. Subvolcanic intrusions with regard to some Neogene magmatites of Metaliferi Mts.-Romania. Rom. J. of Min. Dep., 85, 1, 1-6.

Kamenetsky, V.S., P. Davidson, T.P. Mernagh, A.J. Crawford, J.B. Gemmell, M.V. Portnyagin and R. Shinjo, 2002, Fluid bubbles in melt inclusions and pillow-rim glasses: high-temperature precursors to hydrothermal fluids? Chem. Geol. 183, 349-364.

Kamenetsky V.S., De Vivo B. Naumov V.B., Kamenetsky M., Mernagh T.P., van Achterbergh E., Ryan C.G, Davidson P., 2003. Magmatic inclusions in the search for natural silicate-salt melt immiscibility: methodology and examples, Melt inclusions in volcanic systems, Elsevier, B De Vivo and R.J. Bodnar (ed), Amsterdam, pp. 65-82.

Kamenetsky V.S., 2006. Melt inclusion record of magmatic immiscibility in crustal and mantle magmas, Melt Inclusions in Plutonic Rocks, Mineralogical Association of Canada, Webster J.D. (ed), Montreal, pp. 81-98.

Kamenetsky V.S. and Kamenetsky M.B., 2010. Magmatic fluids immiscible with silicate melts: examples from inclusions in phenocrysts and glasses, and implications for magma evolution and metal transport, Geofluids, 10, (1-2) pp. 293-311.

Kesler S.E., 2005. Ore forming fluids. Elements, 1, 1, 13-18.

Kelly D.P., Vaugham D.J., 1983. Pyrrhotine-pentlandite ore textures: a mechanistic approach. Min. Mag., 47, 453-463.

Kojima S., 1990. A coprecipitation experiment on intimate association of sphalerite and chalcopyrite and its bearings on the genesis of Kuroko ores. Min. Geol., 40(3), 147-158.

Kontak D.J., 2004. Analysis of evaporate mounds as a complement to fluid-inclusion thermometric data: case studies from granitic environments in Nova Scotia and Peru.The Can. Mineral., 42, 1315-1329.

Kouzmanov, K., Pettke, T., Heinrich, C.A., Riemer, S., Ivăşcanu, P.M., Rosu, E., 2003. The porphyry to epithermal transition in a magmatic hydrothermal system: Valea Morii copper gold deposit, Apuseni Mts, Romania. Mineral Exploration and Sustainable Development, Eliopoulos et al. (eds): 303-306.

Kouzmanov, K., Pettke, T., Heinrich, C.A., 2010. Direct analysis of ore-precipitating fluids: combined IR microscopy and LA-ICP-MS study of fluid inclusions in opaque ore minerals. Econ. Geol., 105, 351-373.

Kouzmnov K., Pokrovski G.B., 2012. Hydrothermal contols on metal distribution in porphyry C(-Mo-Au) syatem.SEG, Spec. Publ., 16, 22, 573-618.

Kovacs M., Radu P., Talpoş S., 1982. Contributions to the knowledge of the mineralogical associations from the contact zone of the eruptive body from Mesteacăn-Ţibles spring. D.S. IGG, LXIX/1, 13-30 (in Romanian).

Kovacs M., Molnar F., Kovacs P.P., Lupulescu M., 1995. Fluorapatite from Tibles neogene intrusive massif (East Carpathians, Romania). Rom. J. of Mineral., 77, Suppl. 1, 24-25.

Kovacs M., 2002. Petrogenesis of the subduction magmatic rocks from central-southeast zone of Gutâi Mountains. Dacia Edit., 201 p (in Romanian).

Kovalevich V., Vovnyuk S., 2010. Fluid inclusions in halite from marine salt deposits: are they real micro-droplets of ancient seawater?. Geol. Quarterly, 54, 4, 401-410. Warszawa.

Krüger Y., Stoller P., Rička J., Frenz M., 2007. Femtosecond lasers in fluid inclusion analysis: Overcoming metastable phase states, European Journal of Mineralogy, 19: 693-706.

Landtwing M.R., Pettke T., Halter W.E., Heinrich C.A., Redmond P. B., Einaudi M.T., Kunze K., 2005. Copper deposition during quartz dissolution by cooling magmatic-hydrothermal fluids: The Bingham porphyry: Earth and Planet. Sci. Lett., 235, p. 229-243.

Langenhorst F., 2002. Shock metamorphism of some minerals: basic introduction and microstructural observations. Bull. of the Czech Geol. Surv., 77, 4, 265-282.

Lecumberry-Sanchez P., Steele MacInnis M., Bodnar R.J., 2012. A numerical model to estimate trapping conditions of fluid inclusions that homogenize by halite disappearance. Geochim. Cosmochim.Acta, 92, 14-22.

Lowenstern, J.B., 1995. Applications of silicate-melt inclusions to the study of magmatic volatiles, in Magmas, Fluids and Ore Deposits, Ed. J.F.H. Thompson, Min. Assoc. Canada Short Course vol. 23, 71-99.

Lowenstern J.B., 2003. Melt inclusions come of age: Volatiles, volcanoes, and Sorby's legacy. In Developments in Volcanology 5, Melt Inclusions in Volcanic Systems: Methods, Applications and Problems, (B. DeVivo & R.J. Bodnar, eds.), Elsevier, Amsterdam, 1-21.

Larocque A.C.L., Stimac J.A., Keith J.D., Huminicki M.A.E., 2000. Evidence for open-system behavior in immiscible Fe-S-O liquids in silicate magmas: Implications for contributions of metals and sulfur to ore-forming fluids. Can. Mineral. 38, 1233-1249.

Li Zhaolin, 1994. The silicate melt inclusions in igneous rocks. In Fluid inclusions in minerals: Methods and applications (B. de Vivo, & M.L. Frezzotti eds.), Short Course of the working group (IMA)"Inclusions in minerals", Potignano-Siena, 1-4 sept. 1994, p. 73-93. Italy.

Li Y., Audétat A., Lerchbaumer L., Xiong A.X.L., 2009. Rapid Na, Cu exchange between synthetic fluid inclusions and external aqueous solution: evidence from LA-ICP-MS analysis. Geofluids, 9, 321-329.

Lowenstein T.K., Li J., Brown C.B., 1998. Paleotemperatures from fluid inclusions in halite: method verification and a 100,000 year paleotemperature record, Death Valley CA. Chem. Geo., 150, 223-245.

Madden M.E.E., 2005. Fluids in planetary systems. PhD thesis.Virginia Polytechnic Inst. and State Univ. Blacksburg,VA, USA.

Manilici V., Giuscă D., Stiopol V., 1965. Study of Baia Sprie ore deposit (Baia Mare region) (in Romanian and French). Mem. Com. Geol. Bucharest VII, 113p.

Marias Z. Fr., 1996. Cavnic metalogenetic district. Geostructural and petro-metalogenetic characterization. PhD, 225p. upubl., "Babes-Bolyai" Univ., Cluj-Napoca.

Mason P.R.D., van Bergen M.J., Martinez M., Sumarti S., Valdes, J., Malavassi E., Sriwana T., 2001. Magmatic and hydrothermal controls on trace element output at active volcanoes as recorded by spherules of sulfur in acid crater lakes. Eos Trans. AGU, 82(47), Fall Meet. Suppl., Abstract V42B-1019.

Mason, P.R.D., Nikogosian, I.K., Van Bergen, M., 2008. Major and trace element analysis of melt inclusions by laser ablation ICP–MS. In Laser Ablation ICP–MS in the Earth Sciences: Current Practices and Outstanding Issues (P. Sylvester, ed.). Mineral. Assoc. Can. Short Course Series 40, 219-239.

Ménez B., Simionovici A., Philippot P., Bohic S., Gibert F., Chukalina M., 2001. X-ray-fluorescence micro-tomography of an individual fluid inclusion using a third generation synchrotron light source.Nucl.Instr. and Meth. In Phis. Res sect B: Beam interaction with Mater. and atoms, 181, 1-4, 749-754.

Milu V., Pintea I., 2001. Bolcana porphyry copper deposit. ABCD-GEODE- 2001 Workshop Vaţa-Băi, Romania, Field guidebook. In Rom. J. of Min. Dep., 70, suppl 2, 23-25.

Milu V., Leroy J., Piantone P., 2003. The Bolcana Cu-Au ore deposit (Metaliferi Mountains, Romania): first data on the alteration and related mineralization. C. R. Geosci., 335, 671-680.

Nash T.J., 1976. Fluid-inclusion petrology – data from porphyry copper deposits and applications to exploration: U. S. Geological Survey Prof. Paper 907–D, 16 pp.

Naumov V.B., Tolstykh M.L., Kovalenker V.A., Kononkova N.N., 1996. Fluid overpressure in andesite melts from central Slovakia: Evidence from inclusions in minerals, Petrology 4, 265-276.

Naumov V.B., Prokofiev V.Yu., Kovalenker V.A., Tolstykh M.L., Damian G., Damian F., 2013. Unusual acid melts in the area of the unique Roşia Montană gold deposit, Apuseni Mountains, Romania: Evidence from inclusions in quartz. Geochem. Internat., 51, 11, 876-888.

Naumov V.B., Kovalenker V.A., Damian G., Abramov S.S., Tolstykh M.L., Prokofiev Yu. V., Damian F., Seghedi I., 2014. Origin of the Laleaua Alba dacite (Baia Sprie volcanic area and Au-Pb-Zn ore district, Romania): evidence from study of melt inclusions. Centr. Eur., Geol., 57/1, 83-112.

Nedelcu L., Pintea I., 1993. New data regarding the significance of the pyrite morphology and of the fluid inclusions in quartz crystals at Baia Sprie. Rom. J. Mineral., 76, 1, 79-86.

Nedelcu L., Roşu E., Anastase S., Costea C., Robu L., Ciulavu M., 1995. The morphology and geochemistry of the Valea Morii main ore minerals. An attempt to reconstitute the mineralizing eolution. Rom. J. of Min., 77, Suppl. No 1, p. 32, Abstract volume.

Nedelcu L., Roșu E., Costea C., 1998. Unexpected mineral arborescent-type microstructures related to pyrite of some Neogene ore deposits of Romania. CBGA XVI Congress, Vienna, Abstracts vol., p.417.

Nedelcu L., Pintea I., Rosu E., Ivăşcanu P., Riemer S., 2001. Valea Morii porphyry copper and epithermal gold vein deposit. ABCD-GEODE 2001 workshop Vata-Băi, Romania, 8-12 June, Field guidebook, Rom. J. Min. Dep.79, suppl. 2, p.18-22.

Nedelcu, L., Roşu, E., Costea, C., 2003. Mineral microinclusions hosted in sulfides of main neogene porphyry copper and epithermal ore deposits of the south Apuseni Mountains, Romania. Acta Mineralogical-Petrographica. Abstr. Ser. 1, Szeged, 78.

Palibroda N., Cuna S., Pintea I., 1990. Analiza gazelor din incluziunile fluide din minerale prin cromatografie in faza gazoasa si spectrometrie de masa. (ITIM Cluj-Napoca-IGR Bucuresti) Contract de cercetare nr 1209/1990.

Panaiotu, C.E., (2001). Utilizarea incluziunilor fluide în studiul diagenezei rocilor sedimentare. Ed. Ars Docendi, Bucureşti, p. 32.

Papp D.C., Tecce F., Frezzotti M.L.,Ureche I., 2003. Microthermometric study of fluid inclusions in Neogene shallow intrusions from the inner Carpathian arc (Romania). Journ. of Geochem. Exploration, 3987, 1-5.

Paucă M., 1966. Contributions on the genesis of Miocene salt deposits from Romania. D.S. IGG (IGR), LIII/2(1965-1966), 159-184.

Penniston-Dorland S.C., 2001. Illumination of vein quartz textures in a porphyry copper ore deposit using scanned cathodoluminescence: Grasberg Igneous Complex, Irian Jaya, Indonesia. Amer. Miner., 86, 652–666.

Pettke, T., Halter, W., MacIntosh, I., and Heinrich, C.A., 2001, The porphyry to epithermal link: Preliminary fluid chemical results from Roşia Poieni, Romania, and Famatina, Argentina, Rom. J. Min. Dep., 79, Suppl. 2, ABCD-GEODE, Abstr.vol., p. 81-82, Vaţa Băi, Romania.

Pettke T., 2008. Analytical protocols for element concentration and isotope ratio measurements in fluid inclusions by LA-(MC-)ICP-MS. In Laser Ablation ICP-MS in the Earth Sciences: Current Practices and Outstanding Issues (P. Sylvester, ed.). Mineral. Assoc. Can. Short Course Series 40, 189-217.

Pettke T., Oberli F., Audétat A., Guillong M. , Simon A.C., Hanley J. J. , Klemm L. M., 2012. Recent developments in element concentration and isotope ratio analysis of individual fluid inclusions by laser ablation single and multiple collector ICP-MS. Ore Geology Reviews 44 (2012) 10–38.

Petrichenko O.I., 1973. Metody doslidshennya vkluchen”v mineralakh galogennykh porid. Kiev, Naukova Dumka, 182 p.

Petrichenko O.I., 1977. Atlass microvklucheniy v mineralakh galogennykh porod. Naukova Dumka, Kiev.

Pintea I., 1986. Morphologie et remplissage des inclusions vitreuses piégées dans les phenocrystaux de quartz du dacite macroporphyrique du col de Gutin (carrière “LALEAUA ALBĂ” - départament de Maramures). Significances petrogenetiques. Studia Univ. Babes- Bolyai. Geographia - Geologia, XXXI, 2, 19-25.

Pintea I., 1982. Date privind temperatura de formare a mineralelor din zacamantul Valea Rosie (Sasar, Baia Mare).In Carpatii Orientali, Formatiuni endogene: (I. Petreus, Jakab Gy ed), IPEG Harghita, Gheorgheni, p. 54-62.

Pintea I., 1988. Instalatie microtermometrica pentru studiul incluziunilor fluide din minerale, adaptabila pe microscop.Domeniul de lucru : -190° la + 600°C (77-870K). Tema de proiectare IGG-colectivul de cercetare Cluj-Napoca.

Pintea I., 1991a. Fluid inclusion studies on quartz crystals associated to the REE and sulphide ore body from Jolotca (NW-Ditrau masiff, Transylvania, Romania). ECROFI XI, Plinius , 5, abstr. p. 175, Firenze.Italy.

Pintea I., 1991b. Hypersaline fluid inclusions in miarolitic quartz crystals of the Vlădeasa granite (Apuseni Mountains, Romania). ECROFI XI, Plinius, 5, abstr. p. 176, Firenze. Italy.

Pintea I, 1993a. Contributions to the study of the fluid inclusions in the miarolitic quartz inclusions in the Draganului Valley. Rom. J. Mineralogy, 76, 1, 23-27.

Pintea I., 1993b. Fluid inclusions evidence to the importance of the hydrous saline melts in porphyry - type ore deposits genesis from Apuseni Mts. (Romania). Terra abstr. suppl. no 1, to Terra Nova, v. 5, p. 481, 1993, EUG VII, Stasbourg, France.

Pintea I., 1993c. Microthermometry of the hydrosaline melt inclusions from copper – porphyry ore deposits (Apuseni Mountains, Romania). Arch. Mineral. XLIX,165 – 167, Warsaw, Poland.

Pintea I., 1995a. Fluid inclusions microthermometry. Some typical examples. Rom. J. Mineralogy, 76, 2, 25-36.

Pintea I., 1995b. Fluid inclusion evidence for magmatic immiscibility between hydrous salt melt and silicate melt as primary source of ore metals in porphyry – copper system from Apuseni Mountains, Romania. Bol. Soc. Espagnola Mineralogia, 18 - 1, 184 - 186, Barcelona; suppl. abstract at 3th Symp on Mineralogy, 25-29 August, Baia Mare.

Pintea I., 1996a. New aspects of fluid phase evolution during genesis of the porphyry copper ore deposits from south Apuseni as seen in fluid inclusions. An., IGR, vol. 69. suppl. 1, p.166. Bucureşti.

Pintea I., 1996b. Fluid inclusions study with special view on fluid phases immiscibility associated to porphyry copper genesis from Metaliferi Mountains. Ph D thesis, Univ Bucharest (in Romanian). 172p.

Pintea I., 1997. The significance of the liquid homogenization temperature in salt melt inclusions. A case study in neogene porphyry copper ore deposits from Metaliferi Mountains (western Romania). ECROFI XIV, Nancy , abstract vol., 266 – 267. Nancy, France.

Pintea I., 1998. Fluid inclusion evidence for a porphyry copper ore deposit associated to the Ţibleş-Bran-Măgura Neagră eruptive massif: Petrography and microthermometric preliminary data. Rom. J. Mineral Deposit, 78, Suppl.1.

Pintea I., 1999. New microthermometric data on fluid inclusions from Roşia Montană quartz crystals. In "Mineralogy in the System of Earth Sciences". Abstr. vol suppl. An: XLVIII, p.74 - 75.

Pintea I., 2000. Magmatic - hydrothermal processes in the Alpine Carpathian subvolcanic structures from Romania, inferred by melt and fluid inclusion study. ABCD-GEODE, Workshop, Abstr. vol., p. 68. Borovets, Bulgaria.

Pintea I., 2001a. Contributions to distinguish between porphyry copper and related epithermal ore deposits: a tribute of melt and fluid inclusions. Rom. J. Min. Dep., 79, Suppl. 2, ABCD-GEODE, Abstr.vol., p. 83-84, Vaţa Băi, Romania.

Pintea I., 2001b. Melt and fluid inclusions study in neogene porphyry Cu – Au (Mo) from Metaliferi Mountains. ABCD – GEODE, Field guidebook, 28 - 30.

Pintea I., 2002. Occurrence and microthermometry of the globular sulfide melt inclusions from extrusive and intrusive volcanic rocks and related ore deposits from Alpine Carpathian Chain (Romania). Workshop- Short Course on Volcanic Systems, Geochemical and Geophysical Monitoring, Melt Inclusions: Methods, Applications and Problems, B. De Vivo and R.J. Bodnar, Eds, Proceedings, Sept. 26 – 30th, 2002, Seiano di Vico Equense-Napoli, Italy, pp. 177 – 180.

Pintea I., 2003. Source region of the melt and fluid phases in the porphyry Cu-Au-Mo deposits and other volcanic structures from Alpine Carpathian chain (Romania).Stud.Univ Babes-Bolyai Cluj-Napoca, ser.Geol, Spec. iss.,, p.84.

Pintea I., 2005a. Microthermometry of the magmatic foam glass inclusions in minerals from 'Dej tuff", Transylvania basin, Romania. Ecrofi XVIII - Siena 6-9 July, CD-ROM, abstract 03.Italy.

Pintea I., 2005b. Primary fluid inclusions microthermometry of the badenian salt deposits and modern halite crust from Romania. ECROFI XVIII, Siena 6-9 July, CD-ROM, abstract 04.Italy.

Pintea I., 2006. Melt inclusions texture and microthermometry in volcanic phenoclasts from the central neogene segment, east Carpathians , Romania. An. Inst Geologic al Romaniei. vol. 74, Spec Issue, 171 - 172, Bucharest.

Pintea I., 2007. Peculiar insight of the fluid and melt inclusions features inside the neogene subduction factory in carpathians, Romania. In ESF/LESC Exploratory workshop EW 06-030 New perspectives on volcano behaviour, volcanic hazards and volcanism-related mineral resources, Sovata, Romania, ESF: ESF/LESC Exploratory workshop EW 06-030. p.26 - 27.

Pintea I., 2008a. Fluid and melt inclusion evidence for succession of magmatic and hydrothermal events from Neogene/Quaternary subduction zone in Carpathians. In Pan-American Conference on research on Fluid Inclusions - In memory of Edwin Roedder, Progr. and abstr. p 47.

Pintea I., 2008b. Liquid inclusions microthermometry in the badenian halite and actual evaporate salt crust from Romania. 6 th National Symp. on Economic Geology, Rocksalt and other nonmetalliferous deposits. Sovata, abstr. vol. p 115 – 118.

Pintea I., 2009. Still problematic facts on the fate of brines in the alpine porphyry copper systems in Romania. ECROFI XX, Granada (Spania) abstr. 187 – 188.

Pintea I., 2010. Fluid and melt inclusions evidences for autometasomatism and remelting in the alpine porphyry copper genesis from Romania. Rom. Jour. of Mineral Deposits., 84 Spec. issue, 15 – 18. The 7th Nat Symp on Econ. Geol., "Mineral Resources of Carpathians area", 10 - 12 Sept., 2010, Baia Mare.

Pintea I., 2012. Fluid and melt inclusions: a precious tool in selective exploration strategy. Rom. J. of Min. Dep., 85, 1, 85-89.

Pintea I., 2013. Melt inclusions texture and thermal history in minerals from the Dej Tuff, Transylvania basin, Romania. Rom. J. of Earth Sci., 86, 29-47. Bucharest.

Pintea I., 2014a. The magmatic immiscibility between silicate-, brine-, and Fe-S-O melts from the porphyry (Cu-Au-Mo) deposits in the Carpathians (Romania): a review. Romanian Journal of Earth Sci. 87, 1, 32p, www.igr.ro.

Pintea I., 2014b. Magmatic and hydrothermal features of the fluid and melt inclusions from the quartz xenoliths, fragments and phenocrysts from Săpânţa Valley (Igniş Mountains, Romania). Romanian Jour. of Min. Dep. 87, 1, 79-82.

Pintea I., 2016. A self-perspective research topic revealed during the elaboration of the atlas "Fluid and melt inclusions from Romania". Rom. Jour.of Min. Dep.89, (1-2), 1-6.

Pintea, I., Diamond, L.W., 1994. Immiscible, hypersaline CO_2–H_2O fluids associated with REE and MoS_2 mineralization in the Ditrău alkaline massif, Transylvania, Romania. IMA 16th Gen. Meet. 4–6 Sept., Pisa, Abstr., 328–329.

Pintea I., Iatan L.E., 2013. The magmatic-hydrothermal history of the β-quartz phenocrysts from Rosia Montana dacite inferred by solid-, melt-, and fluid inclusion assemblages. European Current Research On Fluid Inclusions (ECROFI-XXII), Antalya-Turkey, 4-9 June, 2013, Abstract Book, 114-115.

Pintea I., Laczko A.A., 2005. Preliminary microthermometric data related to a complex magmatic-hydrothermal system from Sîntimbru - Băi (South – Harghita Mountains, Romania).“Geo 2005”, Proceedings. Geol. Soc. of Romania, p. 95 - 96.

Pintea I., Mârza I., 1989. Preliminary observations on the CO_2-bearing fluid inclusions in the olivine and pyroxene peridotitic nodules at Hoghiz (Perşani mountains). D. S. IGG (IGR), 74/1, (1987), 1989, 107-116.

Pintea I., Cherebeţiu T., Iurian D., Hiriţ A., Manoilă I., 1992. Termoinc-01, a microthermometric stage for fluid inclusion studies. Rom. Jour. Mineral., Suppl. Abstracts, 75, 34.

Pintea I., Udubaşa G., Nedelcu L., 1999a. Evolution of fluid phases related to a new porphyry copper deposit in Romania: The Ţibles massif. In Proceed. 5th SGA and 10th IAGOD meeting., London Mineral Deposits: Processes to Processing, Stanley et al. (eds), 83-85.

Pintea I., Hopârtean E., Cosma V., Morar G.G., Hopârtean I., Eggenkamp H.G.M., 1999b. Chloride content and chlorine stable isotope ratios of the salt melt inclusions from the Roşia Poieni porphyry copper ore deposit (Metaliferi Mountains, western Romania). ECROFI XV Abstracts, Terra nostra 99/6, 229-230; Rom. J. Mineralogy, vol 79, suppl. nr.1, p.53. Bucharest.

Pintea I., Mosonyi E., Bardocz Z., 2003. Textural features and melt inclusions types in andesites and basaltic andesites from the Eastern Carpathians (Călimani-Gurghiu-Harghita Mts), Romania. Studia Univ. Babes-Bolyai Cluj Napoca, ser. Geol., Spec iss., p.85.

Pintea I., Nutu-Dragomir M.-L., Udubaşa S.S., Birgăoanu D., Iatan E.L., Berbeleac I., Ciobotea-Barbu O.C., 2018. Hydrosilicate aqueous-, and vapor-“melt” inclusions in some specific rocks and minerals from Romania. Romanian Journal of Mineral Deposits, v.91, no 1-2, p.13-18.

Pintea I., Udubaşa S.S., Nuțu-Dargomir L.M., Iatan E.L., Berbeleac I., Petrescu L., Ghinescu E., 2019. Clathrasil compound evidence in fluid and brine inclusions by microthermometry and Raman spectroscopy. Goldschmidt 2019, Barcelona, abstract.

Pintea I., Udubaşa S.S., Iatan E.L., Berbeleac I., Birgăoanu D., Barbu O.C., Ghinescu E., 2019. Microthermometry and Raman spectroscopy of fluid and melt inclusions in the alpine porphyry copper deposits from Romania: insight on micrometallogeny. Rom. J. Mineral Deposits, vol 92, (2019) No. 1-2, p.9-32.

Pintea I., 2019. Fluid and melt inclusions in minerals: applications in geosciences. In „Geosciences in the 21st century” Symposium dedicated to the 80th anniversary of professor Emil Constantinescu, GeoEcoMar, Bucharest, 22.oct. 2019, p.164-169.

Pintea I., Udubaşa S.S., Ghinescu E., Iatan L.E., Berbeleac I., 2020 Melt-melt – fluid immiscibility evidence by microthermometry and Raman spectroscopy in porphyry copper genesis: Bucium Tarnita porphyry Cu-Au(+/-Mo) deposit from Metaliferi Mountains (western Romania). DOI:10.13140/RG.2.2.15160.37120.

Pintea I., Udubaşa S.S., Ghinescu E., Iatan L.E., Berbeleac I., 2020. Melt-melt – fluid immiscibility evidence by microthermometry and Raman spectroscopy in porphyry copper genesis: Bucium Tarnita porphyry Cu-Au(+/-Mo) deposit from Metaliferi

Mountains (western Romania). 12th International Symp. on Ec. Geol., "The future of Mineral Res. in the Circular Economy, extended abstract (in press), Bucharest.

Pintea I., Udubasa S.S., Ghinescu E., Nutu M-L Dragomir, Iatan, L.E., Berbeleac I., 2021. Minerals-, glassy-, globular opaque and fluid inclusions from metamorphic recrystallized "MVT" sulfide mineralization from Blazna-Guşet prospect, Rodna Mountains, Romania. Goldschmidt Conf., Lyon, Abstr. No. 6312.

Pintea I., Iatan L., Udubasa S.S., Berbeleac I., Ghinescu E., 2021. Is there an eutectic mixture of the halite daughter phase with sulphate± carbonate± phosphate± borate± fluoride in the hydrosaline melt inclusions from porphyry Cu- Au (+/-Mo) deposits in Metaliferi Mountains, Western Romania ?. Goldschmidt Conf., Lyon, Abstr. No. 6929.

Pironon J., 1990. Synthesis of hydrocarbon fluid inclusions at low temperature. Amer. Mineral., 75, 226-229.

Pomârleanu V.V., 1958. Dispozitiv pentru determinarea temperaturii de omogenizare a incluziunilor fluide din minerale. An St.Univ. "Al. I. Cuza" din Iași, sect. II (St Naurale),V, 119-124.

Pomârleanu V.V., 1971. Geotermometria si aplicarea ei la unele minerale din Romania. Ed .Acad RSR, 158p.

Pomârleanu V., 1975. Decrepitometria si aplicaţiile ei în prospecţiunea zăcămintelor de minereuri. Ed. Tehn., 180p, București.

Pomârleanu V., Filip D.,1976. Contributions to the method of thermoacoustic research of inclusions from minerals. Rev. Roum. Geol., Geophys.et Geogr., Geologie, 20, 2, 299-306.

Pomârleanu V., Pomârleanu E., 1981. Carbon dioxide in fluid inclusions of pegmatite minerals.Rev. Roum. Geol., Geophys. et Geogr., Geologie, 25,101-108.

Pomârleanu V., 1975. Decrepitometry and their applications in mineral prospection. Edit. Tech., 180p (in Romanian), Bucharest.

Pomârleanu V., Rădut M., Neagu E., 1985. Fluid inclusion study in the Baia Sprie-Suior area; implication for the thermodynamic regime in hydrothermal solutions (in Romanian). Stud Cerc Geol Geogr Ser Geol 30:102–110.

Pomârleanu V., Intorsureanu I., 1986. Salinity of fluid inclusions of the porphyry copper ore deposits and their significance in geobarometry and prospecting (The Lapuşnicu Mare ore deposit-Banat). D.S. Inst. Geol. Geofiz. (IGR)70,-71/2 (1983;1984) 1985, 83-95.

Pomârleanu V., Neagu E.A.(2003) Incluziunile din minerale-mesaje ale unui trecut îndepartat de pe teritoriul României. Rom. Journal of Mineralogy, v. 81, 171p.

Pomârleanu V., Mârza I., 2003. Fluid inclusion in salt (Transylvania Basin, Romania). Stud. Univ. "Babeş-Bolyai", Ser. Geol. Spec. issue, 86-87.

Pomârleanu V., 2007. Microinclusions in minerals from extraterrestrial and terrestrial environments. Ed. AGIR, 173p (in Romanian), Bucharest.

Popescu G., Neacşu A., 2012. Modeling of epithermal gold and porphyry copper deposits from Metaliferi Mountains (Romania). Rom. J. of Mineral Dep., 85, 1, 7-13.

Poty B., Leroy J., Jachimovicz L., 1976. Un nouvel appareil pour la mesure des températures sous le microscope: l'installation de microthermométrie Chaixmeca. Bull. Soc. Fr. Minéral. Cristallogr., 99, 182-186.

Rajamani V., Naldrett A.J., 1978. Pertitioning of Fe, Co, Ni, and Cu between sulfide liquid and basaltic melts and the composition of Ni-Cu sulfide deposits. Econ. Geol., 73, 82-93.

Rădulescu D.P., 1960. Mineralogic researches at Potassium and Magnesium salts from Tg.Ocna- Galeanu. Stud.Cerc.Geol., 6, 3, 519-538 (in Romanian).

Rădulescu D. 1979. Magmatic rocks petrology. Bucharest University (in Romanian). 206p.

Rădulescu D., Dimitrescu R., 1982. Endogeneous petrology of the territory of Romania. Bucharest University. (in Romanian), 120p.

Roberts S.M., Spencer R.J., 1995. Paleotemperatures preserved in fluid inclusions in halite.Geochim. Cosmochim. Acta, 59, 3929-3942.

Roedder E., Ingram B., Hall W.E., 1963. Studies of fluid inclusions III: extraction and quantitative analysis of inclusions in the milligram range. Econ. Geol., 58, 353-374.

Roedder E., 1965. Liquid CO_2 inclusions in olivine-bearing nodules and phenocrysts from basalts. Amer. Min., 30, 1746-1782.

Roedder, E., Coombs, D.S., 1967. Immiscibility in granitic melts, indicated by fluid inclusions in ejected granitic blocks from Ascension Island. J. Petrol. G. B. 8, 417-451.

Roedder E., 1971. Metastability in fluid inclusions. Soc. Min. Geol. Japan, Spec. Issue 3, 327- 334 [Proc. IMA-IAGOD Meetings'70, IAGOD Vol.].

Roedder E., 1972. Composition of fluid inclusions. Geol. Surv. Professional Paper 440-JJ, 164p, 12 Plates.

Roedder E., 1979. Origin and significance of magmatic inclusions: Bull. de Miner. 102, 487-510.

Roedder E., 1984. Fluid inclusions: Reviews in Mineralogy, v. 12, 644 p.

Roedder E., 1984a. The fluid in salt. Amer. Min., 69, 413-439.

Roedder E., 1990. Fluid inclusion analysis – Prologue and epilogue. Geochim. Cosmochim. Acta, 34, 495-507.

Roedder E., 1992. Fluid inclusion evidence for immiscibility in magmatic systems. Geochim. Cosmochim. Acta 56, 5-20.

Roşu E., Nedelcu L., Udubaşa G., Pintea I., Ivăşcanu P., 2001. Neogene ore deposits from south Apuseni Mountains, Romania, constraints and evolution. ABCD - GEODE Field guidebook, p. 22 – 23.

Roşu E., Nedelcu L., Pintea I., Ivăşcanu M.P., Costea C., Şerban A., Alexe V., 2001. The estimation of the formation constraints of the main mineral deposit types. Rom. Jour. of Min. Dep., 79, suppl. 2, Field Guidebook, 23.

Roedder E., Bodnar R.J., 1997. Fluid Inclusion Studies of Hydrothermal Ore Deposits. In Geochemistry of Hydrothermal Ore Deposits, 3rd ed., H. L. Barnes, ed., Wiley & Sons, Inc, New York (657-698).

Rusk B.G., Reed, M.H., Krinsley, D., Bignall, G., and Tsuchiya, N., 2004. Natural and synthetic quartz growth and dissolution revealed by scanningelectron microscope cathodoluminescence. In M. Nakahara, N. Matubayasi, M. Ueno, K. Yasuoka, and K. Watanabe, Eds., Proceedings of 14th international conference on the properties of water and steam, p. 296-302. Maruzen Co., Ltd., Kyoto.

Rusk B.G., Reed M.H., Dilles J.H., 2008. Fluid inclusion evidence for magmatic-hydrothermal fluid evolution in the porphyry copper-molybdenum deposit at Butte, Montana. Econ. Geol., 103, 307-334.

Samson I ., Anderson A., and Marshall D., (eds), 2003. Fluid Inclusions: Analysis and Interpretation: Mineralogical Association of Canada Short Course Volume 32, 370 p.

Săbău G., Massone J-H., 2003. Relationships among eclogite bodies and host rocks in the Lotru Metamorphic Suite (South Carpathian, Romania): Petrological evidence for

multistage tectonic emplacement of eclogites in a medium-pressure terrain. Internat. Geol. Rev., 45, 225-262.

Scambeluri M., Philippot P., 2001. Deep fluids in subduction zones. Lithos, 55, 213-227.

Schmatz J., Urai J.L., 2010. The interaction of fluid inclusions and migrating grain boundaries in a rock analogue: deformation and annealing of polycrystalline camphor-ethanol mixtures. J. Metamorph. Geol., 28, 1-18.

Schmidt C., Chou I-M., Bodnar R.J., Bassett W.A., 1998. Microthermometric analysis of synthetic fluid inclusions in the hydrothermal diamond-anvil cell. Am. Min. 83, 995-1007.

Schmidt C., Bodnar R.J., 2000. Synthetic fluid inclusions: XVI. PVTX- properties in the system H_2O-NaCl-CO_2 at elevated temperatures,pressures, and salinities. Geochim. Cosmochim. Acta, 64, 22, 3853-3869.

Seghedi I., 1982. Contributions on the petrologic study of the Călimani caldera. D.S. IGG (IGR), LXVII/1(1979-1980), 87-126 (in Romanian).

Shepherd T.J., 1981. Temperature-programmable heating-freezing stage for microthermometric analysis of fluid inclusions. Econ. Geol. 76, 1244-1247.

Shepherd, T., Rankin, A.H., and Alderton, D.H.M., 1985. A practical guide to fluid inclusion studies. Blackie, London, 239 p.

Shepherd T.J., Rankin A.H., 1998. Fluid inclusion techniques of analysis. In: Richards J.P., Larson P.B. (eds).”Techniques in hydrothermal ore deposit geology”. Rev. Econ. Geol., 10, 125-149.

Shinohara H., 1994. Exsolution of immiscible vapor and liquid phases from a crystallizing silicate melt: Implications for chlorine and metal transport, Geochim. Cosmochim. Acta 58, 5215-5221.

Shmulovich K.I., Mercury L., Thiéry R., Ramboz C., Mekki El M. 2009. Experimental superheating of water and aqueous solutions. GeochimCosmochim.Acta, 73, 2457-2470.

Siljeström S., 2011. Single fluid inclusion analysis using ToF-SIMS. Implications for ancient Earth biodiversity and paleoenvironment studies. PhD thesis Stockholm Univ. Stockolm, Sweden.

Simon A.C., Frank M.R., Pettke T., Candela P.A., Piccoli P.M., Heinrich C.A., Glascock M., 2007. An evaluation of synthetic fluid inclusions for the purpose of trapping equilibrated, coexisting, immiscible fluid phases at magmatic conditions. Amer. Min., 92, 124-138.

Sîrbescu M.-L., Nabelek P.I., 2003. Dawsonite: An inclusion mineral in quartz from the Tin Mountain pegmatite, Black Hills, South Dakota. Amer. Mineral., 88, 1055-1060.

Sobolev A.V., 1996. Melt inclusions in minerals as a source of principal petrologic information. Petrology 4, 228-239.

Sorby H.C., 1858. On the microscopical structure of crystals, indicating origin of minerals and rocks. Quart. J. Geol. Soc. London 14, 453-500.

Stanciu C., 1984. Hypogene alteration genetic types related to the neogene volcanism of the east Carpathians, Romania. An.Inst Geol. Geofiz. (IGR), LXIV, 235-243.

Sterner S.M., Bodnar R.J., 1984. Synthetic fluid inclusions in natural quartz. I.Compositional types synthesized and applications to experimental geochemistry. Geochim. Cosmochim. Acta 48, 2659-2668.

Sterner M.S., Hall D.L., Bodnar R.J., 1988. Synthetic fluid inclusions.V. Solubility relations in the system NaCl-KCl-H_2O under vapor-saturated conditions. Geochim.Cosmochim. Acta, 52, 989-1005.

Sterner S.M., Bodnar R.J., 1991. Synthetic fluid inclusions.X: experimental determination of P-V-T-X properties in the CO_2-H_2O system to 6 kb and 700°C. Am. J. Sci., 291, 1-54.

Sterner S.M., Hall D.L., Keppler H., 1995. Compositional re-equilibration of fluid inclusions in quartz. Contrib. Mineral. Petrol, 119, 1-15.

Stewart M.L., Pearce T.H., 2004. Sieve-textured plagioclase in dacitic magma: Interference imaging results. Amer. Mineral., 89, 348-351.

Steele - MacInnis- M., Esposito R., Bodnar R.J., 2011.Thermodynamic model for the effect of post-entrapment crystallization of the H_2O-CO_2 systematics of vapor-saturated, silicate melt inclusions. Journ. of Petrology, 52, 12, 2461-2482.

Steele-MacInnis M., Bodnar R.J., 2013. Effect of the vapor phase on the salinity of halite – bearing aqueous fluid inclusions estimated from the halite dissolution temperature.Geochim.Cosmochim.Acta, 115, 205-216.

Stoica C., Gherasie I., 1981. Salt and potassium and magnesium salts from Romania. Ed. Tech. Bucharest, 248 p (in Romanian).

Stoller P., Krüger Y., Frenz M., 2007. Femtosecond lasers in fluid inclusion analysis: Three-diemnsional imaging and determination of inclusion volume in quartz using second harmonic generation microscopy. Earth and Planet. Sci. Lett., 253, 359-368.

Stone W., S., Fleet M.E., 1991. Nickel-copper sulfides from the 1959 eruption of Kilauea volcano, Hawaii: contrasting compositions and phase relations in eruption pumice and Kilauea Iki lava lake. American Mineral., 76, 1363-1372.

Student J.J., Bodnar R.J., 1996. Melt inclusion microthermometry: Petrologic constraints from the H_2O-saturated haplogranite system, Petrology 4 (3) 291-306. From Petrologiya, 4, 3, 1996, 310-325.

Student J.J. Bodnar R.J., 2004. Silicate melt inclusions in porphyry copper deposits: Identification and homogenization behavior. Canadian Mineral. 42, 1583-1599.

Sugaki A., Kitakaze A., Kojima S., 1987. Bulk compositions of intimate intergrowths of chalcopyrite and sphalerite and their genetic implications. Mineral. Deposita, 22, 26-32.

Sugaki A., Kitakaze A.,1998. High form of pentlandite and its thermal stability. Amer. Mineral., 83, 133-140.

Szakács A., Pécskay Z., Silye L., Balogh K., Vlad D., Fülöp A., 2012. On the age of the Dej Tuff, Transylvanian Basin, Romania. Geologica Carpathica, 63, 138-148.

Ştefan A., Istrate G., Udrescu C., 1982. Petrological study of banatites from the Măgureaua-Vaţei-Birtin valley region (South Apuseni mountains). D.S. Inst. Geol. Geofiz. (IGR), LXVII/1 (1979-1980), 145-174.

Ştefan A., Lazăr C., Intorsureanu I., Horvath A., Gheorghiţă I., Bratosin I., Şerbănescu A., Călinescu E., 1985. Petrological study of the banatitic eruptive rocks in the eastern part of the Gilău Mountains. D.S. IGG (IGR), LXIX/1 (1982), 215-246.

Takenouchi S., Imai H., 1975. Glass and fluid inclusions in acidic igneous rocks from some mining areas in Japan. Econ. Geol. 70, 750-769.

Thomas J.B., 2003. Melt inclusion geochemistry. PhD thesis, Virginia Pollytechnic Inst. and State Univ., Blacksburg, Virginia, USA.

Thomas J.B., Bodnar R.J., Shimizu N., Chesner C.A., 2003., Melt inclusion in zircon. In Zircon, Rev. in Mineralogy and Geochemistry, 53, 63 - 87. Min. Soc. America, Geochem. Soc. 495p.

Thomas R., 1994. Estimation of viscosity and water content of silicate melts from melt inclusion data. Eur. J. Mineral. 6, 511-535.

Thomas R., Webster J.D., Heinrich W., 2000. Melt inclusions in pegmatite quartz: Complete miscibility between silicate melts and hydrous fluids at low pressure. Contrib. Mineral. Petrol. 139, 394-401.

Timofeeff M.N., Lowenstein T.K., Blackburn W.H., 2000. ESEM-EDS: an improved technique for major element chemical analysis of fluid inclusions. Chem. Geol., 164, 171-182.

Tissot R.G., Rodriguez M.R., 1999. A practical hot stage for high temperature microanalysis. JCPDS-International centre for diffractionm data. 356-360.

Touret J.L.R., 1977. The significance of fluid inclusions in metamorphic rocks. In: Fraser (ed.), Thermodynamics in Geology, 203-227, D. Reidel - Dordrecht.

Touret J.L.R., Bottinga Y., 1979. Equation d' état pour le CO_2. Application aux inclusions carboniques. Bul. Minéralogie, 102, 577-583.

Touret J.L.R., 1984. Les inclusions fluids: Historie d'un paradoxe. Bull. Mineral., 107, 125-137.

Touret J.L.R., Frezzotti M.- L., 1993. Magmatic remnants in plutonic rocks, Bull. Soc. Geol. France, Huitieme Serie, 164, 229-242.

Touret J.L.R., 2001. Fluids in metamorphic rocks. Lithos, 55, 1-25.

Török K., Bali E., Szabó C., Szakál J.A., 2003. Sr-barite droplets associated with sulfide blebs in clinopyroxene megacrysts from basaltic tuff (Szentbékkalla, western Hungary). Lithos, 66, 275-289.

Trepmannn C.A., Spray J.G., 2006. Shock-induced crystal-plastic deformation and post-shock annealing of quartz: microstructural evidence from crystalline target rocks of the Charlevoix impact structure, Canada. Eur. J. Mineral., 18, 161-173.

Udubaşa G., Istrate G., Dafin E., Braun E., 1976. Polymetallic mineralizations from Bocşa (N Săcărâmb, Metaliferi Mountains). D.S. Inst. geol. geofiz. (IGR), LXII(1974, 1975), 97-124 (in Romanian).

Udubaşa G., Istrate G., Vălureanu M., 1979. Metallogeny of the Coranda-Hondol (Metaliferi Mountains). D. S. Inst. geol. geofiz (IGR), LXVII/2 (1979-1980), 197-232, (in Romanian).

Udubaşa G., Edelstein O., Pop N., Istrate G., Kovacs M., Istvan D., Bogancsik V., Roman L., 1981. Magnesian skarn from Ţibles: preliminary data. D.S. Inst. geol., geofiz. (IGR), LXVI (1979), 139-156.

Udubaşa G., Nedelcu L., Andăr A., Andăr P. 1983. Stratabound lead-zinc pyrite ore deposits in upper Precambrian carbonate rocks, Rodna Mountains, Romania. Mineral Deposita 18, 519-528.

Udubaşa G., 1984. Typomorphhism of some ore minerals and a PvT classification of certain ore deposits. Ann. IGG, LXIV, 141-152.

Udubaşa S.S., Lespinasse M., Udubaşa G., Popescu C.G., Leroy J., Bilal E., 2003. Fluid inclusions data on quartz samples from Costesti gold mineralization, Southern Carpathians,Romania. Acta Mineralogica-Petrographica, Abstract Series 2, 220-221.

Udubaşa G., Răduţ M., Edelstein O., Pop N., Istvan D., Pop V., Stan D., Kovacs M., Roman L., Bernad A., 1984. Metallogeny of the Ţibles eruptive complex, Eastern Carpathians. (in Romanian). D.S. Inst. geol., geofiz. (IGR), LXVIII , 221-241.

Ulrich M.R., Bodnar R.J., 1988. Systematics of stretching of fluid inclusions II: barite at 1 atm confining pressure. Econ. Geol., 83, 1037-1046.

Van den Kerkhof A.M., 1988. CO_2-CH_4-N_2 in fluid inclusions: theoretical modelling and geological applications. Ph.D. Diss. Free Univ., Amsterdam, 206 pp.

Van den Kerkhof A.M., Hein U.F., 2001. Fluid inclusion petrography. In: Andersen T, Frezzotti M.L., Burke E.A.J. ed. Fluid inclusions: phase relationships – methods applications (special issue). Lithos 55 (1-4), 320 pp.

Van den Kerkhof A.M., Sosa G.M., 2012. Fluid inclusions- Petrography and genetic interpretation of fluid inclusions. Application of cathodoluminescence techniques. Postgraduate course. Geowiss. Zentrum Univ. Gottingen (Germany).

Van den Kerkhof A.M., Kronz A., Simon K., 2014. Deciphering fluid inclusions in high-grade rocks. Geosci. Frontieres, 5, 5, 683-695.

Vasyukova O.V., 2011. Types and origin of quartz and quartz-hosted fluid inclusions in mineralised porphyries, 213 p. Ph.D. thesis, University of Tasmania, Hobart.

Varela M.E., 1997. Fluid and melt inclusions in upper mantle xenoliths. Mitt. Österr. Miner. Ges., 142, 111-117.

Vityk M.O., Bodnar R.J., Dudok I.V., 1996. Fluid inclusions in "Marmarosh Diamonds": evidence for tectonic history of the folded Carpathian Mountains, Ukraine. Tectonophysics, 255, 163-174.

Vogelsang H., 1869. Nachtrag zu der abhandlung "über flüssigkeitseinschlusse in gesteinen". Ann. Phys. und Chem., 137, 257-271.

Webster J.W. ed., 2006. Melt inclusions in plutonic rocks. Min. Assoc. of Canada, Short Course series, 36, 237pp.

Webster J.D., Mandeville C.W., 2007. Fluid immiscibility in volcanic environments. Rev. in Min. and Geochem., 65, 313-362.

Weisbrod A., Poty B., 1975. Thermodynamics and geochemistry of the hydrothermal evolution of the Mayres pegmatite. Part I, Petrology, I, 1, 1-16; Part, II Petrology, I, 2, 89-102.

Weisbrod A., 1982. Physical and chemical changes in natural fluids in hydrothermal processes and mineral deposition, studied with fluid inclusions. Ber. Bunsenges. Phys. Chem, 86, 1016-1027.

Weisbrod A., 1984. Utilisation des inclusions fluids in geothermobarometrie. In "Thermometrie et barometrie geologiques" (M. Lagache eds. Vol 1+2, 633 p, 415-459.

Wilkinson J.J., 2001. Fluid inclusions in hydrothermal ore deposits. Lithos, 55, 229-272.

Weiss P., Driesner T., Heinrich C.A., 2012. Porphyry-copper ore shells form at stable pressure-temperature fronts within dynamic fluid plumes. Science, 338,6114, 1613-1616.

Werre, R.W. Jr., Bodnar, R.J., Bethke, P.M., and Barton, P.B. Jr., 1979. A novel gas-flow fluid inclusion heating/freezing stage (abstr.). Geological Society of America Abstracts with Programs, 11, 539.

Williams-Jones A.E., Heinrich C.A., 2005. Vapor transport of metals and the formation of magmatic-hydrothermal ore deposits. Econ. Geol., 100, 7, 1287-1312.

Wyllie P.J., Ryabchikov I.D., 2000. Volatile components, magmas, and critical fluids in upwelling mantle. Jour. of Petrol., 41, 7, 1195-1206.

Yang K., Bodnar R.J., 1994. Magmatic-Hydrothermal evolution in the "Bottoms" of porphyry copper systems: Evidence from silicate melt and aqueous fluid inclusions in granitoid intrusions in the Gyeongsang Basin, South Korea, International Geology Rev. 36, 608-628.

Yardley W.D., Bodnar R.J., 2014. Fluids in the continental crust. Geochem. Perspectives, 3, 1, 136 pp.

Zapunniy, S.A., Sobolev, A.V., Bogdanov, A.A., Slutsky, A.B., Dmitriev, L.V., and Kunin, L.L.. 1989. An apparatus for high-temperature optical research with controlled oxygen fugacity.Geochemistry International, 26, 120-128.

Zhili H., Akbarov H. A., Diquing Z., 2008. In memory of fluid inclusion research pioneers E. Roedder, N. P. Ermakov, H. C. Sorby and Aly Raichan Beruny. Proceed. of the XIII All-Russian conference on thermobarogeochemistry in conjunction with IV APIFIS symposium.10-13.

Zimmermann H., 2001. On the origin of fluids included in Phanerozoic marine halite – basic interpretation strategies. Geochim. Cosmochim. Acta., 65, 1, 35-45.

Zirkel F.,1893. Lehrbuch der petrographie,1, 166-192. Leipzig.